UNIVERSITÀ DEGLI STUDI DI MILANO

Department of Chemistry

Doctoral School in Chemistry

XXXIV Cycle

Synthesis of smart glycosides to enhance glyco-nanomaterials circulation half-life

PhD Thesis

Author: Ruth Mateu Ferrando

Tutor: Prof. Luigi Lay

2019 - 2022

To every woman in science

"Rare sono le persone che usano la mente,
poche coloro che usano il cuore
e uniche coloro che usano entrambi"

Rita Levi Montalcini

ABSTRACT

Nanoparticle (NP)-based therapies have proven to offer potential solutions for conventional medicine while minimizing its side effects. In particular, glycosylated gold NPs (AuGNPs) represent attractive imaging and/or delivery platforms combining the biological activity of carbohydrates with the biocompatibility and physicochemical versatility of the metallic core. However and despite their rapid growth, the full clinical potential of these glyconanosystems will only be reached when their underlying safety concerns are understood and accurately addressed. When placed in biological fluids, AuGNPs, interact with a high number of biomolecules forming a so-called protein corona (PC), a coating that covers them and has severe consequences for their fate, efficacy and toxicity. As a consequence, AuGNPs are often recognized by the immune system and cleared from the blood stream before they have had enough circulation time to reach their therapeutic target.

In order to address the first issue, the initial chapter of the present thesis deals with the preparation of a library of six different AuGNPs functionalized with three monosaccharides (α-mannose, α-galactose and α-fucose) and two polyethylene glycol alternatives (PEG5000 and alkyl-PEG600) as an anchor to the Au nanomaterials (NMs). In collaboration with CICBiomaGUNE (Spain), the interaction of these AuGNPs with different lectins is investigated using Fluorescence Correlation Spectroscopy (FCS) to evaluate the effect of the PEG length on the interaction with proteins and the carbohydrates binding specificity. The second part of the chapter is dedicated to the preparation of an additional set of AuGNPs functionalized with negatively charged monosaccharides such as mannose-6-phosphate, mannose-6-sulfate or *N*-acetyl neuraminic acid. The final goal is to compare the results with neutral mannosylated AuGNPs in terms of colloidal stability and protein binding. These measurements will be performed at RCSI (Ireland) by means of Differential Centrifugal Sedimentation (DCS) and Dynamic Light Scattering (DLS). The final aim of the work described in Chapter I is to provide a better understanding of the PC formation and a correlation to the main NMs' surface characteristics influencing it. The immunosuppressive properties of AuGNPs functionalized with *N*-acetyl neuraminic acid will also be tested *in vivo* in collaboration with Mario Negri Institute (Italy).

The second chapter focuses on the synthesis of ABO blood sugar epitopes, terminal di- (Fucα1-2Galβ1-O-R) and tri-saccharides (GalNAcα1-3(Fucα1-2)Galβ1-O-R and Galα1-3(Fucα1-2)Galβ1-O-R) covering the surface of human red blood cells and other body tissues. Our synthetic derivatives have been prepared adapting previously reported procedures and include a linear aglycone with a free amino group for NM conjugation. Functionalization of NMs with these self-antigens may improve their immunotolerance and biocompatibility in comparison to PEGylated counterparts, prolonging their blood circulation time, improving their delivery efficiency and granting them new therapeutic possibilities. These assumptions are to be tested in the near future in collaboration with RCSI (Ireland).

Chapter III describes the functionalization of mannose (Manα1), dimannose (Manα1-2Manα1) and trimannose (Manα1-3(Manα1-6)Manα1) derivatives with an amine-ending linker at their reducing-end for Au nanorods functionalization at VITO (Belgium). The end goal of the project is to develop a simple and label-free biosensor to detect mannose binding lectin (MBL) from human plasma samples based on optical measurements. The near IR shift due to the effective lectin binding can be correlated to potential cardiovascular disease for prevention and early onset stroke diagnosis.

In summary, this thesis aims to provide a better understanding of AuGNPs' behavior in biological fluids, to face the main concerns impairing nanomedicine translation into clinics and to pave the way towards novel glyco-nanosystems with enhanced therapeutic performance for healthcare applications.

TABLE OF CONTENTS

ABSTRACT.....i

TABLE OF CONTENTS.....iii

ABBREVIATIONS AND ACRONYMS.....vii

INTRODUCTION.....1

1. Nanotechnology.....1

   1.1. Nanotechnologies in nanomedicine.....1

2. Gold: a precious metal for nanomedicine.....3

   2.1. Au NPs as therapeutic agents.....4

   2.2. Au NPs as delivery agents.....5

   2.3. Au NPs in imaging and sensing.....7

   2.4. Synthesis of Au NPs.....8

   2.5. Au NPs concerns.....11

3. Carbohydrate coated Au NPs.....16

   3.1. Synthetic strategies.....17

   3.2. AuGNPs as biosensors for the detection of virus, bacteria and cancer.....18

   3.3. AuGNPs as targeted drug delivery systems.....19

   3.4. AuGNPs in immunology.....20

   3.5. AuGNPs as contrast agents.....21

AIM OF THE PROJECT.....23

CHAPTER I: PROTEIN CORONA STUDIES.....25

1. Introduction.....25

2. Aim of the chapter.....26

3. Results and discussion.....27

   3.1. Synthesis of 3'-aminopropyl α-D-mannopyranoside.....27

   3.2. Synthesis of 3'-aminopropyl α-D-galactopyranoside.....29

   3.3. Synthesis of 3'-aminopropyl α-L-fucopyranoside.....30

   3.4. Synthesis of AuGNPs.....33

4. Negatively charged AuGNPs.....37

   4.1. Synthesis of negatively charged mannose derivatives.....38

   4.2. Synthesis of Sialic Acid.....43

5. Conclusions.....45

CHAPTER II: SYNTHESIS OF BLOOD SUGAR ANTIGENS 47

1. ABO blood group system 47

2. Aim of the chapter 49

3. Results and discussion 50

3.1. Retrosynthetic approach 50

3.2. Synthesis of galactoside acceptors 51

3.3. Synthesis of fucoside donor 53

3.4. Synthesis of disaccharide antigen H derivative 54

3.5. Synthesis of trisaccharide antigen B derivative 56

3.6. Synthesis of trisaccharide antigen A derivative 57

4. Conclusions 58

CHAPTER III: MANNOSYLATED GOLD NANORODS AS BIOSENSORS FOR STROKE DIAGNOSIS 61

1. Aim of the chapter 61

2. Results and discussion 62

2.1. Synthesis of 3'-aminopropyl 2-O-(α-D-mannopyranosyl)-α-D-mannopyranoside 62

2.2. Synthesis of 3'-aminopropyl 3-O-(α-D-mannopyranosyl)-6-O-(α-D-mannopyranosyl)-α-D-mannopyranoside 63

3. Conclusions 63

EXPERIMENTAL SECTION 65

1. Experimental procedures Chapter I 66

1.1. Synthesis of 3'-aminopropyl α-D-mannopyranoside 66

1.2. Synthesis of 3'-aminopropyl α-D-galactopyranoside 72

1.3. Synthesis of 3'-aminopropyl α-L-fucopyranoside 76

1.4. Synthesis of AuGNPs 80

1.5. Synthesis of 3'-aminopropyl 6-O-phospho-α-D-mannopyranoside 84

1.6. Synthesis of 3'-aminopropyl 6-O-sulfo-α-D-mannopyranoside 89

1.7. Synthesis of 3'-aminopropyl *N*-acetyl neuraminic acid 91

2. Experimental procedures Chapter II 96

2.1. Synthesis of galactoside acceptor **50** 96

2.2. Synthesis of fucoside donor **54** 99

2.3. Synthesis of disaccharide antigen H derivative 102

2.4. Synthesis of disaccharide acceptor **56** 103

2.5. Synthesis of galactoside donor **59** 104

2.6. Synthesis of trisaccharide antigen B derivative 105
2.7. Synthesis of donor **62** 106
3. Experimental procedures Chapter III 109
3.1. Synthesis of 3'-aminopropyl 2-O-(α-D-mannopyranosyl)-α-D-mannopyranoside 109
3.2. Synthesis of 3'-aminopropyl 3-O-(α-D-mannopyranosyl)-6-O-(α-D-mannopyranosyl)-α-D-mannopyranoside 114
REFERENCES 119
ACKNOWLEDGEMENTS 135

ABBREVIATIONS AND ACRONYMS

Ac-	Acetyl
ACN	Acetonitrile
AIDS	Acquired immune deficiency syndrome
All-	Allyl
AuGNP	Gold glyconanoparticle
AuNP	Gold nanoparticle
BBB	Blood brain barrier
Bn-	Benzyl
BSA	Bovine serum albumin
CA	Contrast agent
Cbz-	Benzyloxycarbonyl
ConA	Concanavalin A
COVID-19	Coronavirus disease 2019
CSA	Camphorsulfonic acid
CT	Computed tomography
CTAB	Cetyltrimethylammonium bromide
Da	Dalton
DBAD	Di-tert-butyl azodicarboxylate
DBU	1,8-Diazabicyclo(5.4.0)undec-7-ene
DCM	Dichloromethane
DCS	Differential centrifugal sedimentation
DFM	Dark field microscopy
DIAD	Diisopropyl azodicarboxylate
DIPEA	N,N-Diisopropylethylamine
DLS	Dynamic light scattering
DMAP	4-Dimethylaminopyridine
DMF	N,N-Dimethylformamide
DTT	Dithiothreitol
DNA	Deoxyribonucleic acid
EDC	1-Ethyl-3-(3-dimethylaminopropyl)carbodiimide
EMA	European medicines agency
EPR	Enhanced permeability and retention
ESI	Electrospray ionization
ESR	Early-stage researcher
ETN	European training network
EtOAc	Ethyl acetate
FBS	Fetal bovine serum
FCS	Fluorescence correlation spectroscopy
FCCS	Fluorescence cross correlation spectroscopy
FDA	Food and drug administration

GlcN	Glucosamine
Hex	Hexane
HIV	Human immunodeficiency virus
HMBC	Heteronuclear multiple bond correlation
HMDS	Hexamethyldisilazane
HPMA	*N*-(2-Hydroxypropyl)methacrylamide
HPTLC	High performance thin layer chromatography
HSQC	Heteronuclear single quantum coherence spectroscopy
Ig	Immonuglobulin
IR	Infrared
ISBT	International Society of Blood Transfusion
LbL	Layer-by-layer
LecA	Lectin A
LSPR	Localized surface plasmon resonance
MBL	Mannose binding lectin
mCPBA	*m*-Chloroperbenzoic acid
Me-	Methyl
MeOH	Methanol
M6P	Mannose-6-phosphate
MGPR	Mannose-6-phosphate receptor
M6S	Mannose-6-sulfate
miRNA	micro Ribonucleic acid
MR	Mannose receptor
MRI	Magnetic resonance imaging
MS	Mass spectrometry
MSA	Mercaptosuccinic acid
MW	Molecular weight
Neu	Neuraminic acid
Neu5Ac	*N*-Acetyl neuraminic acid
NIH	National Institutes of Health
NIS	*N*-Iodo succinimide
NM	Nanomaterial
NMR	Nuclear magnetic resonance
NP	Nanoparticle
NR	Nanorod
OCT	Optical coherence tomography
PA	Photoacustic imaging
PC	Protein corona
PDT	Photodynamic therapy
PEG	Polyethylene glycol
PET	Positron emission tomography
Ph-	Phenyl

PFP	Pentafluorophenol
PMB-	*p*-Methoxybenzyl
PS	Photosensitizer
PTT	Photothermal therapy
PVP	Polyvinylpyrrolidone
RAFT	Reversible addition fragmentation chain transfer
RBC	Red blood cell
RCSI	Royal College of Surgeons in Ireland
Rh	Rhesus
RNA	Ribonucleic acid
ROS	Reactive Oxygen Species
RPTLC	Reverse phase thin layer chromatography
RT	Room temperature
SARS-Cov-2	Severe acute respiratory syndrome coronavirus 2
SERS	Surface enhanced Raman spectroscopy
SNA-II	*Sambucus nigra* agglutinin II
Siglec	Sialic acid-binding immunoglobulin lectin
siRNA	Small interfering Ribonucleic acid
SPION	Superparamagnetic iron oxide nanoparticles
Sulfo-NHS	*N*-hydroxysulfosuccinimide
sym-Collidine	2,4,6-Trimethylpyridine
TACA	Tumor associated carbohydrate antigen
TBAB	Tetrabutylammonium bromide
TBAF	Tetrabutylammonium fluoride
TBAI	Tetrabutylammonium iodide
TBDMS-	*tert*-Butyldimethylsilyl
TEM	Transmission electron microscopy
TEA	Triethylamine
TF	Thomsen Friedenreich antigen
TfOH	Trifluoromethanesulfonic acid
THF	Tetrahydrofuran
TLC	Thin layer chromatography
TMS-	Trimethylsilyl
TMSOTf	Trimethylsilyl trifluoromethanesulfonate
Tn	Thomsen Nouveau antigen
TNFα	Tumor necrosis factor alpha
TOAB	Tetraoctylammonium bromide
UEA-I	*Ulex europaeus* agglutinin I
XEPA	*N,N*-Diethyl-1,5-dihydro-2,3,4-benzodioxaphosphepin-3-amine

INTRODUCTION

1. Nanotechnology

It all started with the famous lecture imparted by the physicist R. P. Feynman in 1959: "There is plenty of room at the bottom: an invitation to enter a new field of physics" in which he discussed the possibility of direct manipulation of individual atoms or molecules for the fabrication of macroscale products[1]. Although versions of the talk were published in a few popular magazines, it went largely unnoticed and did not inspire the conceptual beginnings of nanotechnology until the early 1980s when the development of the scanning tunneling microscope allowed to "see" individual atoms.

Nanotechnology is nowadays an emerging field of science devoted to the manipulation of matter in the nanoscale[2]. The fundamental component of nanotechnology are nanomaterials (NMs), which may be defined as an assembly of atoms, molecules, or ions with at least one of their three dimensions theoretically between one and a few hundred nanometers, according to the definition coined by the European Commission (EC)[3]. A NM can be considered a nanoparticle (NP) if all its three dimensions are similar in size.

When reduced to the nanoscale, materials present unusual or peculiar chemical and physical properties that differ from the properties of bulk materials or macroscopic systems. Furthermore, as a consequence of the quantum effect, these properties are size-dependent. The discovery of this unprecedented phenomenon conferred new purpose to already existing materials.

1.1. Nanotechnologies in nanomedicine

Over millennia, nature has perfected the art of biology at the nanoscale. Hemoglobin, the protein that carries oxygen through the body, is 5.5 nm in diameter. A strand of DNA, one of the building blocks of life, is about 2 nm in diameter. The smallest cellular life forms, the bacteria of the genus *Mycoplasma*, are around 200 nm in length. By sharing the same dimension range, nanomaterials have demonstrated a fine interaction with biological processes (Figure 1). The application of nanotechnology for prevention, treatment, diagnosis and/or monitoring of diseases has recently been referred to as "nanomedicine" by the National Institutes of Health (NIH).

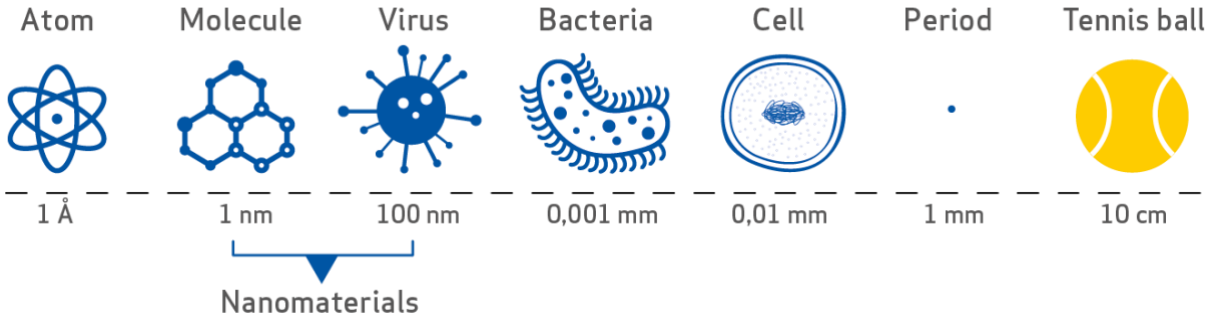

Figure 1. From atoms to macromaterials. Size comparison[4]

Given their unique and tunable properties, NMs are being explored as novel drug delivery systems able to overcome the limitations of conventional medical treatments[5]. On the one hand, their size allows them to mediate molecular interactions and cross biological barriers. Some NMs have also proven to

ameliorate the water solubility of poorly soluble drugs, protect them from degradation and facilitate a controlled release, reducing side effects and increasing patient's compliance. On the other hand, NMs can be coated with bioactive molecules and/or with imaging probes allowing accumulation in target tissues and/or monitoring of the drug distribution respectively. The combination of diagnostic and therapeutic capabilities into a single agent is nowadays labelled with the term "theranostics" and is paving the way towards the development of personalized medicines.

However, like for any breakthrough discovery, the promising possibilities that nanomedicine offers have to be counterweighted against the risks. Robust and precise characterization of the interactions between nanoengineered materials and biosystems is vital for the development of safe and efficient nanomedicines and this emerging area of research is known as nanotoxicology.

1.1.1. Nanomaterials classification

NMs can be broadly divided into various categories based on their composition, size and morphology. According to their composition they can be divided in organic, inorganic and carbon-based. Organic NMs can be made of dendrimers, lipids, polymers and ferritin, or hollow spheres, such as liposomes for slow and controlled release of the cargo. Metal and metal oxide based NMs are generally categorized as inorganic and they include silver, gold, iron, copper, aluminum, cadmium, cobalt, zinc, titanium oxide, iron oxide, silicon dioxide, cerium oxide and zinc oxide amongst others. The carbon-based NMs are made entirely of carbon, and they can be classified into fullerenes, graphene, nanotubes, nanofibers and carbon black[6,7].

The size and size distribution of NMs dictate their biological fate, toxicity and targeting ability[5]. Generally, NPs with diameters below 100 nm are preferred for drug delivery purposes since they are more efficient in permeating biological barriers, present improved solubility, bioavailability and circulation times. However, smaller particles present a larger surface area, which translates into a greater risk of aggregation and hence, it becomes a challenge to formulate NMs with the smallest size but maximum stability. Finally, NMs come in a variety of shapes that can be classified based on the number of dimensions outside the nanoscale (1 to 100 nm). Accordingly, in *zero-dimensional* (0D) NMs all the dimensions are below 100 nm: the prime example are spherical nanoparticles, but also nanocubes, fullerenes or quantum dots can be included in this category. *One-dimensional* (1D), include NMs with one dimension outside the nanoscale, e.g. nanorods, nanotubes, and nanowires. In *two-dimensional* (2D) NMs, two dimensions are above 100 nm: this class exhibits plate-like shapes such as graphene, nanodiscs, nanofilms or nanolayers. Whereas *three-dimensional* (3D) NMs are not confined to the nanoscale in any dimension. Morphology can have a significant impact in the drug loading, transport capabilities and optical properties of the NMs.

1.1.2. Nanomaterials in the clinic

Despite the significant potential of nanomedicine for the treatment of many pathologies, we are still in the early stages of its clinical development. As of today, there are some nanotechnology-based diagnostics and therapeutic agents already on the market, many more are under clinical trials and by far the largest part, are still under development[6,8–10]. Most nanoformulations in clinical use are based on liposomal or polymeric platforms. However, colloidal elemental particles, such as gold or metal oxides are also gaining interest.

Liposomal anticancer drugs such as doxorubicin (Doxil), daunorubicin and cytarabine (Vyxeos) have been FDA approved and over 50 liposomal chemotherapeutics are undergoing clinical trials in the US alone. These liposomal formulations present long circulating times and controlled drug release. Liposomal vaccines, also known as virosomes, have also been approved, e.g. an influenza vaccine (Inflexal V) and a hepatitis A vaccine (Epaxal) which encapsulate key viral proteins that can generate an immune response. These formulations contain low levels of ovalbumin and are thus less allergenic than traditional vaccines. Liposomes are being also used as a vector to administer anesthetics like morphine and antibiotics like amphotericin with reduced toxicity. Abraxane is a marketed albumin-bound nanoformulation of paclitaxel, used to treat a number of cancers, improving the poor water solubility of the drug itself. VivaGel is a dendrimeric mucoadhesive gel, delivered vaginally to relieve the symptoms of bacterial vaginosis and reduce the risk of recurrence.

Superparamagnetic iron oxide nanoparticles (SPIONs) are being extensively studied as Magnetic Resonance Imaging (MRI) contrast agents (CA). Sienna+ is a dextran-coated SPION approved by the European Commission in 2011, whereas Ferumoxytol is a SPION coated with polyglucose sorbitol carboxymethyl ether used for anemia treatment in patients with chronic kidney disease. Gold NPs (Au NPs) functionalized with tumor necrosis factor alpha (TNFα) have shown to improve tumor cell killing effect while reducing side effects. The drug, marketed as Aurimune, has undergone human clinical trials in combination with chemotherapy.

Undoubtedly, the most recent and greatest milestone in the nanomedicine field is the use of lipid nanoparticles entrapping a strand of mRNA. This nanotechnology has proven to be a fast and efficient approach to develop a safe vaccine against severe acute respiratory syndrome coronavirus (SARS-CoV-2), the virus responsible of the COVID-19 disease and global pandemic in 2019. The lipid nanoformulation entraps a strand of mRNA encoding for the spike glycoprotein of SARS-CoV-2. By decoding this mRNA sequence cells can develop an immune response against the virus. This nanotechnology has proven to be safe, fast and efficient in the vaccines distributed by Pfizer/BioNTech and Moderna in 2020[10,11].

2. Gold: a precious metal for nanomedicine

Gold is a transition metal represented by the symbol **Au**, from Latin: *aurum*, and atomic number 79. In its bulk form it is a dense, soft, malleable and ductile metal with a characteristic bright yellow hue known as golden color. This noble metal is one of the least reactive chemical elements, nevertheless it presents peculiar properties at the nano-metric scale attractive for biomedical applications.

Au NMs can be readily prepared with well controlled sizes, geometries and surface properties. Established methods for the synthesis of Au colloids will be discussed in the next section. Despite the metal inertness, Au NMs react with sulfur-containing compounds, such as thiols or disulfides, forming effectively covalent bonds or with nitrogen-based compounds like amines or pyridines[12,13], being this interaction more electrostatic in nature. A comprehensive study of the not-so-straightforward nature of these interactions has been reported by Reimers et al.[14] Thus, Au NMs can be easily and robustly functionalized with bioactive molecules and/or drugs exploiting this unusual chemistry, in order to create multifunctional platforms with enhanced therapeutic benefits and low toxicity. The excellent *in vivo* biocompatibility of Au NMs, when used in low concentrations, has been associated to the inertness of the metal[15,16].

Given its high atomic number and density, gold presents excellent X-ray absorption coefficient in comparison to human tissues, hence Au NMs are emerging as ideal biocompatible contrast agents in X-ray computed tomography imaging. Another exclusive optical characteristic of Au NMs is the Localized Surface Plasmon Resonance (LSPR) effect, due to the oscillation of free electrons on the conductive metal surface. LSPR is sensitive to changes in the NMs local environment such as size, morphology and solvent dielectric constant and it is the main responsible of the characteristic colors associated with Au colloids. Moreover, LSPR leads to a unique optical phenomenon in which light is scattered or absorbed when the metal is irradiated with light of a specific wavelength that matches the plasmon oscillation cycle. Unlike most metallic NMs that absorb light in the UV region, spherical Au NPs absorb visible light and anisotropic Au NMs absorb light in the near infrared region, where biological tissues exhibit the highest optical transparency, increasing their imaging and therapeutic possibilities.

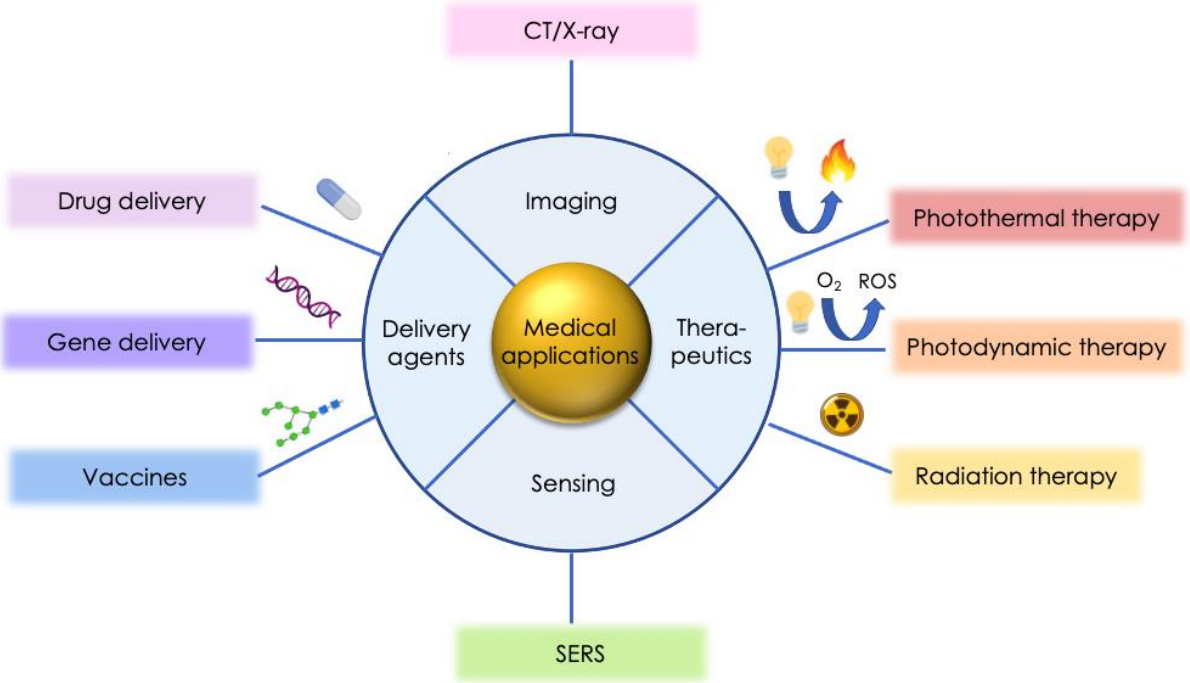

Figure 2. Medical applications of Au NMs

Given their versatile and tailorable optical properties and their peculiar physicochemical characteristics, Au NPs can be exploited in a wide range of medical applications summarized in Figure 2 and explained more in detail in the section below.

2.1. Au NPs as therapeutic agents

Au NP can be delivered into specific cells through either passive or active targeting. Passive targeting is based on the enhanced permeability and retention (EPR) effect, where the Au NPs accumulate within tumors through their irregular and leaky vasculature. In the case of active targeting, NPs are conjugated with a bioactive molecule that binds to a specific receptor in the target cells. Thanks to this controlled accumulation and their intrinsic optical properties, Au NPs can be exploited as therapeutic agents in some unconventional cancer treatments such as photothermal therapy, photodynamic therapy and radiotherapy.

2.1.1. Photothermal therapy (PTT)

An important step forward in the fight against cancer is the so-called photothermal therapy (PTT). This emerging treatment is based on the ability of certain nanomaterials to convert absorbed light into heat. The generated heat is confined around the NMs, enabling localized tumoral cell killing. The additional focusing of the external light source, allows better control to eradicate cancer cells without compromising healthy tissues[16].

Au NMs represent optimal candidates for PTT since they present enhanced tumor avidity, an excellent light to heat conversion strengthened by the LSPR phenomenon and they can be coated with additional anti-cancer drugs for synergic treatments. Au nanorods (Au NRs) have been actively studied as PTT tools since they absorb light in the near IR (NIR) region[17–20], allowing deeper penetration of tissues than light of other wavelengths. Au NPs[21,22], Au nanoshells[23,24] and Au nanocages[25] have also been investigated as PTT agents for chemotherapy resistant tumors or to prevent tumor recurrence after surgery.

2.1.2. Photodynamic therapy (PDT)

Photodynamic therapy (PDT) is another incipient cancer treatment that, unlike PTT, uses a photosensitizer (PS) that upon excitation by light of specific wavelengths, converts oxygen from tissues into reactive oxygen species (ROS) that lead to cell death by apoptosis. Au NPs functionalized with PS can improve PDT efficiency by enhancing reactive oxygen species (ROS) formation thanks to the LSPR effect[26]. Au NPs incorporating a PS can be used for dual PTT/PDT therapy as proved by Kuo and co-workers who used Au NPs and Au NRs simultaneously for PTT/PDT and as contrast agents. The results showed enhanced destruction of cancer cells as compared with PTT and PDT alone[27]. Wang et al. adapted the LSPR wavelength of Au nanostars to fit that of the PS, to induce both PDT and PTT upon a single NIR laser irradiation, greatly simplifying the treatment process[28].

2.1.3. Radiotherapy

Au NPs can also be exploited as potential radiosensitizers in radiotherapy treatments. Given gold's high density and atomic number, Au NPs present a large interaction cross section with γ-rays, X-rays, and with ion radiation, and thus, increase the production of free radicals that lead to cancer cells damage[29,30]. Although the radiosensitizing potential of Au NPs has been tested in brain, breast and colon tumors amongst others, its translation into clinics still faces many challenges that have been detailed elsewhere[31].

2.2. Au NPs as delivery agents

Au NMs have also come to the fore as promising vehicles for drug, gene or antigen delivery. These therapeutic agents can be loaded onto Au NPs exploiting the Au-S and Au-N chemistry, by electrostatic interactions or covalently grafted to a polymer attached to the Au surface. Generally, the attachment to Au nanosystems improves the payload pharmacokinetics and pharmacodynamics. For example, the solubility and permeability of small drug molecules is ameliorated, the enzymatic degradation of nucleic acids is prevented, and the immunogenicity of antigens is boosted.

2.2.1. Drug delivery

Chemotherapeutic agents are often toxic and poorly soluble and colloidal gold represents an alternative for their safer distribution. Astra Zeneca in partnership with Cytimmune is preparing polyethylene glycol (PEG) stabilized Au NPs functionalized with the protein TNFα, named Aurimune (CYT-6091). This nanoformulation can efficiently deliver TNFα to tumor sites and is the first Au NP-based formulation to enter human clinical trials for the treatment of solid tumors in combination with chemotherapy[32]. An analog of CYT-6091 including paclitaxel derivatives is also under development[33]. Other examples of anticancer drugs loaded onto Au NPs are doxorubicin[34] and methotrexate[35]. Additionally, these nanosystems can be used in synergistic combination with PTT and radiotherapy for the treatment of persistent cancers.

Antibiotics have also been electrostatically bound[36] or chemically grafted[37,38] to Au NPs showing greater stability and higher inhibition of bacterial growth than their free counterparts.

2.2.2. Gene delivery

The use of nucleic acids to treat and control diseases is termed 'gene therapy'. In comparison to viral vectors, Au NPs represent attractive candidates for DNA and RNA delivery given the reduced cytotoxicity and immunogenicity. While in comparison to other non-viral vectors such as liposomes, dendrimers or polymers, Au NPs allow targeted deliver and simultaneous *in vivo* tracking/monitoring of the biodistribution[39]. Furthermore, nucleic acids can be covalently or electrostatically attached to AuNPs without altering or inhibiting their biological activity.

Mirkin *et al.* synthesized Au NPs covalently linked with a dense monolayer of thiol-modified polyvalent nucleic acids (pNA–Au NPs) and proved the stability against nucleases[40]. They functionalized these platforms with siRNA for gene silencing[41] *and* miRNA for tumor suppression[42]. More recently, the same group added a monoclonal antibody to the pNA–AuNPs conjugates providing better selectivity and gene knockdown in cells that overexpress the target antigen[43]. Similar pNA-AuNPs can be used to transdermally deliver siRNA in an effective manner without clinical nor histological evidence of toxicity in treated skin[44]. The negative charge of nucleic acids makes cationic AuNPs obvious partners for self-assembly. In early studies, Rotello *et al.* created effective delivery vehicles for plasmid DNA using ammonium–functionalized Au NPs[45]. In a similar manner, Au colloids functionalized with dendritic cationic amino acids provide a scaffold for effective DNA and siRNA in *in vitro* delivery[46,47] whereas layer-by-layer (LbL) deposition of positive polyelectrolytes and negative siRNA on top of Au NPs provided an efficient strategy for the controlled release of nucleic acids[48,49].

2.2.3. Vaccines

Thanks to gold immunomodulating properties, Au nanocarriers have raised attention as vaccine platforms with potential advantages over traditional vaccines. Gold acts simultaneously as carrier and adjuvant, displaying several copies of an antigen directly to macrophages, dendritic cells or other immune cells, enhancing immunogenicity while reducing systemic toxicity. For a more extensive review about the use of Au NMs coated with protein and carbohydrate antigens against viral, parasitic or bacterial infections, as well as for the development of therapeutic vaccines against cancer or autoimmune disorders we refer the reader to a recent review published by Mateu et al[50].

2.3. Au NPs in imaging and sensing

Optical microscopic techniques represent essential tools for early detection and prognosis of a disease, but they still suffer from drawbacks associated to resolution, sensitivity, speed, and penetration depth. Au NPs with their strong X-ray absorption coefficient, represent an interesting alternative to current contrast agents. Moreover, exploiting their inherent LSPR effect they can increase the sensitivity of conventional optical sensitizers, acting as innovative sensors for the detection of biological relevant molecules or processes.

2.3.1. Computed tomography (CT)

Computed tomography is a standard imaging modality routinely used in clinics owing to its fast operation time, low cost and high temporal and spatial resolution. CT is a non-invasive technique that measures the X-ray transmission through the body, and the tissue-dependent attenuation rate that can be reconstructed as a 3D image. Imaging soft tissues can be challenging unless a contrast agent is used, nowadays the most diffused CT contrast agents are iodinated compounds which tend to have fast renal clearance and renal toxicity. Au NPs exhibit larger X-ray attenuation, longer circulation times and specific accumulation[51]. In 2006, Smilowitz and coworkers, used for the first time citrated stabilized Au NPs as *in vivo* CT contrast agents with encouraging results[52]. Following this paper, numerous studies have investigated the possibility of using Au NPs as CT contrast agents, active targeting ligands such as antibodies, folic acid or glucose have been grafted to the surface of Au NPs to improve their accumulation and tumor targeting specificity[53–55]. Regardless of their advantages, the long retention time in the body of Au NMs limits their practical applications as contrast agents. Ultrasmall Au nanoclusters often display good tumor contrast and better renal clearance[56,57].

2.3.2. Positron emission tomography (PET)

Nuclear imaging techniques, such as positron emission tomography (PET), have a much higher sensitivity and accuracy compared to CT imaging, but they require the presence of radioactive substances to emit radiation and external detectors to capture the radiation emission. Application of radionuclide embedded Au NPs in nuclear imaging is also a very attractive possibility. Zheng and co-workers were the first who doped ^{198}Au into glutathione protected gold nanoclusters to achieve a performance similar to clinical available radionuclides and faster renal clearance[58]. Alternatively, PET-active radionuclides have been incorporated to Au NPs by functionalization of the gold surface with suitable thiol-ended chelating agents , as it is the case of ^{68}Ga [59].

2.3.3. Fluorescence imaging

Fluorescence imaging relies on the sequential irradiation and delayed photon emission from the sample. Its high sensitivity, resolution and low cost render this technique popular for the semi-quantitative analysis, although its depth penetration is limited. Au NPs reduced to the subnanometer scale (0.5 to 1 nm), known as gold nanoclusters, exhibit photoluminescent properties and present enhanced photostability and biocompatibility in comparison to fluorescent dyes and quantum dots[60]. Yang et al. have synthesized α-lactalbumin stabilized ultrasmall Au NPs with good *in vivo* fluorescence imaging of human breast cancer cells[61]. Pyo et al. found that functionalization with folate ligands boosted the fluorescence quantum yield of Au nanoclusters by energy transfer[62].

2.3.4. Surface enhanced Raman spectroscopy (SERS) for imaging and sensing

Raman signals are molecule specific and thus constitute a "fingerprint" that can be exploited for its detection. The main drawback of this technique are the long exposure times required to register a single spectrum. Thanks to the LSPR effect, Au NPs can amplify the Raman signal of the molecules close to them, enhancing the sensitivity and reducing the exposure time. This SERS enhancement is generally applied in sensing of bioactive molecules such as proteins, nucleic acids or small molecules[63–65]. When a molecule with a well-known Raman pattern is directly attached to the gold core, SERS can be implemented for more conventional imaging purposes such as the detection of tumors or to follow drug distribution[66–68]. More detailed reviews on the topic can be found[69,70].

More recently, Au NP probes have also been designed to access molecular imaging using other modalities such as Magnetic Resonance Imaging (MRI), dark field microscopy (DFM), optical coherence tomography (OCT), photoacoustic imaging (PAI) and so forth, although those modalities remain comparatively underexplored.

Despite Au NPs increasing number of applications, their greatest potential resides in the possibility to exploit some of their properties simultaneously e.g., they can deliver drugs and monitor their distribution using CT imaging or transport chemotherapeutic agents and enhance their action by PTT or radiotherapy. However, some drawbacks associated with their use will be discussed in section 2.5.

2.4. Synthesis of Au NPs

As many other NMs, Au NPs can be prepared by either "top down" or "bottom up" approaches (Figure 3). In the "top down" strategy, bulk gold is systematically broken down to generate nanoparticles of desired dimensions using mechanical methods such as milling, laser ablation, electron beam lithography or ion sputtering. In spite of the easy large-scale production, "top down" methods are limited concerning the control of the size, shape and surface functionalization and find reduced applicability in nanomedicine.

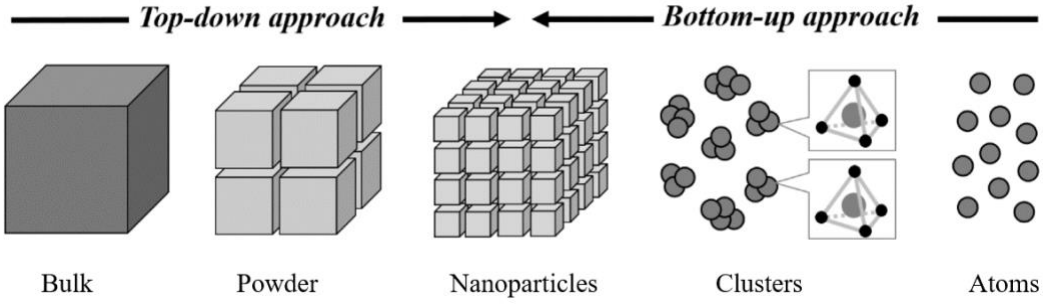

Figure 3. Schematic representation of the "top-down" and "bottom-up" approaches

In contrast, in the "bottom up" approach, Au NPs are generated by assembling individual atoms generated via reduction of precursor ions. The most classical approach involves the reduction of Au (III) salts in solution in the presence of reducing and stabilizing agents to form gold colloids. These colloidal nanoparticles tend to aggregate, thus the role of the stabilizing agents is to prevent aggregation via electrostatic or steric repulsion. This stabilizing agent can then be replaced or attached to biologically relevant molecules, such as drugs or targeting scaffolds, in order to obtain Au NPs suitable for biomedical purposes. In the next section, the most common "bottom up" strategies and their modifications for the preparation of Au colloids will be discussed.

2.4.1. Turkevich synthesis

In 1951 J. Turkevich et al. developed the most popular strategy for the preparation of Au NPs, and consequently, the recommended by the National Institute of Standards and Technology (NIST) for reference material preparation[71]. The method adds trisodium citrate (Na_3Ct) into a refluxing solution of tetrachloroauric acid ($HAuCl_4$) in water. The citrate ions act both as reducing and stabilizing agent preventing uncontrolled growth and aggregation and they can be easily replaced post-synthesis by other ligands, in favor of the NPs functionalization. In spite of the fairly simple experimental procedure, much research has been carried out on the topic with the aim to understand and optimize the synthesis conditions, however there are still diverse hypotheses[72–74]. It is commonly believed that the synthesis is divided into nucleation and growth stages. In the early instants of the reaction a partial reduction of the gold precursor leads to the formation of small clusters or seeds. During the growing stage, the residual metal precursor is reduced on the surface of the preformed seeds inducing their growth until the gold is fully consumed[75].

The Turkevich method offers the possibility to obtain electrostatically stabilized Au colloids with diameters between 10 and 50 nm. The non-toxic citrate ions can be easily replaced by thiolated molecules. An important limitation of this protocol is the modest control of the particle size, due to the many factors that can influence the growth step.

In 1973, Frens et al. further refined this method by changing the gold-to-citrate ratio[76]. High concentration of citrate allows to rapidly cap the nanoparticles by stopping their growth at dimensions comprised between 10 and 20 nm. Instead, a low concentration is reflected in an incomplete capping of the NP surface, leading to their aggregation and the formation of bigger and irregular NPs[77]. While the Na_3Ct to $HAuCl_4$ molar ratio has shown to have a great effect on the particle size, temperatures ranging from 50 to 100 °C only play subtle roles[78]. The size of NPs formally increases with reaction time[79]. By adding $HAuCl_4$ to a warm solution of Na_3Ct, Ojea-Jimenez and co-workers revealed how inverting the order of addition of the reagents substantially reduces the inhomogeneous mixing, improving the size distribution[80]. The pH of the reaction medium is also a fundamental parameter affecting the particle size and the size distribution. The smallest and most monodisperse Au NPs of about 10 nm are produced while the pH of the solution is kept between 5.4 and 6.8. Below pH 4 or above pH 7.5 both the size and size distribution dramatically increase[72]. On this basis, nearly monodispersed Au NPs with sizes ranging from 10 to 40 nm have been synthesized upon variation of the solution pH[79,81,82]. To minimize the citrate buffer effect, Xia et al. modified the Frens procedure, by adding a pre-mixed solution of citrate and tetrachloroauric acid to boiling water to maintain the pH stable throughout the growing step. They also used traces of $AgNO_3$ to suppress the secondary nucleation and reshape the polycrystallinity in an almost-spherical shape[83].

Noteworthy, a control over the core morphology can be implemented by adding surfactants or templating agents, for example, the presence of cetyl trimethylammonium bromide (CTAB) and $AgNO_3$ favors the elongation of the gold crystals to form Au nanorods[84] and L-tyrosine leads to the formation of gold nanoflowers[85]. Murphy and co-workers presented an interesting seed-mediated route to multiple-shaped Au NPs by systematic variation of the synthetic parameters such as the CTAB, $HAuCl_4$, ascorbic acid and $AgNO_3$ quantities[86]. In a similar manner, Silvestri et al. prepared star shaped, anisotropic and symmetric NPs in a one-pot protocol by accurate modulation of the reagent's ratio[54]. Although a large variety of geometries have been produced, there is still much room for improvement before rational nanoparticle design is achieved.

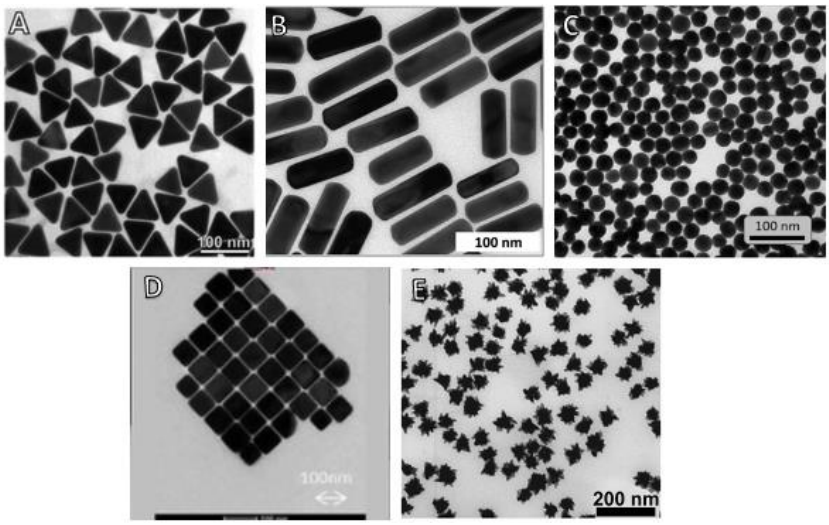

Figure 4. Transmission Electron Microscopy (TEM) of A)Au nanotriangles B) Au nanorods C) Au nanoparticles D) Au nanocubes E) Au nanostars

2.4.2. Brust-Schiffrin synthesis

A second method for the production of gold colloids was ideated in 1994 by M. Brust and D. J. Schiffrin[87]. The protocol takes place in a two-phase aquatic-organic environment in which $HAuCl_4$ acts as gold precursor, sodium borohydride ($NaBH_4$) as a strong reducing agent and the produced nanoparticles are directly passivated by means of aliphatic thiols. Initially, Au (III) ions are transferred from the water phase to the organic phase, with the aid of a phase transfer reagent such as tetraoctylammonium bromide (TOAB). Then, a specific amount of thiol (RSH) is added, which reduces Au(III) to Au(I)-SR. Finally, the reduction of Au(I)-SR with $NaBH_4$ leads to the formation of Au nanoparticles. This methodology produces low dispersity Au NPs with sizes ranging from 2 to 8 nm. Since the sulfur-containing agents inhibit the growth process, larger thiol-to-gold molar ratios give smaller average core sizes. Fast $NaBH_4$ addition and cooled solutions also produce smaller, more monodispersed Au NPs[79]. Another highly reproducible phase-transfer method was described by Martin and coworkers[88]. They used $NaBH_4$ as reducing agent and NaOH and HCl as stabilizers to obtain a narrow distribution between 3 and 5 nm. A significant improvement is the abandonment of the biphasic system in favour of a single monophasic system, in which both the gold precursor and the thioalkane are soluble (e.g., methanol) to avoid the use of toxic TOAB[89]. Less reports on morphology variations using the Brust-Shiffrin approach have been published[90].

The Brust-Schiffrin method allows the synthesis of small and very stable nanoparticles with better size control. Unlike the Turkevich method, where the NPs obtained are post-functionalized with the desired ligands by citrate replacement, Brust-Schiffrin allows direct functionalization with thiolated ligands during the so-called passivation step. Both procedures are widely diffused since they allow large scale preparation in relatively easy conditions and without particular or expensive instrumentation. Apart from Na_3Ct and $NaBH_4$, ascorbic acid[91], hydroquinone[92], hydroxylamine[82] or other biomolecules have been used as reducing agents in the Turkevich protocol.

2.4.3. Green synthesis: a novel approach

Recent efforts have been directed towards a greener approach for the synthesis of Au NPs as an eco-friendly and cost-effective alternative to harsh and expensive chemicals used in the syntheses described above. A plethora of biomolecules and organisms have been tested for their potential to operate as

reducing agents and stabilizers during the synthesis, ranging from plant and plant extracts[93,94] to bacteria[95,96], algae[97,98], and fungi[99]. Bhaskaran et al.[100] interestingly showed how Au NPs can be shaped according to the pH of the natural extract. These green alternatives may reduce the toxicity concerns associated with traditionally prepared Au NPs, but their greatest hurdles are the recovery of the nanoparticles from the reaction mixture after the synthesis, the long reaction times and the difficulties to scale-up. An encouraging thought is that given the wide range of species present in the marine, plant and bacterial realm, new materials and conditions for the synthesis of unprecedented Au NMs have yet to be discovered.

2.5. Au NPs concerns

Despite the medical potential of Au NMs, their translation from laboratory to clinics is proceeding at a pace significantly lower than expected. Only a few Au NPs have entered clinical trials, and none have reached clinical practice. The main concerns are related to their biodistribution and circulation times in the blood stream, their long- and short-term toxicities and their clearance rate. Although most of these safety issues have been addressed in several studies, the results seem inconclusive. Comparison between outcomes obtained from different research groups using diverse experimental conditions is not a simple task. Since many research groups began their projects independently, there is a great scatter in experimental design, including synthesis method, size, shape and surface functionalization, *in vivo* animal models, doses or method of administration and *in vitro* tissues or cells lines. This section does not aim to provide an exhaustive coverage of all published work regarding Au NMs concerns, it only seeks to integrate the most relevant data available in literature to give a better understanding of factors that may contribute to the safety of Au NPs.

2.5.1. Toxicity

Extensive and comprehensive reviews have been published in the field of nanotoxicology[101–103]. Most evaluations are conducted using *in vitro* cell models that cannot fully approximate the complexity of living organisms. Although the majority of studies have shown negligible toxicity to cells[98,99], there are also studies that present conflicting results[106–108]. The *in vivo* results are scarcer and also controversial, but in general, Au NPs are biocompatible on exposure to low doses (< 0.5 mg/kg daily) during short periods of time (approximately a weeklong)[15,101].

The lower size toxicity boundary is associated with Au colloids of 1 to 2 nm in diameter and is determined by their high surface area, increasing their ability to irreversibly bind to key biomolecules such as DNA and to produce undesired reactive oxygen species[103,109]. Additionally, they show considerable accumulation in filtering organs with the kinetics of their elimination being really slow. Citrate-coated Au NPs up to 100 nm do not evidence noticeable toxicity in low concentrations[101]. Regarding the morphology, different capping molecules are used to shape Au NPs and therefore, comparing the results of different studies is complicated[102]. Bhamidipati et al. noted that morphology and size only affected cell viability, but the CTAB used for the synthesis contributed to cell toxicity[110]. Wang and co-workers prepared rod-, cage- and hexapod-like Au NPs and the latter exhibited the lowest cytotoxicity and the highest cellular uptake *in vitro*[111]. Goodman et al. investigated the toxicity of anionic and cationic 2 nm NPs. Cationic NPs functionalized with quaternary amines proved to be seven-fold more toxic than their anionic counterparts coated with carboxylic acids[112]. A plausible explanation to these results is that the positive groups interact with the negative cell surface leading to its disruption.

Given the scatter in experimental conditions, comparison of countless toxicity studies becomes an arduous task. Hence, sequential modification of a single NMs' variable at a time becomes crucial in order to gain a clearer understanding of the effect of each parameter on biological activity and to help researchers evaluate and compare results. Carnovale et al., for the first time, provided an interesting systematic study on the influence of Au NPs size, shape, and surface coating on cellular uptake and toxicity while attempting to keep the other variables constant[113]. When considering the shape: Au nanorods and nanocubes are more biocompatible than nanospheres (NS) and Au nanoprisms (NPr), although NS and NPr as also well tolerated. The higher toxicity of NS may be due to their higher cellular uptake. Regarding the size, smaller particles evidenced increased uptake by number, but not necessarily by total gold. They also found that surface coating elicited remarkably different cellular uptakes and cytotoxic responses. Overall, increased uptake levels were observed for Au NS stabilized with tryptophan and tyrosine amino acids compared to those stabilized with citrate and CTAB/citrate. Additionally, their work did not find a direct correlation between the nanoparticle surface charge and their cellular uptake.

Keeping in mind countless reports on *in vitro* toxicity, it would be important to translate these results to *in vivo* conditions. Nevertheless, before safely moving into clinical trials, more systematic studies in the line of the one presented by Carnovale et al. are of paramount importance, as well as more defined guidelines and standards from regulatory bodies such as the FDA or the EMA.

2.5.2. Biodistribution

As for toxicity results, the scatter of experimental data makes difficult the comparison between biodistribution studies. However, unlike toxicity studies, biodistribution and circulation time essays are more limited since they need to be performed *in vivo*.

The nanoformulation size has a significant influence on the *in vivo* biodistribution, circulation time and clearance. NPs between 5 and 10 nm are within renal glomerular filtration range and hence, quickly removed by the kidneys. While NPs above 100 nm are quickly recognized by the immune system, mainly taken up by phagocytes and accumulated in the liver and spleen for long periods of time[108-110]. As a result, particles with sizes between 10 and 100 nm should present enough circulation time to reach the target organs without causing long term toxicity in the liver and spleen. In this size range, the fate of NPs is likely to be influenced by a range of factors, including shape and surface chemistry.

Two early studies performed independently by De Jong et al. and Sonavave et al., proved that the tissue distribution of Au NPs is size dependent with 10 nm and 15 nm possessing the most widespread organ distribution including blood, liver, lung, spleen, kidney, brain, heart, stomach, etc. after intravenous administration. On the other hand, larger particles (from 50 to 250 nm) were only significantly deposited in the liver, spleen and blood. Regarding the blood brain barrier (BBB) penetration, the results present some discrepancies, while 50 nm NPs were identified in the mouse brain[117], they were not present in the rat brain[118]. The delivery of NPs into the brain is particularly worthy of attention since central nervous system diseases impose a heavy burden on society. The cells in the blood-brain barrier have low endocytic activity, preventing the vast majority of drugs to reach the brain, and thus, the upper penetration limit of NPs through the BBB is commonly established at about 15 nm[115,119].

Arnida et al. compared the *in vivo* fate of Au NPs (50 nm) and NRs (10 x 45 nm) in mice and the result showed that after 6 h, the concentration of NPs in blood was less than 1% and they mostly accumulated in the liver, while 11 % of the NRs remained in blood. In addition, the accumulation of NRs in tumor

tissues was significantly higher than that of nanospheres[120]. A more recent study by Zhang and co-workers, claims that size rather than geometry dominates the *in vivo* fate of Au NMs: while NRs and spherical NPs bigger than 20 nm are retained mainly in the spleen, nanoclusters of smaller size (3 and 7 nm) are rapidly cleared through the kidneys[121].

The surface charge properties also affect the endocytosis rate and the circulation time. Since cell membranes are negatively charged, positively charged NPs are relatively easy absorbed by targeted cells, but equally trapped by macrophages, limiting the circulation time[115]. Elci and co-workers proved that 2 nm positively charged Au NPs are rapidly taken up by the liver whereas their neutral and negatively charged counterparts tend to circulate longer[122].

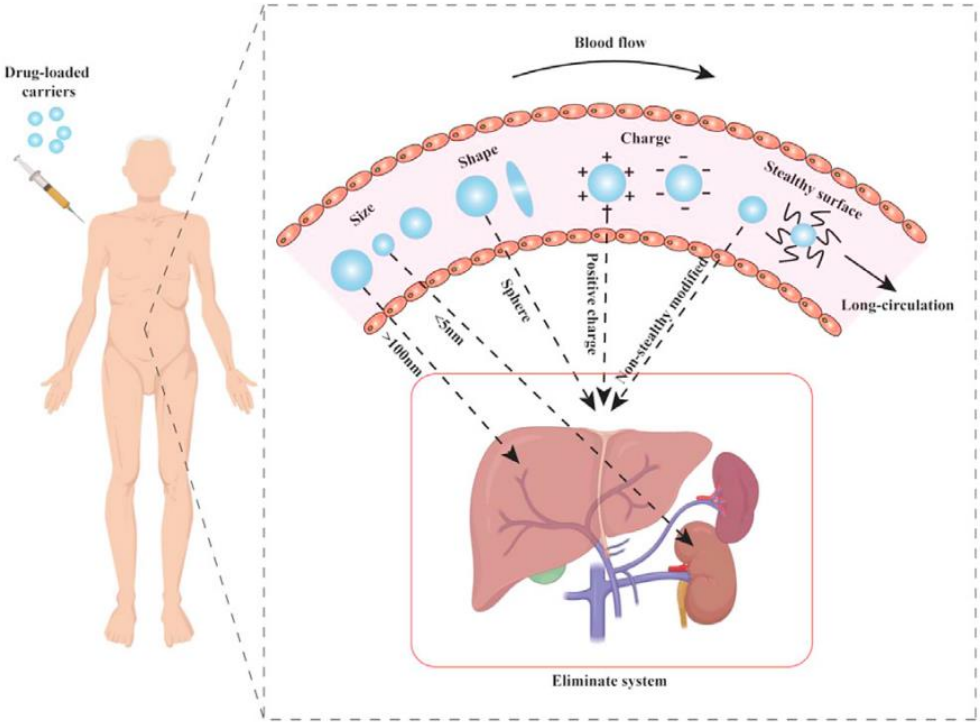

Figure 5. Physical and chemical properties that affect the circulation of Au NPs: size, shape, charge, "stealthy" surface. Adapted from[115]

Relationships between NPs characteristics and *in vivo* behavior and excretion pathways are summarized in Figure 5. In general, non-spherical NPs with sizes between 10 and 100 nm and neutral or negative surface charges, tend to remain longer in the bloodstream, increasing the chances to reach their target. However, NMs clearance must be efficient enough to avoid long term toxicities. Given the lack of biodistribution studies, any assumption regarding the *in vivo* fate of novel Au NMs should be validated by experimental data on a case-to-case basis before advancing to clinical settings.

2.5.3. Protein Corona

The NMs' biodistribution is strongly correlated to their interaction with the physiological environment. Relatively little is known about this interface, and this is now a serious bottleneck in the whole nanomedicine enterprise. Upon systemic administration, NPs are immediately exposed to blood, which carries roughly 3700 identified proteins and other biomolecules[106,107]. A subset of these proteins will progressively and selectively adsorb onto its surface, forming a coating shell that is commonly known as the protein corona (PC)[123]. The adsorbed proteins confer to the NPs a unique "biological identity"

that differs from the "synthetic identity" and leads to unpredictable *in vivo* performance. While the pristine surface remains inaccessible, the PC directly engages with the physiological environment dictating the NPs' behavior.

The PC is made up of two component layers: the "hard" corona, represented by strongly adsorbed proteins at the nanomaterial surface and the "soft" corona, a more external layer of proteins with a weaker binding affinity[124]. The 'soft corona' represents a more dynamic exchangeable layer of proteins that constantly interact with the environment and is much more elusive to isolate and characterize based on current available techniques.

The PC can be considered unique for each given nanomaterial and even in the case of NPs constituted by the same material, it greatly depends on physicochemical properties such as the size[125–127], surface functionalization[126,127] and morphology[128–131]. In general, NPs with higher surface area tend to adsorb more proteins. However, very small NPs with highly curved surfaces can suppress protein interaction to the point where it no longer occurs[132]. Spherical NPs minimize the interactions with the environment when compared to nanostars[131,133], nanorods[128–130] or other geometries. In regards to the surface chemistry, NPs with charged surfaces tend to adsorb more proteins and denature them with greater extent than those with neutral surfaces[132,134].

At the same time, the composition of the PC in terms of protein types, relative abundance, and conformation has an important impact on NPs colloidal stability, circulation time, biodistribution and toxicity, as illustrated in Figure 6[123,135]. Generally speaking, adsorption of opsonins such as immunoglobulins, complement factors and fibrinogens activate the host innate immune response promoting NPs uptake by macrophages, release of proinflammatory cytokines and even blood clotting[132]. Whereas adsorption of dysopsonins such as albumin, clusterins or apolipoproteins may increase the circulation lifetime in blood and biocompatibility[136].

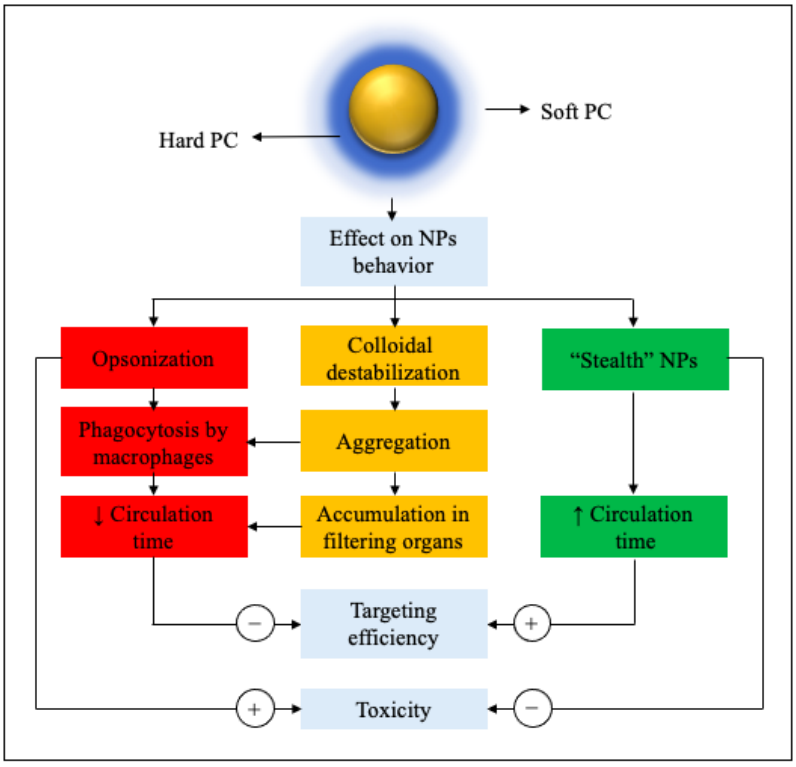

Figure 6. Schematic flow chart summarizing the positive and negative implications of the PC formation

Several studies also report that adsorption of proteins may mask the targeting ligands grafted on the NPs' surface, reducing recognition by cellular receptors and leading to unspecific accumulation[134]. One approach to overcome this issue is to engineer the protein corona composition for active targeting. For example, decoration of NPs with apolipoproteins can be useful for NPs to transport into brain due to the high expression of lipoprotein receptors at the BBB[136].

Some serum proteins, such as fibrinogens, may induce NPs destabilization, aggregation and undesired accumulation in filtering organs[137] while others, such as clusterins, may play a fundamental role to avoid clearance by macrophages increasing the circulation time and conferring the so-called "stealth" feature[138]. The role of some abundant serum proteins such as albumin is still controversial since the results strongly depend on the experimental conditions[139,140].

Although several determinant factors involved in protein corona formation have been identified from *in vitro* studies, specific relationships between the NMs synthetic identity and its ensuing biological identity under realistic *in vivo* conditions remains elusive mainly because of the difficulty to capture NPs and isolate associated proteins after administration. An interesting arising alternative is the application of molecular dynamic simulations to predict the proteins-NPs interactions[141,142].

Based on the aforementioned results, one can conclude that the field of PC and its implications is still in its early stage. Comprehensive and detailed studies are required to better understand the role of each protein in the corona and the cumulative effects of the entire corona on the biological response of nanoparticles. Mastering this phenomenon will have a great impact for nanomedicine since in the future, the corona itself might be controlled and used as a novel means to achieve the desired biodistribution and safety profiles.

2.5.4. PEGylation as strategy to overcome Au NMs' concerns

Researchers have widely sought for a NMs surface coating able to limit protein opsonization and extend systemic circulation long enough to reach their therapeutic target. Unlike toxicity and biodistribution, that can be modulated according to the NPs physicochemical characteristics, the PC represents an ungovernable phenomenon. The most widespread strategy to reduce nonspecific protein binding without compromising NMs' safety[109] is the surface modification with hydrophilic, neutral and hydrogen bond accepting polymers (i.e. with lone electron pairs)[143]. All these characteristics are fulfilled by poly(ethylene glycol) (PEG), a rather inexpensive, biocompatible, versatile, and FDA approved polymer[144]. Moreover, PEG is commercially available in different molecular weights and bearing various functional groups. The thiol group on one end is anchored to the Au NPs surface whereas amines or carboxylic acids on the other end allow secondary tethering of the NPs surface with biologically relevant molecules such as peptides, carbohydrates or drugs to improve the delivery efficiency and avoid nonspecific accumulation. This is the principle behind Aurimune, the only gold nanoformulation undergoing clinical trials, where the PEG moiety acts as a bridge between 30 nm Au NPs and TNFα.

Surface modification with PEG derivatives, also referred as PEGylation, confers steric stabilization, preventing aggregation, increases particle hydrophilicity and guarantees a fine control over the NPs' surface, thus minimizing the attachment of opsonins and the clearance by macrophages, conferring a "stealth" behavior able to extend the NPs circulation half-life with reduced immunogenicity. Despite its antifouling characteristics, PEG cannot completely avoid the protein adsorption. To ensure minimal non-specific protein binding, three critical factors to consider are the PEG chain length (MW)[145,146], the surface charge[134,147], and the grafting density[148,149] which determines the conformation adopted by the

flexible polymer chains on the NPs surface (Figure 7)[150]. If the grafting density is low, PEG chains are present in a condensed or "mushroom" conformation. As the number of PEG chains per surface area increases, the distance between chains decreases and they adopt a more extended or "brush" footprint. In the last case, the PEG layer is much thicker, reducing the PC formation[148,151], however, too dense PEGylation can also entrap a targeting ligand inside the PEG interface and suppress its interaction with the target receptor. In these cases, backfilling with shorter PEG chains can help to both reduce the PC formation while assuring ligand accessibility[152].

As for the chain length, it has been proven that PEG molecular weight up to 5 - 10 kDa reduce protein adsorption, whereas above this MW no significant decrease in biomolecules interactions can be noticed. Furthermore, if the chain length is too long, the large hydrodynamic diameter may prevent efficient renal clearance from the body. This aspect is important since despite its biocompatibility, PEG is not biodegradable. PEG may accumulate in the liver an lysosomes and its repeated dosage can eventually evoke recognition by the immune system, leading to the formation of anti-PEG IgM antibodies, accelerated blood clearance and undesired side effects[153].

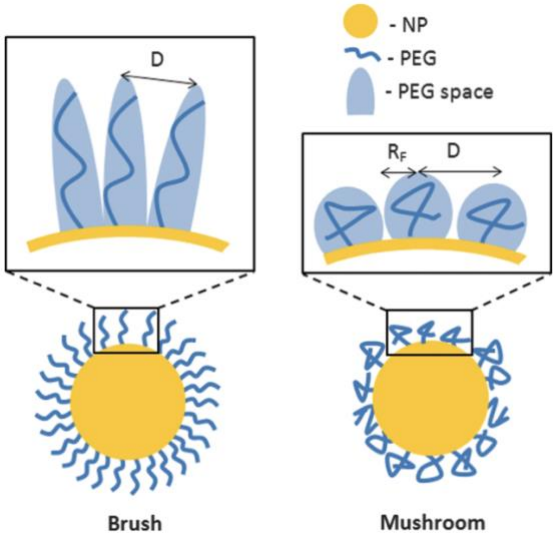

Figure 7. Brush and mushroom conformation of PEG on spherical NPs. Shaded blue area indicates space that PEG molecules may occupy[150]

This has prompted the search for PEG alternatives with improved antifouling properties and reduced immunogenicity[154]: poly(vinylpyrrolidone) (PVP)[155], poly(*N*-(2-hydroxypropyl) methacrylamide (pHPMA)[156], zwitterionic polymers[157] or naturally occurring structures such as polysaccharides[158] and polyaminoacids[159] represent promising candidates that have yet to be translated into clinical trials.

3. Carbohydrate coated Au NPs

Carbohydrates, alongside proteins, lipids and nucleic acids, might be considered essential molecules of life since they are ubiquitous in nature and play crucial roles in a great deal of biological processes[160–162]. Beyond their well-established structural and energetic functions, carbohydrates modulate protein function and decorate the external surface of all cells, forming the so-called glycocalyx where they mediate interactions with the external environment. As such, glycans are involved in many physiologically relevant functions that include cell proliferation, differentiation, migration and apoptosis, host-pathogen interactions and host immune response, inflammation and blood group

determination. Correct glycosylation patterns are essential for normal cell and organism function whereas aberrant glycosylation is a hallmark of numerous human diseases such as cancers or congenital disorders. Carbohydrates present a high degree of specificity for their receptors (even if the affinity is typically poor) and can be exploited as targeting molecules, as antigens for vaccine development or as biomarkers for different physiological and pathological conditions.

Au NMs represent excellent platforms for carbohydrate presentation since they can mimic their natural multivalent disposition on the cell surface, thus allowing to overcome the inherently weak nature of the interactions with their receptors[163]. On their behalf, glycans increase colloidal stability and biocompatibility of Au NMs while preventing unspecific interactions with proteins in the media, hence the saccharide coating can be exploited as an alternative to PEGylation to obtain stealth NMs[164].

Therefore, the synergic combination of carbohydrates and Au NPs to obtain carbohydrate-coated Au NPs (AuGNPs) is finding increasing interest in nanomedicine. AuGNPs combine in a single entity the biological information encoded by carbohydrates with Au NPs' therapeutic potential. The present chapter focuses on the most diffused protocols for the synthesis of AuGNPs and the main parameters to take into account when designing a new glyco-nanosystem. The last three sections summarize the achievements and ongoing studies published in the last years, with a special focus on glyco-gold nanoparticle applications in biosensing field, as drug and antigen carriers or contrast agents and as tools in the immunological field.

3.1. Synthetic strategies

In general, there are three main methods that one can use for the synthesis of AuGNPs and they are summarized in Figure 8. The first one, introduced by de la Fuente and co-workers in 2001, was the first ever report of AuGNPs and it consists in a one-step preparation of ultrasmall spherical Au NPs coated with thiol-ending glycosides using the Brust-Schiffrin approach[165]. This synthetic procedure allows to introduce different ligands in controlled ratios and has been extensively explored[59,166–168].

The second approach is based on the two steps protocol introduced by Turkevich et al[71]. It consists on the preparation of citrate-capped spherical nanoparticles, with diameters between 10 and 50 nm, followed by ligand exchange to introduce the thiolated saccharide molecules[169–171]. This methodology allows an easier control of the morphology by using surfactants or templating agents[172] but, the main drawbacks are the longer reaction times and the difficulty for a fine control of the organic shell composition.

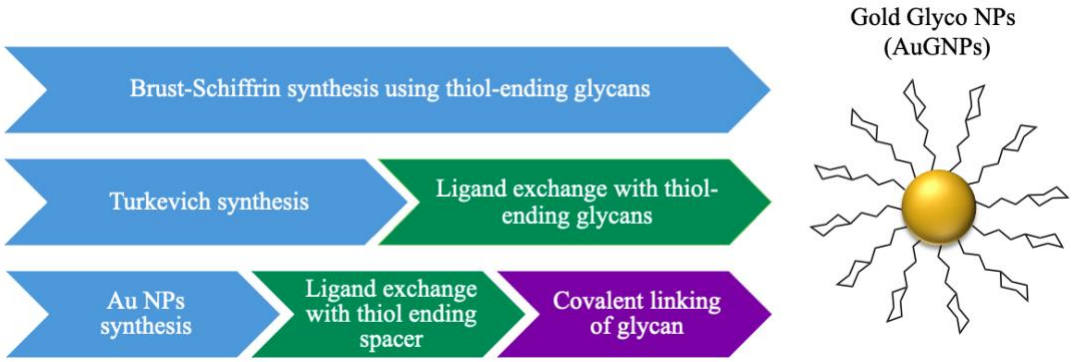

Figure 8. Schematic overview on AuGNPs main synthetic approaches. Adapted from[173]

The third method consists in the synthesis of Au NPs with specific ligands that will in a subsequent step react with suitably functionalized carbohydrates. Various types of reactions such as click chemistry[174], amidation[175] or oxime formation[176] have been used to introduce the carbohydrate moiety. Even if this three-steps approach is certainly time-consuming, it requires the use of lower amounts of precious sugar residues. More details regarding the synthesis of AuGNPs can be found in the reviews by Penadés and co-workers[177] and also in a recent review by Compostella et al.[173]

The carbohydrate density and exposure are relevant factors influencing the interaction of AuGNPs with their ligands and they are strongly related to the NMs' shape, morphology and the spacer in-between the NP and the carbohydrate. A deep knowledge of every aspect that can influence the AuGNP behavior is important to drive the correct design of the glyco-nanosystem for the final bio-application.

Generally, when the diameter grows, NPs present a smaller curvature which allows higher ligand packing density[173,178,179]. However, not always a high carbohydrate density is translated in an improved affinity. For example lectins, the most-common carbohydrate binding proteins, present characteristic distances between binding pockets, so a well-controlled carbohydrate density can result in a more efficient recognition[180]. Even if the carbohydrate loading is relevant, the disposition may be more important than the density itself. Studies by Kikkeri et al. proved that rod-shaped AuGNPs coated with mannose and galactose derivatives presented better affinity to *E. coli*[172], stronger bacterial inhibition[181] and better internalization in cancer cell lines[182] in comparison to spherical and star shaped AuGNPs. At the same time, Au glyco-nanostars evidenced prolonged circulation times in zebrafish models, demonstrating their potential therapeutic efficacy in drug delivery[168].

Often, a too high carbohydrate density on the NPs surface can hamper accessibility of the glycans to protein receptors. This issue can be addressed through the choice of the linker or tether between the glycan and the Au surface. In general, longer linkers favor interaction with receptors[178,183]. Grant and co-workers, performed molecular dynamics simulations of surface-conjugated glycans to evaluate the role of the spacer in the glycan recognition[184]. The authors considered different types of spacers in terms of chemical structure, length and rigidity to prove that longer linkers gave a better access to the protein pocket. Furthermore, they showed that rigid spacers could hinder the binding, by creating unfavorable interactions with the protein surface, while flexible spacers resulted in a better carbohydrate presentation and subsequent easier interaction with the target.

The continuous advances in NMs' synthesis together with the ever-growing understanding of the physiological and pathological processes regulated by glycans and the advent of new technologies for their isolation, synthesis and characterization, will continuously unravel novel opportunities for AuGNPs.

3.2. AuGNPs as biosensors for the detection of virus, bacteria and cancer

In the last decade, a variety of biosensors have been developed exploiting the color changes and LSPR shifts as Au NPs either aggregate or disperse, in the presence of analytes (Figure 9). To date AuGNPs have proven effective for lectin detection, including those associated with viruses and bacteria.

The specific interaction between glucosamine-functionalized Au NPs and the plant lectin Concanavalin A (ConA) has been reported by Di Silvio et al. to study the intracellular exchange of PC[185]. Apart from the detection of plant lectins, a more interesting approach is the use of AuGNPs for the development of convenient and portable sensors for the rapid detection of viruses and bacteria. The affinity between

hemagglutinin, a protein on the surface of *Influenza* virus, and sialic acid on the host cell, has been explored for the development of a diagnostic tool. A collection of Au NPs functionalized with seven different sialic acid derivatives has been used to detect and discriminate between *Influenza* strains based on a simple and fast colorimetric change due to the aggregation of Au NPs on the viral surface[186]. Based on the same concept, Baker and co-workers prepared *N*-acetyl neuraminic acid-functionalized AuGNPs for the rapid and low-cost detection of SARS-CoV2[187]. The system was transferred into lateral flow format enabling a rapid, sensitive detection of virus-like particles presenting the SARS-CoV2 spike protein. In addition, several studies have proven the ability of AuGNPs to bind DC-SIGN receptors and hence, prevent viral cell, such as HIV or Ebola, internalization[188–190].

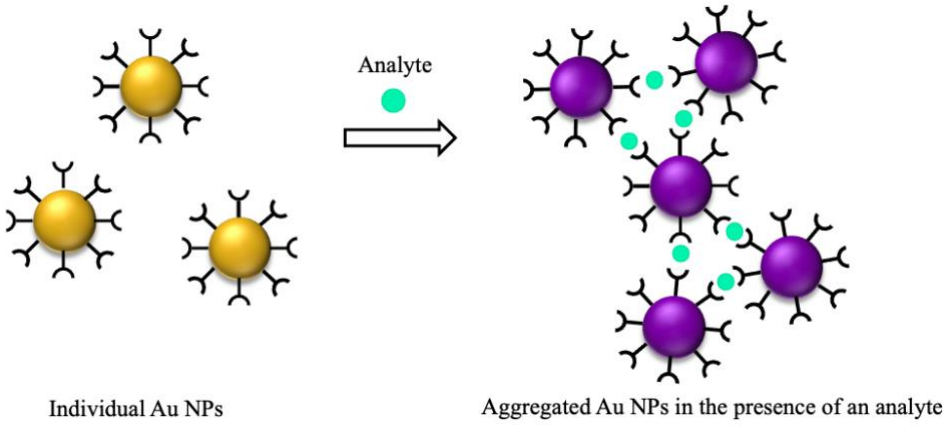

Figure 9. Schematic representation of the biosensing principle. Au NPs change in color due to induced aggregation in the presence of an analyte

A turn on-based fluorescent system afforded a simple means to detect *E. coli* based on the fluorescent properties of glucose-acrylamides, quenched when attached to Au NPs and restored in the presence of a glucose-binding target[191]. Whereas Zhang and co-workers prepared Au NPs functionalized with D-galactose and L-fucose owing to their selective recognition towards LecA and LecB respectively, key virulence factors of *P. aeruginosa.* Subsequently, the AuGNPs were loaded with florescent agents or antibiotics in order to simultaneously detect and kill the pathogen[192].

Imaging and early detection of tumors is vital for patient survival. Sialic acid and galactose binding lectins, siglecs and galectins, are cancer markers of increasing interest[193]. Schofield et al. designed sialic acid functionalized Au NPs for their detection[194]. The assay provides a color change upon aggregation of the Au NPs in the presence of siglecs, notably the aggregation could also be localized in cell lines by TEM. García Calavia et al. reported bi-functional AuGNPs containing lactose to target galectins, and a phthalocyanine derivative as photosensitizer[195]. The AuGNPs could be used to achieve selective breast cancer cell death upon irradiation of the PS, resulting harmless to healthy cells. Recently, Au NPs stabilized with acetylated mannose were used in an image-based assay to detect lung cancer cells[196].

3.3. AuGNPs as targeted drug delivery systems

AuGNPs represent efficient and safe drug delivery systems, able to deliver toxic and insoluble payloads to specific tissues thanks to the carbohydrates targeting abilities, lowering side effects attributed to non-specific delivery.

Given the aberrant expression of carbohydrate-binding receptors on the surface of some cancer cells, AuGNPs have been extensively studied to target and treat tumors[197,198]. In this contest, Vargas-

Berenguel et al. prepared AuGNPs functionalized with lactose and β-cyclodextrins. This nanoformulation targeted galectins overexpressed in cancer cells in order to selectively deliver anticancer methotrexate transported on the β-cyclodextrin cavity[199]. Yilmaz et al. successfully synthesized mannose tagged AuGNPs by covering the metallic core with methacrylic acid derivatives as a toolbox for pH-sensitive doxorubicin delivery. These nanoconjugates were applied to cancer cell lines to assess the cytotoxicity and cellular uptake, showing significant potential in human neuroblastoma cell lines[200]. Galactose-polymers attached to AuGNPs were used by Adokoh and co-workers for the delivery of anticancer Au (I) triphenylphosphine targeting the asialoglycoprotein receptors overexpressed in hepatocellular carcinomas[201]. Glucose functionalized Au NPs have also proven to be optimal radiosensitizers for radiotherapy taking advantage of cancer cell's elevated glucose consumption[202,203]. A recent study exhibited efficient internalization by lung cancer cell lines of Au NPs stabilized by *n*-gluconamidoalkyl disulfides suggesting that they could be an alternative for the delivery of anti-cancer drugs[204].

The antiviral activity of glucose-coated Au NPs loaded with anti-HIV prodrug candidates was tested by Chiodo and co-workers. The glucose moiety improved cellular uptake and biocompatibility whereas the pH-mediated release of the drugs proved to inhibit viral replication[205]. Hence, the loading of multiple antiretroviral molecules on AuGNPs could lead to efficient and selective drug delivery systems able to overcome the toxic side effects of current antiretroviral therapies.

AuGNPs have also been briefly investigated as novel antimicrobial agents to bypass resistance to traditional antibiotics. Chitosan-streptomycin AuGNPs could overcome antibiotic resistance on microbial biofilms[206]. Similarly, a novel recyclable AuGNP nanoformulation, carrying both a targeting glycopolymer and an antibacterial polymer, resulted able to reliably bind and kill *E. coli*[207].

3.4. AuGNPs in immunology

Pathogens present characteristic glycosylation patterns on their cell surface that can be tailored onto Au NPs for vaccine development. AuGNPs not only display several copies of the carbohydrate antigen, but also stimulate the immune response by presenting them directly to antigen presenting cells such as macrophages, dendritic cells or other immune cells, without the need of carrier proteins or adjuvants[208,209]. Thus, AuGNPs could play an important role in vaccine development as carriers and adjuvants, enhancing the immunogenicity of antigens and reducing toxicity.

AuGNPs decorated with antigenic carbohydrates have been investigated as prophylactic vaccine candidates against infections caused by virulent bacteria, such as *Streptococcus pneumonia* serotypes 19F and 14[210,211], *Burkholderia pseudomallei*[212] or *Listeria monocytogenes*[213]. An effective vaccine against HIV still represents a challenge to prevent infection and progression of the acquired immune deficiency syndrome (AIDS), especially in developing countries. The HIV-1 envelope glycoprotein is known to be covered by high-mannose *N*-glycans, hence Martínez-Álvarez et al. prepared a library of Au NPs' using different oligomannosides, spacers and densities to study the binding to DC-SIGN, receptor involved in the first steps of HIV infection[214]. More recently, Chiodo and co-workers prepared Au NPs functionalized with tetra- and penta-mannosides. The latter not only elicited broadly neutralizing antibodies against the virus *in vitro*, but also inhibited its binding to DC-SIGN receptors, preventing viral entry[215]. Other groups have proved that addition of di- and tetra-mannosides to Au NPs coated with antigenic peptides, improved antigen capture by dendritic cells and the immune response against HIV[216,217].

Cancer cells can be distinguished from healthy cells by the expression of a series of tumor associated carbohydrate antigens (TACAs) and AuGNPs constitute a brilliant template for their multivalent presentation. The most prevalent TACAs are the Thomsen Noveau (Tn), the Thomsen Friedenreich (TF) and the sialyl-Tn (sTn) and they are usually linked to tumoral mucins, a family of aberrant glycoproteins overexpressed on tumor cells. AuGNPs were coated with mucin glycopeptides functionalized with the TF disaccharide antigen. Immunization of mice with these nanoformulations, elicited a small but encouraging immune response[218]. A polymeric version of the Tn antigen was synthesized by reversible addition-fragmentation chain transfer (RAFT) polymerization and conjugated to Au NPs. *In vivo*, these AuGNPs, induced a significant production of IgG antibodies, selective to the Tn antigen glycan, providing cross-protective immunity toward mucin glycoproteins displaying Tn antigens[219]. Au NPs directly coated with mucin glycoproteins have also been evaluated as antigens in the quest towards effective cancer vaccines[220,221]. Alternatively, Terán-Navarro and co-workers presented a novel nanovaccine against cutaneous melanoma using Au NPs loaded with both β-D-glucose and a listeriolysin peptide with anti-metastatic properties (LLO_{91-99}). The results on monocyte dendritic cells from melanoma patients promoted antigen presentation whereas in mice models this immunotherapy evidenced tumor regression and improved survival[222].

3.5. AuGNPs as contrast agents

Combining Au NPs X-ray absorption properties with carbohydrates targeting ability, makes AuGNPs ideal candidates for the next generation of contrast agents in CT. In this context, glucose coated AuGNPs proved to efficiently accumulate in tumors exploiting overexpressed glucose receptors and to act as potential contrast agent for *in vivo* CT imaging when compared to non-targeted Au NPs[216]. Similar encouraging results were obtained with glucosamine AuGNPs targeting lung inflamed cells[52]. Jølk and co-workers produced a nanogel composed by sucrose acetate isobutyrate and poly(*N*-isopropylacrylamide) coated Au NPs, allowing 2D X-ray visualization *in vivo* in healthy mice and canine cancer patients[224]. Furthermore, AuGNPs functionalized with Gd^{3+} complexes[225,226] or ^{68}Ga[59] have also been described as MRI or PET contrast agents respectively to improve discrimination between lesion and neighboring tissues. However, given the lack of literature reports in this area, there is still a long way to go in the field of AuGNPs for imaging.

In conclusion, AuGNPs represent versatile platforms suitable for biosensing, targeted delivery of drugs or other payloads, vaccine formulation, radiation therapies, imaging or even combinations thereof. The field continues to progress at vertiginous pace, but the full therapeutic potential of these glyco-nanosystems will only be achieved when all the concerns regarding Au NPs are fully understood and accurately addressed. New discoveries in the complex and fascinating world of carbohydrates will also play an important part in this nanorevolution.

AIM OF THE PROJECT

The work described in this thesis is part of NanoCarb (Glyco-Nanoparticles for Applications in Advanced Nanomedicine), a European Training Network (ETN) with the final goal to develop novel glycosylated nanoparticles with enhanced therapeutic performance for healthcare applications.

As highlighted in section 3, AuGNPs combine in a single entity the biological information encoded in carbohydrates with Au NMs therapeutic possibilities. However, despite their rapid growth, the full potential of these glyconanosystems will only be achieved when the underlying safety concerns associated with Au NMs (described in section 2.5) are understood and accurately addressed. In the NanoCarb project, 15 Early-Stage Researchers (ESRs) with expertise in the fields of glycoscience and nanotechnology are combining their efforts to overcome the existing limitations and pave the way towards the next generation of AuGNPs with improved clinical performance.

In this context, our contribution to the project from Professor Lay's group at the University of Milan has focused on the synthesis of carbohydrates suitable for NMs functionalization. The present work is divided in three chapters:

The first chapter focuses on the influence of the NM's surface coating on the interaction with proteins in the media. For that purpose, a set of six different AuGNPs are prepared combining three monosaccharides (mannose, galactose and fucose) and two PEG derivatives (PEG5000 and Alkyl-PEG600). In collaboration with the CIC BiomaGUNE (Spain), this project aims to evaluate how pre-incubation with proteins can dictate the AuGNPs' behavior *in vitro*. In a second part of the chapter, mannose is modified with anionic groups in order to prepare negatively charged AuGNPs and compare them to the neutral counterparts in terms of colloidal stability and interaction with proteins in the media, these measurements will be performed at RCSI (Dublin). In addition, Au NPs functionalized with a synthetic derivative of sialic acid (a naturally occurring negatively charged monosaccharide) are included in this study. The immunomodulatory properties of these sialylated AuGNPs are investigated *in vivo* at Mario Negri Institute (Italy). The final aim of this chapter is to provide a better understanding of the PC formation and a correlation to the main NMs' characteristics influencing it.

The second chapter describes the synthesis of ABO blood sugar antigens, terminal di- and tri-saccharides covering the surface of human red blood cells and other body tissues. As hydrophilic, neutral and hydrogen-bond accepting molecules, carbohydrates represent an excellent PEG alternative to reduce non-specific interactions with proteins in the media while increasing biocompatibility and biodegradability. Specifically, NMs' functionalization with ABO self-antigens, ubiquitous in the human organism, may improve their immunotolerance, minimizing macrophages uptake and granting enough circulation time to reach their therapeutic target. These biomimetic glyco-NPs may present upgraded "stealth" behavior and reduced immunogenicity and these assumptions will be tested in the near future in collaboration with RCSI.

The last chapter deals with the synthesis of mannose (Manα1), dimannose (Manα1-2Manα1) and trimannose (Manα1-3(Manα1-6)Manα1) derivatives equipped with an amine-ending linker at their reducing-end for Au NRs functionalization at VITO (Belgium). The end goal of the project is to develop a high-throughput biosensor to detect mannose binding lectin (MBL) from human plasma samples and to correlate the results to potential cardiovascular disease development.

CHAPTER I: PROTEIN CORONA STUDIES

1. Introduction

Previous studies from Prof. Lay's group in collaboration with Dr. Sergio Moya (CIC BiomaGUNE) evaluated the interaction of Au NPs with proteins in the media as a function of their surface coating using fluorescence correlation spectroscopy (FCS)[227]. FCS is a spectroscopic technique that translates the diffusion coefficients of fluorescently labelled NPs in solution into hydrodynamic diameters and it is particularly suited to study the PC evolution because of the possibility to perform experiments *in situ* in complex biological matrixes[228,229]. For that purpose, Au NPs were functionalized with four different ligands: a long chain PEG of 5 kDa (PEG5000), an amphiphilic polymer composed of a short PEG of 600 Da and an alkyl chain (alkyl-PEG600), mercaptosuccinic acid (MSA) and *N*-(4-mercaptobutyroyl) glucosamine (GlcN) (Figure 10).

The results confirmed that the surface coating influences the colloidal stability and the protein binding. In cell growth media enriched with fetal bovine serum (FBS), GlcN and MPS coated Au NPs showed strong affinity toward proteins and once internalized by cells, they presented reduced stability and more prominent formation of aggregates. In contrast, both PEGylated NPs maintained constant the diffusion values over time in enriched cell culture media and intracellularly, proving their great colloidal stability and lower protein binding. In summary, FCS results evidenced that surface functionalization with negatively charged molecules or single monosaccharides was not enough to guarantee a "stealth" performance and the presence of an antifouling polymer was required.

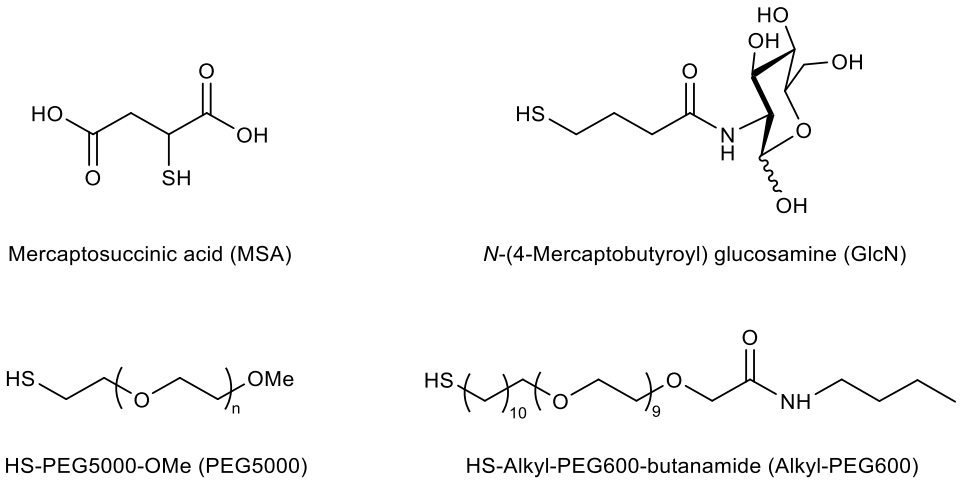

Figure 10. Ligands selected to coat Au NPs[227]

In a subsequent study, the linker with the best antifouling performance, Alkyl-PEG600, was functionalized with a terminal glucosamine and used to coat Au NPs[185] (Figure 11). The goal was to study the stability of a pre-formed PC *in vitro*. For that purpose, they used ConcanavalinA (ConA), a protein with well-known affinity for GlcN, and Bovine Serum Albumin (BSA), the most abundant protein in plasma, but with non-specific interaction with the sugar. Using FCCS, a variation of FCS in which both NPs and proteins are fluorescently labelled, they provided valuable information on the stability and exchangeability of pre-incubated proteins around AuGNPs forming a sort of PC.

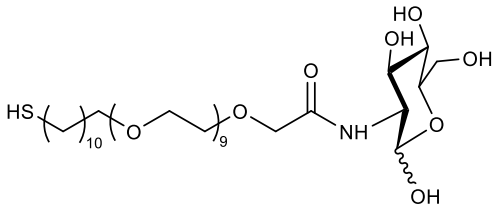

HS-Alkyl-PEG600-glucosamine (Alkyl-PEG600-GlcN)

Figure 11. Ligands selected coating Au NPs in follow-up study[185]

In enriched cell culture media, alkyl-PEG600-GlcN Au NPs showed higher affinity towards ConA whereas competitive assays proved the ability of ConA to replace a pre-formed BSA corona, but not otherwise. These experiments highlighted an interesting point: the binding ability of the sugar coating is retained even in the presence of a non-specific PC. Inside cells, the ConA corona remained stable over time and prevented NPs aggregation, whereas the BSA corona was lost faster and NPs aggregates were found. These findings pose a question of increasing interest, is it possible to engineer a PC to increase colloidal stability and more important, to modulate NMs fate?

2. Aim of the chapter

In line with previous findings, the initial aim of this chapter was to prepare six new Au NPs to further evaluate the effect of the surface coating on the PC. Three monosaccharides with affinity for commercially available lectins and two PEG derivatives with confirmed antifouling properties were chosen (Figure 12).

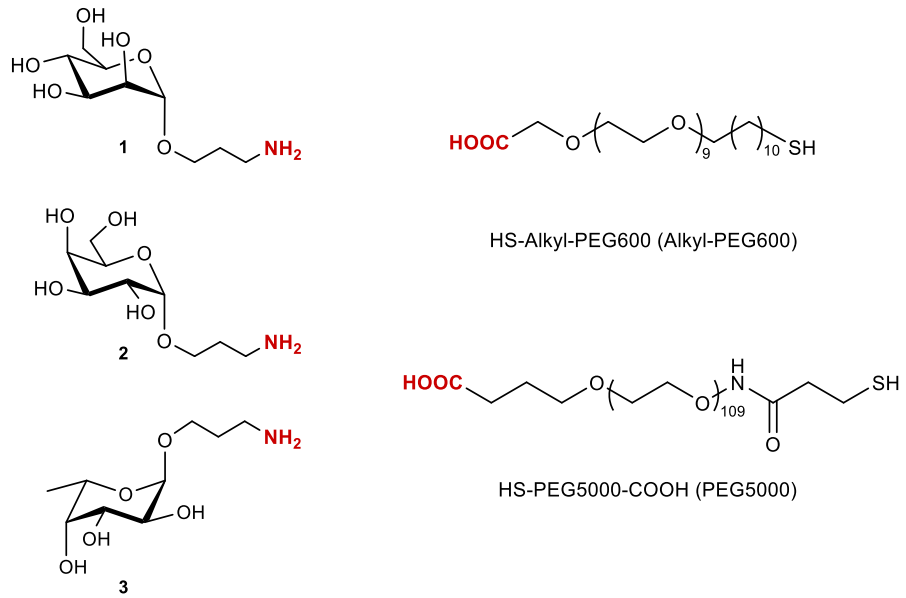

Figure 12. Monosaccharides and ligands selected to coat the Au NPs target of this chapter

Our contribution to the project focused on the modification of monosaccharides with a short anomeric linker with a terminal amine which could be conveniently conjugated to PEG derivatives through the carboxylic acid group. After conjugation, these new linkers were used to functionalize Au NPs which have been sent to the CIC BiomaGUNE (Spain) to perform FCS in collaboration with Dr. S Moya's group.

The end goal of the project is, in first place, to determine if the choice of PEG (in terms of chain length and hydrophilicity) may affect the carbohydrates disposition on the NPs' surface and hence their interaction with lectins in the media. Previous studies proved that Alkyl-PEG600 guarantees great carbohydrate presentation and efficient interaction with lectins, while PEG5000 may entrap the small carbohydrates, due to its length and flexibility, thus reducing ligand affinity. In second place, to corroborate if the binding specificity of carbohydrates is retained even in the presence of a pre-formed PC. Positive results could have huge implications for the targeted delivery of AuGNPs even in in complex physiological media. Finally, this study will keep looking into the repercussions of protein pre-incubation on the aggregation sate and intracellular fate of AuGNPs. Hopefully the results will shed some light into the PC formation and the factors governing it, with the future prospect to minimize it or eventually engineer it to control the NMs biodistribution and safety profiles.

3. Results and discussion

3.1. Synthesis of 3'-aminopropyl α-D-mannopyranoside

Mannose was chosen as a first target since it binds to commercially available plant lectins such as ConA or Sambucus Nigra II (SNA-II)[230]. Moreover this monosaccharide is involved in essential biological functions[231] and has been extensively studied for NMs functionalization[180,200,232].

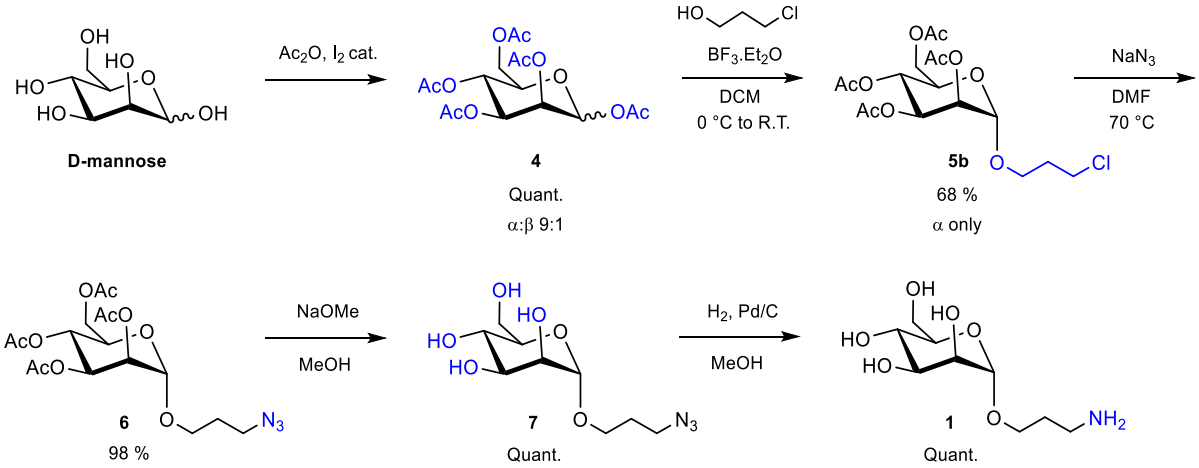

Scheme 1. Synthesis of 3'-aminopropyl α-D-mannopyranoside

The synthesis of compound **1** started with per-acetylation of D-mannose using acetic anhydride and iodine as catalyst to obtain compound 4 mainly in α configuration[233]. The subsequent linker introduction involved the formation of a glycosidic bond between the anomeric position of mannose and the hydroxyl group of the linker (Scheme 2). This reaction was tested in different conditions and a summary is reported in Table 1.

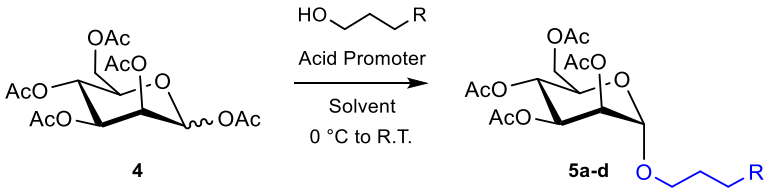

Scheme 2. General linker introduction conditions

Table 1. Conditions for the linker introduction

Entry	Linker (3 eq.)	Acid promoter	Solvent	Yield
1	HO–Br	$BF_3{\cdot}Et_2O$ (3 eq)	DCM	60 %
2	HO–Cl	$BF_3{\cdot}Et_2O$	DCM	68 %
3	HO–NHCbz	$BF_3{\cdot}Et_2O$	DCM	32 %
4	HO–NHCbz	$BF_3{\cdot}Et_2O$	ACN	30 %
5	HO–Cl	TMSOTf (0.5 eq)	DCM	40 %
6	HO–N_3	$BF_3{\cdot}Et_2O$	DCM	42 %

Thanks to the anchimeric assistance of the axial 2-O-acetyl, shown in Scheme 3, compound **5** was always obtained as the preferentially lectin-binding α-anomer. In general, 3-bromo- and 3-chloro-propanol were more reactive than the *N*-Cbz protected aminopropanol or the 3-azidopropanol. Using $BF_3{\cdot}Et_2O$ as acid promoter the reaction was typically slow (~ 48 h) and the yield of the glycosylation varied from 30 up to 68 %. With a stronger acid such as trimethylsilyl trifluoromethanesulfonate (TMSOTf), the reaction rate increased (~ 16 h), but some deacetylation of the starting material was observed which decreased the overall yield (Table 1, entry 5). The change of solvent had no significant influence in the final reaction outcome (Table 1, entries 3 and 4).

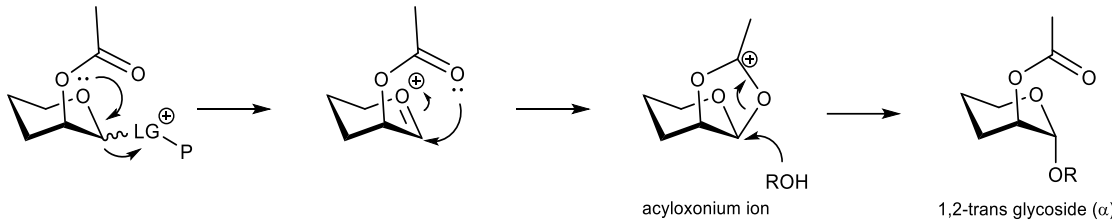

Scheme 3. Mechanism 2-O-Ac participating effect in mannose series. LG represents a leaving group and P an acid promoter

Given the moderate yields obtained with the first approach, the anomeric position was equipped with a better leaving group. For that purpose, the 1-O-acetyl was selectively removed by treatment with hydrazine acetate followed by activation in the presence of trichloroacetonitrile and catalylic amounts of 1,8-diazabicyclo(5.4.0)undec-7-ene (DBU), to afford the thermodynamically stable α-thrichloroacetimidate according to Scheme 4. In this case, the glycosylation step was faster (~ 2h) and higher yielding, but with the addition of two new steps to the synthesis, this strategy was not atom-efficient, and the initial strategy, presented in Scheme 1, was adopted.

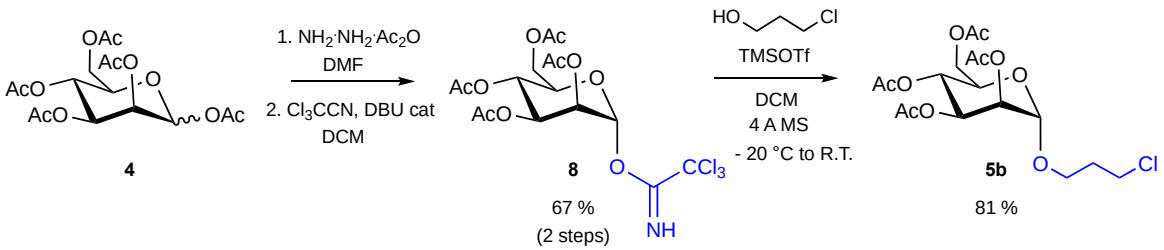

*Scheme 4. Activation of the anomeric position and glycosylation to obtain compound **5b***

After glycosylation with 3-chloropropanol, the chlorine atom was replaced by an azido group via nucleophilic substitution to obtain compound **6**. Deacetylation under Zemplen conditions provided 3'-azidopropyl α-D-mannopyranoside **7**. The final step involved the reduction of the azido group and

for that, two different conditions were tested: the Staudinger reaction using supported PPh_3 and hydrogenation in the presence of H_2 and a catalytic amount of Pd/C. Even if the use of supported PPh_3 allowed to get rid of Ph_3PO formed as a side-product of the reaction, hydrogenation proved to be a faster and cleaner way to afford the target compound. The reduction could be monitored by ^1H NMR given an up-field shift of the two aliphatic protons close to the nitrogen atom from 3.43 ppm in compound **7** to 2.77 ppm in compound **1**.

Compound **1** and other intermediates of the synthesis are being used for different purposes within the NanoCarb network. For example, compound **7** has been used for the preparation of self-induced polymeric NPs at Prof. A. Heise's group (RCSI). Also at RCSI, Dr. M. Monopoli's group is using compound **1** to perform complementary protein binding assays by means of DLS and DCS. In addition, compound **1** is being employed by Dr. I. Nelissen's team at VITO (Belgium) for the functionalization of Au NRs, as discussed in detail in Chapter III.

3.2. Synthesis of 3'-aminopropyl α-D-galactopyranoside

D-Galactose was chosen as the second target since it interacts with readily available plant lectins such as LecA, from *Pseudomonas aeruginosa*[230]. This 4-epimer of D-glucose is an essential energy source in the human organism and it can be exploited for galectin binding, a human lectin implicated in a wide range of diseases such as cancer, HIV, autoimmune disease or chronic inflammation. As opposed to the common belief, monovalent galactose is not big enough to attach to the binding pocket of anti-α-gal antibodies[234] and has been used in several studies as biocompatible sugar for Au NPs functionalization[235,236].

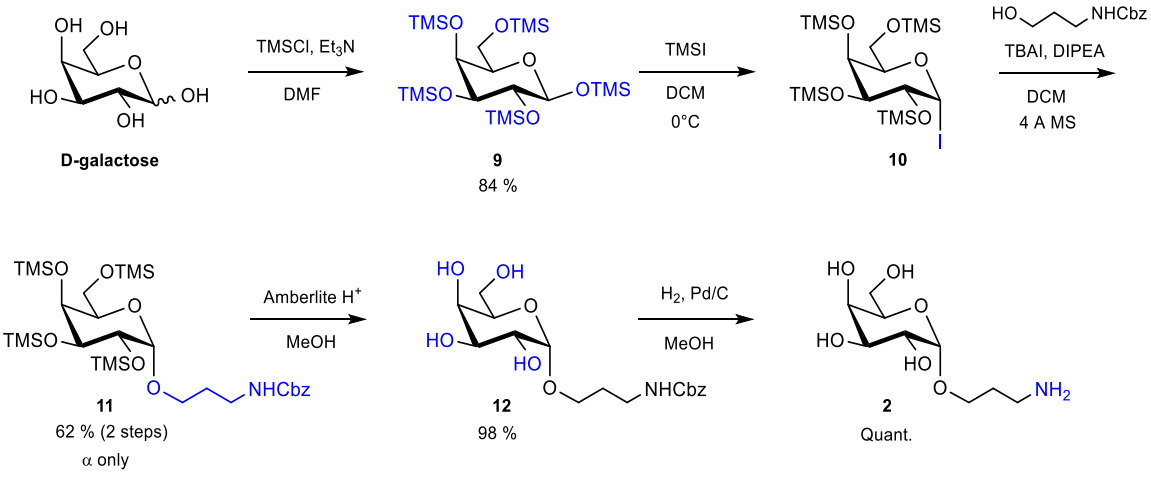

Scheme 5. Synthesis of 3'-aminopropyl α-D-galactopyranoside

Initially, D-galactose was treated with chlorotrimethylsilane (TMSCl) and triethylamine (Et_3N) in DMF to obtain the per-silylated compound **9**. Reaction of **9** with iodotrimethylsilane (TMSI) in DCM at 0 °C gave the α-glycosyl iodide **10** which in the presence of linker in excess afforded compound **11** in excellent stereoselectivity thanks to the tetrabutylammonium iodide (TBAI) contribution. This protocol is known as "*in situ* anomerization" and was first reported by Lemieux and co-workers[237], the mechanism is represented in Scheme 6. In absence of TBAI, the thermodynamically stable α-glycosyl iodide favours the equatorial nucleophilic attack and the formation of a 1,2-trans glycoside. In the presence of TBAI an equilibrium between the thermodynamic (α) and the kinetic (β) glycosyl iodide is

established. Since the kinetic glycosyl iodide is more reactive, it quickly undergoes nucleophilic attack to form the 1,2-cis product.

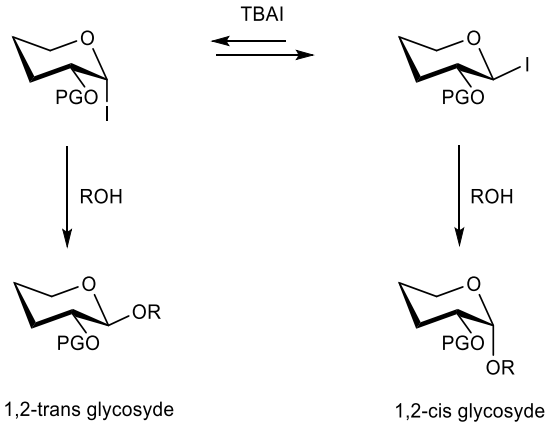

Scheme 6. Mechanism of Lemieux in situ anomerization procedure

Table 2. Glycosylation yields using different linkers

Entry	Acceptor (2 eq.)	Yield (2 steps)
1	HO NHCbz	62 %
2	HO NHCbz	40 %
3	HO N_3	52 %

Different linkers were tested to try to improve the yield of the glycosylation step (Table 2) and the best results were obtained using commercially available 3-(benzyloxycarbonyl)-aminopropanol. The deprotection of compound **11** involved the cleavage of the acid labile silyl ethers using an ion exchange resin, Amberlite (H^+), and a final step of hydrogenation to afford the free amine, according to Scheme 5.

3.3. Synthesis of 3'-aminopropyl α-L-fucopyranoside

L-fucose or 6-deoxy-L-galactose is often displayed is often displayed in α configuration at the non-reducing end of many glycoconjugates and plays key roles in several biological settings including blood transfusions and oncogenic events[238,239]. Lectins that predominantly recognize α-fucose include LecB from *Pseudomonas aeruginosa* and *Ulex europaeus* agglutinin-I (UEA-I)[230] and therefore, L-fucose represents an ideal target for PC studies.

The introduction of the same aminopropylic aglycon on peracetylated fucose afforded exclusively the undesired 1,2-trans-fucopyranoside (β anomer) due to the neighboring participation effect. A new strategy was adopted, using thricholoacetimidate **13**, already present in Prof Lay's laboratory, synthesized in 8 steps from L-fucose[240]. This crystalline solid presents a non-participating 2-O-benzyl group and 3,4-O-acetyl groups to provide stability with respect to the fully benzylated imidate.

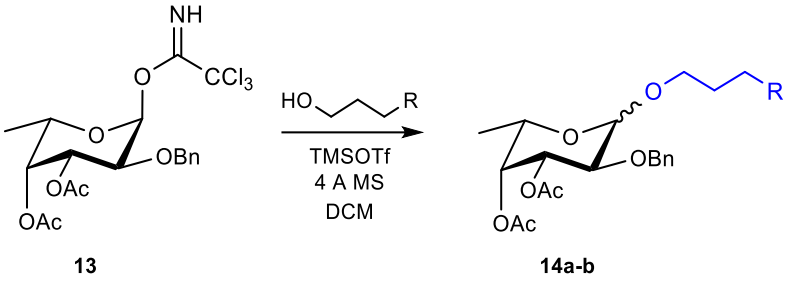

13 **14a-b**

Scheme 7. General linker introduction conditions

Table 3. Conditions for the linker introduction step

Entry	Acceptor (2 eq.)	Temperature	Approach	α : β
1	HO NHCbz	-20 ºC to 0 ºC	Classical	3:7
2	HO NHCbz	0 ºC	Classical	4:6
3	HO NHCbz	0 ºC to r.t.	Inverse	1:1
4	HO Br	0 ºC to r.t.	Classical	1:1
5	HO Br	0 ºC to r.t.	Inverse	1:1

In the first two attempts, both donor and linear alcohol were dissolved in DCM and TMSOTf (0.05 to 0.2 eq.) was added to promote the reaction, under classical glycosylation conditions (Table 3, entries 1 and 2). Alternatively, the inverse procedure (pioneered by Schmidt et al.[241]) consisted in a slow addition of the donor to a solution of the linker and the acid promoter. Different linkers, rates of addition and temperatures were tested but the outcome was always a mixture of the two anomers in yields up to 80 %. The α/β ratio of the products was determined by integration of typical anomeric signals in the corresponding ^{1}H NMR spectra. The β anomeric signal appears at 4.4 ppm as a doublet with a $J_{1\text{-}2}$ = 7.7 Hz whereas the α anomeric signal can be found at 5.15 ppm with $J_{1\text{-}2}$ = 3.2 Hz. Despite numerous efforts, the desired α anomer could not be isolated using traditional separation methods such as column chromatography or crystallization and this approach was abandoned.

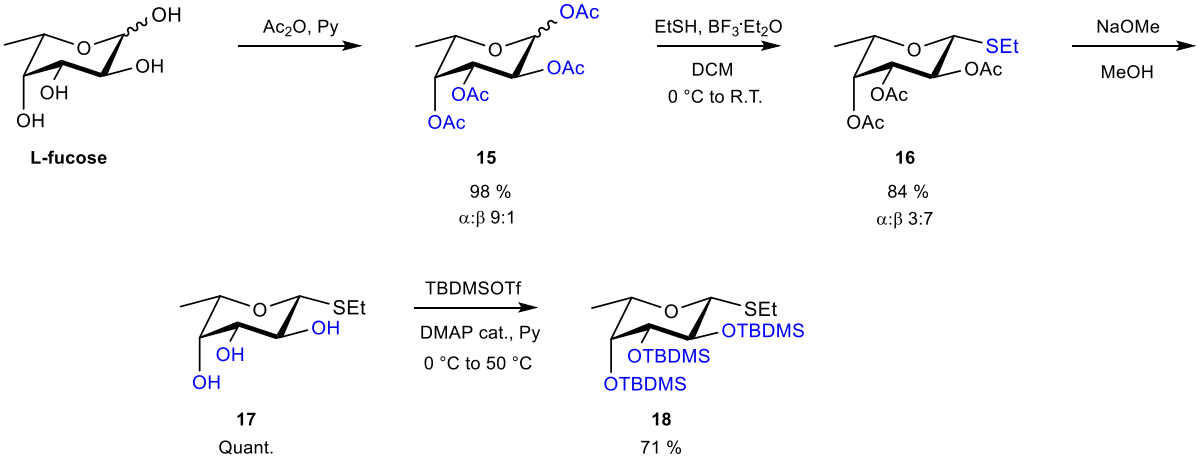

*Scheme 8. Synthesis of "super armed" donor **18***

Recently, Daly and co-workers suggested the use of bulky tert-butyldimethylsilyl (TBDMS) ethers as protective groups for improved stereocontrol of fucose donors[239]. The preparation of the new donor **18** started with per-acetylation of L-fucose and activation on the anomeric position as an ethyl

thioglycoside by treatment with etanthiol (Scheme 8). The thiofucopyranoside **16** was obtained as a mixture of two anomers and upon isolation of the β anomer, the acetyl groups were replaced by non-participating and sterically hindered O-TBDMS ethers, TBDMSOTf was used as silylating agent since it proved to be more efficient than TBDMSCl to obtain the fully protected donor **18**. Apart from their non-participating nature, silyl ethers offer enhanced reactivity due to the "super arming" effect. This effect was first described by Pedersen et al. and it is related to a conformational change induced by the steric bulk of silyl protective groups [242]. Significant line broadening in the ^{1}H NMR suggested that compound **18** was being forced out of the usual $^1C_4$ conformation.

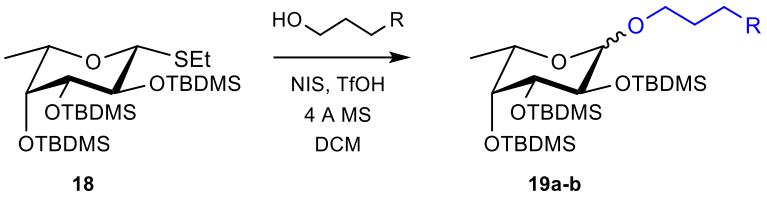

Scheme 9. General linker introduction conditions

Thiofucoside **18** was coupled with different linkers in the presence of freshly recrystallized *N*-iodosuccinimide (NIS) and triflic acid (TfOH) (Scheme 9). The reaction was carried out at increasing temperature (Table 4) to favor the S_N2 over the S_N1 mechanism since according to Scheme 10, reaction through the fucosyloxocarbenium ion would result in a loss of steric control. Even if Daly et al. reported excellent α-selectivity using this same donor[239], compound **19** was again obtained as an indistinguishable mixture of two anomers. This might be due to the fact that linear alcohols have more conformational freedom compared to traditional saccharide acceptors, and thus they feel the steric effect of the protecting groups to a lesser extent, allowing attack from both faces of the donor even under S_N2 control.

Table 4. Specific linker introduction conditions

Entry	Acceptor (2 eq.)	Temperature	Yield	α : β
1	HO NHBoc	-20 °C	70 %	6:4
2	HO NHBoc	-10 °C	72 %	7:3
3	HO NHBoc	0 °C	57 %	7:3
4	HO NHCbz	0 °C	65 %	7:3

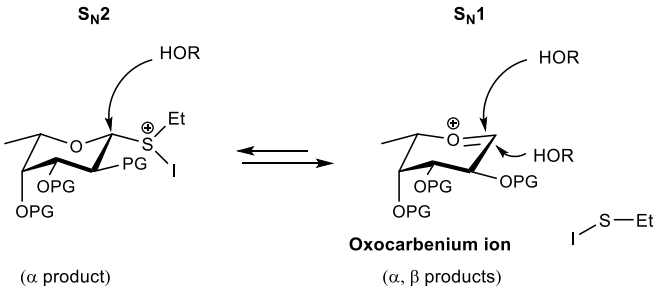

Scheme 10. S_N1 vs S_N2 mechanism of glycosylation with ethylthio β-fucopyranosides

In a third attempt, the ethyl β-thiofucopyranoside **18** was converted into the α-fucosyl bromide **20** using bromine (Br_2) in DCM at 0 °C. The bromine in excess was quenched with 1,4-ciclohexadiene and the glycosyl bromide was reacted without further purification with the linear aglycon in the presence of tetrabutylammonium bromide (TBAB). Under *in situ* anomerization conditions, the desired α-anomer

was obtained exclusively and in excellent yield using both 3-(benzyloxycarbonyl)-aminopropyl and 3-(tert-butoxycarbonyl)-aminopropyl as linkers in 92 % and 80 % respectively. In reaction Scheme 11, only the results with the best outcome have been reported. The silyl ethers were removed using TBAF in THF, followed by an additional acetylation step to remove traces of TBAF. Compound **22** was deacetylated and the -NHCbz group was cleaved using H_2 and Pd/C to obtain the target compound **3** in 10 steps with an overall yield of 36 %.

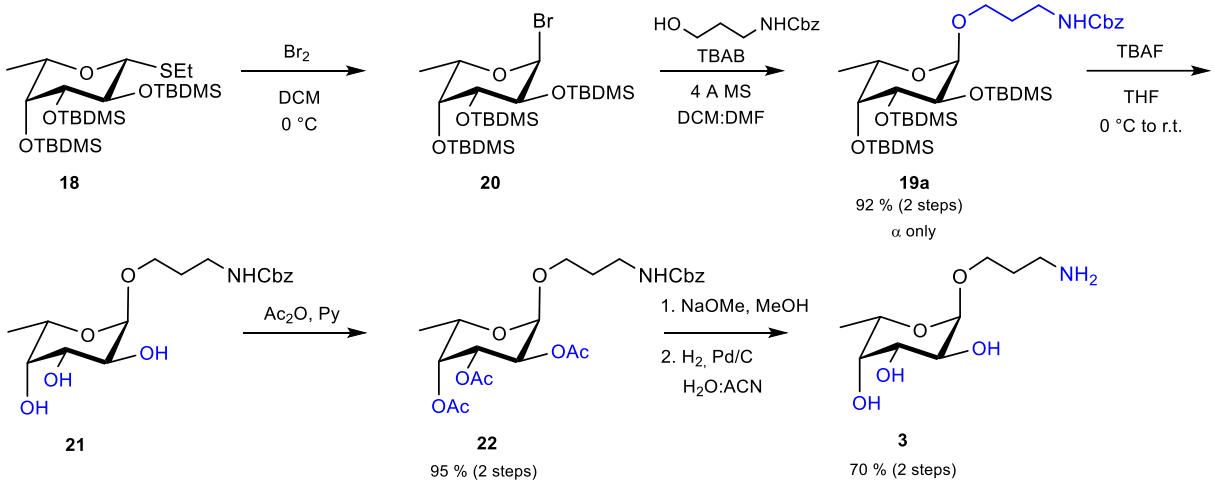

Scheme 11. Third approach for the synthesis of 3'-aminopropyl α-L-fucopyranoside

In parallel, compound **3** was successfully prepared using, the same strategy reported in Scheme 5 to prepare 3'-aminopropyl α-galactopyranoside. This strategy, first reported by Hindsgaul and co-workers[243] for the preparation of α-fucosides, afforded 3'-aminopropyl α-fucopyranoside as a single anomer in less steps and better overall yield (Scheme 12).

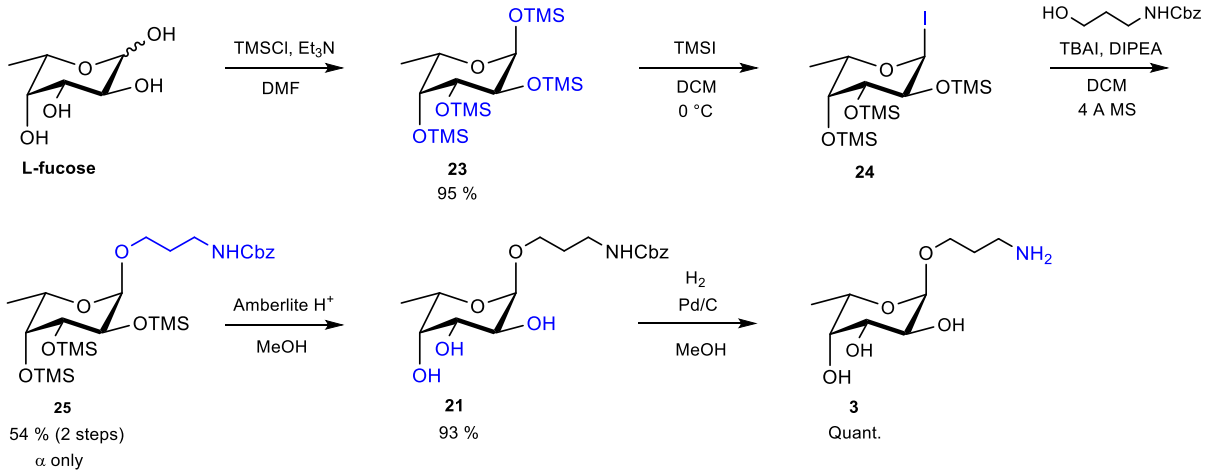

Scheme 12. Fourth approach for the synthesis of 3-aminopropyl α-L-fucopyranoside

3.4. Synthesis of AuGNPs

In order to perform PC studies, monosaccharides **1**, **2** and **3** were coupled to polyethylene glycol (PEG) spacers to favor their interaction with lectins since, according to previous findings, direct functionalization of NMs with sugars would limit their accessibility[184]. In our case, two PEG derivatives were chosen, differing in length and hydrophilicity:

-HS-PEG5000-COOH is amongst the most used surface coatings in the design of stealth NPs for biomedical application and it consists in a long, hydrophilic chain of 5000 g/mol.

-HS-Alkyl-PEG600-COOH is constituted by a short aliphatic chain (undecanthiol) attached to a PEG chain of 600 g/mol. Its amphiphilic nature guarantees a tighter ligand packing and has proven to efficiently reduce non-specific interactions with proteins in the media[227,244].

Both polymers present a thiol moiety to be anchored to the gold surface and a carboxylic group that, upon activation, reacted with the free amino group in the target monosaccharides. PEG5000 was activated as a pentafluorophenyl ester and purified by precipitation in Et_2O according to a procedure reported by Pitirollo et al.[245]. Then, it was coupled to the different monosaccharides in the presence of *N,N*-diisopropylethylamine (DIPEA) as reported in Scheme 13. The coupling was confirmed by ^1H NMR.

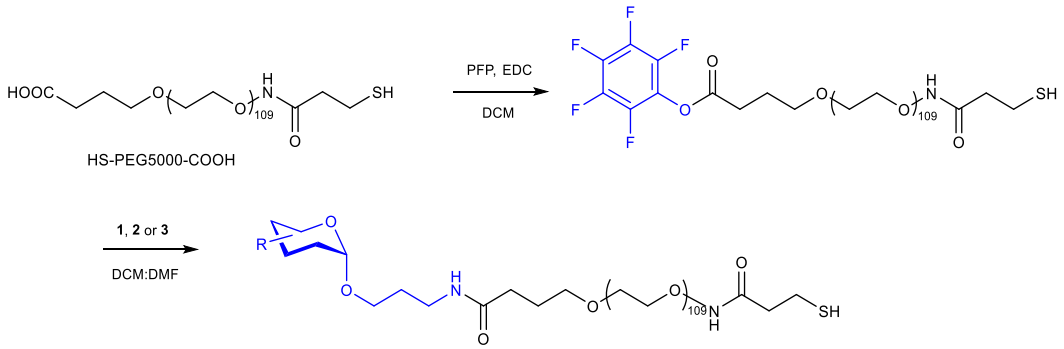

Scheme 13. PEG5000-Sugar coupling

Since the pentafluofophenyl ester of Alkyl-PEG600 resulted to be an oil, its purification could not be attained by simple precipitation in Et_2O or other common organic solvents. Hence, in this case, the carboxylic acid group was activated *in situ* using 1-ethyl-3-(3-dimethylaminopropyl)carbodiimide (EDC) and *N*-hydroxysulfosuccinimide (sulfo-NHS) followed by reaction with the target sugars as shown in Scheme 14. Once again, ^1H NMR confirmed the attachment.

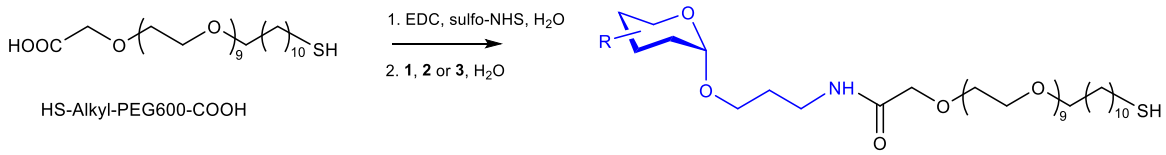

Scheme 14. Alkyl-PEG600-Sugar coupling

It is important to note that in both cases, before coupling to the Au NPs, the previously prepared linkers were treated with dithiothreitol (DTT) to ensure the reduction of potential disulfide bonds into free thiols for more efficient coupling to gold.

The synthesis of Au NPs was performed in collaboration with Dr. Laura Polito's team at CNR-SCITEC following their optimized seed mediated Turkevich protocol[54] which allowed to obtain isotropic nanoparticles without intermediate purifications and with great control over the morphology, size and size distribution.

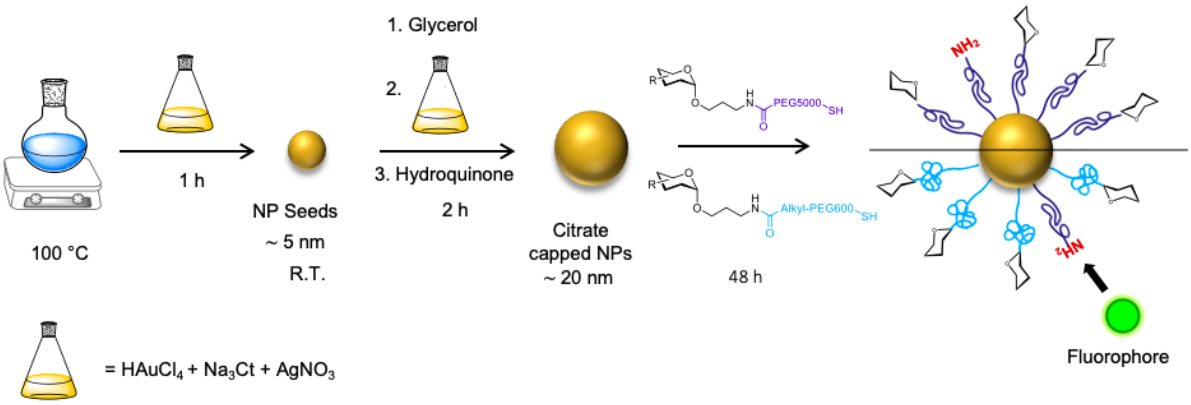

Figure 13. Preparation of 20 nm Au glyco-NPs

The synthesis started by adding a pre-incubated mixture of $HAuCl_4$, sodium citrate (Na_3Ct) and silver nitrate ($AgNO_3$) to a refluxing water solution. The sodium citrate immediately reduced Au (III) to Au (0) to form NPs seeds, but to ensure complete reduction of the gold precursor and homogenization of the gold crystals, the reaction mixture was kept under stirring at 100 ºC for 1 h. The second stage consisted in the growth of the preformed seeds and for that, the solution was cooled down to room temperature before adding glycerol and new pre-incubated mixture of $HAuCl_4$, $AgNO_3$ and Na_3Ct. Immediately after, a solution of hydroquinone, acting as second reducing agent, was added. The addition of glycerol during the growing stage ensured control over uniformity and size distribution whereas $AgNO_3$ acted as templating agent to suppress the secondary nucleation and reshape the polycrystallinity. During 2 h the NPs were allowed to grow at room temperature, to obtain citrate stabilized NPs of about 20 nm. At this point, the nanoparticles were prevented from further growing by adding the thiolated linkers previously prepared (Scheme 13Scheme 14) and stirred for 48 h to obtain the desired AuGNPs. For all particles, 10 % of the surface was coated with HS-PEG5000-NH_2 to allow subsequent labeling with a fluorophore. The functionalized AuGNPs were purified and concentrated to a final volume of 10 ml using Amicon centrifugal filters (30 KDa cut-off).

The same procedure summarized in Figure 13, was applied to prepare a panel of six AuGNPs wich were characterized by means of Transmission Electron Microscopy (TEM), UV-Vis spectroscopy, and Dynamic Light Scattering (DLS) and the results are summarized in Table 5. TEM micrographs showed that Au NPs range in diameter from 13 to 23 nm (Figure 14 and Figure 15). The subsequent steps at CIC BiomaGUNE are the fluorescent labelling of these NPs and incubation with lectins in order to study the interaction using FCS and FCCS.

a.

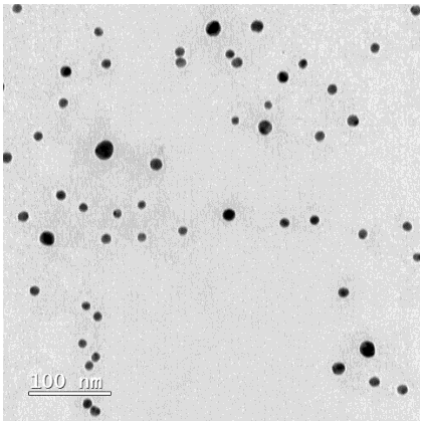

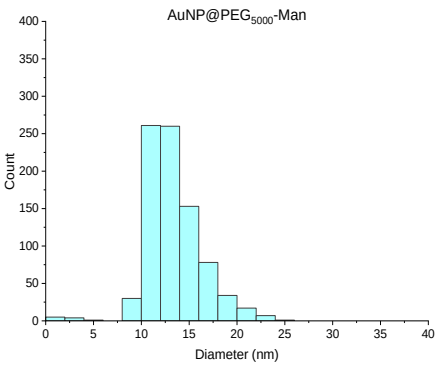

b.

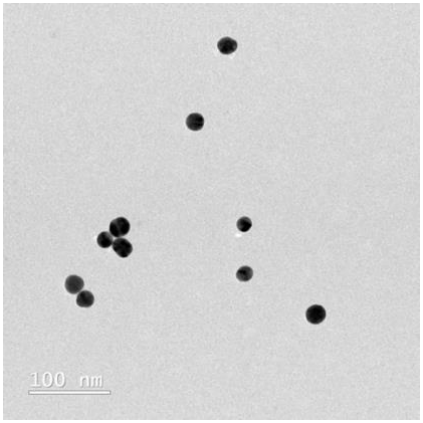

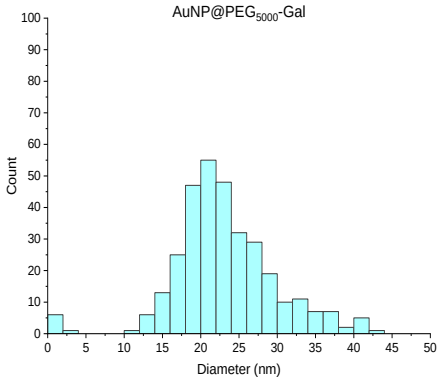

c.

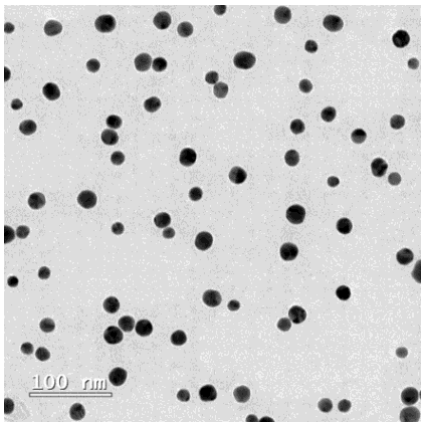

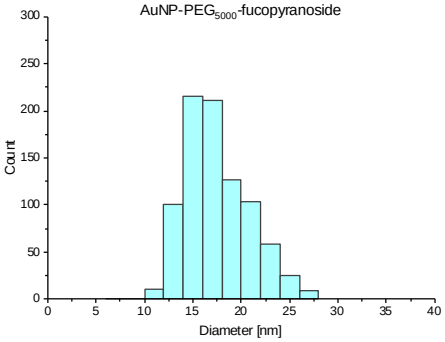

Figure 14. TEM images of a. AuNPs-PEG5000-Man (D: 13.4 ± 3.0 nm), b. AuNPs-PEG5000-Gal (D: 23.1 ± 6.7nm) c. AuNPs-PEG5000-Fuc (D: 17.5 ± 3.3 nm)

a.

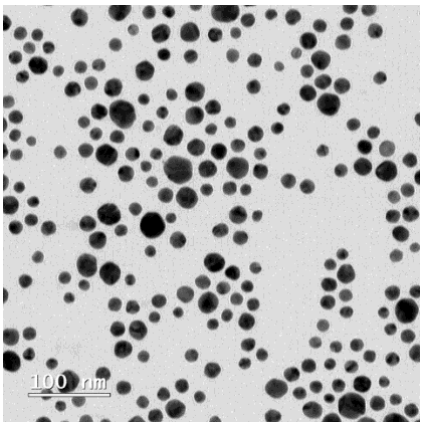

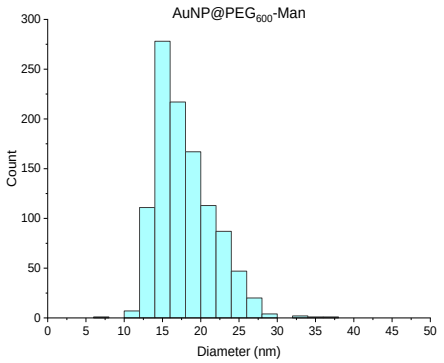

b.

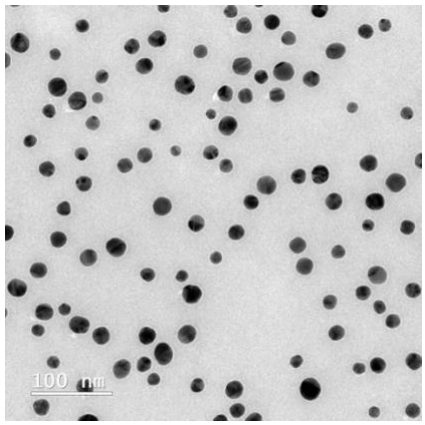

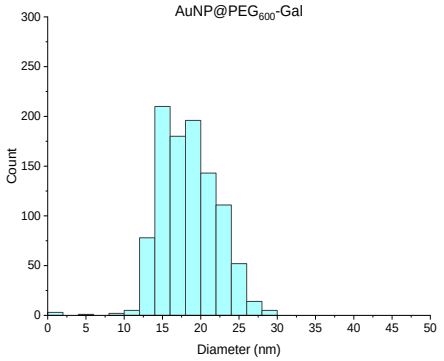

c. 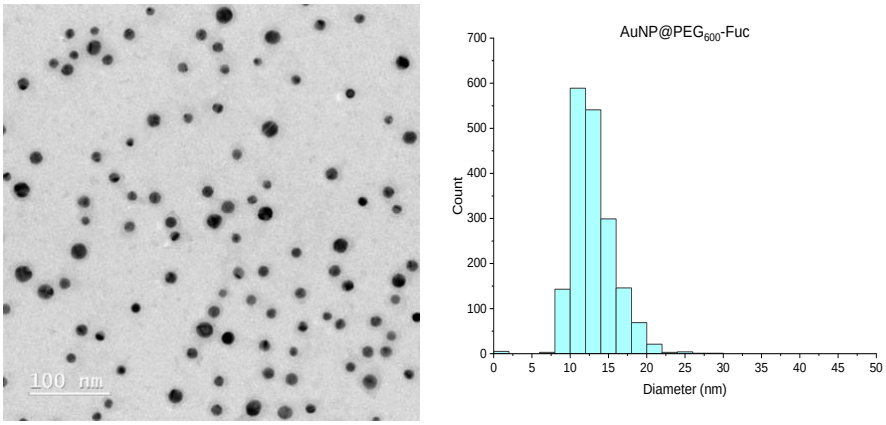

Figure 15. TEM images of a. AuNPs-Alkyl-PEG600-Man (D: 17.9 ± 3.7 nm), b. AuNPs-Alkyl-PEG600-Gal (D:18.4 ± 3.7 nm) c. AuNPs-Alkyl-PEG600-Fuc (D: 13.0 ± 2.7 nm)

Table 5. Summary of the AuGNPs characterization

	TEM		**DLS**		**UV**
	Core D (nm)	SD (nm)	D_H (nm)	PDI (nm)	λ_{max}
Au-PEG5000-Man	13.4 ± 3.0	3.0	39.4	0.2	524 nm
Au-PEG5000-Gal	23.1 ± 6.7	6.7	46.9	0.3	520 nm
Au-PEG5000-Fuc	17.5 ± 3.3	3.3	40.0	0.2	524 nm
Au-PEG600-Man	17.9 ± 3.7	3.7	32.3	0.3	525 nm
Au-PEG600-Gal	18.4 ± 3.7	3.7	33.7	0.1	526 nm
Au-PEG600-Fuc	13.0 ± 2.7	2.7	29.2	0.2	520 nm

4. Negatively charged AuGNPs

The correlation between NMs surface functionalization and interaction with proteins in the media has been extensively studied, however, the effect of the surface charge is not so well-established. The scarce *in vivo* studies generally report that negatively-charged Au NPs evidence lower phagocytic uptake in comparison to positively-charged equivalents, thereby contributing to the elongation of their circulation times, accumulation in target tissues and biocompatibility[122,246,247]. *In vitro*, charged NPs present a loss of tendency towards aggregation via electrostatic repulsion, but tend to adsorb more proteins than neutral NPs[248]. Nicoarã et al. proved how negatively charged NPs absorbed less BSA than their positive counterparts, the results can be explained by considering the isoelectric point of the protein, which at physiological pH is slightly negatively charged[134]. Likewise, negatively charged NPs will be covered by positively charged proteins. Immunoglobulins and other opsonins are known to have a negative net charge, interacting preferentially with positively charged NPs. This is consistent with the widely accepted understanding that positive NPs are more likely to attract macrophages, be cleared and display stronger acute toxicity. However, negatively charged NPs have been investigated less thoroughly and need further research.

As outlined in the "aim of the project" section, in order to elucidate how and if the surface charge may affect the colloidal stability and the interaction with proteins in the media, the second part of this chapter focused on the preparation of negatively charged monosaccharides bearing a linker suitable for subsequent NMs functionalization (Figure 16). The first two targets were mannose derivatives with a

phosphate or sulfate group in position 6 (**26** and **27**, respectively) which upon coupling to Au NPs through PEG derivatives will allow direct comparison with the previously prepared mannosylated AuGNPs in terms of colloidal stability and PC attenuation by means of dynamic light scattering (DLS) and Differential Centrifugal Sedimentation (DCS). These studies will be performed in the near future in collaboration with Dr. M. Monopoli's research group at the Royal College of Surgeons in Ireland (RCSI). Sialic acid was chosen as a third target given its intrinsic negative charge and immunomodulatory features. Sialylated Au NPs have been prepared at the CNR-SCITEC and used in Mario Negri's institute to perform *in vivo* tests.

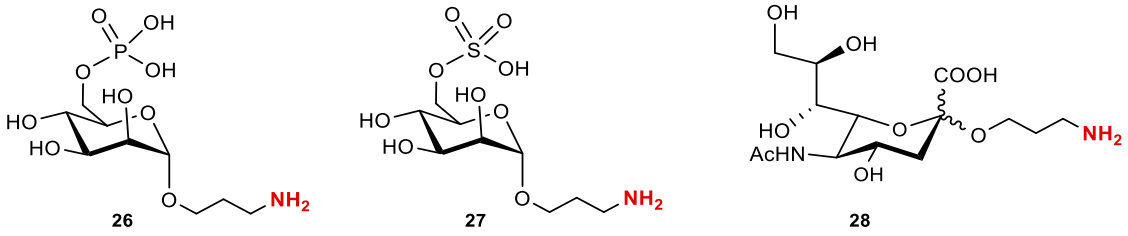

Figure 16. Negatively charged targets

4.1. Synthesis of negatively charged mannose derivatives

The synthesis of the two negatively charged mannose derivatives started from intermediate 7 (Scheme 15). Initially, the primary alcohol was regioselectively protected with bulky TBDMSCl and the remaining hydroxy groups were benzylated to form compound **30**. The cleavage of the silyl ether using TBAF afforded intermediate **31** with the 6-OH free for functionalization with negatively charged groups.

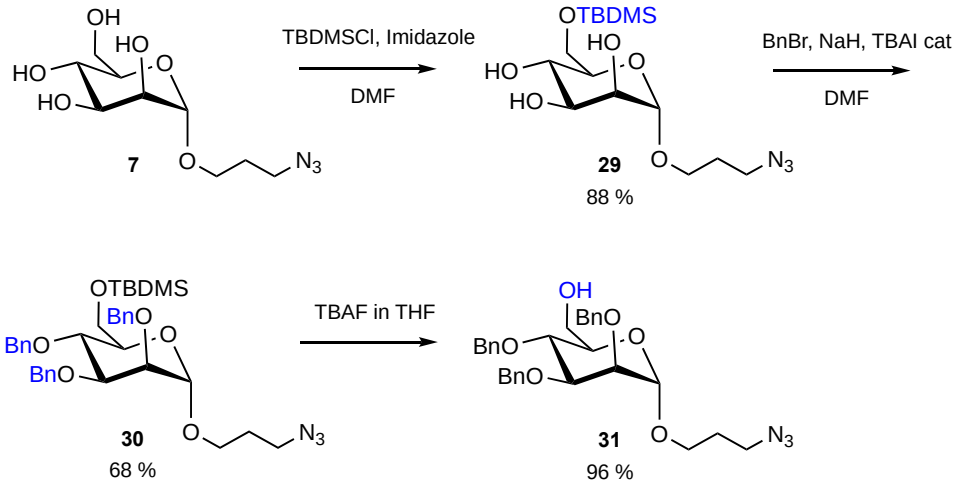

*Scheme 15. Synthesis of 3'-aminopropyl 2,3,4-tri-O-benzyl-α-D-mannopyranoside **31***

4.1.1. Synthesis of 3'-aminopropyl 6-O-phospho-α-D-mannopyranoside

Within the cell, mannose is phosphorylated by hexokinases to produce mannose-6-phosphate (M6P), a key targeting signal that binds lysosomal hydrolases and transports them into the lysosomes where they are recognized by mannose 6-phosphate receptors (M6PR)[249]. Moreover, this receptor is overexpressed in other pathologies such as solid tumors, particularly breast cancer[250], fibrosis or neurodegenerative diseases[251], hence, it can be considered as a mean to address cytotoxic drugs to lysosomes[251,252].

The phosphorylation of intermediate **31** took place in two steps first described by Watanabe and co-workers[253] (Scheme 16).

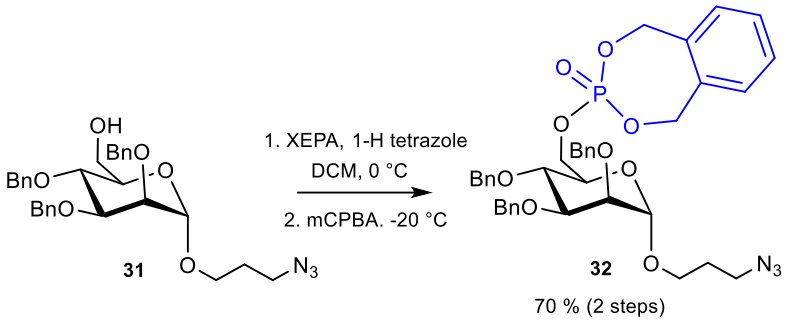

*Scheme 16. Synthesis of compound **32***

The mechanism of the first step is detailed in Scheme 17: initially, the amino group of *N*,*N*-diethyl-1,5-dihydro-2,3,4-benzodioxaphosphepin-3-amine (XEPA) is protonated in the presence of 1H-tetrazole. The resulting tetrazolide anion can displace the protonated amine to form a more reactive species which can undergo a nucleophilic attack from 6-OH of intermediate **31** to afford the intermediate phosphite. In a second step, the posphite was oxidized to phosphate in the presence of m-chloroperbenzoic acid (mCPBA).

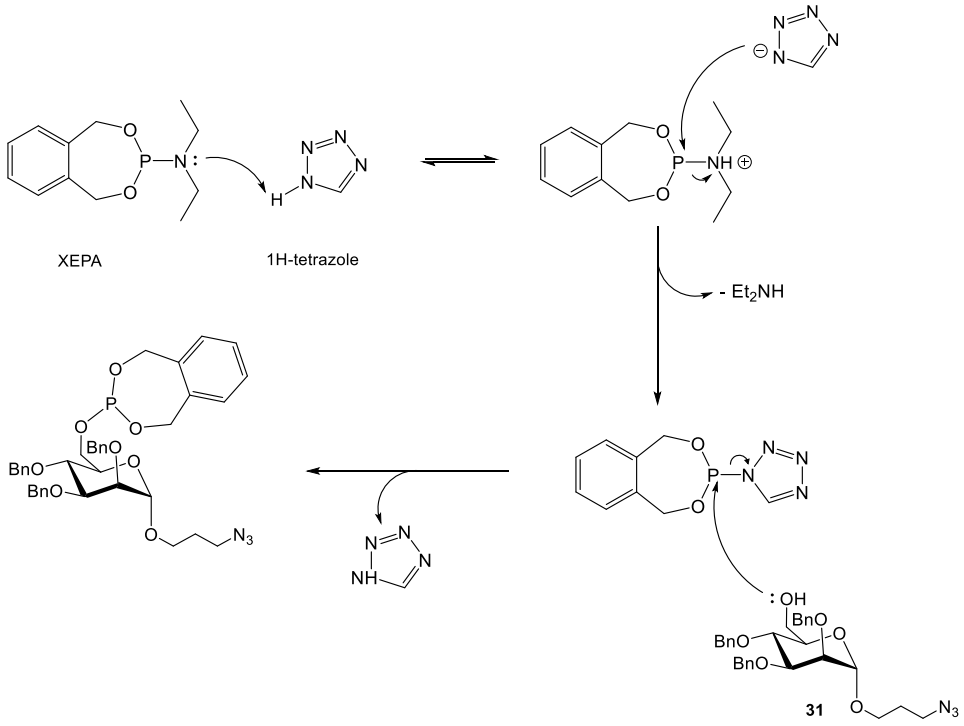

*Scheme 17. Mechanism of phosphytilation of intermediate **31***

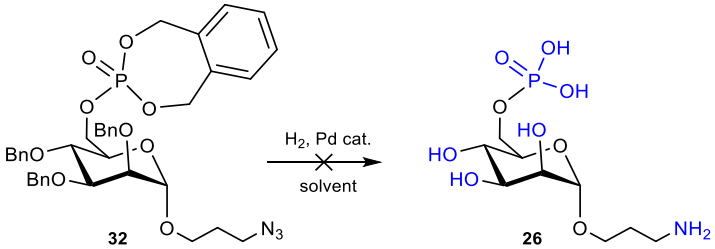

*Scheme 18. Hydrogenation of compound **32***

The use of XEPA as phosphorylating agent had been previously reported in Prof. Lay's group[254] given the effectiveness of the coupling and the convenience of the deprotection, which theoretically should afford the target molecule **26** in a single hydrogenation step as shown in Scheme 18.

However, even though numerous conditions were tested, the full deprotection of compound **32** was not achieved. Initially, the reaction was performed at atmospheric pressure, but according to ^{1}H NMR some benzyl groups were still present after several days of reaction (Table 6, entry 1). In a second attempt, a drop of acetic acid (AcOH) was added to the reaction mixture to avoid the poisoning of the Pd catalyst by the free amine forming, but the results were similar (Table 6, entry 2). Neither the pressure increase nor the change of catalyst (Table 6, entries 3 and 4) afforded the fully deprotected compound **26**, and a new strategy was adopted.

*Table 6. Conditions for the hydrogenation of compound **32***

Entry	H_2 pressure	Solvent	Catalyst	Time
1	atm	MeOH:H_2O 1:1	Pd/C	3 days
2	atm	MeOH:H_2O 1:1 + AcOH drop	Pd/C	3 days
3	5 bars	MeOH:H_2O 1:1 + AcOH drop	Pd/C	2 days
4	atm	MeOH:H_2O 1:1 + AcOH drop	Pd black	4 days

In a second attempt, the phosphate moiety was introduced directly through a Mitsunobu coupling, using dibenzyl phosphate as a phosphorous source. Unlike diphenyl phosphate, the former allows the final hydrogenolysis in a single step, facilitating the formation of target **26**.

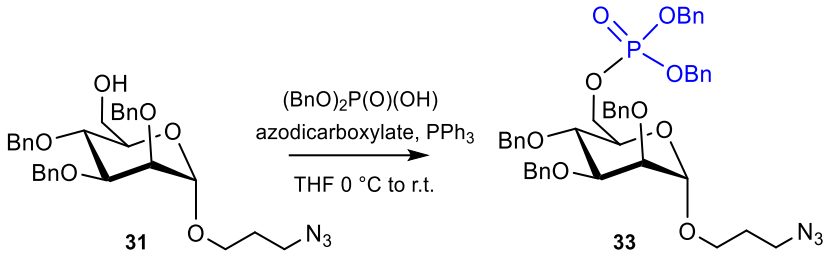

*Scheme 19. Synthesis of compound **33***

Thus, compound **31** reacted in the presence of dibenzyl phosphate, triphenylphosphine (PPh_3) and diisopropyl azadicarboxylate (DIAD) in dry THF at 0°C to afford compound **33** (Scheme 19). The mechanism of the Mitsunobu reaction is reported in Scheme 20. Initially, PPh_3 attacks the azodicarboxylate to generate a phosphonium intermediate that binds the 6-OH of compound **31**, activating it as a leaving group. Then, the previously deprotonated dibenzylphosphate performs a nucleophilic attack on the activated 6-OH to form the desired phosphate **33** and triphenylphosphineoxide (Ph_3PO) as side-product.

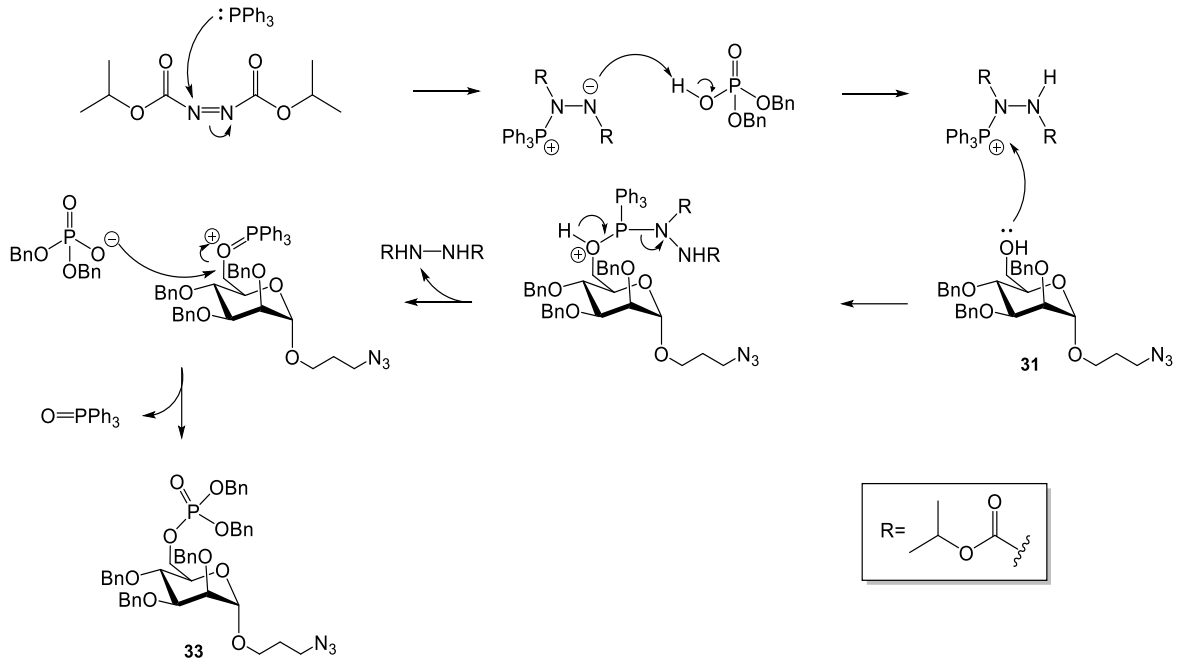

Scheme 20. Mechanism of the Mitsunobu coupling

Compound **33** was analyzed by ^{31}P NMR to confirm the presence of the characteristic phosphate peak around -2 ppm. Even if ^{1}H NMR showed no traces of Ph_3PO, it revealed the prevalence of DIAD even after an extra purification step. Therefore, DIAD was replaced by the less common di-tert-butyl azadicarboxylate (DBAD) since this reagent and its reduced form can be converted to volatile by-products (N_2, CO_2 and isobutylene) and water-soluble materials (N_2H_4) by simple acid treatment as seen in Scheme 21[255].

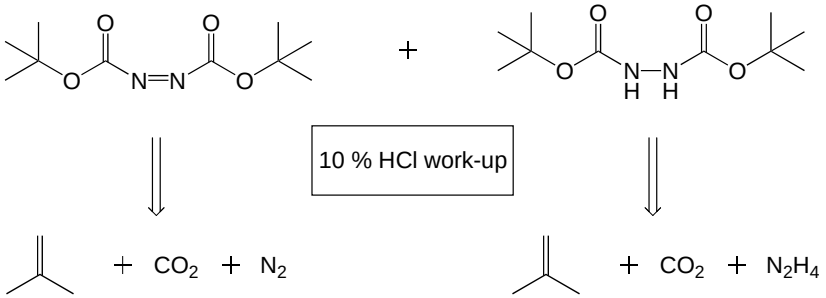

Scheme 21. Decomposition of DBAD under acid work-up

With this modified strategy, compound **33** could be obtained in 87% yield. The latter underwent hydrogenation using new conditions (Table 7), but only the use of $Pd(OH)_2/C$ as a catalyst could guarantee the full conversion of compound **33** into compound **26** in 98 % yield.

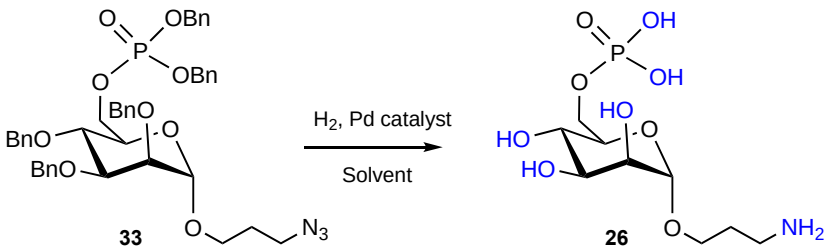

*Scheme 22. Hydrogenation of compound **33** to afford 3'-aminopropyl 6-O-phospho-α-D-mannopyranoside*

*Table 7. Conditions for the hydrogenation of compound **33***

Entry	H_2 pressure	Solvent	Pd-Catalyst	Time
1	atm	MeOH	Pd/C	2 days
2	atm	MeOH:H_2O – 1:1	Pd/C	3 days
3	3 bars	Dioxane:H_2O – 1:1	Pd/C	2 days
4	3 bars	Dioxane:H_2O – 1:1	$Pd(OH)_2$/C	4 days

4.1.2. Synthesis of 3'-aminopropyl 6-O-sulfo-α-D-mannopyranoside

Mannose-6-sulfate (M6S) has been chosen as a M6P analogue since it differs in charge density and electronic delocalization while maintaining the ability to bind M6PR[250]. Moreover, sulfonated substrates have already proven to absorb less proteins as opposed to their carboxylated counterparts[256]. Little to no reports of the use of M6S as ligands for NMs functionalization are found in literature, however, sulphated polysaccharides such as heparin sulfate and derivatives are used as anticoagulants and recently, they have proven to bind to the spike protein of SARS-CoV-2 *in vitro* inhibiting viral infection[257,258].

The sulfation of intermediate **31** was performed using a sulfur trioxide pyridine complex (SO_3·Py). After purification by column chromatography, the fractions containing the product were concentrated and eluted through a Dowex 50WX8 resin (Na^+ form) column to form the salt **34**.

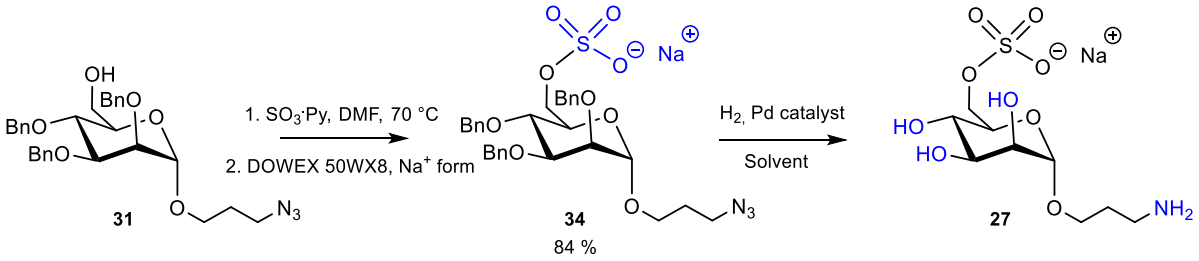

Scheme 23. Synthesis of 3'-aminopropyl 6-O-sulfo-α-D-mannopyranoside

Hydrogenation of the protected sulfo-derivative 34 was first attempted using Pd/C as catalyst and MeOH as solvent. After 20 days of reaction, compound **27** was isolated along with traces of *N*-mono- and *N*,*N*-dimethylated amine according to ^{1}H NMR and ESI^+ MS results. These unexpected side-products could be forming as a result of a slightly modified Eschweiler-Clark reductive amination in the presence of MeOH and Pd. A plausible reaction mechanism is suggested in Scheme 24.

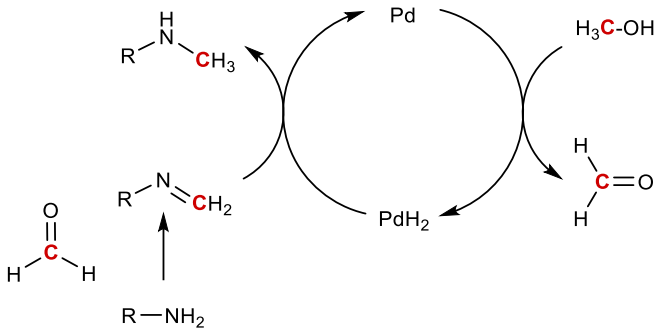

Scheme 24. Proposed mechanism for Pd-catalyzed methylation of amines

Initially, Pd abstracts hydrogen from MeOH and produces formaldehyde and Pd-H_2. Subsequently, an imine is formed via condensation with formaldehyde and hydrogenated in the presence of Pd-H_2 species to form *N*-methylaniline and restore Pd. Then, *N*-methylaniline again undergoes condensation with formaldehyde followed by the hydrogenation to give *N,N*-dimethylamine[259].

Therefore, compound **34** was prepared again and hydrogenated using a mixture of water:dioxane 1:1 to avoid this undesired side-product. However, after more than 15 days of reaction, the ^{1}H NMR spectrum still showed some remaining benzyl ethers. Once again, only the use of $Pd(OH)_2/C$, could afford target compound **27** in 84 % yield.

4.2. Synthesis of Sialic Acid

More than 60 structural modifications of the basic neuraminic acid molecule, 5-amino-3,5-dideoxy-2-nonulosonic acid (Neu), can be found. The most prevalent variant in human cells is *N*-acetylneuraminic acid (Neu5Ac) with an acetyl group at position 5. The naturally occurring isomeric form, in which the carboxylic group in the anomeric center is in the axial orientation, is by convention, referred to as the α-form.

In our organism, Neu5Ac, is often found at the nonreducing end of glycoconjugates and it is associated with important biological recognition events and disease states. It is recognized as a "self" marker by major serum protein complement factor H avoiding complement system activation and presents strong immunomodulatory properties via sialic acid-binding immunoglobulin-like lectins or Siglecs, immunosuppressive receptors on the surface of immune cells[260]. Neu5Ac not only attenuates the immune response, it also facilitates active targeting owing to its ability to bind E- and P-selectins, transmembrane glycoproteins up-regulated as part of the host response to injury or disease[261,262].

Thus, sialylation of therapeutic formulations has been explored as an alternative to improve their pharmacokinetics[263]. In a similar manner, surface functionalization of NMs with sialic acid derivatives could grant them new therapeutic possibilities. Apart from being a self-antigen, Neu5Ac can help by-pass the immune system conferring the nanosystems the ability to circulate in the bloodstream over a prolonged period of time for successful delivery. In addition, specific delivery can be achieved by exploiting its targeting ability. Both *in vivo* and *in vitro* results on nanocarriers, modified with different Neu5Ac derivatives, have highlighted the great potential of this approach[261,264–266]. For example, Kim and co-workers[263] proved that functionalization of Au NPs with sialic acid decreased phagocytosis by macrophages *in vitro* and conferred prolonged systemic circulation and improved tumor targeting ability *in vivo*. This observation implies the potential application of surface modification with sialic acid derivatives as a safe way to obtain long-circulating nanocarriers with enhanced tumor accumulation.

For that purpose, to facilitate the functionalization of NMs, commercially available Neu5Ac was functionalized with the same C3 spacer with a free amino group (Scheme 25). As a first step, the carboxylic acid was masked as a methyl ester to obtain compound **35**. Acetyl chloride was then used to simultaneously acetylate all the hydroxy groups and activate the anomeric position as a β-sialyl chloride.

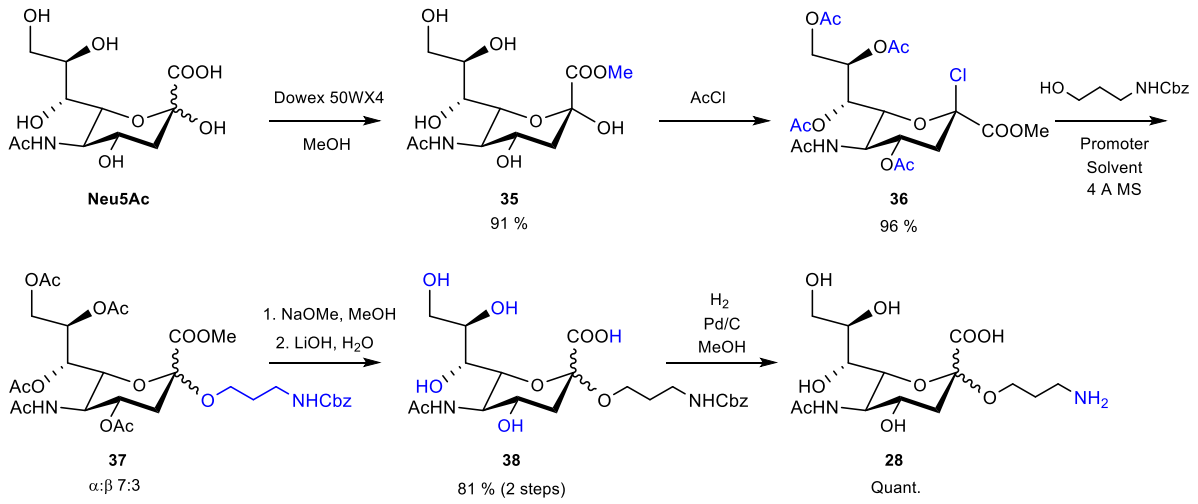

*Scheme 25. Synthesis of compound **28***

Compound **36** was reacted with different linkers, silver-based promoters and solvents at room temperature and under the exclusion of light according to the classical Koenigs-Knorr conditions (Table 8). The best outcome was obtained using 3'-(benzyloxycarbonyl)-aminopropyl as linker (Table 8, entry 4). Once again, control of the stereoselectivity proved to be challenging, even in the presence of apolar solvents favoring the S_N2 mechanism. Compound **37** was always obtained as a mixture of anomers (α:β 7:3) indistinguishable by column chromatography. The moderate yield of the reaction was attributed to the challenging separation, the presence of some unreacted starting material and some undesired glycal formation due to an elimination side reaction. The deprotection to afford the target **28** involved three consecutive steps, O-acetyl cleavage under Zemplen conditions, methyl ester hydrolysis using LiOH and the *N*-Cbz removal using H_2 and Pd/C as a catalyst.

Table 8. Conditions for the linker introduction step

Entry	Acceptor (2 eq.)	Promoter	Solvent	T	Yield	α : β
1	HO–NHBoc	AgOTf	ACN	R.T.	24 %	7:3
2	HO–NHBoc	AgOTf	DCM	R.T.	35 %	7:3
3	HO–NHBoc	Ag_2CO_3	DCM	R.T.	38 %	7:3
4	HO–NHCbz	Ag_2CO_3	DCM	R.T.	46 %	7:3

The poor yield and stereocontrol of the glycosylation reaction is one of the most challenging aspects in the preparation of naturally occurring α-sialosides given the sterically constrained tertiary anomeric center, the presence of an electron-withdrawing carbonyl group which destabilizes the formation of the oxocarbenium ion, favoring the elimination reaction, and the absence of a participating substituent adjacent to the anomeric center. All this becomes a bigger challenge if a flexible, linear alcohol is used as an acceptor.

Compound **28** has been successfully employed to functionalize Au NPs through a PEG5000 spacer at CNR-SCITEC in collaboration with Dr. L. Polito's group. These AuGNPs are being used for *in vivo* studies in collaboration with Dr. Paolo Bigini's group at Mario Negri institute in order to evaluate their circulation times and biodistribution.

5. Conclusions

In summary, this chapter has reported the synthesis of six biologically relevant monosaccharides with an anomeric linker as a handle for NMs conjugation. Several reaction conditions were tested to optimize the yield and the stereochemistry of the linker introduction step. However, it is interesting to note that no general method was found, and protocols needed to be tailored for each specific sugar. Moreover, the linker's conformational flexibility, made the stereocontrol of the reaction exceedingly challenging, especially in the case of L-fucose and *N*-acetyl-neuraminic acid.

The first three targets: 3'-aminopropyl α-D-mannopyranoside, 3'-aminopropyl α-D-galactopyranoside and 3'-aminopropyl α-L-fucopyranoside were coupled to PEG derivatives differing in length and hydrophilicty, before being used for the preparation of AuGNPs. This small library of AuGNPs are now undergoing PC studies at CIC BiomaGUNE using FCS to provide deeper insight into the PC formation. Moreover, thanks to the versatility of the short C3 linker, these aminopropyl glycosides are being used by other partner organizations at NanoCarb to functionalize NMs with different purposes.

Apart from surface coating, surface charge may be a primary determinant of protein binding. In the second part of the chapter, phosphate and sulfate groups were regioselectively introduced to mannose primary hydroxy group to obtain 3'-aminopropyl 6-O-phospho-α-D-mannopyranoside and 3'-aminopropyl 6-O-sulfo-α-D-mannopyranoside. These sugars will be used to coat Au NPs and perform comparative studies with neutral mannosylated Au NPs to try to assess how and if the NMs' surface charge can influence their colloidal stability and interaction with proteins in the media. For that purpose, NPs will be incubated with different lectins in order to perform comparative assays by means of DLS and DCS at RCSI. Hopefully, the combined results of these two studies will provide a better understanding of the effect of the surface functionalization and charge on the PC formation paving the way towards more promising glycosylated Au NPs for biomedical applications.

Finally, *N*-acetyl neuraminic acid was also modified with the same short spacer and employed in the functionalization of Au NPs. These sialylated Au NPs are expected to show increased colloidal stability and reduced protein binding due to the negative charge but also an increased circulation time thanks to the immunosuppressive characteristics of the sugar. All these assumptions will be tested *in vivo* at Mario Negri institute.

CHAPTER II: SYNTHESIS OF BLOOD SUGAR ANTIGENS

1. ABO blood group system

The Austrian immunologist K. Landsteiner discovered the ABO histo-blood group system in 1900 after noting patterns of agglutination during blood transfusions, his finding earned him the Nobel Prize in Medicine in 1930. However, the structure of the underlying carbohydrate epitopes behind each group were not elucidated until 1957 by W. M. Watkins and W. J. Morgan[267]. The three antigenic determinants represented in Figure 17 can be found at the termini of oligosaccharide chains linked to glycoproteins and glycolipids on the surface of human red blood cells (RBC), other body fluids and tissues such as epithelial and endothelial cells[268].

Apart from defining an individuals' blood group, the physiological role of ABO blood group antigens remains a mystery. However, many biological phenomena associated with them have been found: some pathogens, such as *E. coli*, display blood group antigens on their cell surface to evade the immune system of the human host[269] whereas others, such as *C. jejuni*[270] and *Norovirus*[271], exploit these antigens as receptors for colonization[272]. They can be used as diagnostic and prognostic markers since they are aberrantly expressed during oncogenesis and inflammatory processes[273,274]. Numerous associations between increased susceptibility to certain infectious and non-infectious diseases and particular ABO phenotypes have been made[275–277]. Finally, they are key factors to take into account during both blood transfusion and organ transplantation.

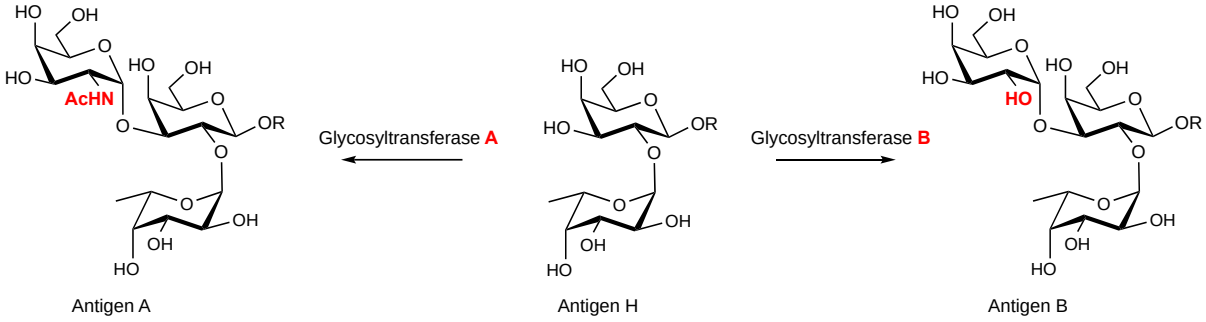

Figure 17. Structures of the A, B and H(O) antigens. R = Glycoprotein, glycolipid or free oligosaccharide

As shown in Figure 17, the H determinant consists of a fucose residue α1-2 linked to a galactose. This disaccharide is the common backbone that almost all individuals express and may be converted into A or B antigens by adding a terminal *N*-acetyl-galactosamine or galactose α1-3-linked to the non-reducing end of the galactose residue, respectively. The addition is catalyzed by a specific glycosyltransferase dependent on an individual's inherited allele, a subtle genetic difference with a critical impact: individuals of a particular blood group only tolerate the antigen found in their system and produce IgM and IgG antibodies, also known as allo-antibodies, against the other antigen as indicated in Table 9. This is crucial in blood transfusion and organ transplantation since mismatched antigens are recognized by antibodies in the recipient plasma and destructed by means of complement-mediated lysis, leading to intravascular hemolysis, coagulation and eventual death.

Type O blood is considered "universal" since it contains neither A nor B antigens and thus, can be transfused safely into recipients of any ABO blood group. A novel approach to overcome blood incompatibilities and increase the overall blood supply is the use of bacterial glycosidases to selectively

hydrolyze the αGalNAc and αGal monosaccharides from group A and B structures[278]. However, the major obstacle towards clinical implementation of this method is the large quantities of enzyme required. An alternative protocol suggests masking any antigenic epitope on the RBC surface by attachment of long, hydrophilic, biocompatible polymers such as PEG[279].

Table 9. Blood group antigens and antibodies in different blood types where R represents the six disaccharide subtypes

Blood Group	Antigenic epitope	Antibody in serum
A	GalNAcα1-3(Fucα1-2)Galβ1-O-R	Anti-B
B	Galα1-3(Fucα1-2)Galβ1-O-R	Anti-A
AB	GalNAcα1-3(Fucα1-2)Galβ1-O-R Galα1-3(Fucα1-2)Galβ1-O-R	None
O (H)	Fucα1-2Galβ1-O-R	Anti-A Anti-B

The ABO antigens can be further grouped into six subtypes (I-VI) based on the composition and the linkages of the disaccharide precursor attached to the galactose on their reducing end (Table 10)[276]. The role of these subtypes is still unclear, but they have been isolated from different tissues of the same individual[268,273] suggesting that they do not have a significant influence on the ABO immunogenicity.

Table 10. Disaccharide precursors responsible for the six subtypes of human blood, where R are the ABO antigens and R' are proteins or lipids on the cell membrane

Sub-type	Disaccharide precursor
I	R-Galβ1-3GlcNAcβ-R'
II	R-Galβ1-4GlcNAcβ-R'
III	R-Galβ1-3GalNAcα-R'
IV	R-Galβ1-3GalNAcβ-R'
V	R-Galβ1-3Galβ-R'
VI	R-Galβ1-4Glcβ-R'

In addition to the most immunogenic ABO blood group, the International Society of Blood Transfusion (ISBT) has recently recognized 32 other blood groups, 4 of which have antigens of carbohydrate nature: LEWIS, P1Pk, Ii and GLOB[280]. The Rhesus (Rh) system is the second most prominent blood system, and it is normally described with a *positive* (+) or *negative* (−) suffix after the ABO type depending on the presence or absence of an immunogenic D-antigen. The combination of these two systems gives rise to the most acknowledged 8 blood groups: O, A, B, AB with Rh + or −.

2. Aim of the chapter

The majority of NMs are being designed for parenteral or oral administration, which implies their systemic distribution throughout the body. However, keeping NPs in blood for sufficiently long times so as to allow them to reach their therapeutic target or to act as efficient contrast agents still represents a major challenge. Upon administration into blood, they are quickly opsonized and accumulated into filtering organs, thereby limiting their circulation times. Surface-modification with PEG derivatives was the first strategy to confer a so-called "stealth" effect, minimizing the attachment of opsonins and prolonging NPs circulation time, but the transient nature of this effect due to the eventual production of anti-PEG antibodies, is rendering obvious the need to look for alternatives.

Accordingly, surface modification with molecules already present in our system (self-antigens) could be an efficient strategy to obtain "stealth" NMs tolerated by the immune system. Erythrocytes are the most abundant endogenous cells that circulate through the body[281]. For decades, researchers have explored the encapsulation of drugs, biomolecules, imaging probes and even NMs inside RBCs[282–284] or attached to their membrane[281,285–287] to protect the cargo from immune recognition. However, these erythrocyte-based delivery systems often alter RBC function causing acute hemolytic reactions. Recently, the membrane of erythrocytes has been proposed as a more sophisticated strategy to cloak polymeric[288,289], gold[290,291] and iron oxide (Fe_3O_4)[292] nanosystems[293] (Figure 18). Meanwhile, other groups have focused on the preparation of artificial polymeric delivery vehicles mimicking the size, shape and elasticity of RBCs with promising results[294]. In a similar and yet unexplored manner, we envisaged a simpler approach based on the functionalization of NMs with carbohydrate antigens present on the surface of RBC, exploiting biomimicry to increase immunotolerance, elongating NMs' systemic circulation and thus, their ability to reach the desired tissues. Eventually, other targeting ligands can be also grafted onto the NMs' surface in order to avoid non-specific accumulation and off-target side effects. To the best of our knowledge, no literature reports concerning NMs functionalized with these self-markers have been published, Slaney et al. prepared silica microparticles functionalized with A or B (type I and II) blood group antigens for the detection of antigen-recognizing B cells via flow cytometry with the final aim to develop a new tool for precise and effective clinical management of ABO-incompatible transfusions[295].

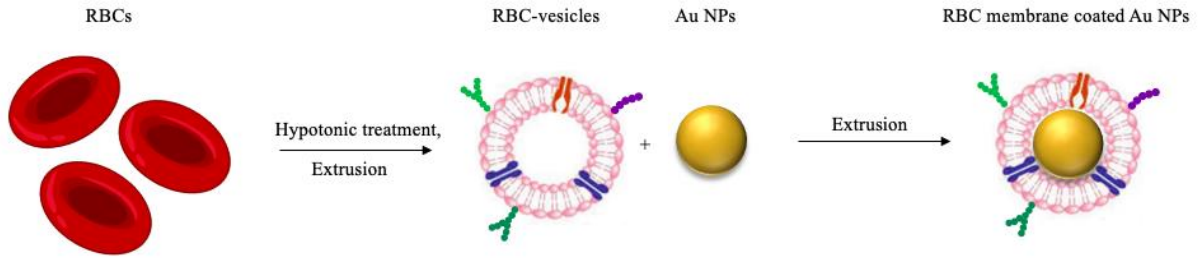

Figure 18. Schematic illustration of the preparation of RBC membrane-coated Au NPs

Note that, as opposed to one-size-fits-all approach of conventional medicine, we foresee a much more specific and personalized treatment where the NPs mimicking RBC need to match the patient's blood types to be recognized as self-markers and avoid harmful immunogenic reactions. Nevertheless, being aware of the difficulties that this approach entails from an industrial point of view, a way to implement the clinical translation would be the functionalization of nanomaterials with type O antigens which would be applicable to the entire human population regardless of their blood type.

3. Results and discussion

3.1. Retrosynthetic approach

Our synthetic efforts have been focused on the preparation of the three core ABO sugar epitopes for later NMs functionalization. A propylic aglycone with a terminal amino group was added to the reducing end of the three antigens to allow conjugation to NMs using polymers with terminal carboxylic acid groups.

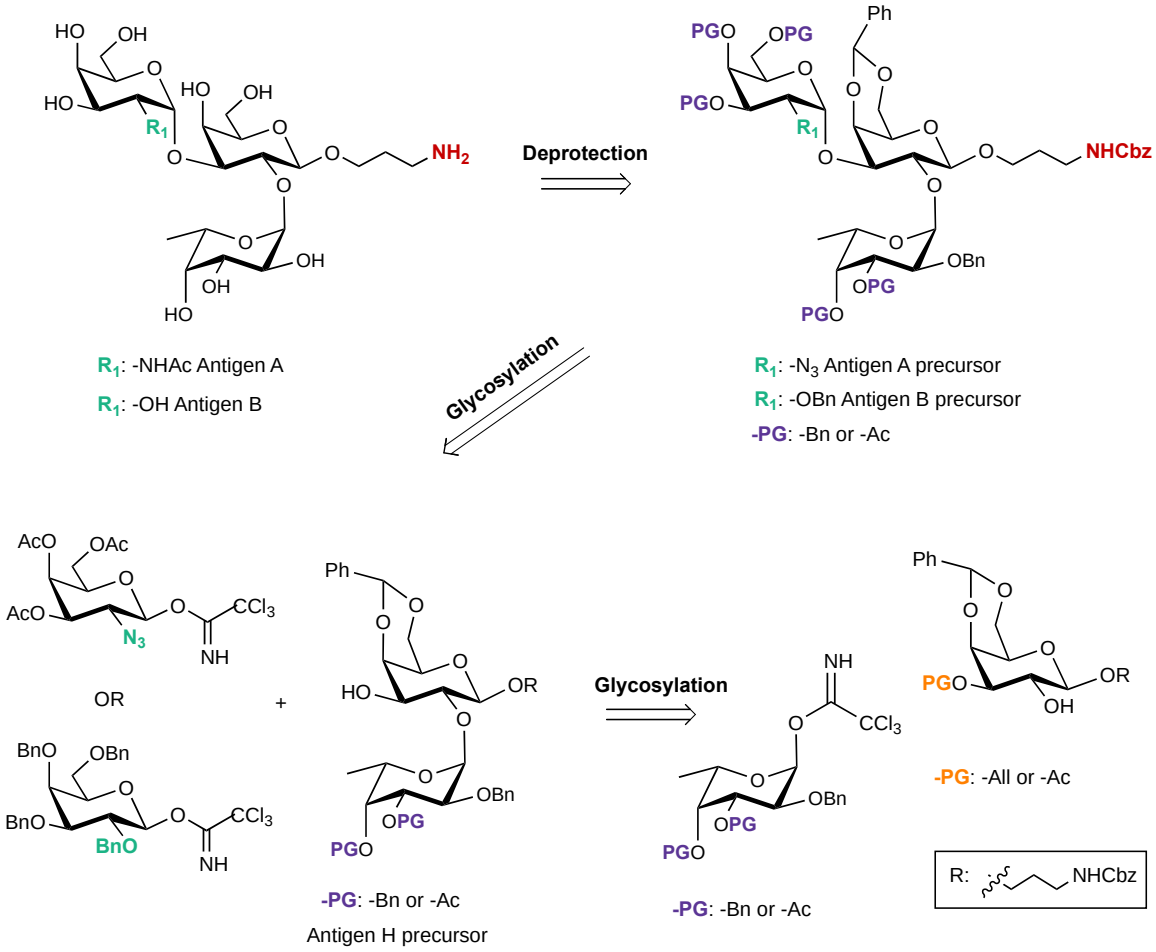

Scheme 26. Retrosynthetic approach to ABO blood sugar antigen derivatives

As the two trisaccharide antigens A and B only differ in one functional group highlighted in green in Scheme 26, they can be prepared from a common disaccharide backbone upon glycosylation with 3,4,6-tri-O-acetyl-2-azido-2-deoxy-β-D-galactopyranosyl trichloroacetimidate or 2,3,4,6-tetra-O-benzyl-β-D-galactopyranosyl thrichloroacetimidate respectively. For the synthesis of the disaccharide antigen H precursor, two building blocks were envisaged: a galactosyde acceptor with a temporary protecting group at 3-OH, in orange, for subsequent elongation, and an unprotected 2-OH to perform a nucleophilic attack on a fucosyde donor with the anomeric position activated with a leaving group. In both cases, donor and acceptor were equipped with different PG so as to "match" the reactivity of the pair and try to find the most suitable glycosylation approach to obtain the target disaccharide in good yield and α-stereoselectivity.

3.2. Synthesis of galactoside acceptors

The synthesis of three different galactoside building blocks is reported in this section, all of them with an orthogonal temporary protecting group in position 3 for further elongation and a free hydroxy group in position 2. The first two steps were the linker introduction as *N*-Cbz protected 3-aminopropanol using $BF_3{\cdot}Et_2O$ as Lewis acid to obtain compound **39** which was subsequently deacetylated to obtain 3'-(benzyloxycarbonyl)-aminopropyl β-D-galactopyranoside **40**, intermediate for the preparation of different acceptors.

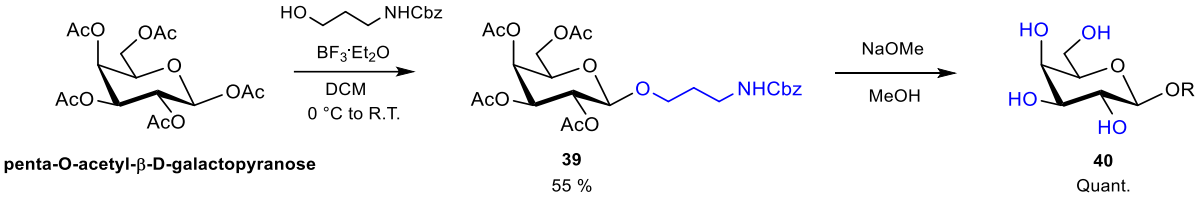

*Scheme 27. Synthesis of 3'-(benzyloxycarbonyl)-aminopropyl β-D-galactopyranoside **40***

For the preparation of the first acceptor with a benzylidene ring simultaneously masking positions 4 and 6 and a temporary *p*-methoxybenzyl (PMB) ether in position 3, a one-pot approach described by different groups for the preparation of similar glucopyranoside building blocks was adopted[296–298]. The first step involved per-silylation of intermediate **40** using hexamethyldisilazane (HMDS) activated using catalytic amount of TMSOTf as described by Wang and co-workers[299]. The procedure proved to be faster and cleaner than the traditional protection using TMSCl and TEA in DMF. The acid labile O-TMS protecting groups played an essential role in the next regioselective one-pot reaction. The first catalytic step involved a selective protection of 4-OH and 6-OH as a benzylidene acetal. In the second catalytic cycle, the TMSOTf promoted the site-selective formation of an open chain mixed acetal at 3-OH reduced in the presence of Et_3SiH to produce the 3-O-PMB protected **43**. The final step was the cleavage of the remaining 2-O-TMS using TBAF in THF (Scheme 28).

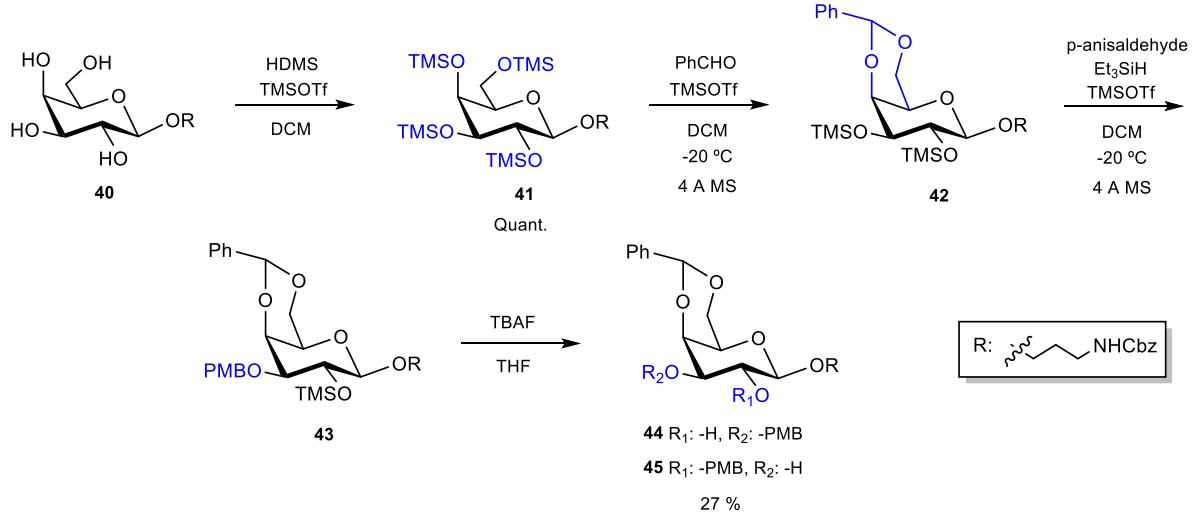

*Scheme 28. First approach to the synthesis of Acceptor **44***

However, a complex mixture of compounds was formed from which the target compound **44** could not be isolated. An undistinguishable mixture of **44** and **45** was recovered in 27 % yield. Upon acetylation, separation via column chromatography and deacetylation, the desired compound **44** represented 70 % of the mixture while the regioisomer with 2-O-PMB represented 30 %. Other by-products of this one-

pot approach were the 2,3-di-O-benzylated, the 2,3-di-O-PMB compounds or combinations with one hydroxyl protected as benzyl ether and other as p-methoxybenzyl ether.

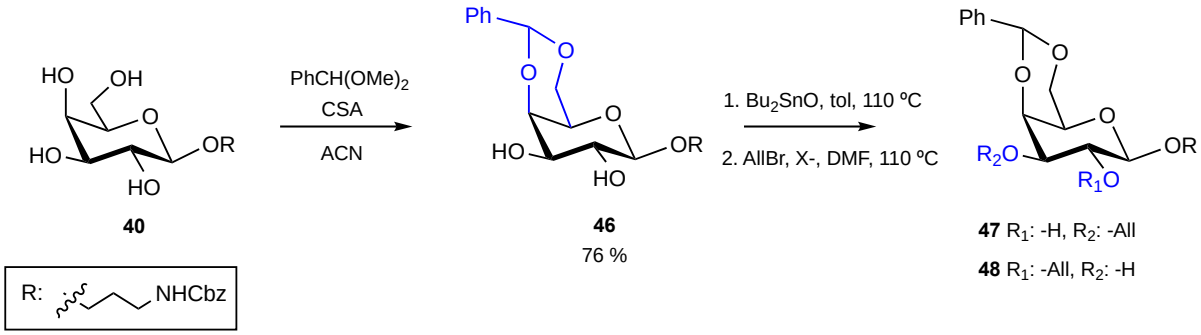

*Scheme 29. Synthesis of Acceptor **47***

Hence, despite the convenience of this protocol for the synthesis of glucopyranose building blocks, the regioselectivity for galactopyranose derivatives proved to be low, and target acceptor **44** could only be isolated in 19 % yield after an additional step of acetylation. A more traditional approach consisted in the 4,6-O-benzylidenation in the presence of camphorsulfonic acid (CSA) and subsequent regioselective introduction of an orthogonal protective group in position 3 using a dibutyl tin oxide mediated alkylation (Scheme 29). The first step presumably involves the formation of a dibutylstannylene acetal between positions 2 and 3. Successively, a halide ion coordinates to the tin intermediate enhancing the nucleophilicity of one of the two bound oxygen atoms and favoring the regioselective attack to the alkyl halide. However, the mechanism of the reaction has not been demonstrated. Halides such as cesium fluoride (CsF) or tetrabutyl ammonium iodide (TBAI) were tested[300]. The reaction using CsF lead yet again to a mixture of the two regioisomers which could be separated by column chromatography only after acetylation. Even if Scheme 29 only shows AllBr as alkylating agents, PMBCl was also tested with similar results (Table 11). The reaction using TBAI however, did not yield the desired compounds since the smaller and more electronegative fluorine ions may have a better ability to coordinate to tin, leading to a more efficient cleavage of the Sn-O bond and a faster nucleophilic attack.

Table 11. Conditions for regioselective alkylation

Entry	RX	X^-	Yield	
1	PMBCl	CsF	67 %	33 % 2-O-PMB (**45**)
				67 % 3-O-PMB (**44**)
2	AllBr	CsF	77%	40 % 2-O-All (**48**)
				60 % 3-O-All (**47**)
3	AllBr	TBAI	-	

Surprisingly, it was observed that inverting the order of the steps (Scheme 30) afforded exclusively the 3-O-allylated product **47**. Probably due to the formation of a dibutylstannylene acetal between positions 3 and 4 of intermediate **40** which could better differentiate the nucleophilicity of the two hydroxyl groups (Scheme 31). As opposed to fluorine, iodine ions can coordinate to Sn in a weaker manner, leading to a slower reaction but with improved regioselectivity. The preparation of the 3-O-PMB product using the same protocol was not attempted for the sake of time, but similar results should be envisaged.

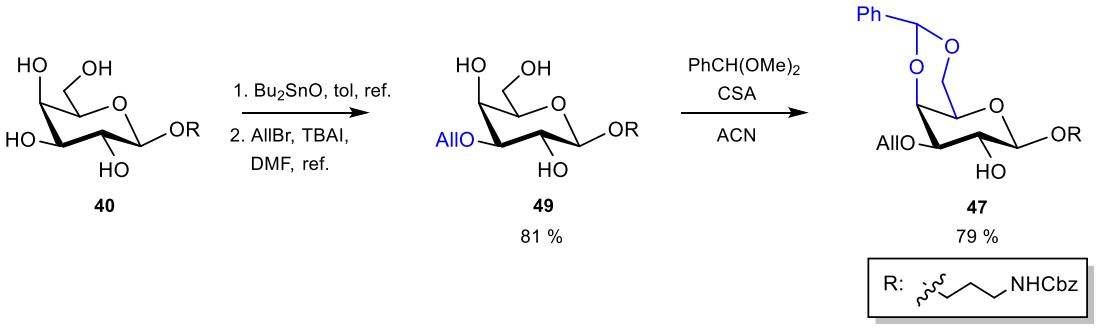

*Scheme 30. Alternative approach for the synthesis of Acceptor **47***

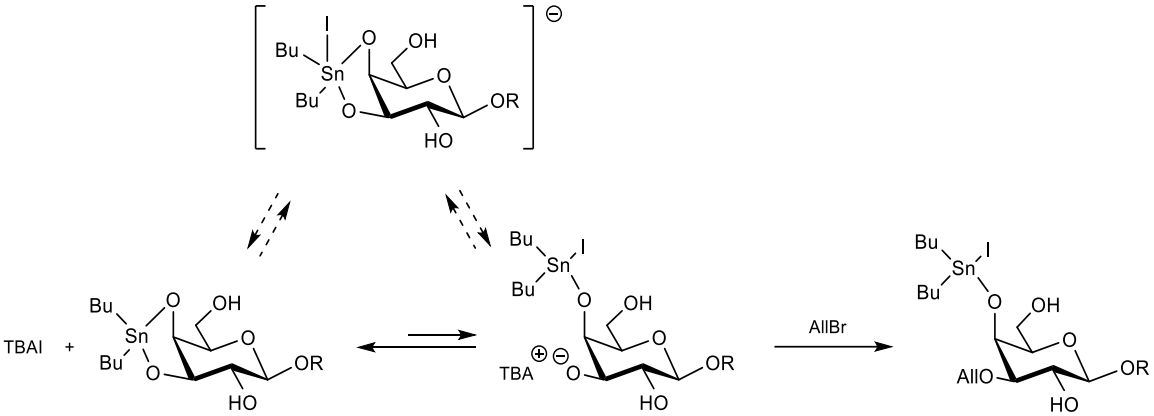

Scheme 31. Proposed mechanism for halide promoted organotin mediated alkylation of deprotected galactopyranosides

For the preparation of the third acceptor, intermediate **46** was orthogonally protected with an acetyl group in position 3 to afford the new acceptor **50**. In this case, the reaction proceeded in excellent yields and regioselectivity adapting a procedure described in literature[301], involving a 2,4,6-trimethylpyridine (sym-collidine) as a hindered base and acetyl chloride (AcCl) as acylating agent at -20 ºC (Scheme 32). The excellent regioselectivity is probably due to the stronger electrophilic nature of AcCl over PMBCl or AllBr.

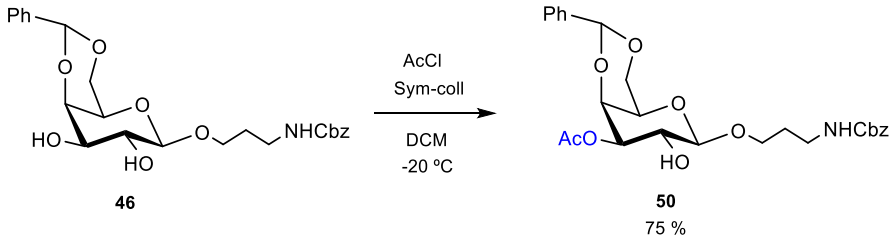

*Scheme 32. Synthesis of acceptor **50***

3.3. Synthesis of fucoside donor

Synthesis of fucopyranosyl trichloroacetimidate **54** was achieved following an already established procedure first described by Schmidt and co-workers (Scheme 33)[302]. Treatment of L-fucose with Amberlite H^+ in refluxing methanol afforded a complex mixture of the methyl α/β-L-fucofuranoside and α/β-L-fucopyranoside forms. Upon several crystallization attempts the methyl α-L-fucopyranoside **51** could be isolated in 42 % yield. Benzylation of **51** and subsequent acid hydrolysis of the methyl

ether gave 2,3,4-tri-O-benzyl-L-fucopyranose which was then activated to obtain the highly reactive donor **54** as a mixture of two anomers (α:β 8:2).

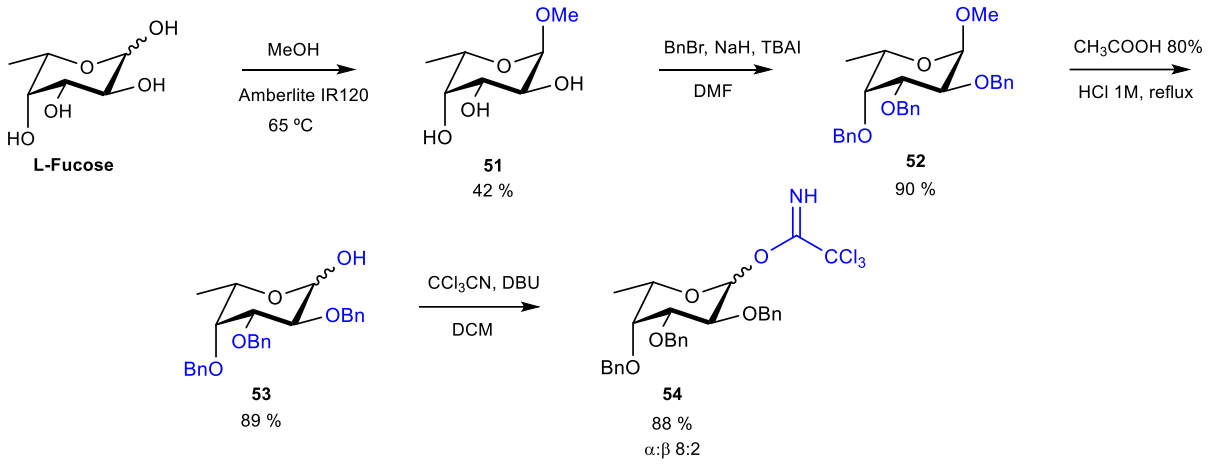

*Scheme 33. Synthesis of donor **54***

3.4. Synthesis of disaccharide antigen H derivative

One of the cornerstones of carbohydrate chemistry is the glycosylation reaction which couples a donor and an acceptor via a new glycosidic bond. Although many different strategies have been described for the successful coupling, control of the stereoselectivity of the newly formed glycosidic linkage, remains a challenge and successful protocols must be established on a case-by-case basis. The outcome of the reaction is influenced by many different parameters, such as the leaving group on the glycosyl donor, the acid promoter, the solvent, the temperature and the protecting groups on both reaction partners.

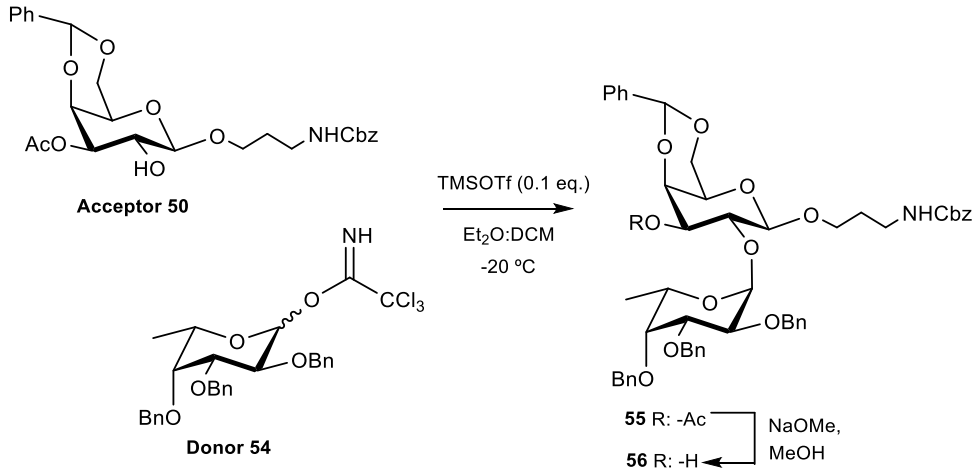

*Scheme 34. Synthesis of disaccharide antigen H precursor **55** and acceptor **56***

Access to the disaccharide H antigen was first achieved by glycosylation between acceptor **50** and trichloroacetimidate **54** in the presence of 0.1 equivalents of TMSOTf at -20 ºC (Scheme 34). Diethyl ether was chosen as a non-polar solvent since it should favor the formation of the 1,2-cis product through a stabilization of the oxacarbenium ion, in absence of a participating group in position 2. However, given the poor solubility of the acceptor, in some cases dichloromethane (DCM) was used to ensure solubilization at -20 ºC. The first two attempts (Table 12, entries 1 and 2) were performed using the isolated α-trichloroacetimidate whereas the third reaction (Table 12, entry 3) was performed using

only the β-trichloroacetamide. In both cases the outcome of the reaction was similar, suggesting that the reaction mainly proceeds through and S_N1-like mechanism. For the following attempts (Table 12, entries 4 and 5) the mixture of the two anomers was used as a donor.

*Table 12. Conditions for the synthesis of disaccharide **55***

Entry	Procedure	Donor: Acceptor	Solvent	4 Å MS	Yield α	Yield β
1	Classical	2	Et_2O:DCM 7:3	NO	49 %	15 %
2	Inverse	2	Et_2O:DCM 8:2	NO	52 %	Not isolated
3	Classical	2	Et_2O:DCM 8:2	NO	40 %	Not isolated
4	Classical	2.5	Et_2O	YES	49 %	16 %
5	Inverse	2.7	Et_2O:DCM 9:1	NO	60 %	12 %

Initially a classical glycosylation approach was adopted, but some unreacted acceptor and a lot of rearranged donor were recovered, suggesting an unmatched reactivity between the two building blocks. The inverse procedure, in which a solution of the donor was added dropwise to a solution containing the acceptor and the acid promoter allowed to overcome to certain extent some of those issues. Disaccharide **55** was always obtained as a mixture of two anomers which could be separated by column chromatography. The ^{1}H NMR spectrum of the α anomer showed an anomeric proton signal appearing at 5.30 ppm as a doublet with a $J_{1\text{-}2}$ = 3.7 Hz, while the spectrum of the β anomer showed an anomeric proton signal at 4.36 ppm as a doublet with a coupling constant of 7.8 Hz. After isolation of the α anomer, the next step was the removal of the acetyl group to afford the common disaccharide **56** acceptor for elongation.

In order to improve the yield and the stereoselectivity of the reaction, an alternative glycosylation was suggested (Scheme 35). It was envisioned that the presence of an electron donating group in position 3 of acceptor 47 would increase its reactivity, converting it in a better match for the highly reactive donor 54. However, this new acceptor was much more difficult to dissolve and target disaccharide **57** could only be isolated in 26 % yield due to its similar chromatographic behavior to the hydrolyzed donor.

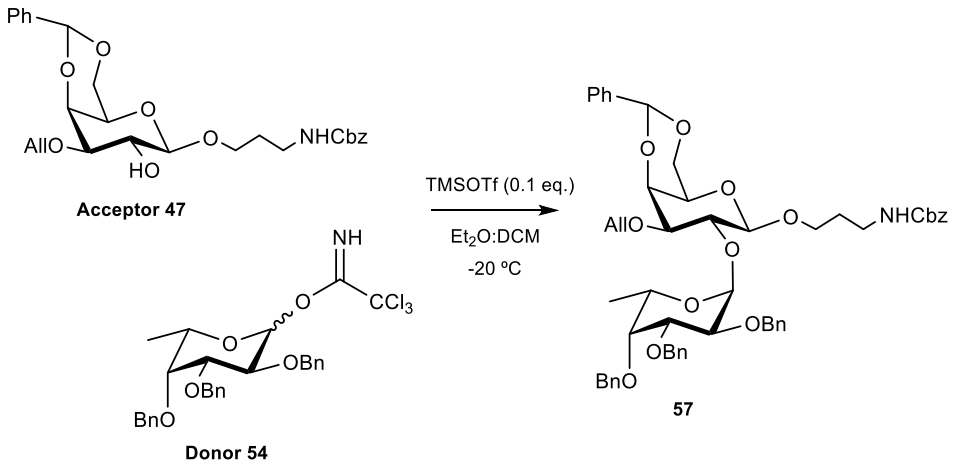

*Scheme 35. Alternative synthesis of disaccharide antigen H precursor **57***

One last glycosylation attempt between the 3-O-allylated acceptor **47** and the less reactive donor **13**, already present in our laboratory, was performed (Scheme 36). As indicated in Table 13, different

conditions were tested, but the amount of isolated α-anomer was again low, mainly due to the poor solubility and poor reactivity of the acceptor and the difficult separation between the two anomers.

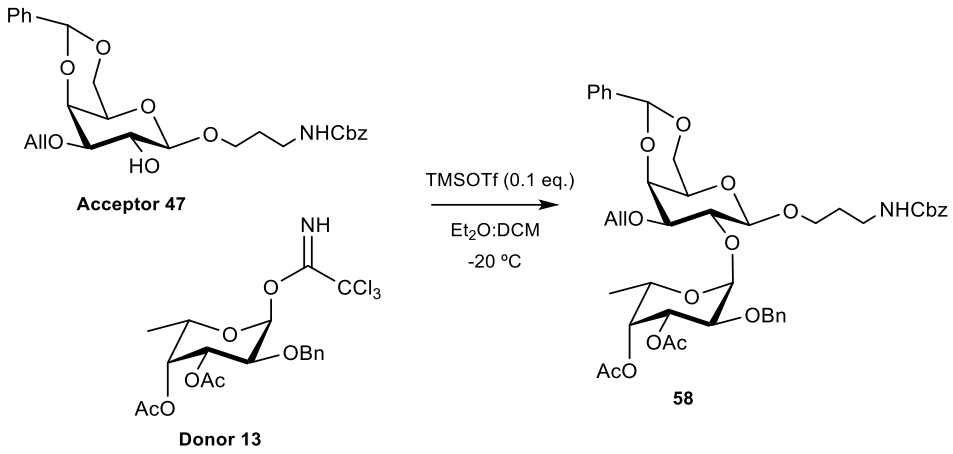

*Scheme 36. Alternative synthesis of disaccharide antigen H precursor **58***

*Table 13. Conditions for the synthesis of disaccharide **58***

Entry	Procedure	Donor: Acceptor	Solvent	4 Å MS	Yield	
					α	β
1	Classical	2	Et_2O:DCM 1:1	NO	28%*	Not isolated
2	Inverse	2	Et_2O:Tol 6:4	NO	21 %*	Not isolated
3	Classical	2	DCM	NO	30 %*	Not isolated

*Mixed fractions

Based on these results, the final strategy adopted for the disaccharide synthesis was the first one reported in Scheme 34 since the dissolution of the acceptor was easier, the separation of the α-product was less challenging and the yields were higher. Moreover, the deacetylation to yield acceptor **56** is much simpler and cost effective than the deallylaltion, which proceeds in two steps and requires the use of an expensive iridium catalyst.

3.5. Synthesis of trisaccharide antigen B derivative

For the elongation of disaccharide **56**, a new donor was prepared in one step from commercially available 2,3,4,6-tetra-O-benzyl-galactopyranose (Scheme 37). In this case, potassium carbonate replaced DBU as a weaker base to favor the formation of the kinetic β-trichloroacetimidate which could be isolated in up to 90 % yield from the crude mixture. If the glycosylation happens under S_N2-like conditions, the anomeric configuration of the donor in the absence of a participating group in position 2 may dictate the stereochemical outcome of the glycosylation, favoring the formation of the desired α-trisaccharide.

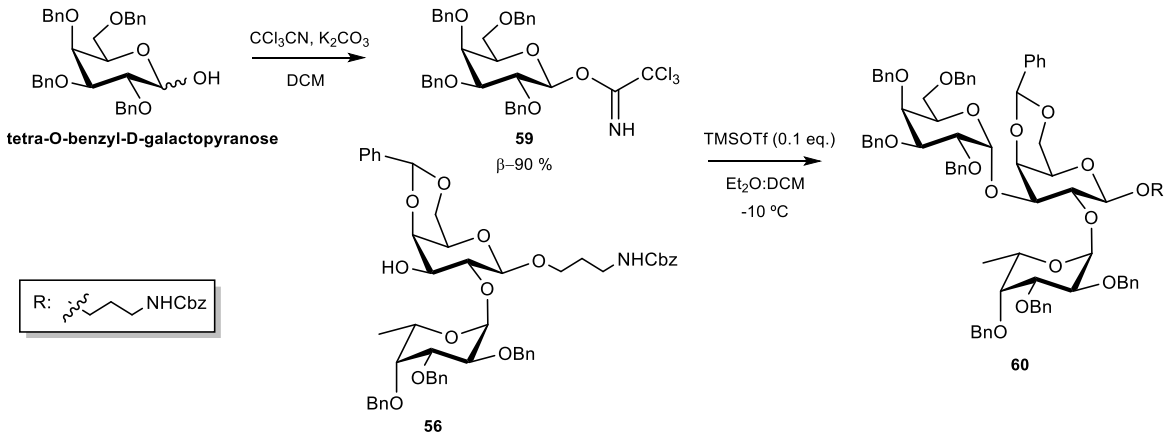

*Scheme 37. Synthesis of donor 59 and glycosylation with acceptor **56** to afford trisaccharide antigen B*

Access to the B antigen was achieved by glycosylation between disaccharide acceptor **56** and trichloroacetimidate **59** in the presence of 0.1 equivalents of TMSOTf at -10 ºC (Scheme 37). The reaction was attempted in different conditions (Table 14) and the best results were obtained using an inverse glycosylation protocol. The main challenge faced during this glycosylation was the dissolution of the acceptor in most common solvents used in glycosylation reactions: toluene, Et_2O, DCM… The main side-products of the reaction were some unreacted acceptor and the rearranged donor. Traces of the β anomer could not be isolated probably due to the small scale of the reaction.

*Table 14. Conditions for the synthesis of trisaccharide **60***

Entry	Procedure	Donor: Acceptor	Solvent	4 Å MS	Yield	
					α	β
1	Classical	3	Et_2O:DCM 9:1	NO	28%	Not isolated
2	Classical	1.5	DCM	YES	38 %	Not isolated
3	Inverse	3	Et_2O:DCM 9:1	NO	50 %	Not isolated
4	Inverse	2	DCM	YES	68 %	Not found

The stereochemistry of the newly formed glycosidic linkage was confirmed using ^{1}H NMR. The new anomeric proton of α-D-galactopyranoside moiety appeared at 5.50 ppm as a doublet with a coupling constant of 2.5 Hz. The hydrogenation of trisaccharide **60** will yield the target B blood group determinant derivative.

3.6. Synthesis of trisaccharide antigen A derivative

The preparation of trisaccharide antigen A derivative required a new donor, the synthesis of which started from D-galactosamine hydrochloride. A diazotransfer reaction with imidazole-1-sulfonyl azide hydrogen sulfate, prepared as described by Potter and co-workers[303], led to the azido derivative which was peracetylated to afford compound **61**. The acetyl group in anomeric position was selectively removed by treatment with hydrazine acetate followed by activation as a trichloroacetimidate (Scheme 38). In this case, even if K_2CO_3 was used as a base, imidate **62** was obtained as a mixture of two anomers (α:β 4:6).

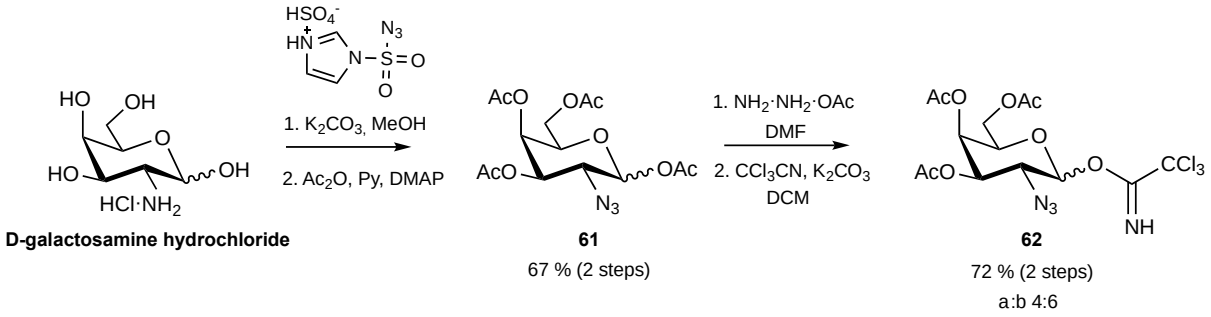

D-galactosamine hydrochloride

61
67 % (2 steps)

62
72 % (2 steps)
a:b 4:6

*Scheme 38. Synthesis of donor **62***

In the near future, this donor will be coupled with acceptor **56** to afford the protected trisaccharide precursor which, upon azido reduction, acetylation and hydrogenation, will lead to the last target antigen A.

4. Conclusions

Since their discovery in 1957, the chemical synthesis of the three antigenic ABO determinants and their subtypes has been described in several works[272,304–307] and even comprehensive reviews summarizing the synthetic efforts have been published[308]. These synthetic glycans have been mostly used to try to elucidate their elusive physiological role, but to the best of our knowledge, no reports have exploited these self-antigens for NMs functionalization.

For that reason, the effort of this work was not directed towards the discovery of a new and groundbreaking synthetic protocol, but rather to adapt the existing ones in order to obtain sufficient amount of the target compounds in a fast and efficient manner. A simplified version of the work performed by Meloncelli and co-workers[304] has been adopted, replacing some protective groups and modifying specific conditions.

In summary, this section has reported the synthesis of the B and H histo-blood group antigens attached to a linear aglycone with a free amino group for nanomaterial conjugation. Key to the synthesis was the preparation of the common reducing-end disaccharide **56**, which served as the core upon which the two trisaccharides will be built. The regioselectivity of this glycosylation was lower than expected, regardless of the reaction conditions and this was probably due to the lack of anchimeric assistance and the unmatched reactivity between the reaction pair. The best attempt to date afforded the target disaccharide **56** in 60 % yield. In the near future, a new glycosylation using ethylthio 2,3,4-tri-O-TBDMS-β-L-fucopyranoside **18** as a donor, described in Chapter I, will be attempted to try to improve both the yield and especially the regioselectivity.

Trisaccharide antigen B could be obtained by coupling **56** with 2,3,4,6-tetra-O-benzyl-β-D-galactopyranose trichloroacetimidate. The inverse glycosylation procedure afforded trisaccharide **60** in up to 68 % yield. The synthesis of trisaccharide antigen A will be attempted in the near future with donor **62** already in our hands.

Hydrogenation of disaccharide **56** and trisaccharide **60** will afford the underlying blood sugar carbohydrate epitopes H and B. After the three targets have been prepared, our next endeavor will be to couple them to different NPs through polymeric spacers with the final aim to test the ability of these novel nanosystems to act as RBC mimics and thus, minimize the interaction with the immune system

upon systemic administration. Preliminary studies will be carried out in plasma to determine the ability of these novel NMs to bind allo-antibodies and other biomolecules in the biological milieu.

CHAPTER III: MANNOSYLATED GOLD NANORODS AS BIOSENSORS FOR STROKE DIAGNOSIS

1. Aim of the chapter

A stroke occurs when a blood vessel that carries oxygen and nutrients to the brain is either blocked by a clot (ischemic stroke) or ruptures (hemorrhagic stroke) preventing blood supply to the brain and causing brain damage, long-term disability or even death. Despite recent substantial progress in prevention and disease management, stroke still remains a largely unmet medical challenge. Several studies indicate that some activators of the lectin complement pathway, particularly mannose-binding lectin (MBL), have a key role in cerebral ischemic episodes[309–312]. Hence, the choice of MBL as stroke biomarker in liquid biopsies could represent an attractive alternative for prevention and early onset diagnosis.

As explained in the introductory section, Au NPs can be exploited to produce biosensors as the binding of biomolecules to the NP's surface leads to LSPR shifts that can be readily measured[313,314]. As opposed to spherical Au NPs, the anisotropy of Au nanorods (Au NRs) leads to a splitting of the optical absorption band into two separate LSPR peaks corresponding to resonances along the short and long axes of the rod, termed the transverse and longitudinal bands respectively. The longitudinal resonance peak position is highly size dependent and thus, it can be fine-tuned from the visible to the near infrared, where biological tissues exhibit the highest optical transparency[314–317]. This allows measurements directly in complex biological fluids such as blood, enabling a broad range of *in vitro* and *in vivo* applications[318]. Moreover, the longitudinal peak position is highly sensitive to refractive index changes in the local environment, such as those caused by binding of biomolecules to the rod surface. Therefore, Au NR-based LSPR sensors represent an important advancement towards the rapid, simple, label-free and sensitive detection of biomolecules[319–323].

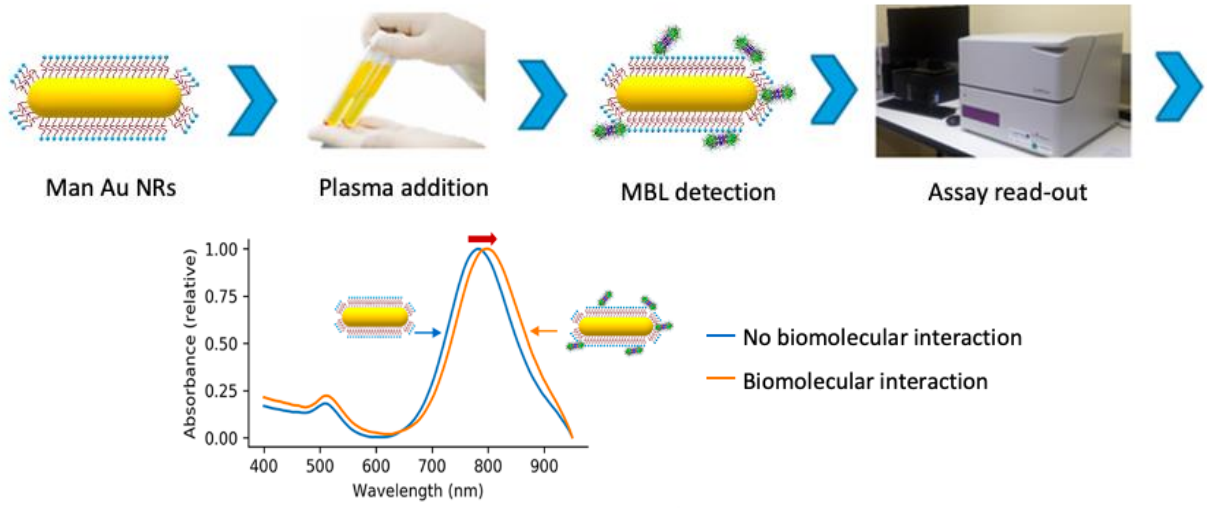

Figure 19. Mannosylated Au NRs incubated with plasma to detect MBL

To enable LSPR-based biosensing, Au NRs must be decorated with recognition units tethered to the surface by a ligand. In this context, we hypothesized that Au NRs bearing mannose derivatives could be a high-throughput design towards MBL detection, and hence, for stroke diagnosis. For that reason, mannose (Manα1), dimannose (Manα1-2Manα1) and trimannose (Manα1-3(Manα1-6)Manα1)

structures were equipped with an amine-ending anomeric linker with a free amino group to obtain compounds **1**, **68** and **73**. These compounds are being used by Dr. Inge Nelissen's group at VITO (Belgium) for the functionalization of Au NRs coated with polymers with a terminal carboxylic group. These mannosylated nanosystems are then incubated with human serum plasma in order to detect MBL based on simple optical (near IR) measurements according to Figure 19. The final aim of the project is to correlate the absorbance shift with potential cardiovascular disease development.

2. Results and discussion

2.1. Synthesis of 3'-aminopropyl 2-O-(α-D-mannopyranosyl)-α-D-mannopyranoside

Starting from benzyl 3-O-benzyl-4,6-O-benzylidene-2-O-(2,3,4,6-tetra-O-acetyl-α-D-mannopyranosyl)-α-D-mannopyranoside **63**, already present in our laboratory, benzyl ethers and benzylidene group were first removed by hydrogenolysis. This reaction was initially performed at atmospheric pressure using H_2, Pd/C as a catalyst and MeOH as a solvent, but after more than 10 days, the one benzyl ether in the anomeric position was still present according to the HMBC NMR spectrum. Increasing the pressure to 10 bars for 4 more days finally afforded compound **64**. The simplest way to introduce a leaving group at the reducing end of the sugar was per-acetylation of compound **64** using acetic anhydride in pyridine and a catalytic amount of 4-dimethylaminopyridine (DMAP).

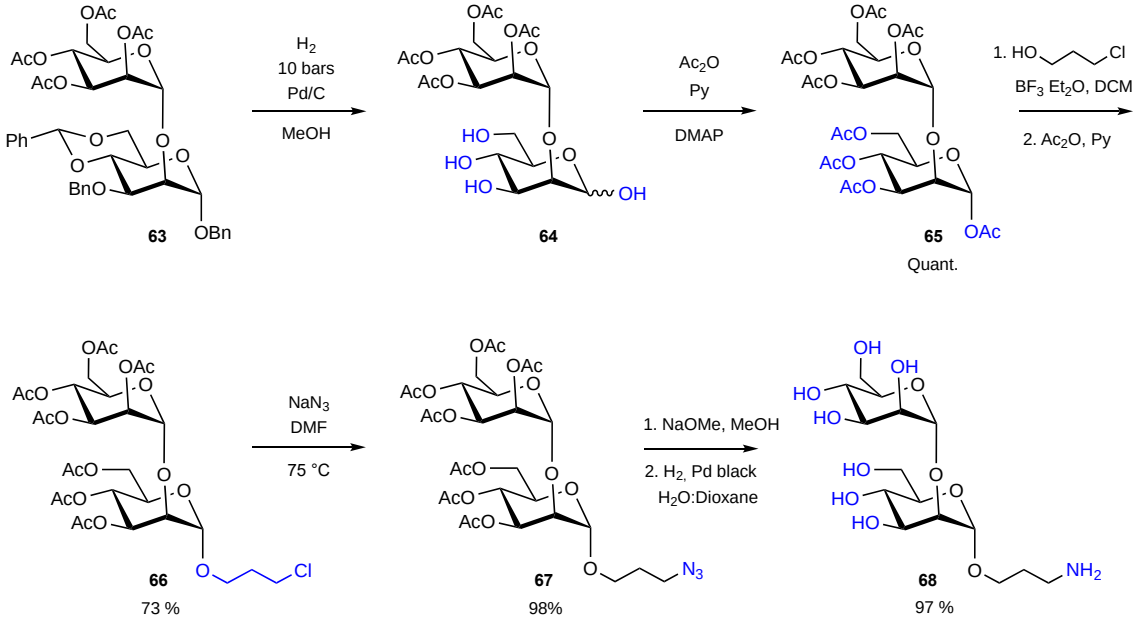

*Scheme 39. Synthesis of 3'-aminopropyl 2-O-(α-D-mannopyranosyl)-α-D-mannopyranoside **68***

Per-acetylated compound **64** was then functionalized with a C3 linker in the anomeric position following the same protocol optimized for the synthesis of 3'-chloropropyl α-D-mannopiranoside **5a** (Table 1, entry 2) to obtain compound **66** in relatively fair yield. Given the limited amount of starting material, the crude of the reaction was always acetylated to facilitate the recovery of any traces of deacetylated product or unreacted starting material. Then, the azido group was introduced by nucleophilic replacement of the chlorine to obtain intermediate **67**, which was deacetylated using NaOMe in MeOH and hydrogenated in the presence of Pd black and a mixture of water and dioxane as a solvent to obtain the target **68** (Scheme 39).

2.2. Synthesis of 3'-aminopropyl 3-O-(α-D-mannopyranosyl)-6-O-(α-D-mannopyranosyl)-α-D-mannopyranoside

Functionalization of commercially available 3-O-(α-D-mannopyranosyl)-6-O-(α-D-mannopyranosyl)-α,β-D-mannopyranose started with per-acetylation. The introduction of the linker was then attempted in the same conditions described before, but in this case the reaction proceeded with much lower yields and the acetylation of the crude proved to be a key step to recover as much product as possible and all the precious unreacted started material for future trials. Different alternatives were tested to improve the outcome of this step, such as the use of TMSOTf as acid promoter or the use of 3-chloropropanol both as reagent and solvent, but the yield never exceeded 37 %. The nucleophilic displacement to afford the azido derivative **71** and its deprotection were carried out in the same conditions previously used to produce the target compound **73** as shown in Scheme 40.

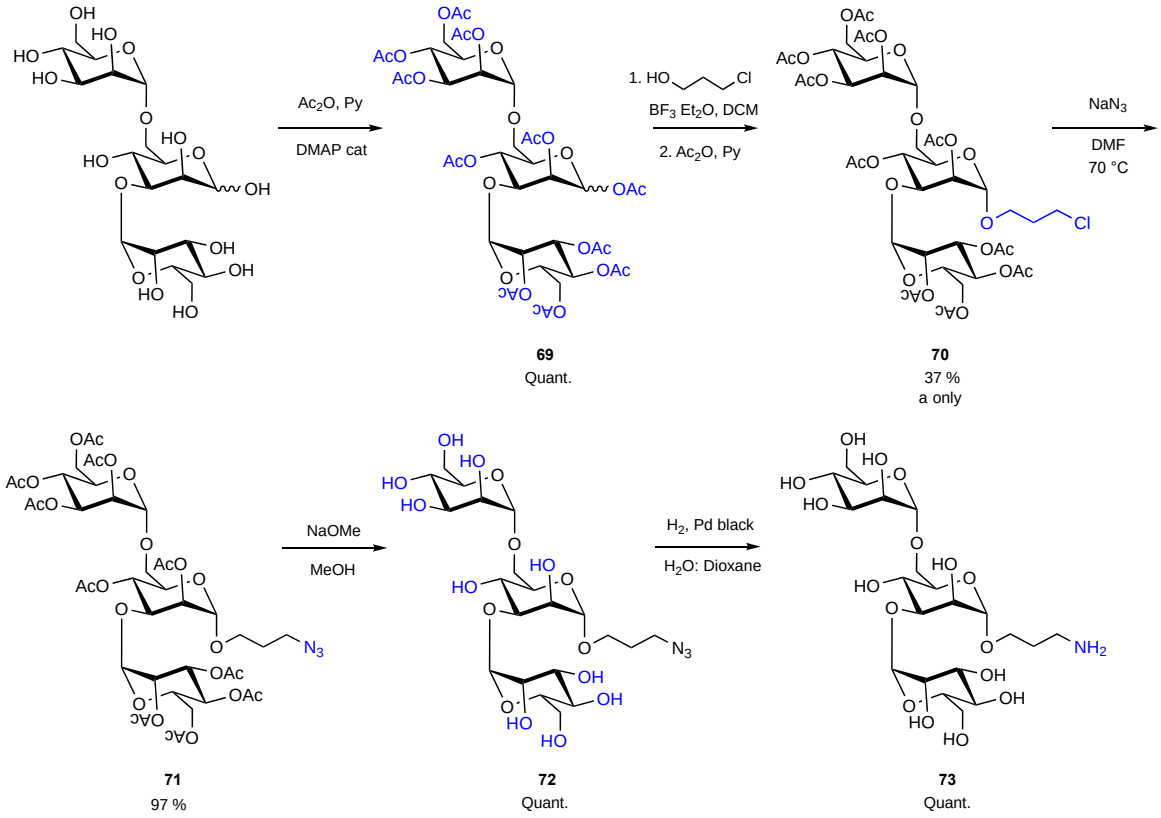

*Scheme 40. Synthesis of 3'-aminopropyl 3-O-(α-D-mannopyranosyl)-6-O-(α-D-mannopyranosyl)-α-D-mannopyranosode **73***

3. Conclusions

3'-Aminopropyl α-D-dimannoside was prepared in 69 % overall yield, whereas 3'-aminopropyl α-D-trimannoside could be obtained with an overall yield of 53 % considering the recovery of the peracetylated intermediate **69** after the linker introduction step. In both cases the linker glycosylation was the most challenging reaction, probably due to the inaccessibility of the anomeric center, much more evident in the trisaccharide's case.

Compounds **68** and **73** along with 3'-aminopropyl α-D-mannopyranoside **1**, prepared in Chapter I, were sent to VITO where they are being coupled to Au NRs through carboxylated PEG spacers. These nanosensors are then incubated with human plasma and the presence of MBL is detected via a LSPR shift with the final aim to correlate this shift with early stroke diagnosis.

EXPERIMENTAL SECTION

All chemicals were purchased from commercial sources and used without further purification unless otherwise stated. Dry solvents were purchased from Sigma-Aldrich. All reactions containing moisture or air-sensitive reagents were carried out under nitrogen or argon atmosphere.

Reactions were monitored by Thin Layer Chromatography (TLC) and High-Performance Thin Layer Chromatography (HPTLC) using Merck precoated 60 F_{254} glass plates (0.25 mm and 0.2 mm, respectively). Compounds were visualized, when appropriate by UV light (254 nm), followed by staining and charring at 473 K. The solution used as stains were:

- Molybdic solution: 21 g of $(NH_4)_4Mo_4O_{24}$, 1 g of $Ce(SO_4)_2$, 31 ml of H_2SO_4 98%, 970 ml H_2O
- Sulfuric acid solution: 50 ml of H_2SO_4 98%, 450 ml of MeOH, 450 ml H_2O
- Ninhydrin solution: 2.7 g of 2,2-dihydroxyindane-1,3-dione, 27 ml of AcOH, 900 ml of EtOH

Compounds were purified by flash chromatography using silica gel (SiO_2, high-purity grade, pore size 60 Å, mesh particle size 230-400) from Sigma-Aldrich. Biotage SP1 was also used to purify some compounds using Biotage SNAP cartridges ranging from 5 g to 50 g.

NMR spectra were recorded using a Bruker AMX 400 NMR spectrometer (^{1}H: 400 MHz, ^{13}C: 100.6 MHz, ^{31}P: 162 MHz and ^{19}F: 376 MHz). The probe temperature during the experiments was kept at 298 K unless otherwise stated. Samples were prepared using deuterated solvents ($CDCl_3$, CD_3OD, D_2O…) purchased from Eurisotop. All products were fully characterized by means of ^{1}H, ^{13}C, ^{31}P, ^{19}F 1D-NMR techniques and ed-HSQC, HMBC and COSY 2D-NMR techniques by using pulse sequences provided by the manufacturer. Chemical shifts (δ) are reported in ppm using residual solvent peaks as internal standards. Coupling constants (*J*) are expressed in Hz. Coupling patterns are given as *s* (singlet), *d* (doublet), *t* (triplet), multiplet (m) or combinations thereof.

Low resolution mass analyses were recorded in negative or positive mode on a Thermo Finnigan LCQ Advantage equipped with an electrospray ionization (ESI) source.

Freeze-drying of aqueous solutions was performed using Lio5P Lyophilizer.

1. Experimental procedures Chapter I

1.1. Synthesis of 3'-aminopropyl α-D-mannopyranoside

*Synthesis of acetyl 2,3,4,6-tetra-O-acetyl-α,β-D-mannopyranoside (**4**)*

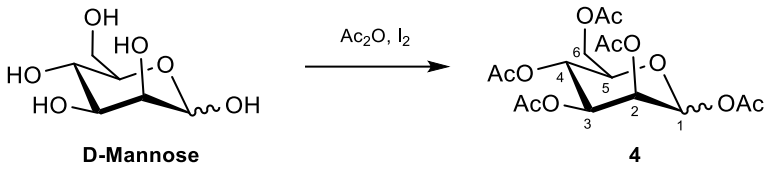

D-Mannose **4**

To an ice-cooled solution of D-mannose (7.0 g, 38.9 mmol) in acetic anhydride (60.0 ml, 634.7 mmol) catalytic I_2 (0.5 g, 2.0 mmol) was added. The reaction mixture was monitored by TLC (Hex:EtOAc - 1:1) and after 18 h, the I_2 in excess was quenched with $Na_2S_2O_3$ until transparency, washed with DCM (2 x 40 ml) and extracted. After washing with sat. $NaHCO_3$ (2 x 30 ml) and brine (2 x 30 ml), the organic phase was collected, dried over anhydrous Na_2SO_4, filtered and the excess of solvent was removed with a rotary evaporator to obtain the desired compound **4** as a white solid (15.6 g, quant., α:β 9:1).

TLC: R_f: 0.53 (Hex:EtOAc - 1:1).

NMR data for α anomer:

^{1}H NMR (400 MHz, $CDCl_3$, 25 ºC): δ= 6.09 (d, 1H, $J_{1\text{-}2}$ = 1.8 Hz, H-1), 5.37 – 5.33 (m, 2H, H-3, H-4), 5.26 (dd, 1H, $J_{2\text{-}1}$= 1.8 Hz, $J_{2\text{-}3}$= 2.6 Hz, H-2), 4.28 (dd, 1H, $J_{6a\text{-}6b}$= 12.3 Hz, $J_{6a\text{-}5}$ = 4.8 Hz, H-6a), 4.10 (dd, 1H, $J_{6b\text{-}6a}$= 12.3 Hz, $J_{6b\text{-}5}$ = 2.4 Hz, H-6b), 4.05 (m, 1H, $J_{5\text{-}6a}$= 4.8 Hz, $J_{5\text{-}6b}$ = 2.4 Hz, H-5), 2.18 (s, 3H, -$COCH_3$), 2.17 (s, 3H, -$COCH_3$), 2.09 (s, 3H, -$COCH_3$), 2.05 (s, 3H, -$COCH_3$), 2.00 (s, 3H, -$COCH_3$) ppm.

^{13}C NMR (100.6 MHz, $CDCl_3$, 25 ºC): δ= 171.3 – 167.7 (-$\underline{C}OCH_3$), 90.8 (C-1), 70.8 (C-5), 68.9 (C-4 or C-3), 68.5 (C-2), 65.8 (C-3 or C-4). 62.3 (C-6), 21.0 (-CO$\underline{C}H_3$), 20.9 (-CO$\underline{C}H_3$), 20.8 (-CO$\underline{C}H_3$), 20.8 (-CO$\underline{C}H_3$), 20.75 (-CO$\underline{C}H_3$) ppm.

*Synthesis of 3'-bromopropyl 2,3,4,6-tetra-O-acetyl-α-D-mannopyranoside (**5a**)*

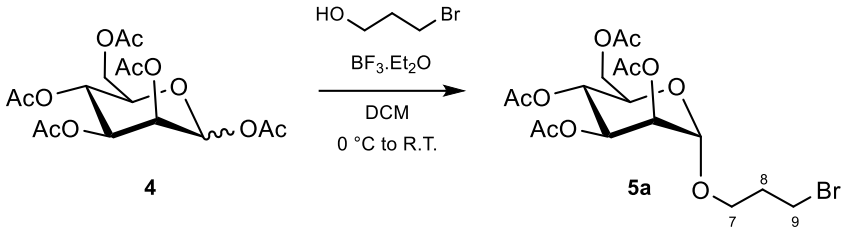

To an ice-cooled solution of **4** (2.0 g, 5.0 mmol) in DCM (40 ml, 0.1 M), $BF_3 \cdot Et_2O$ (2.5 ml, 20.4 mmol) and 3-bromo-1-propanol (1.8 ml, 20.4 mmol) were added dropwise. The reaction mixture was stirred overnight at r.t and monitored by TLC (Hex:EtOAc - 1:1). After 48h, the reaction mixture was cooled down with an ice bath, quenched with K_2CO_3 0.25 M until neutral pH and extracted with DCM (2 x 10 ml). The organic phase was washed with brine (2 x 10 ml), dried over anhydrous Na_2SO_4, filtered and concentrated in vacuo. The crude product was purified by column chromatography (Hex:EtOAc 8:2 → 6:4) to obtain mannopyranoside **5a** as a pale-yellow syrup (1.4 g, 60 %).

TLC: R_f: 0.67 (Hex:EtOAc - 1:1).

NMR data:

^{1}H NMR (400 MHz, $CDCl_3$, 25 ºC): δ= 5.30 – 5.28 (m, 2H, H-3, H-4), 5.23 (dd, 1H, $J_{2\text{-}1}$ = 1.6 Hz, $J_{2\text{-}3}$= 2.6 Hz, H-2), 4.82 (d, 1H, $J_{1\text{-}2}$= 1.6 Hz, H-1), 4.26 (dd, 1H, $J_{6a\text{-}6b}$= 12.3 Hz, $J_{6a\text{-}5}$= 5.4 Hz, H-6a), 4.09 (dd, 1H, $J_{6b\text{-}6a}$= 12.3 Hz, $J_{6b\text{-}5}$= 2.4 Hz, H-6b), 4.00 (m, 1H, H-5), 3.86 (m, 1H, H-7a), 3.55 (m, 1H, H-7b), 3.49 (m, 2H, H-9), 2.17 – 2.07 (m, 2H, H-8), 2.11 (s, 3H, -$COCH_3$), 2.06 (s, 3H, -$COCH_3$), 2.01 (s, 3H, -$COCH_3$), 1.95 (s, 3H, -$COCH_3$) ppm.

^{13}C NMR (100.6 MHz, $CDCl_3$, 25 ºC): δ= 171.3 – 169.7 (-$\underline{C}OCH_3$), 97.6 (C-1), 69.5 (C-2), 69.0 (C-3 or C-4), 68.7 (C-5), 66.0 (C-3 or C-4), 65.5 (C-7), 62.4 (C-6), 32.0 (C-8), 30.1 (C-9), 20.8 (-CO$\underline{C}H_3$), 20.7 (-CO$\underline{C}H_3$), 20.6 (-CO$\underline{C}H_3$) ppm.

*Synthesis of 3'-chloropropyl 2,3,4,6-tetra-O-acetyl-α-D-mannopyranoside (**5b**)*

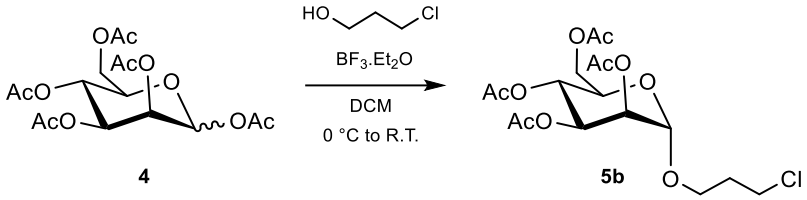

To an ice-cooled solution of **4** (4.5 g, 11.5 mmol) in DCM (50 ml, 0.2 M), $BF_3 \cdot Et_2O$ (5.6 ml, 46.0 mmol) and 3-chloro-1-propanol (3.8 ml, 46.0 mmol) were added dropwise. The reaction mixture was stirred overnight at r.t and monitored by TLC (Hex:EtOAc - 4:6). After 48h, the reaction mixture was quenched and extracted with $NaHCO_3$ (2 x 30 ml) and brine (2 x 30 ml), dried over anhydrous Na_2SO_4, filtered and concentrated in vacuo. The crude product was purified by column chromatography (Hex:EtOAc 9:1 $\rightarrow$ 6:4) and the eluent was removed in vacuo to afford compound **5b** as a pale-yellow syrup (3.3 g, 68 %).

TLC: R_f = 0.53 (Hexane:EtOAc 4:6).

NMR data:

^{1}H NMR (400 MHz, $CDCl_3$, 25 ºC): δ= 5.31 – 5.26 (m, 2H, H-3, H-4), 5.24 (dd, 1H, $J_{2\text{-}1}$ = 1.6 Hz, $J_{2\text{-}3}$= 2.9 Hz, H-2), 4.83 (d, 1H, $J_{1\text{-}2}$= 1.6 Hz, H-1), 4.28 (dd, 1H, $J_{6a\text{-}6b}$= 12.2 Hz, $J_{6a\text{-}5}$ = 5.3 Hz, H-6a), 4.13 (dd, 1H, $J_{6b\text{-}6a}$= 12.2 Hz, $J_{6b\text{-}5}$= 2.4 Hz, H-6b), 3.99 (ddd, 1H, $J_{5\text{-}4}$= 9.8 Hz, $J_{5\text{-}6a}$= 5.3 Hz, $J_{5\text{-}6b}$= 2.4 Hz, H-5), 3.92 (m, 1H, H-7a), 3.67 (m, 2H, H-9), 3.59 (m, 1H, H-7b), 2.16 – 2.07 (m, 2H, H-8), 2.16 (s, 3H, -$COCH_3$), 2.11 (s, 3H, -$COCH_3$), 2.05 (s, 3H, -$COCH_3$), 2.00 (s, 3H, -$COCH_3$) ppm.

^{13}C NMR (100.6 MHz, $CDCl_3$, 25 ºC): δ= 171.3 – 169.7 (-$\underline{C}OCH_3$), 97.7 (C-1), 69.5 (C-2), 68.8 (C-3 or C-4), 68.7 (C-5), 66.0 (C-3 or C-4), 64.4 (C-7), 62.5 (C-6), 42.0 (C-9), 32.3 (C-8), 21.0 (-CO$\underline{C}H_3$), 20.7 (-CO$\underline{C}H_3$), 20.6 (2 x -CO$\underline{C}H_3$) ppm.

*Synthesis of 3'-azidopropyl 2,3,4,6-tetra-O-acetyl-α-D-mannopyranoside (**6**)*

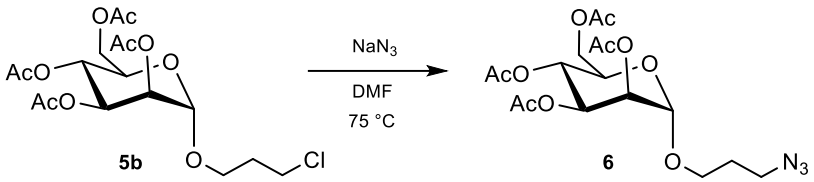

Sodium azide (0.75 g, 11.76 mmol) was added portionwise to a stirred solution of compound **5b** (1.23 g, 2.90 mmol) in DMF (20 mL, 0.1 M). The reaction mixture was heated up to 75 °C for 12 h until TLC (Hex:EtOAc - 1:2) showed the disappearance of the starting material. The reaction mixture was dissolved in Et_2O (100 ml) and H_2O (30 ml), extracted and the water phase was further washed with Et_2O (2 x 30 ml). The organic phases were combined, washed with $NaHCO_3$ (2 x 30 ml) and brine (2 x 30 ml), dried over anhydrous Na_2SO_4, filtered and the excess of solvent was evaporated to give compound **6** (1.24 g, 98 %) as a colorless syrup.

TLC: R_f: 0.67 (Hex:EtOAc - 1:1).

IR: peak at 2100.1 cm^{-1}, -N=N=N stretching.

NMR data:

^{1}H NMR (400 MHz, $CDCl_3$, 25 ºC): δ= 5.32 – 5.29 (m, 2H, H-3 and H-4), 5,24 (dd, 1H, $J_{2\text{-}1}$= 1.7 Hz, $J_{2\text{-}3}$= 3.2 Hz, H-2), 4.82 (d, 1H, $J_{1\text{-}2}$= 1.7 Hz, H-1), 4.28 (dd, 1H, $J_{6a\text{-}6b}$= 12.2 Hz, $J_{6a\text{-}5}$= 5.4 Hz, H-6a), 4.12 (dd, 1H, $J_{6b\text{-}6a}$= 12.2 Hz, $J_{6b\text{-}5}$= 2.4 Hz, H-6b), 3.96 (ddd, 1H, $J_{5\text{-}4}$= 9.3 Hz, $J_{5\text{-}6a}$= 5.4 Hz, $J_{5\text{-}6b}$= 2.4 Hz, H-5), 3.85 – 3.75 (m, 1H, H-7a), 3.53 (m, 1H, H-7b), 3.43 (t, 2H, $J_{9\text{-}8}$= 6.5 Hz, H-9), 2.16 (s, 3H, -$COCH_3$), 2.11 (s, 3H, -$COCH_3$), 2.05 (s, 3H, -$COCH_3$), 2.00 (s, 3H, -$COCH_3$), 1.95 – 1.82 (m, 2H, H-8) ppm.

^{13}C NMR (100.6 MHz, $CDCl_3$, 25 ºC): δ= 172.4 – 169.7 (-$\underline{C}OCH_3$), 97.8 (C-1), 69.7 (C-2), 69.2 (C-3 or C-4), 68.8 (C-5), 66.3 (C-4 or C-3), 65.0 (C-7), 62.6 (C-6), 48.2 (C-9), 28.8 (C-8), 21.0 – 20.8 (-CO$\underline{C}H_3$) ppm.

*Synthesis of 3'-azidopropyl α-D-mannopyranoside (**7**)*

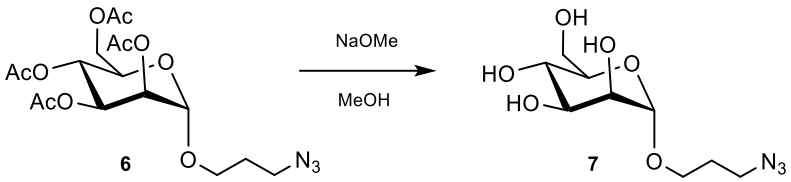

Compound **6** (1.02 g, 2.36 mmol) was dissolved in MeOH (20 ml, 0.1M) and NaOMe (0.10 g, 1.84 mmol) was added. The reaction mixture was stirred at r.t. until TLC (DCM:MeOH - 7:3) showed the consumption of the starting material. After 3 h, the reaction mixture was quenched using Amberlite IR120 (H^+ form), filtered over cotton and concentrated in vacuo to afford compound **7** (0.65 g, quant.) as a colorless syrup.

TLC: R_f: 0.87 (DCM:MeOH - 7:3).

NMR data:

^{1}H NMR (400 MHz, CD_3OD, 25 ºC): δ= 4.77 (d, 1H, $J_{1\text{-}2}$= 1.7 Hz, H-1), 3.86 – 3.73 (m, 2H, H-6a and H-7a), 3.82 (dd, 1H, $J_{2\text{-}3}$= 3.3 Hz, $J_{2\text{-}1}$= 1.7 Hz, H-2), 3.72 (dd, 1H, $J_{6b\text{-}6a}$= 12.2 Hz, $J_{6b\text{-}5}$= 5.9 Hz, H-6b), 3.70 (dd, 1H, $J_{3\text{-}4}$= 9.5 Hz, $J_{3\text{-}2}$ = 3.3 Hz, H-3), 3.63 (t, 1H, $J_{4\text{-}3}$= 9.5, Hz, $J_{4\text{-}5}$= 9.4 Hz, H-4), 3.56 – 3.50 (m, 2H, H-5 and H-7b), 3.43 (td, 2H, $J_{9\text{-}8}$= 6.7 Hz, $J_{9\text{-}7}$ = 3.1 Hz, H-9), 1.88 (m, 2H, H-8) ppm.

^{13}C NMR (100.6 MHz, CD_3OD, 25 ºC): δ=101.7 (C-1), 74.8 (C-5), 72.6 (C-3), 72.1 (C-2), 68.5 (C-4), 65.3 (C-7), 62.8 (C-6), 49.5 (C-9), 29.9 (C-8) ppm.

MS (ESI+): theoretical mass: 263.25 m/z, experimental mass $[M+Na]^+$: 286.13 m/z.

*Synthesis of 3'-aminopropyl α-D-mannopyranoside (**1**)*

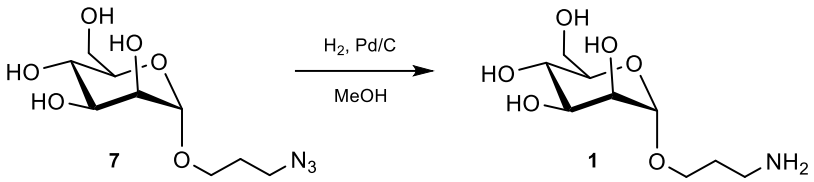

To a solution of compound **7** (0.51 g, 1.94 mmol) in MeOH (20 ml, 0.1 M), a catalytic amount of Pd/C was added. The reaction atmosphere was purged with H_2/vacuum cycles and then, stirred under H_2 atmosphere. After 3 h, the Pd/C was filtered through a Whatman syringe filter and concentrated under vacuum to give compound **1** as a colorless syrup (0.46 g, quant.).

NMR data:

^{1}H NMR (400 MHz, D_2O, 25 ºC): δ= 4.87 (d, 1H, $J_{1\text{-}2}$= 1.7 Hz, H-1), 3.95 (dd, 1H, $J_{2\text{-}1}$= 1.7 Hz, $J_{2\text{-}3}$= 3.5 Hz, H-2), 3.90 (dd, 1H, $J_{6a\text{-}6b}$= 12.34 Hz, $J_{6a\text{-}5}$= 1.8 Hz, H-6a), 3.84 - 3.74 (m, 3H, H-3, H-6b and H-7a), 3.67 - 3.56 (m, 3H, H-4, H-5 and H-7b), 2.77 (td, $J_{9\text{-}8}$= 7.3 Hz, $J_{9\text{-}7}$= 3.0 Hz, 2H, H-9), 1.84 (m, 2H, H-8) ppm.

^{13}C NMR (100.6 MHz, D_2O, 25 ºC): δ= 99.7 (C-1), 72.9 (C-4 or C-5), 70.7 (C-3), 70.3 (C-2), 66.8 (C-4 or C-5), 65.8 (C-7), 60.8 (C-6), 37.9 (C-9), 30.9 (C-8) ppm.

MS (ESI+): theoretical mass: 237.25 m/z, experimental mass $[M+Na]^+$: 260.09 m/z.

1.2. Synthesis of 3'-aminopropyl α-D-galactopyranoside

*Synthesis of acetyl 2,3,4,6-tetra-O-trimethylsilyl-β-D-galactopyranoside (**9**)*

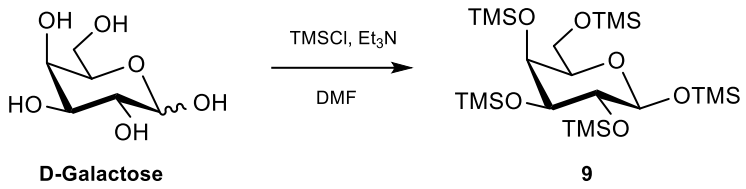

D-Galactose **9**

To a suspension of D-galactose (2.04 g, 11.10 mmol) in DMF (75 ml, 0.15 M), TEA (8.5 ml, 61.1 mmol) was added. The mixture was cooled down to 0 °C followed by the dropwise addition of TMSCl (7.8 ml, 61.1 mmol). After 17 h, the reaction mixture was diluted in 100 ml of hexane and extracted with cold water (2 x 100 ml). The organic phase was dried over anhydrous Na_2SO_4, filtered and the excess of solvent was removed in vacuo providing compound **9** (5.02 g, 84 %) as a colorless syrup.

TLC: R_f: 0.89 (Hex:EtOAc - 7:3).

NMR data:

^{1}H NMR (400 MHz, $CDCl_3$, 25 ºC): δ= 5.07 (d, 1H, $J_{1\text{-}2}$= 2.1 Hz, H-1), 3.91 (m, 2H, H-3 and H-5), 3.84 (m, 2H, H-2 and H-4), 3.64 (dd, $J_{6a\text{-}6b}$= 9.5 Hz, $J_{6a\text{-}5}$= 7.9 Hz, 1H, H-6a), 3.55 (dd, $J_{6b\text{-}6a}$= 9.5 Hz, $J_{6b\text{-}5}$= 5.4 Hz, 1H, H-6b), 0.16 (s, 18H, -OSi$(CH_3)_3$), 0.15 (s, 9H, -OSi$(CH_3)_3$), 0.13 (s, 9H, -OSi$(CH_3)_3$), 0.12 (s, 9H, -OSi$(CH_3)_3$) ppm.

^{13}C NMR (100.6 MHz, $CDCl_3$, 278 K): δ= 94.8 (C-1), 72.4 (C-3 or C-5), 71.3 (C-3 or C-5), 70.7 (C-2 or C-4), 70.1 (C-2 or C-4), 61.2 (C-6), 0.7 (-OSi$(CH_3)_3$), 0.6 (-OSi$(CH_3)_3$), 0.4 (-OSi$(CH_3)_3$), 0.3 (-OSi$(CH_3)_3$), -0.4 (-OSi$(CH_3)_3$) ppm.

MS (ESI+): theoretical mass: 541.07 m/z, experimental mass $[M+Na]^+$: 563.61 m/z.

Synthesis of N-(benzyloxycarbonyl)aminopropyl 2,3,4,6-tetra-O-trimethylsilyl-α-D-galactopyranoside ***(11)***

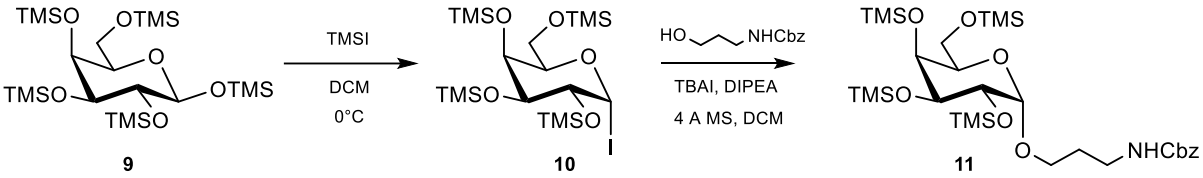

Compound **9** (1.96 g, 3.62 mmol) was dissolved in dry toluene and the solvent was evaporated, the process was repeated three times to get rid of any water traces. After 12 h, compound **9** was dissolved in dry DCM (20 ml, 0.18 M) under Ar atmosphere and cooled down to 0 °C followed by the dropwise addition of TMSI (0.52 ml, 3.66 mmol). The reaction mixture was stirred for 90 mins at 0 °C and monitored by TLC (Hex:EtOAc 8:2). After disappearance of the starting material, the excess of solvent was removed to obtain the galactosyl iodide **10**.

In a separate flask, benzyl *N*-(3-hydroxypropyl) carbamate (1.14 g, 5.43 mmol) was dissolved in toluene and the solvent was evaporated, the process was repeated three times to ensure dryness. After 15 h, it was dissolved in 10 ml of dry DCM and 4 Å MS, TBAI (4.01 g, 10.86 mmol) and DIPEA (1.3 ml, 7.24 mmol) were added. The mixture was stirred for 15 mins before the addition of a solution of the intermediate **10** in 15 ml of DCM. The reaction mixture was stirred for 15 h and monitored by TLC (Hex:EtOAc 8:2). Once the reaction was complete, it was filtered over celite, the excess of solvent was removed and the crude was purified by column chromatography (Hex:EtOAc 95:5 → 9:1 + 0.5% TEA) to afford glycoside **11** (2.37 g, 62 %) as a white solid.

TLC: R_f: 0.61 (Hex:EtOAc - 7:3).

NMR data:

^{1}H NMR (400 MHz, $CDCl_3$, 25 ºC): δ= 7.38 – 7.28 (m, 5H, H_{arom}), 5.81 (m, 1H, -NH), 5.10 (s, 2H, -NHCOOC$\underline{H}_2$Ph), 4.70 (d, 1H, $J_{1\text{-}2}$= 3.7 Hz, H-1), 3.92 (m, 3H, H-2, H-4, H-7a), 3.78 (m, 2H, H-3, H-5), 3.61 (m, 3H, H-6a, H-6b, H-9a), 3.40 (m, 1H, H-7b), 3.14 (m, 1H, H-9b), 1.81 (m, 2H, H-8), 0.15 (s, 9H, -OSi$(CH_3)_3$), 0.13 (s, 9H, -OSi$(CH_3)_3$), 0.11 (s, 9H, -OSi$(CH_3)_3$), 0.10 (s, 9H, -OSi$(CH_3)_3$) ppm.

^{13}C NMR (100.6 MHz, $CDCl_3$, 25 ºC): δ= 157.2 (-NH$\underline{C}$OOCH$_2$Ph), 128.5 and 128.1 (C_{arom}), 100.8 (C-1), 72.6 (C-2 or C-4), 71.8 (C-3 or C-5), 71.3 (C-3 or C-5), 69.9 (C-2 or C-4), 68.9 (C-7), 66.5 (-NHCOO$\underline{C}$H$_2$Ph), 61.7 (C-6), 40.5 (C-9), 29.4 (C-8), 0.9 (-OSi$(CH_3)_3$), 0.7 (-OSi$(CH_3)_3$), 0.4 (-OSi$(CH_3)_3$), -0.3 (-OSi$(CH_3)_3$) ppm.

*Synthesis of N-(benzyloxycarbonyl)aminopropyl α-D-galactopyranoside (**12**)*

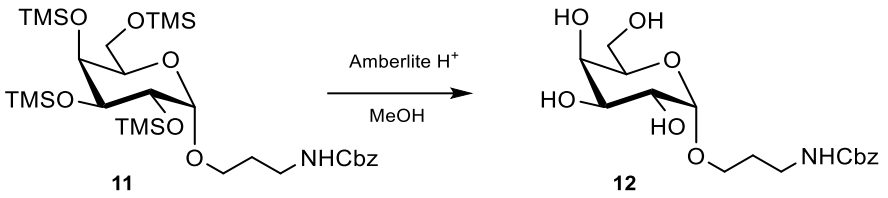

Compound **11** (1.67 g, 2.53 mmol) was dissolved in MeOH and Amberlite IR120 was added. The reaction mixture was stirred until TLC (DCM:MeOH - 8:2) showed disappearance of the starting material. The Amberlite was filtered off using a cotton and the excess of solvent was evaporated to obtain compound **12** as a colorless oil (0.92 g, 98 %).

TLC: R_f: 0.46 (DCM:MeOH - 8:2).

NMR data:

^{1}H NMR (400 MHz, CD_3OD, 25 ºC): δ= 7.40 – 7.28 (m, 5H, H_{arom}), 5.09 (s, 2H, -NHCOOC$\underline{H}_2$Ph), 4.81 (d, 1H, $J_{1\text{-}2}$= 3.7 Hz, H-1), 3.89 (dd, $J_{4\text{-}3}$= $J_{4\text{-}5}$ < 2 Hz, 1H, H-4), 3.84 – 3.79 (m, 2H, H-3 and H-7a), 3.85 – 3.75 (m, 2H, H-2 and H-5), 3.71 (m, 2H, H-6), 3.49 (m, 1H, H-7b), 3.27 (m, 2H, H-9), 1.82 (m, 2H, H-8) ppm.

^{13}C NMR (100.6 MHz, CD_3OD, 25 ºC): δ= 129.6 and 129.1 H_{arom}), 100.6 (C-1), 72.6 (C-3), 71.7 (C-2 or C-5), 71.2 (C-4), 70.4 (C-2 or C-5), 67.5 (-NHCOO$\underline{C}H_2$Ph), 66.7 (C-7), 62.9 (C-6), 38.2 (C-9), 30.8 (C-8) ppm.

MS (ESI+): theoretical mass: 371.39 m/z, experimental mass $[M+Na]^+$: 394.33 m/z.

*Synthesis of 3'-aminopropyl α-D-galactopyranoside (**2**)*

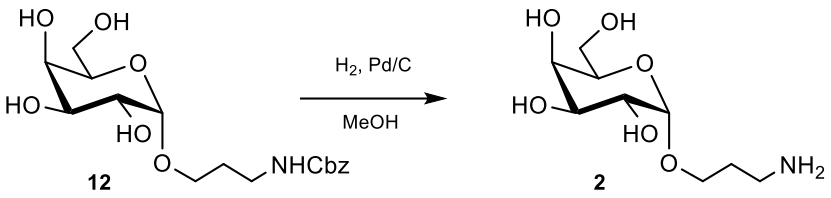

To a solution of compound **12** (0.54 g, 1.45 mmol) in MeOH (10 ml, 0.01 M), Pd/C was added. The reaction atmosphere was purged with H_2/vacuum cycles and then, stirred under H_2 atmosphere. After 3 h, the Pd/C was filtered through a whatman syringe filter and concentrated under vacuum to obtain compound **2** as a colorless foam (0.34 g, quant.).

NMR data:

^{1}H NMR (400 MHz, D_2O, 25 ºC): δ= 4.95 (d, 1H, $J_{1\text{-}2}$= 3.0 Hz, H-1), 3.98 (bs, 1H, H-4), 3.93 (m, 1H, H-5), 3.88 – 3.80 (m, 3H, H-2, H-3, H-7a), 3.75 (m, 2H, H-6), 3.59 (m, 1H, H-7b), 2.91 (m, 2H, H-9), 1.88 (m, 2H, H-8) ppm.

^{13}C NMR (100.6 MHz, D_2O, 25 ºC): δ= 98.1 (C-1), 70.7 (C-5), 69.0, 68.8 and 67.6 (C-2, C4 or C-3), 65.46 (C-7), 60.8 (C-6), 37.9 (C-9), 26. 2 (C-8) ppm.

MS (ESI+): theoretical mass: 237.25 m/z, experimental mass $[M+H]^+$: 238.05 m/z.

1.3. Synthesis of 3'-aminopropyl α-L-fucopyranoside

*Synthesis of acetyl 2,3,4-tri-O-trimethylsilyl-α-L-fucopyranoside (**23**)*

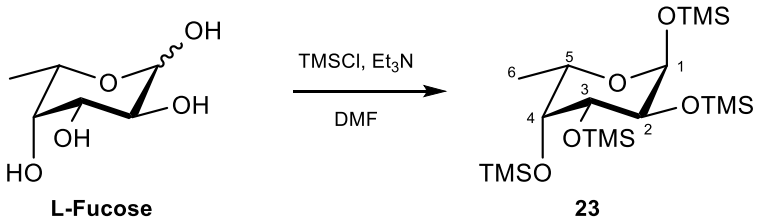

L-Fucose **23**

To a suspension of L-fucose (1.08 g, 6.58 mmol) in DMF (50 ml, 0.1 M), TEA (3.7 ml, 26.32 mmol) was added. The mixture was cooled down to 0 °C followed by the dropwise addition of TMSCl (3.3 ml, 26.3 mmol). After 15 h, the reaction mixture was diluted in 50 ml of hexane and extracted with cold water (2 x 50 ml) and brine (2 x 50 ml). The organic phase was dried over anhydrous Na_2SO_4, filtered and the excess of solvent was removed under vaccuum to afford compound **23** (2.83 g, 95 %) as a colorless syrup.

TLC: R_f: 0.88 (Hex:EtOAc - 1:1).

NMR data:

^{1}H NMR (400 MHz, $CDCl_3$, 25 ºC): δ= 5.03 (d, 1H, J_{1-2}= 2.9 Hz, H-1), 4.04 (dq, 1H, J_{5-6}= 6.4 Hz, J_{5-4} *< 1* Hz, H-5), 3.81 (m, 2H, H-2 and H-3), 3.6 (m, 1H, H-4), 1.12 (d, 3H, J_{6-5}= 6.4 Hz, H-6), 0.14 (s, 27H, -OSi$(CH_3)_3$), 0.10 (s, 9H, -OSi$(CH_3)_3$) ppm.

^{13}C NMR (100.6 MHz, $CDCl_3$, 25 ºC): δ= 94.8 (C-1), 76.6 (C-4), 71.1 (C-2 or C-3), 69.8 (C-2 or C-3), 67.1 (C-5), 17.1 (C-6), 0.82 (-OSi$(CH_3)_3$), 0.58 (-OSi$(CH_3)_3$), 0.44 (-OSi$(CH_3)_3$), 0.31 (-OSi$(CH_3)_3$) ppm.

MS (ESI+): theoretical mass: 452.89 m/z, experimental mass $[M+Na]^+$: 475.36 m/z.

*Synthesis of N-(benzyloxycarbonyl)aminopropyl 2,3,4-tri-O-trimethylsilyl-α-L-fucopyranoside (**25**)*

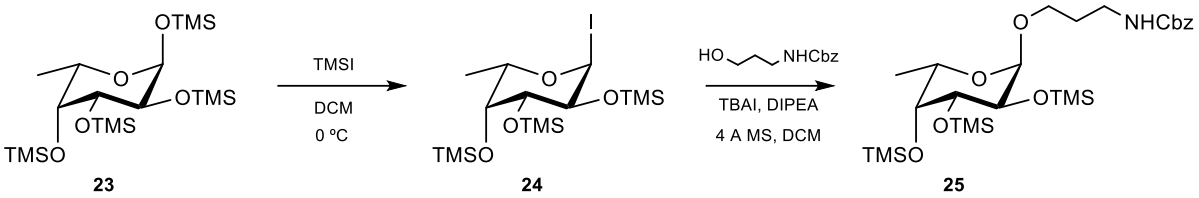

23 **24** **25**

Compound **23** (1.40 g, 3.09 mmol) was dissolved in dry toluene and the solvent was evaporated, the process was repeated three times to get rid of any water traces. After 15 h, compound **23** was dissolved in dry DCM (25 ml, 0.12 M) under Ar atmosphere and cooled down to 0 °C followed by the dropwise addition of TMSI (0.44 ml, 3.09 mmol). The reaction mixture was stirred for 60 mins at 0 °C and monitored by TLC (Hex:EtOAc 8:2). After disappearance of the starting material, the excess of solvent was removed to obtain the fucosyl iodide **24**.

In a separate flask, benzyl *N*-(3-hydroxypropyl) carbamate (1.14 g, 5.45 mmol) was co-evaporated with toluene. After 16 h, it was dissolved in 10 ml of dry DCM and 4 Å MS, TBAI (1.14 g, 3.09 mmol) and DIPEA (1.0 ml, 6.18 mmol) were added. The mixture was stirred for 15 mins before the addition of a solution of the intermediate **24** in 10 ml of dry DCM. The reaction mixture was stirred for 15 h and monitored by TLC (Hex:EtOAc 8:2). Once the reaction was complete, it was filtered over celite, the excess of solvent was removed and the crude was purified by column chromatography (Hex:EtOAc 9:1 → 8:2 + 1 % TEA) to afford the fucosyde **25** (0.95 g, 54 %) as a transparent oil.

TLC: R_f: 0.67 (Hex:EtOAc - 1:1).

NMR data:

^{1}H NMR (400 MHz, $CDCl_3$, 25 ºC): δ= 7.37 – 7.27 (m, 5H, H_{arom}), 5.82 (m, 1H, -N<u>H</u>), 5.07 (s, 2H, -NHCOOC<u>H</u>$_2$Ph), 4.67 (d, 1H, $J_{1\text{-}2}$= 3.7 Hz, H-1), 3.92 – 3.83 (m, 3H, H-2, H-5, H-7a), 3.76 (dd, 1H, $J_{3\text{-}2}$= 9.7 Hz, $J_{3\text{-}4}$= 2.9 Hz, H-3), 3.58 (m, 2H, H-4, H-9a), 3.37 (m, 1H, H-7b), 3.15 (m, 1H, H-9b), 1.78 (m, 2H, H-8), 1.13 (d, 3H, $J_{6\text{-}5}$= 6.4 Hz, H-6), 0.14 (s, 9H, -OSi(CH_3)$_3$), 0.09 (s, 9H, -OSi(CH_3)$_3$), 0.08 (s, 9H, -OSi(CH_3)$_3$) ppm.

^{13}C NMR (100.6 MHz, $CDCl_3$, 25 ºC): δ= 128.6 and 128.0 (C_{arom}), 100.6 (C-1), 75.9 (C-4), 71.3 (C-3), 69.3 (C-2 or C-5), 69.0 (C-7), 67.1 (C-2 or C-5), 66.4 (-NHCOO<u>C</u>H$_2$Ph), 40.5 (C-9), 29.3 (C-8), 17.0 (C-6), 0.8 (-OSi(CH_3)$_3$), 0.6 (-OSi(CH_3)$_3$), 0.4 (-OSi(CH_3)$_3$) ppm.

MS (ESI+): theoretical mass: 571.93 m/z, experimental mass $[M+Na]^+$: 594.66 m/z.

*Synthesis of N-(benzyloxycarbonyl)aminopropyl α-L-fucopyranoside (**21**)*

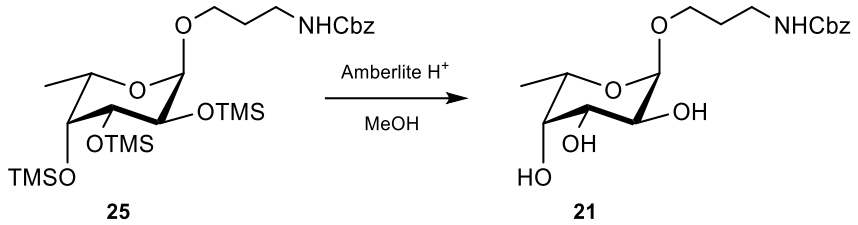

25 **21**

Compound **25** (0.95 g, 1.66 mmol) was dissolved in MeOH (10 ml, 0.16 M) and Amberlite IR120 was added. The reaction mixture was stirred until TLC (DCM:MeOH - 9:1) showed disappearance of the starting material. The Amberlite was filtered off using cotton and the excess of solvent was evaporated to obtain compound **21** as a colorless oil (0.55 g, 93 %).

TLC: R_f: 0.32 (DCM:MeOH - 9:1).

NMR data:

^{1}H NMR (400 MHz, CD_3OD, 23 ºC): δ= 7.41 – 7.30 (m, 5H, H_{arom}), 5.10 (s, 2H, -NHCOOC$\underline{H}_2$Ph), 4.76 (d, 1H, $J_{1\text{-}2}$= 2.9 Hz, H-1), 3.96 (m, 1H, H-5), 3.80 – 3.73 (m, 3H, H-2, H-3, H-7a), 3.67 (m, 1H, H-4), 3.48 (m, 1H, H-7b), 3.29 (m, 2H, H-9b), 1.83 (m, 2H, H-8), 1.21 (d, 3H, $J_{6\text{-}5}$= 6.5 Hz, H-6), ppm.

^{13}C NMR (100.6 MHz, CD_3OD, 23 ºC): δ= 130.2 – 128.5 (C_{arom}), 100.6 (C-1), 73.7 (C-4), 71.9 (C-2 or C-3), 70.2 (C-2 or C-3), 67.7 (C-5), 67.6 (-NHCOO$\underline{C}H_2$Ph), 66.7 (C-7), 39.2 (C-9), 30.8 (C-8), 16.8 (C-6) ppm.

MS (ESI+): theoretical mass: 355.39 m/z, experimental mass $[M+Na]^+$: 378.24 m/z.

*Synthesis of 3'-aminopropyl α-L-fucopyranoside (**3**)*

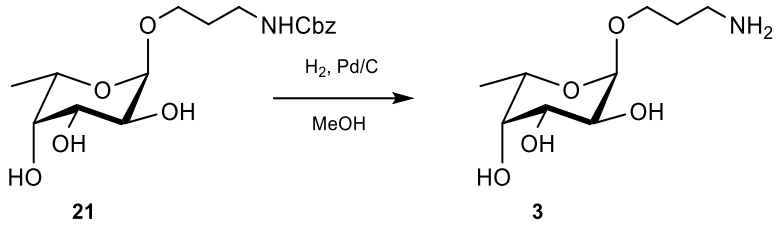

21 **3**

To a solution of compound **21** (0.54 g, 1.52 mmol) in MeOH (15 ml, 0.10 M), Pd/C was added. The reaction atmosphere was purged with H_2/vacuum cycles and then, stirred under H_2 atmosphere. After 3 h, the Pd/C was filtered through a whatman syringe filter and concentrated under vacuum to give compound **3** as a colorless foam (0.34 g, quant.).

NMR data:

^{1}H NMR (400 MHz, D_2O, 25 ºC): δ= 4.90 (d, 1H, $J_{1\text{-}2}$= 3.5 Hz, H-1), 4.07 (dq, 1H, $J_{5\text{-}6}$= 6.5 Hz, $J_{5\text{-}4}$< *1* Hz, H-5), 3.88 (m, 1H, H-7a), 3.85 – 3.78 (m, 3H, H-2, H-3, H-4), 3.59 (m, 1H, H-7b), 3.15 (m, 2H, H-9), 2.00 (m, 2H, H-8), 1.22 (d, 3H, $J_{6\text{-}5}$= 6.5 Hz, H-6) ppm.

^{13}C NMR (100.6 MHz, D_2O, 25 ºC): δ= 100.9 (C-1), 74.0, 71.9, 70.1 (C-2, C-3 and C-4), 69.00 (C-5), 68.3 (C-7), 40.1 (C-9), 28.7 (C-8), 17.52 (C-6) ppm.

MS (ESI+): theoretical mass: 221.37 m/z, experimental mass $[M+Na]^+$: 244.03 m/z.

1.4. Synthesis of AuGNPs

All glassware employed for Au NPs synthesis was previously cleaned using aqua regia ($HCl:HNO_3$ - 3:1). MilliQ water, was employed for the aqueous solutions. The solution of $HAuCl_4 \cdot 3H_2O$ 10 mM was stored at 4°C under the exclusion of light, whereas $NaCt_3 \cdot 2H_2O$, $AgNO_3$ and hydroquinone solutions were freshly prepared before every synthesis. HS-PEG5000-COOH and HS- PEG5000-NH_2 were purchased from Rapp Polymer GmbH and HS-Alkyl-PEG600-COOH was synthesized by Chorisis srl following a reported procedure[244]. All polymers were stored at -20 °C under Ar atmosphere.

Size exclusion chromatography was performed using Sephadex G-25 or Sephadex G-10 (Sigma Aldrich) depending on the PEG MW. The purification and concentration of Au NPs was achieved by ultrafiltration employing Millipore Amicon Centrifugal Filter Units (30 KDa cut-off). The size of the Au NPs was determined by transmission electron microscopy (TEM) operated on a LaB 6-TEM JEOL JEM 1400 (40 - 120 kV) microscope. The TEM samples were prepared by deposition of the NPs suspension (3 μL) onto a carbon-coated microscopy copper grid. The particle size distribution was obtained by measuring at least 800 nanoparticles. Agilent 8453 spectrometer was employed to register UV/Vis spectra. A 1 cm optical path length cuvette was employed for the measurements. Dynamic Light Scattering (DLS) measurements were performed employing a 90 Plus Particle Size Analyzer (Brookhaven Instrument Corporation). Samples were equilibrated for 3 min prior to measurement and at least three independent measurements of 10 runs (10 s each one) were performed for each sample.

1.4.1. General procedures

General procedure A: Synthesis of HS-PEG5000-sugar

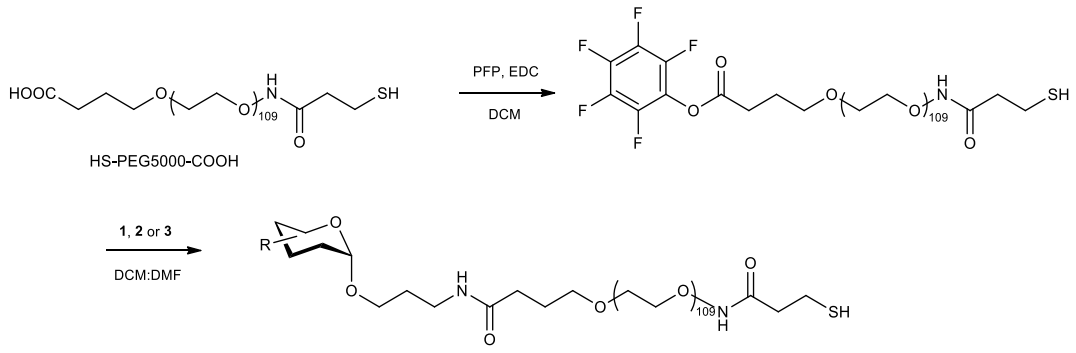

To a solution of HS-PEG5000-COOH (1 eq.) in dry DCM (0.02 M), pentafluorophenol (3 eq.) and 1-ethyl-3-(3-dimethylaminopropyl)carbodiimide (3 eq.) were added. The reaction progress was monitored by TLC (DCM:MeOH - 9:1). After 48 h the excess of DCM was evaporated, the crude was re-dissolved in cold Et_2O and centrifuged for 6 min at 6000 rpm. The supernatant was removed, and the centrifugation process was repeated for 5 times until the formation of a white HS-PEG5000-COO-PFP precipitate.

^{19}F NMR (376 MHz, $CDCl_3$, 25 ºC): δ= -152.75 (dd, 2F, F_{ortho}), -158.9 (t, 1F, F_{para}), -162.37 (dt, 2F, F_{meta}) ppm.

HS-PEG5000-PFP (1 eq.) was dissolved in dry DCM (0.02 M). *N*,*N*-diisopropylethylamine (DIPEA) (3 eq.) was added, followed by dropwise addition of monosaccharides **1**, **2** or **3** (3 eq.) previously dissolved in dry DMF. The reaction was monitored by TLC (DCM:MeOH - 8:2) and after 36 h, the

solvent was removed under vacuum. The crude product was redissolved in water and purified by Sephadex G-25.

Before adding to the NPs solution, the product was dissolved in a phosphate buffer saline water solution at pH 7.4 (0.02 M) and 1,4-dithiothreitol (DTT) (4 eq.) was added. The reaction mixture was stirred at 50 °C and after 3 h, the excess of solvent was removed under reduced pressure. The crude was purified by Sephadex G-25 before addition to the Au NPs.

General procedure B: Synthesis of HS-Alkyl-PEG600-sugar

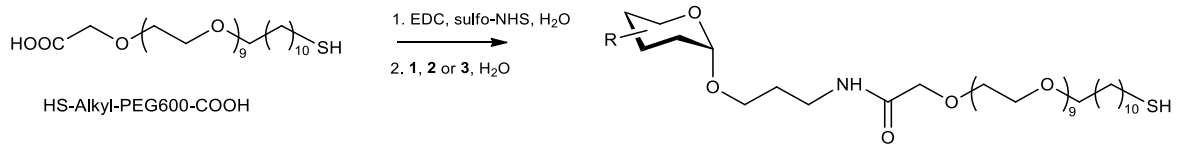

To a solution of HS-Alkyl-PEG600-COOH (1 eq.) in H_2O (0.1 M), 1-ethyl-3-(3-dimethylaminopropyl) carbodiimide (EDC) (2 eq.) and *N*-hydroxysulfosuccinimide (sulfo-NHS) (2 eq.) were added in order to activate the carboxylic moiety and stirred for 1 h at r.t. Monosaccharides **1**, **2** or **3** (1.5 eq.), dissolved in H_2O, were subsequently added. After 48 h, the solvent was evaporated under reduced pressure and the crude product was purified by Sephadex G-10.

Before adding to the NPs solution, the product was dissolved in a phosphate buffer saline water solution at pH 7.4 (0.02 M) and DTT (4 eq.) was added. The reaction mixture was stirred at 50 °C and after 3 h, the excess of solvent was removed under reduced pressure. The crude was purified by Sephadex G-10 and directly employed for Au NPs functionalization.

General AuGNPs synthesis

A water solution of $HAuCl_4 \cdot 3H_2O$ (7.5 ml, 10 mM), sodium citrate dihydrate (9 ml, 67 mM), and $AgNO_3$ (420 µl, 5.9 mM) was prepared and mixed at r.t. for 6 minutes. The pre-incubated mixture was added to 250 ml of H_2O at 100 °C and the mixture was vigorously stirred for 1 h. Afterwards the reaction solution was cooled down to r.t. and glycerol (5 ml, 68.5 mmol) was added. After 15 mins, a second mixture of $HAuCl_4 \cdot 3H_2O$ (7.5 ml, 10 mM), sodium citrate dihydrate (10 ml, 34 mM) and $AgNO_3$ (426 µl, 5.9 mM) pre-mixed for 6 minutes, was added to the reaction solution. Immediately followed by a hydroquinone solution (8 ml, 91 mM). Then, the colloidal solution was left to age for 2 h stirring at r.t. AuGNPs were obtained by adding the prepared HS-PEG-monosaccharides to the colloidal solution containing citrate-capped Au NPs. For all particles, 10 % of HS-PEG5000-NH_2 was added to allow subsequent coupling to a fluorescent tag. The reaction mixture was stirred at r.t. for 48 h and the functionalized AuGNPs were purified using Amicon centrifugal filter units to a final volume of 10 mL to obtain the desired AuGNPs.

1.4.2. AuGNPs synthesis.

Preparation of Au-PEG5000-Mannose

Compound **1** (7.6 mg, 0.032 mmol) was reacted with HS-PEG5000-PFP (53.2 mg, 0.011 mmol) according to General procedure A to obtain HS-PEG5000-Man (50.0 mg) as a white foam.

^{1}H NMR (400 MHz, D_2O, 25 ºC): δ= 4.88 (d, 1H, $J_{1\text{-}2}$= 1.7, H-1), 3.95 (dd, 1H, $J_{2\text{-}1}$= 1.68 Hz, $J_{2\text{-}3}$= 3.46 Hz, H-2), 3.99 – 3.49 (m, 480 H, H-3, H-4, H-5, H-6, H-7a and -O-CH_2-CH_2-O), 3.54 (m, 1H, H-7b), 2.71 (m, 2H, H-9), 2.61 (t, 2H, -O-C$\underline{H}_2$-CH_2-), 2.50 (t, 2H, HS-C$\underline{H}_2$-CH_2-), 2.33 (m, 4H, -CH_2-C$\underline{H}_2$-CONH- and -CH_2-C$\underline{H}_2$-CONH-), 1.85 (m, 4H, H-8 and -CH_2-C$\underline{H}_2$-CH_2-) ppm.

Au-PEG5000-Man NPs were obtained by adding 25.2 mg of HS-PEG5000-Man and 3 mg of HS-PEG5000-NH_2 to a colloidal solution containing citrate-capped Au NPs prepared according to the general procedure for AuGNPs synthesis.

Preparation of Au-PEG5000-Galactose

Compound **2** (8.5 mg, 0.036 mmol) was reacted with HS-PEG5000-PFP (46.5 mg, 0.009 mmol) according to General procedure A to obtain HS-PEG5000-Gal (40.8 mg) as a white foam.

^{1}H NMR (400 MHz, D_2O, 25 ºC): δ= 4.94 (d, 1H, $J_{1\text{-}2}$= 3.6 Hz, H-1), 3.98 (d, 1H, H-4), 3.89 (m, 3H, H-2, H-3, H-5), 3.93 – 3.42 (m, 523 H, H-6, H-7a and -O-CH_2-CH_2-O), 3.55 (m, 1H, H-7b), 2.73 (m, 2H, H-9), 2.68 (t, 2H, -O-C$\underline{H}_2$-CH_2-), 2.57 (t, 2H, HS-C$\underline{H}_2$-CH_2-), 2.40 (m, 4H, -CH_2-C$\underline{H}_2$-CONH- and -CH_2-C$\underline{H}_2$-CONH-), 1.86 (m, 4H, H-8 and -C$\underline{H}_2$-CH_2-COONH) ppm.

Au-PEG5000-Gal NPs were obtained by adding 23.3 mg of HS-PEG5000-Gal and 3 mg of HS-PEG5000-NH_2 to a colloidal solution containing citrate-capped Au NPs prepared according to the general procedure for AuGNPs synthesis.

Preparation of Au-PEG5000-Fucose

Compound **3** (11.3 mg, 0.051 mmol) was reacted with HS-PEG5000-PFP (60.7 mg, 0.012) according to General procedure A to obtain HS-PEG5000-Fuc (57.1 mg,) as a white foam.

^{1}H NMR (400 MHz, D_2O, 25 ºC): δ= 4.89 (d, 1H, $J_{1\text{-}2}$= 3.7 Hz, H-1), 3.93 (m, 2H, H-5, H-7a), 3.89 – 3.77 (m, 3H, H-2, H-3, H-4), 3.73 – 3.55 (m, 386 H, -O-CH_2-CH_2-O), 3.26 (m, 1H, H-7b), 2.73 (m, 2H, H-9), 2.61 (t, 2H, -O-C$\underline{H}_2$-CH_2-), 2.54 (t, 2H, HS-C$\underline{H}_2$-CH_2-), 2.24 (m, 4H, -CH_2-C$\underline{H}_2$-CONH- and -CH_2-C$\underline{H}_2$-CONH-), 1.70 (m, 4H, H-8 and -CH_2-C$\underline{H}_2$-CH_2-), 1.31 (d, 3H, $J_{6\text{-}5}$= 6.8 Hz, H-6) ppm.

Au-PEG5000-Fuc NPs were obtained by adding 26.2 mg of HS-PEG5000-Fuc and 3 mg of HS-PEG5000-NH_2 to a colloidal solution containing citrate-capped Au NPs prepared according to the general procedure for AuGNPs synthesis.

Preparation of Au-Alkyl-PEG600-Mannose

Initially HS-Alkyl-PEG600-COOH (52 mg, 0.08 mmol) reacted with EDC (33 mg, 0.172 mmol) and sulfo-NHS (35 mg, 0.16 mmol). After 1 h, a solution of compound **1** (32 mg, 0.135 mmol) in 0.5 ml of H_2O was added according to General procedure B to obtain HS-Alkyl-PEG600-Man as a white foam (58 mg).

^{1}H NMR (400 MHz, D_2O, 25 ºC): δ= 4.86 (d, 1H, $J_{1\text{-}2}$= 1.7, H-1), 3.93 (s, 2H, -O-CH_2-COO-), 3.87 – 3.56 (m, 48 H, H-2, H-3, H-4, H-5, H-6, H-7 and -O-CH_2-CH_2-O), 3.52 (t, 2H, -CH_2-C$\underline{H}_2$-O-), 3.10 (m, 2H, H-9), 2.53 (t, 2H, -SH-C$\underline{H}_2$-CH_2-), 1.87 (m, 2H, H-8), 1.31 (m, 16 H, -CH_2-CH_2-) ppm.

Au-Alkyl-PEG600-Man NPs were obtained by adding 20.4 mg of HS-Alkyl-PEG600-Man and 2 mg of HS-PEG5000-NH_2 to a colloidal solution containing citrate-capped Au NPs prepared according to the general procedure for AuGNPs synthesis.

Preparation of Au-Alkyl-PEG600-Galactose

HS-Alkyl-PEG600-COOH (69 mg, 0.09 mmol) reacted with EDC (41 mg, 0.22 mmol) and sulfo-NHS (35 mg, 0.18 mmol). After 1 h, a solution of compound **2** (42 mg, 0.18 mmol) in 0.5 ml of H_2O was added according to General procedure B to obtain HS-Alkyl-PEG600-Gal as a white foam (72 mg).

^{1}H NMR (400 MHz, D_2O, 25 ºC): δ= 4.94 (H-1), 3.95 (s, 2H, -O-CH_2-COO-), 3.82 – 3.59 (m, 48 H, H-2, H-3, H-4, H-5, H-6, H-7 and -O-CH_2-CH_2-O), 3.54 (t, 2H, -CH_2-C$\underline{H}_2$-O-), 3.17 (m, 2H, H-9), 2.54 (t, 2H, -SH-C$\underline{H}_2$-CH_2-), 1.81 (m, 2H, H-8), 1.32 (m, 16 H, -CH_2-CH_2-) ppm.

Au-Alkyl-PEG600-Gal NPs were obtained by adding 24.0 mg of HS-Alkyl-PEG600-Gal and 3 mg of HS-PEG5000-NH_2 to a colloidal solution containing citrate-capped Au NPs prepared according to the general procedure for AuGNPs synthesis.

Preparation of Au-Alkyl-PEG600-Fucose

HS-Alkyl-PEG600-COOH (50 mg, 0.07 mmol) reacted with EDC (33 mg, 0.17 mmol) and sulfo-NHS (34 mg, 0.16 mmol). After 1 h, a solution of compound **3** (42 mg, 0.19 mmol) in 0.5 ml of H_2O was added according to General procedure B to obtain HS-Alkyl-PEG600-Fuc as a white foam (42 mg).

^{1}H NMR (400 MHz, D_2O, 25 ºC): δ= 4.86 (d, 1H, $J_{1\text{-}2}$= 3.6, H-1), 3.90 (s, 2H, -O-CH_2-COO-), 3.8 – 3.56 (m, 50 H, H-2, H-3, H-4, H-5, H-7 and -O-CH_2-CH_2-O-), 3.46 (t, 2H, -CH_2-C$\underline{H}_2$-O-), 3.17 (m, 2H, H-9), 2.54 (t, 2H, -SH-C$\underline{H}_2$-CH_2-), 1.85 (m, 2H, H-8), 1.29 (m, 16 H, -CH_2-CH_2-), 1.18 (d, 3H, $J_{6\text{-}5}$= 6.8 Hz, H-6) ppm.

Au-Alkyl-PEG600-Fuc NPs were obtained by adding 23.6 mg of HS-Alkyl-PEG5000-Fuc and 3 mg of HS-PEG5000-NH_2 to a colloidal solution containing citrate-capped Au NPs prepared according to the general procedure for AuGNPs synthesis.

1.5. Synthesis of 3'-aminopropyl 6-O-phospho-α-D-mannopyranoside

*Synthesis of 3'-azidopropyl 6-O-tert-butyldimethylsilyl-α-D-mannopyranoside (**29**)*

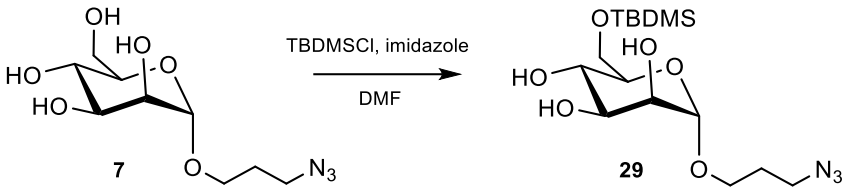

Compound **7** (0.46 g, 1.75 mmol) was dissolved in dry DMF (15 ml, 0.1 M), imidazole (0.43 g, 3.85 mmol) and TBDMSCl (0.51 g, 3.33 mmol) were added at 0 °C and the reaction mixture was stirred for 48 h at r.t. until TLC ($CHCl_3$:MeOH - 85:15) showed complete conversion of the starting material. The excess of solvent was concentrated under reduced pressure and the crude was purified by column chromatography (Hex:EtOAc 9:1 → 7:3) to obtain compound **29** as a transparent oil (0.58, 1.53 mmol, 88%).

TLC: R_f: 0.48 ($CHCl_3$:MeOH 85:15).

NMR data:

^{1}H NMR (400 MHz, CD_3OD, 25 ºC): δ= 4.67 (d, 1H, $J_{1\text{-}2}$ = 1.47 Hz, H-1), 3.92 (dd, 1H, $J_{6a\text{-}6b}$= 11.1 Hz, $J_{6a\text{-}5}$ = 1.6 Hz, H-6a), 3.77 (m, 1H, H-7a), 3.81 (dd, 1H, $J_{2\text{-}3}$ = 3.5 Hz, $J_{2\text{-}1}$ = 1.5 Hz, H-2), 3.71 (dd, 1H, $J_{6b\text{-}6a}$= 11.1 Hz, $J_{6b\text{-}5}$ = 5.4 Hz, H-6b), 3.61 (m, 1H, H-3), 3.50 – 3.45 (m, 2H, H-4 and H-5), 3.43 (m, 1H, H-7b), 3.35 (m, 2H, H-9), 1.81 (m, 2H, H-8), 0.87 (s, 9H, -OSiC($C\underline{H}_3$)$_3$), 0.05 (s, 6H, -OSi($C\underline{H}_3$)$_2$) ppm.

^{13}C NMR (100.6 MHz, CD_3OD, 25 ºC): δ= 101.7 (C-1), 75.6 (C-4 or C-5), 72.9 (C-3), 72.3 (C-2), 68.8 (C-4 or C-5), 65.4 (C-7), 64.8 (C-6), 49.7 (C-9), 30.0 (C-8), 26.4 (-OSiC($\underline{C}H_3$)$_3$), 19.3 (-OSi$\underline{C}$(CH_3)$_3$), -5.1 (-OSi($\underline{C}H_3$)$_2$) ppm.

MS (ESI+): theoretical mass: 485.25 m/z, experimental mass $[M+Na]^+$: 508.44.

*Synthesis of 3'-azidopropyl 2,3,4-tri-O-benzyl-6-O-tert-butyldimethylsilyl-α-D-mannopyranoside (**30**)*

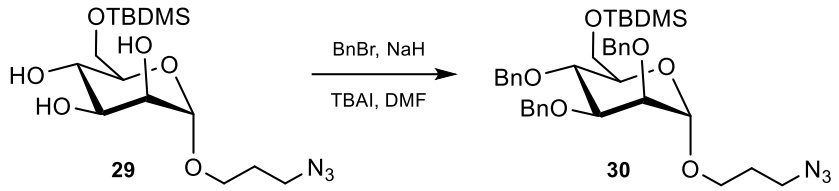

Compound **29** (1.86 g, 4.49 mmol) was dissolved in dry DMF (50 ml, 0.1 M), BnBr (4.5 ml, 37.03 mmol), NaH (0.54 g, 22.50 mmol) and TBAI (81 mg, 0.22 mmol) were added to the reaction mixture under Ar atmosphere. The reaction was stirred at r.t. and monitored by TLC (Hex: EtOAc - 7:3). After 24 h, the excess of NaH was quenched with MeOH and the reaction mixture was diluted in H_2O (50 ml) and Et_2O (50 ml). The organic phase was further washed with $NaHCO_3$ (2 x 30 ml) and brine (2 x 30 ml) and then, dried over anhydrous Na_2SO_4, filtered and concentrated in vacuo. The crude was purified by column chromatography (Hex:EtOAc 9:1 → 7:3) to yield compound **30** as a yellowish oil (2.19 g, 3.37 mmol, 68%).

TLC: R_f: 0.66 (Hex:EtOAc - 7:3).

NMR data:

^{1}H NMR (400 MHz, $CDCl_3$, 25 ºC): δ= 7.39 – 7.27 (m, 15H, H_{arom}), 4.91 (d, 1H, J_{gem}= 10.9 Hz, O$\underline{C}H_2$Ph), 4.79 (d, 1H, $J_{1\text{-}2}$= 1.7 Hz, H-1), 4.74 (d, 1H, J_{gem}= 12.4 Hz, -O$\underline{C}H_2$Ph), 4.68 – 4.59 (m, 4H, -O$\underline{C}H_2$Ph), 3.92 – 3.85 (m, 2H, H-3 and H-4), 3.83 (m, 2H, H-6a and H-6b), 3.75 – 3.70 (m, 2H, H-2 and H-7a), 3.55 (ddd, 1H, $J_{5\text{-}4}$= 10.9 Hz, $J_{5\text{-}6a}$= 7.3 Hz, $J_{5\text{-}6b}$= 2.5 Hz, H-5), 3.41 (m, 1H, H-7b), 3.29 (m, 2H, H-9), 1.78 (m, 2H, H-8), 0.89 (s, 9H, -OSiC(C$\underline{H}_3$)$_3$), 0.07 (s, 3H, -OSi(C$\underline{H}_3$)$_2$), 0.06 (s, 3H, -OSi(C$\underline{H}_3$)$_2$) ppm.

^{13}C NMR (100.6 MHz, $CDCl_3$, 25 ºC): δ= 128.6 ($C_{arom.}$), 98.4 (C-1), 79.9 (C-3 or C-4), 75.4 (C-2), 75.1 (-O$\underline{C}H_2$Ph), 75.0 (C-3 or C-4), 73.6 (C-5), 72.7 – 72.2 (-O$\underline{C}H_2$Ph), 62.4 (C-7), 63.0 (C-6), 48.7 (C-9), 29.6 (C-8), 25.7 (-OSiC($\underline{C}H_3$)$_3$), 18.3 (-OSi$\underline{C}$(CH$_3$)$_3$), -5.1 and -5.0 (-OSi($\underline{C}H_3$)$_2$) ppm.

*Synthesis of 3'-azidopropyl 2,3,4-tri-O-benzyl-α-D-mannopyranoside (**31**)*

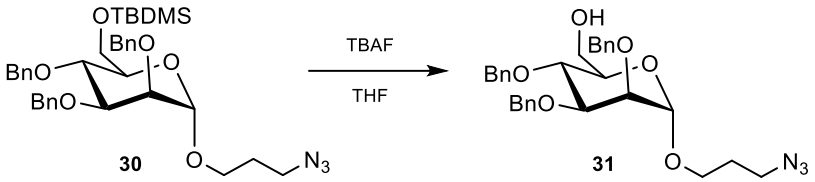

Compound **30** (2.19 g, 3.37 mmol) was dissolved in dry THF (30 ml, 0.1 M) and TBAF (0.1 M in THF, 7 ml) was added. The reaction mixture was stirred at r.t. and after 14 h, TLC (Hex:EtOAc - 7:3) showed complete disappearance of the starting material. The solvent was removed under vacuum and the crude was purified by column chromatography (Hex:EtOAc 8:2 → 6:4), the eluent in excess was evaporated to isolate compound **31** as white solid (1.74 g, 3.26 mmol, 96%).

TLC: R_f: 0.19 (Hex:EtOAc - 7:3).

NMR data:

^{1}H NMR (400 MHz, $CDCl_3$, 25 ºC): δ= 7.33 – 7.20 (m, 15H, H_{arom}), 4.88 (d, 1H, J_{gem}= 10.9 Hz, -OC$\underline{H}_2$Ph), 4.76 – 4.71 (m, 2H, H-1 and -OC$\underline{H}_2$Ph), 4.65 – 4.57 (m, 4H, -OC$\underline{H}_2$Ph), 3.91 (t, 1H, $J_{4\text{-}3}$= 9.5 Hz, $J_{4\text{-}5}$= 9.5 Hz, H-4), 3.79 (dd, 1H, $J_{3\text{-}4}$= 9.5 Hz, $J_{3\text{-}2}$ = 3.0 Hz, H-3), 3.78 (dd, 1H, $J_{6a\text{-}6b}$= 11.9 Hz, $J_{6a\text{-}5}$= 3.0 Hz, H-6a), 3.74 – 3.69 (m, 2H, H-2 and H-6b), 3.65 (m, 1H, H-7a), 3.55 (ddd, 1H, $J_{5\text{-}4}$= 9.5 Hz, $J_{5\text{-}6a}$= 3.0 Hz, $J_{5\text{-}6b}$= 4.8 Hz, H-5), 3.35 (dt, 1H, $J_{7a\text{-}7b}$= 9.9 Hz, $J_{7b\text{-}8}$= 6.5 Hz, H-7b), 3.25 (m, 2H, H-9), 1.73 (m, 2H, H-8) ppm.

^{13}C NMR (100.6 MHz, $CDCl_3$, 25 ºC): δ= 129.0 (C_{arom}), 98.7 (C-1), 80.5 (C-3), 75.5 (-O$\underline{C}H_2$Ph), 75.1 (C-2), 75.0 (C-4), 73.1 (-O$\underline{C}H_2$Ph), 72.8 (C-5), 72.4 (-O$\underline{C}H_2$Ph), 64.40 (C-7), 62.7 (C-6), 48.9 (C-9), 30.0 (C-8) ppm.

MS (ESI+): theoretical mass: 533.25 m/z, experimental mass $[M+Na]^+$: 556.67 m/z.

*Synthesis of 3'-azidopropyl 2,3,4-tri-O-benzyl-6-O-dibenzylphosphate-α-D-mannopyranoside (**33**)*

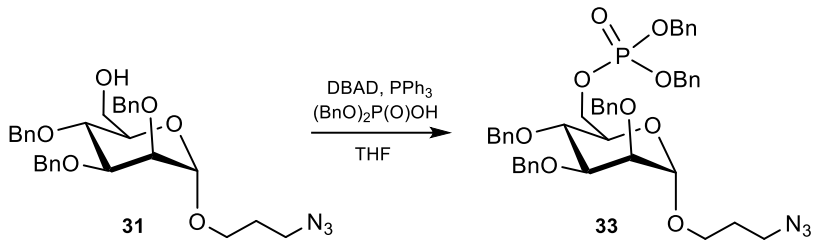

After co-evaporation with toluene and ACN respectively, compound **31** (0.18 g, 0.33 mmol) and dibenzyl phosphate (0.11 g, 0.40 mmol) were dissolved in dry THF (2 mL, 0.2 M) under Ar atmosphere. The reaction mixture was cooled down to 0 ºC and PPh_3 (0.19 g, 0.73 mmol) and DBAD (0.17 g, 0.73 mmol) were added. The reaction was monitored by TLC (Hex:EtOAc - 7:3). After 24 h the crude product was diluted with aq. HCl 10 % (10 ml) and extracted with DCM (10 ml). The water phase was further washed with DMC (2 x 10 mL). The combined organic phases were dried over Na_2SO_4 and concentrated in vacuo. The crude product was purified by column chromatography (Hex:EtOAc 9:1 → 7:3) to obtain phosphate **33** as a transparent syrup (0.23 g, 0.30 mmol, 87%).

TLC: R_f: 0.28 (Hex:EtOAc - 7:3).

NMR data:

^{1}H NMR (400 MHz, $CDCl_3$, 25 ºC): δ= 7.36–7.24 (m, 25H, H_{arom}), 5.09–5.01 (m, 4H, -P(O)O($C\underline{H}_2Ph)_2$), 4.90 (d, 1H, J_{gem}= 10.9 Hz, -O$C\underline{H}_2$Ph), 4.74 (d, 1H, $J_{1\text{-}2}$= 1.5 Hz, H-1), 4.71 (d, 1H, J_{gem}= 12.3 Hz, -O$C\underline{H}_2$Ph), 4.65 – 4.56 (m, 4H, -O$C\underline{H}_2$Ph), 4.35 – 4.25 (m, 2H, H-6a and H-6b), 3.94 (dd, 1H, $J_{4\text{-}3}$= 9.8 Hz, $J_{4\text{-}5}$= 9.5 Hz, H-4), 3.86 (dd, 1H, $J_{3\text{-}2}$= 2.9 Hz, $J_{3\text{-}4}$= 9.8 Hz, H-3), 3.73 (dd, 1H, $J_{2\text{-}1}$ = 1.5 Hz, $J_{2\text{-}3}$= 2.9 Hz, H-2), 3.71 – 3.65 (m, 2H, H-5 and H-7a), 3.35 (m, 1H, H-7b), 3.25 (m, 1H, H-9), 1.73 (m, 2H, H-8) ppm.

^{13}C NMR (100.6 MHz, $CDCl_3$, 25 ºC): δ= 128.2 (C_{arom}), 98.6 (C-1), 80.2 (C-3), 75.5 (-O$\underline{C}H_2$Ph), 75.1 (C-2), 73.4 (C-4), 73.2 (-O$\underline{C}H_2$Ph), 72.3 (-O$\underline{C}H_2$Ph), 71.4 (C-5), 69.4 – 69.3 (C-10 and C-11), 67.0 (C-6), 64.6 (C-7), 48.4 (C-9), 29.6 (C-8) ppm.

^{31}P NMR (162 MHz, $CDCl_3$, 25 ºC): δ= -0.98 ppm.

MS (ESI+): theoretical mass: 793.31 m/z, experimental mass $[M+H]^+$: 794.63 m/z.

*Synthesis of 3'-aminopropyl 6-O-phospho-α-D-mannopyranoside (**26**)*

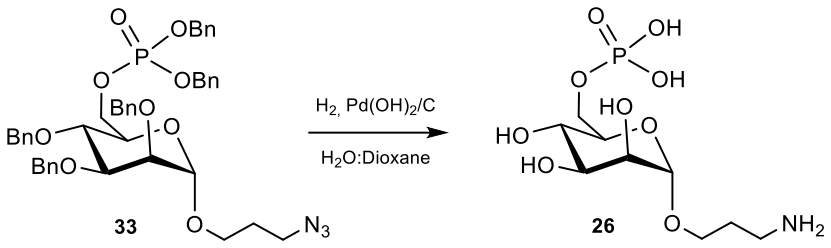

To a suspension of compound **33** (56.3 mg, 0.07 mmol) in H_2O:dioxane 1:1 (8 ml), a catalytic amount of $Pd(OH)_2/C$ was added. The solution was stirred in an autoclave at room temperature and under a H_2 pressure of 3 bars. After 4 days, the $Pd(OH)_2/C$ was filtered off through a Whatman filter and the excess of solvent was removed under vacuum and freeze dried to give compound **26** as a transparent solid (21.8 mg, 0.06 mmol, 98%).

NMR data:

^{1}H NMR (400 MHz, D_2O, 25 ºC): δ= 4.89 (s, 1H, H-1), 4.15 and 4.03 (m, 2H, H-6a and H-6b), 3.96 (m, 1H, H-2), 3.87 (m, 1H, H-7a), 3.81 (dd, 1H, $J_{3\text{-}2}$= 2.9 Hz, $J_{3\text{-}4}$= 9.8 Hz, H-3), 3.77 – 3.70 (m, 2H, H-5 and H-4), 3.66 (m, 1H, H-7b), 3.14 (t, 2H, $J_{9\text{-}8}$= 7.4 Hz, H-9), 2.03 (m, 2H, H-8) ppm.

^{13}C NMR (100.6 MHz, D_2O, 25 ºC): δ= 99.9 (C-1), 72.1 (C-4 or C-5), 70.6 (C-3), 70.5 (C-2), 66.5 (C-4 or C-5), 65.3 (C-7), 64.1 (C-6), 38.2 (C-9), 27.0 (C-8) ppm.

^{31}P NMR (162 MHz, D_2O, 25 ºC): δ= 1.17 ppm.

MS (ESI-): theoretical mass: 317.23 m/z, experimental mass [M-H]: 316.98 m/z.

1.6. Synthesis of 3'-aminopropyl 6-O-sulfo-α-D-mannopyranoside

*Synthesis of 3'-azidopropyl 2,3,4-tri-O-benzyl-6-O-sulfo-α-D-mannopyranoside sodium salt (**34**)*

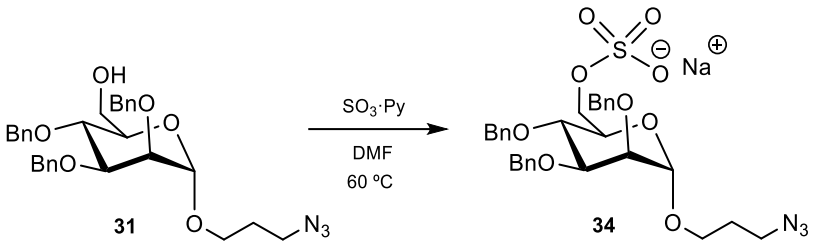

To a solution of compound **31** (0.20 g, 0.38 mmol) in dry DMF (3 mL, 0.1 M), SO_3·Py (0.30 g, 1.90 mmol) was added. The reaction mixture was warmed up to 60 °C and monitored by TLC (MeOH: $CHCl_3$ - 2:8). After 5 h, the reaction mixture was quenched with MeOH and concentrated under vacuum. The crude was purified by column chromatography (MeOH:$CHCl_3$ 1:9), the fractions containing the product were concentrated and eluted through a Dowex 50WX8 resin (Na^+ form) column to obtain compound **34** as a transparent solid (0.20 mg, 0.32 mmol, 84%).

TLC: R_f: 0.40 (MeOH:$CHCl_3$ - 2:8).

NMR data:

^{1}H NMR (400 MHz, $CDCl_3$, 25 ºC): δ= 7.36 – 7.19 (m, 15H, H_{arom}), 4.93 – 4.77 (m, 4H, H-1 and -OC$\underline{H}_2$Ph), 4.67 (d, 1H, J_{gem}= 10.2 Hz, -OC$\underline{H}_2$Ph), 4.52 (m, 2H, -OC$\underline{H}_2$Ph), 4.37 (m, 2H, H-6a and H-6b), 4.10 (dd, 1H, $J_{4\text{-}3}$= 9.5 Hz, $J_{4\text{-}5}$= 9.2 Hz, H-4), 3.78 (dd, 1H, $J_{3\text{-}2}$= 2.8 Hz, $J_{3\text{-}4}$= 9.2 Hz, H-3), 3.69 (m, 1H, H-2), 3.64 (m, 1H, H-5), 3.57 (m, 1H, H-7a), 3.29 (m, 1H, H-7b), 3.08 (m, 2H, H-9), 1.58 (m, 2H, H-8) ppm.

^{13}C NMR (100.6 MHz, $CDCl_3$, 25 ºC): δ= 129 (C_{arom}), 98.2 (C-1), 79.9 (C-3), 75.6 (-O$\underline{C}H_2$Ph), 74.5 (C-4), 73.4 (-O$\underline{C}H_2$Ph), 72.7 (-O$\underline{C}H_2$Ph), 70.7 (C-5 and C-2), 66.7 (C-6), 65.0 (C-7), 48.9 (C-9), 28.7 (C-8) ppm.

MS (ESI+): theoretical mass: 635.19 m/z, experimental mass $[M+Na]^+$: 658.78 m/z.

*Synthesis of 3'-aminopropyl 6-O-sulfo-α-D-mannopyranoside sodium salt (**27**)*

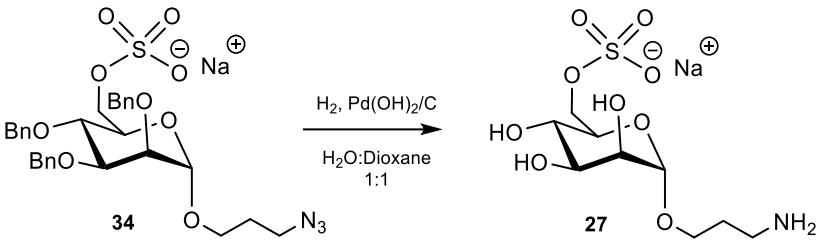

To a solution of compound **34** (80.3 mg, 0.13 mmol) in H_2O:dioxane 1:1 (8 ml), catalytic amount of $Pd(OH)_2/C$ was added. The solution was stirred in an autoclave at room temperature and under a H_2 pressure of 5 bars. After 5 days, the $Pd(OH)_2/C$ was filtered off through a Whatman filter and the excess of solvent was removed under vacuum and freeze dried to afford compound **27** as a yellowish solid (36.4 mg, 0.11 mmol, 84 %).

NMR data:

^{1}H NMR (400 MHz, D_2O, 25 ºC): δ= 4.88 (m, 1H, H-1), 4.30 – 4.18 (m, 2H, H-6a and H-6b), 3.98 (m, 1H, H-2), 3.90 – 3.79 (m, 3H, H-3, H-5, H-7a), 3.73 – 3.57 (m, 2H, H-4, H-7b), 3.08 (m, 2H, H-9), 1.98 (m, 2H, H-8) ppm.

^{13}C NMR (100.6 MHz, D_2O, 25 ºC): δ= 99.9 (C-1), 70.9 (C-3 or C-5), 70.4 (C-3 or C-5) 69.8 (C-2), 67.6 (C-6), 66.6 (C-4), 65.3 (C-7), 38.2 (C-9), 27.4 (C-8) ppm.

MS ESI (-): theoretical mass: 317.31 m/z, experimental mass $[M-H]^-$: 316.83 m/z.

1.7. Synthesis of 3'-aminopropyl *N*-acetyl neuraminic acid

*Synthesis of methyl (5-acetamido-3,5-dideoxy-D-glycero-α-D-galacto-2-nonulopyranosid)onate (**35**)*

Neu5Ac **35**

N-Acetyl neuraminic acid (2.05 g, 6.63 mmol) was stirred with Dowex 50WX4 (0.50 g) in dry MeOH (60 mL, 0.11 M) overnight. The resin was filtered off and evaporation of MeOH in vacuo afforded methyl ester **35** (1.95 g, 6.03 mmol, 91 %) as a white solid.

NMR data:

^{1}H NMR (400 MHz, CD_3OD, 25 ºC): δ= 4.07 (ddd, 1H $J_{4\text{-}3ax}$= 11.7 Hz, $J_{4\text{-}3eq}$= 5.0 Hz, $J_{4\text{-}5}$= 10.1 Hz, H-4), 4.02 (dd, 1H, $J_{6\text{-}5}$= 10.7 Hz, $J_{6\text{-}7}$= 1 Hz, H-6), 3.87 – 3.82 (m, 2H, H-5, H-9a), 3.80 (s, 3H, -COOC$\underline{H}_3$), 3.73 (ddd, 1H, $J_{8\text{-}9a}$= 2.8 Hz, $J_{8\text{-}9b}$= 5.4 Hz, $J_{8\text{-}7}$= 9.4 Hz, H-8), 3.64 (dd, 1H, $J_{9b\text{-}9a}$=10.9 Hz, $J_{9b\text{-}8}$= 5.4 Hz, H-9b), 3.50 (dd, 1H, $J_{7\text{-}8}$= 9.4 Hz, $J_{7\text{-}6}$= 1 Hz, H-7), 2.24 (dd, 1H, $J_{3eq\text{-}3ax}$= 12.9 Hz, $J_{3eq\text{-}4}$= 5.0 Hz, H-$3_{equatorial}$), 2.04 (s, 3H, -NHCOC$\underline{H}_3$), 1.92 (dd, 1H, $J_{3ax\text{-}3eq}$= 12.9 Hz, $J_{3ax\text{-}4}$= 11.7 Hz, H-3_{axial}) ppm.

^{13}C NMR (100.6 MHz, CD_3OD, 25 ºC): δ= 175.2 (-$\underline{C}OOCH_3$), 171.9 (-NH$\underline{C}OCH_3$), 96.7 (C-2), 72.3 (C-6), 71.8 (C-8), 70.4 (C-7), 68.1 (C-4), 65.0 (C-9), 54.4 (-COO$\underline{C}H_3$), 53.3 (C-5), 40.8 (C-3), 22.8 (-NHCO$\underline{C}H_3$) ppm.

*Synthesis of methyl (5-acetamido-4,7,8,9-tetra-O-acetyl-2-chloro-2,3,5-trideoxy-D-glycero-β-D-galacto-2-nonulopyranosid)onate (**36**)*

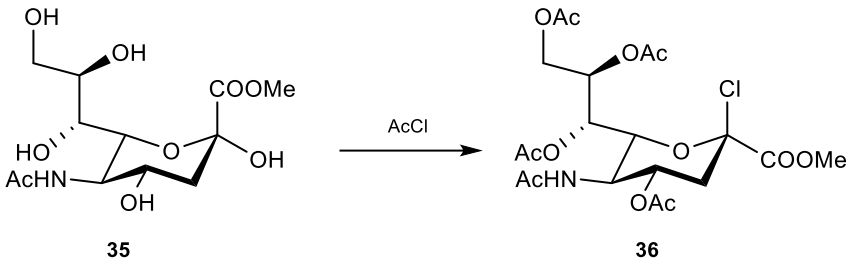

35 **36**

Methyl ester **35** (0.91 g, 2.82 mmol) was dissolved in acetyl chloride (10 ml, 0.28 M). The reaction flask was sealed and the mixture stirred at r.t. After 48 h, the excess of solvent was removed to give the β sialyl chloride **36** (1.37 g, 2.70 mmol, 96 %) as a white foam.

NMR data:

^{1}H NMR (400 MHz, $CDCl_3$, 25 ºC): δ= 5.47 (dd, 1H, $J_{7\text{-}8}$= 7.3 Hz, $J_{7\text{-}6}$= 2.3 Hz, H-7), 5.40 (ddd, 1H $J_{4\text{-}3ax}$= 11.7 Hz, $J_{4\text{-}3eq}$= 4.8 Hz, $J_{4\text{-}5}$= 10.1 Hz, H-4), 5.18 (ddd, 1H, $J_{8\text{-}9a}$= 2.6 Hz, $J_{8\text{-}9b}$= 5.8 Hz, $J_{8\text{-}7}$= 7.3 Hz, H-8), 4.42 (dd, 1H, $J_{9a\text{-}9b}$= 12.5 Hz, $J_{9a\text{-}8}$= 2.6 Hz, H-9a), 4.35 (dd, 1H, $J_{6\text{-}7}$= 2.3 Hz, $J_{6\text{-}5}$= 10.8 Hz, H-6), 4.21 (dd, 1H, $J_{5\text{-}6}$= 10.8 Hz, $J_{5\text{-}4}$= 10.1 Hz, H-5), 4.06 (dd, 1H, $J_{9b\text{-}9a}$= 12.5 Hz, $J_{9b\text{-}8}$= 5.8 Hz, H-9a), 3.89 (s, 3H, -COOC$\underline{H}_3$), 2.78 (dd, 1H, $J_{3eq\text{-}3ax}$= 13.9 Hz, $J_{3eq\text{-}4}$= 4.8 Hz, H-$3_{equatorial}$), 2.28 (dd, 1H, $J_{3ax\text{-}3eq}$= 13.9 Hz, $J_{3ax\text{-}4}$= 11.7 Hz, H-3_{axial}), 2.10 (s, 3H, -$COCH_3$), 2.08 (s, 3H, -$COCH_3$), 2.06 (s, 3H, -$COCH_3$), 2.05 (s, 3H, -$COCH_3$), 1.91 (s, 3H, -NHCOC$\underline{H}_3$)ppm.

^{13}C NMR (100.6 MHz, $CDCl_3$, 25 ºC): δ= 172.5 – 166.1 (-$\underline{C}OOCH_3$ and -$\underline{C}OCH_3$), 97.1 (C-2), 74.5 (C-6), 70.1 (C-8), 69.1 (C-4), 67.2 (C-7), 62.4 (C-9), 54.1 (-COO$\underline{C}H_3$), 49.2 (C-5), 41.0 (C-3), 24.4 (-NHCO$\underline{C}H_3$), 21.5 – 20.4 (-CO$\underline{C}H_3$) ppm.

*Synthesis of methyl (5-acetamido-4,7,8,9-tetra-O-acetyl-2-O-(N-benzyloxycarbonyl)aminopropyl-3,5-dideoxy-D-glycero-α,β-D-galacto-2-nonulopyranosid)onate (**37**)*

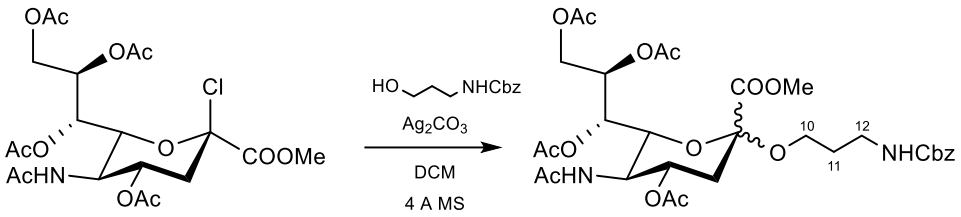

36 **37**

Sialyl chloride **36** (0.60 g, 1.18 mmol) and *N*-Cbz-aminopropyl (0.49 g, 2.35 mmol) were co-evaporated with toluene. After 5 h in the pump, the mixture was dissolved in dry DCM (10 mL, 0.11 M) and 4 Å MS were added, the mixture was stirred for 30 mins before adding Ag_2CO_3 (0.61 g, 2.21 mmol). After 16 h stirring at room temperature with exclusion of light, Ag_2CO_3 was filtered through Celite and the crude was purified by column chromatography (Hex:EtOAc 5:5 → 3:7) to obtain compound **37** (0.37 g, 46 %, α:β 7:3) as a colorless foam.

TLC: R_f: 0.27 (Hex:EtOAc - 1:9).

NMR data for α anomer:

^{1}H NMR (400 MHz, $CDCl_3$, 25 ºC): δ= 7.40 – 7.28 (m, 5H, H_{arom}), 5.37 (ddd, $J_{8\text{-}9a}$= 2.5 Hz, $J_{8\text{-}9b}$= 6.2 Hz, $J_{8\text{-}7}$= 8.3 Hz, 1H, H-8), 5.32 (dd, 1H, $J_{7\text{-}8}$= 8.3 Hz, $J_{7\text{-}6}$= 2.1 Hz, H-7), 5.11 (s, 2H, -NHCOOC$\underline{H}_2$Ph), 4.85 (ddd, 1H $J_{4\text{-}3ax}$= 11.6 Hz, $J_{4\text{-}3eq}$= 4.6 Hz, $J_{4\text{-}5}$= 10.2 Hz, H-4), 4.27 (dd, 1H, $J_{9a\text{-}9b}$= 12.4 Hz, $J_{9a\text{-}8}$= 2.6 Hz, H-9a), 4.16 – 3.97 (m, 3H, H-5, H-6, H-9b), 3.84 (m, 1H, H-10a), 3.77 (s, 3H, -COOC$\underline{H}_3$), 3.36 (m, 1H, H-10b), 3.29 (m, 2H, H-12), 2.55 (dd, 1H, $J_{3eq\text{-}3ax}$= 12.8 Hz, $J_{3eq\text{-}4}$= 4.6 Hz, H-$3_{equatorial}$), 2.17 – 1.95 (m, 13H, H-3_{axial}, -COC$\underline{H}_3$), 1.88 (s, 3H, -NHCOC$\underline{H}_3$), 1.76 (m, 2H, H-11) ppm.

^{13}C NMR (100.6 MHz, $CDCl_3$, 25 ºC): δ= 171.7 – 168.8 (-$\underline{C}OOCH_3$ and -$\underline{C}OCH_3$), 156.5 (-NH$\underline{C}OOCH_2Ph$), 98.8 (C-2), 72.7 (C-6), 69.2 (C-4), 68.6 (C-8), 67.5 (C-7), 66.7 (-NHCOO$\underline{C}H_2Ph$), 63.0 (C-10), 62.5 (C-9), 53.0 (-COO$\underline{C}H_3$), 49.8 (C-5), 38.2 (C-3 and C-12), 29.5 (C-11), 23.4 (-NHCO$\underline{C}H_3$), 21.3 – 20.9 (-CO$\underline{C}H_3$) ppm.

MS (ESI+): theoretical mass: 682.67 m/z, experimental mass $[M+Na]^+$: 705.62 m/z.

*Synthesis of 5-acetamido-2-O-(N-benzyloxycarbonyl)aminopropyl-3,5-dideoxy-D-glycero-α,β-D-galacto-2-nonulopyranosidonic acid (**38**)*

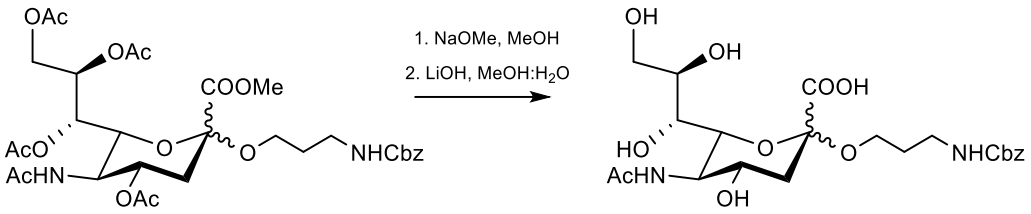

37 **38**

Compound **37** (0.37 g, 0.54 mmol) was dissolved in MeOH (5 ml, 0.11 M) and NaOMe (0.04 g, 0.54 mmol) was added. After stirring for 16 h, the solution was neutralized with Amberlite IR120 (H^+ form), filtered and concentrated in vacuo. The residue was dissolved in H_2O:MeOH (4:1, 5 ml), treated with LiOH (0.02 g, 0.54 mmol) and the solution was stirred overnight. After neutralization with Amberlite IR120 (H^+ form), the resin was filtered off and the filtrate was concentrated to remove the methanol and then, freeze dried to afford the deprotected glycoside **38** as a transparent oil (0.22 g, 81 %).

NMR data for α anomer:

^{1}H NMR (400 MHz, CD_3OD, 25 ºC): δ= 7.40 – 7.25 (m, 5H, H_{arom}), 5.06 (s, 2H, -NHCOOC$\underline{H}_2$Ph), 3.88 – 3.81 (m, 3H, H-8, H-9a, H-10a), 3.75 – 3.66 (m, 2H, H-4, H-5), 3.63 (dd, 1H, $J_{9b\text{-}9a}$= 11.2 Hz, $J_{9b\text{-}8}$= 5.4 Hz, H-9b), 3.60 – 3.52 (m, 2H, H-6, H-7), 3.48 (m, 1H, H-10b), 3.20 (t, 2H, $J_{12\text{-}11}$= 6.7 Hz, H-12), 2.72 (dd, 1H, $J_{3eq\text{-}3ax}$= 12.9 Hz, $J_{3eq\text{-}4}$= 4.4 Hz, H-$3_{equatorial}$), 2.04 (s, 3H, -NHCOC$\underline{H}_3$), 1.71 (m, 3H, H-3_{axial}, H-11) ppm.

^{13}C NMR (100.6 MHz, CD_3OD, 25 ºC): δ= 175.4 and 172.7 (-NH$\underline{C}OCH_3$ and -$\underline{C}$OOH), 159.2 (-NH$\underline{C}OOCH_2Ph$), 100.3 (C-2), 74.9 (C-6 or C-7), 72.8 (C-8), 70.1 (C-6 or C-7), 68.9 (C-4 or C-5), 67.4 (-NHCOO$\underline{C}H_2Ph$), 64.5 (C-9), 62.5 (C-10), 54.0 (C-4 or C-5), 41.9 (C-3), 38.9 (C-12), 30.9 (C-11), 22.6 (-NHCO$\underline{C}H_3$) ppm.

MS (ESI+): theoretical mass: 500.50 m/z, experimental mass $[M+2Na]^{2+}$: 546.89 m/z.

*Synthesis of 5-acetamido-2-O-(3'aminopropyl)-3,5-dideoxy-D-glycero-α,β-D-galacto-2-nonulopyranosidonic acid (**28**)*

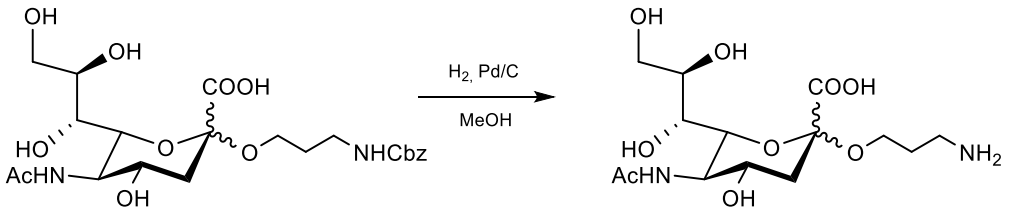

38 **28**

To a solution of compound **38** (0.11 g, 0.21 mmol) in MeOH (10 ml, 0.02 M), Pd/C was added. The reaction atmosphere was purged with H_2/vacuum cycles and then, stirred under H_2 atmosphere. After 15 h, the Pd/C was filtered through a whatman syringe filter and concentrated under vacuum to obtain compound **28** as a white foam (0.08 g, quant.).

NMR data for α anomer:

^{1}H NMR (400 MHz, CD_3OD, 25 ºC): δ= 3.80 (m, 1H, H-10a), 3.76 – 3.67 (m, 2H, H-9a, H-10a), 3.66 – 3.55 (m, 2H, H-4, H-5 and H-6 or H-7), 3.55 – 3.45 (m, 2H, H-9b, H-10b), 3.40 (q, 1H, *J*= 9.9 Hz, H-6 or H-7), 2.92 (t, 2H, $J_{12\text{-}11}$= 6.5 Hz, H-12), 2.68 (dd, 1H, $J_{3eq\text{-}3ax}$= 11.9 Hz, $J_{3eq\text{-}4}$= 3.8 Hz, H-$3_{equatorial}$), 1.92 (s, 3H, -NHCOC$\underline{H}_3$), 1.76 (m, 2H, H-11), 1.51 (m, 1H $J_{3ax\text{-}3eq}$= 11.9 Hz, H-3_{axial}) ppm.

^{13}C NMR (100.6 MHz, CD_3OD, 25 ºC): δ= 175.8 and 174.8 (-NH$\underline{C}OCH_3$ and -$\underline{C}OOH$), 102.1 (C-2), 74.6 (C-6 or C-7), 73.1 (C-8), 70.3 (C-6 or C-7), 69.2 (C-4 or C-5), 64.6 (C-9), 63.3 (C-10), 54.3 (C-4 or C-5), 42.6 (C-3), 39.8 (C-12), 29.1 (C-11), 22.6 (-NHCO$\underline{C}H_3$) ppm.

MS (ESI-): theoretical mass: 366.36 m/z, experimental mass $[M-H]^-$: 365.67 m/z.

2. Experimental procedures Chapter II

2.1. Synthesis of galactoside acceptor 50

*Synthesis of N-(benzyloxycarbonyl)aminopropyl 2,3,4,6-tetra-O-acetyl-β-D-galactopyranoside (**39**)*

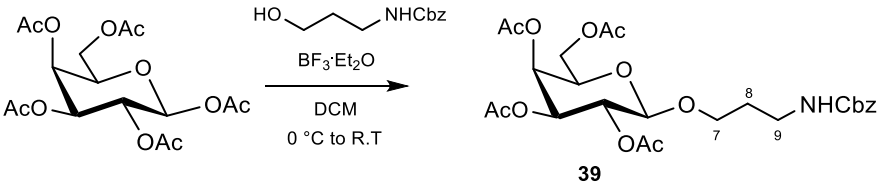

39

Acetyl 2,3,4,6-tetra-O-acetyl-β-D-galactopyranoside (3.06 g, 7.84 mmol) and benzyl *N*-(3-hydroxypropyl)carbamate (3.92 g, 18.64 mmol) were dissolved in dry toluene and co-evaporated three times. After one night in the pump, the reagents were dissolved in dry DCM (60 ml, 0.13 M). The solution was ice-cooled to 0 °C and $BF_3 \cdot Et_2O$ (1.9 ml, 15.38 mmol) was added dropwise. The reaction mixture was stirred overnight at r.t and monitored by TLC (Hex:EtOAc 4:6), as the reaction proceeded a change in color from transparent to pale yellow was observed. After 24h, more $BF_3 \cdot Et_2O$ (1.0 ml, 8.09 mmol) was added. After 48h, when the spot corresponding to the starting material disappeared, the solution was extracted with sat. $NaHCO_3$ (2 x 60 ml), water (1 x 60 ml) and brine (1 x 60 ml) and dried over anhydrous Na_2SO_4. The excess of solvent was evaporated and the crude product was purified by column chromatography (Hex:EtOAc 7:3 → 2:1) to obtain glycoside **39** as a white foam (2.28 g, 55 %).

TLC: *Rf:* 0.57 (Hex:EtOAc 4:6).

NMR data:

^{1}H NMR (400 MHz, $CDCl_3$, 25 °C): δ= 7.41 – 7.33 (m, 5H, H_{arom}), 5.40 (d, 1H, $J_{4\text{-}3}$= 3.4 Hz, $J_{4\text{-}5}$ < 1 Hz, H-4), 5.22 (dd, 1H, $J_{2\text{-}1}$= 7.9 Hz, $J_{2\text{-}3}$= 10.3 Hz, H-2), 5.12 (s, 2H, -NHCOOC$\underline{H}_2$Ph), 5.02 (dd, 1H, $J_{3\text{-}2}$= 10.3 Hz, $J_{3\text{-}4}$= 3.3 Hz, H-3), 4.48 (d, 1H, $J_{1\text{-}2}$= 7.9 Hz, H-1), 4.20-4.11 (m, 2H, H-6a, H-6b), 3.99 – 3.88 (m, 2H, H-5 and H-7a), 3.61 (m, 1H, H-7b), 3.35 (m, 1H, H-9a), 3.27 (m, 1H, H-9b), 2.15 (s, 3H, -$COCH_3$), 2.05 (s, 6H, -$COCH_3$), 2.00 (s, 3H, -$COCH_3$), 1.82 (m, 2H, H-8) ppm.

^{13}C NMR (100.6 MHz, $CDCl_3$, 25 °C): δ= 170.2 – 169.53 (-$\underline{C}OCH_3$), 156.8 (-NH$\underline{C}OOCH_2$Ph), 128.6 (C_{arom}), 102.0 (C-1), 71.4 (C-5 and C-3), 69.4 (C-2), 68.2 (C-7), 67.5 (C-4), 66.9 (-NHCOO$\underline{C}H_2$Ph), 61.6 (C-6), 39.4 (C-9), 30.4 (C-8), 21.4 – 20.9 (-CO$\underline{C}H_3$) ppm.

*Synthesis of N-(benzyloxycarbonyl)aminopropyl 4,6-O-benzylidene-β-D-galactopyranoside (**46**)*

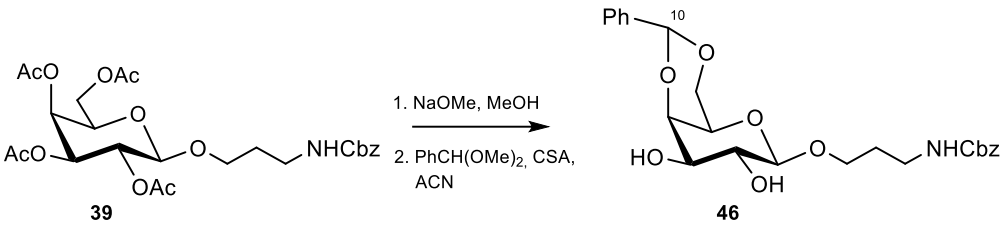

Compound **39** (2.28 g, 4.21 mmol) was dissolved in MeOH (40 ml, 0.11 M) and NaOMe (0.10 g, 1.68 mmol) was added. The reaction mixture was stirred at r.t. until TLC (DCM:MeOH - 7:3) showed the consumption of the starting material. After 3 h, the reaction mixture was quenched using Amberlite IR120 (H^+ form), filtered and concentrated using the rotary evaporator. After some hours in the vacuum pump to remove any traces of MeOH, the intermediate was dissolved in dry ACN (40 ml, 0.1 M), $PhCH(OMe)_2$ (1.9 ml, 12.62 mmol) and CSA (0.2 g, 0.84 mmol) were added. TLC (DCM:MeOH - 9:1) showed full conversion after 4h. The CSA in excess was quenched with TEA, the solvent was removed and the crude product was purified by column chromatography (Hex:EtOAc 1:3 → 1:5) to obtain compound **46** as a white solid (1.47 g, 76%).

TLC: R_f: 0.44 (DCM:MeOH - 9:1).

NMR data:

^{1}H NMR (400 MHz, $CDCl_3$, 25 °C): δ= 7.51 (m, 2H, H_{arom}), 7.40-7.35 (m, 8H, H_{arom}), 5.57 (s, 1H, H-10), 5.22 (b.t., 1H, NH), 5.11 (s, 2H, -NHCOOC$\underline{H}_2$Ph), 4.35 (dd, 1H, $J_{6a\text{-}6b}$= 12.2 Hz, $J_{6a\text{-}5}$= 1.2 Hz, H-6a), 4.29 (d, 1H, $J_{1\text{-}2}$= 7.5 Hz, H-1) 4.23 (dd, 1H, $J_{4\text{-}3}$= 3.6 Hz, $J_{4\text{-}5}$ < 1 Hz, H-4), 4.10 (dd, 1H, $J_{6b\text{-}6a}$= 12.2 Hz, $J_{6b\text{-}5}$= 1.7 Hz, H-6b), 4.05 (m, 1H, H-7), 3.76 (dd, 1H, $J_{2\text{-}1}$= 7.5 Hz, $J_{2\text{-}3}$= 8.2 Hz, H-2), 3.71 (dd, 1H, $J_{3\text{-}2}$= 8.2 Hz, $J_{3\text{-}4}$= 3.6 Hz, H-3), 3.64 (m, 1H, H-7), 3.54 (m, 1H, H-9a), 3.50 (m, 1H, H-5), 3.32 (m, 1H, H-9b), 1.88 (m, 1H, H-8a), 1.80 (m, 1H, H-8b) ppm.

^{13}C NMR (100.6 MHz, $CDCl_3$, 25 °C): δ= 157.1 (-NH$\underline{C}$OOCH_2Ph), 137.9 – 136.8 (C_{arom}), 128.2 - 126.9 (C_{arom}), 103.7 (C-1), 101.6 (C-10), 75.9 (C-4), 73.1 (C-3), 72.1 (C-2), 69.5 (C-6), 66.9 (C-7, C-5, -NHCOO$\underline{C}$H$_2$Ph), 38.5 (C-9), 30.5 (C-8) ppm.

MS (ESI+): theoretical mass: 459.49 m/z, experimental mass $[M+H]^+$: 460.08 m/z.

*Synthesis of N-(benzyloxycarbonyl)aminopropyl 3-O-acetyl-4,6-O-benzylidene-β-D-galactopyranoside (**50**)*

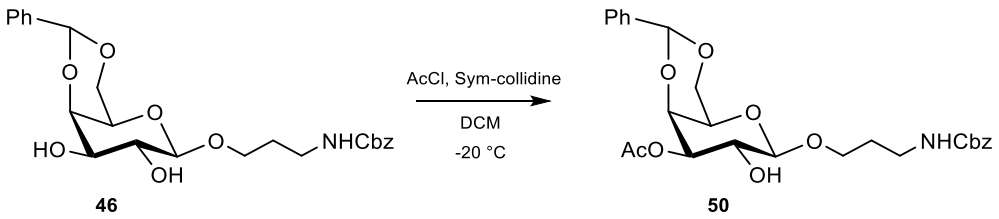

Compound **46** (0.62 g, 1.31 mmol) was dissolved in dry DCM (25 mL, 0.07 M). Sym-collidine (0.9 ml, 6.75 mmol) was added and the solution was cooled down to -20 °C. Acetyl chloride (0.12 ml, 1.62 mmol) was added dropwise and the reaction progress was monitored by TLC (Hex:EtOAc - 2:8). After 90 mins, the reaction mixture was diluted with H_2O and washed with aq. HCl 5% (2 x 20 ml) and sat. $NaHCO_3$ (2 x 20 ml). The organic phase was dried over Na_2SO_4 and the solvent was removed under reduced pressure. The crude was purified by column chromatography (Hex:EtOAc 1:1 → 3:7) to give compound **50** (0.50 g, 75 %) as a white foam.

TLC: R_f: 0.28 (Hex:EtOAc - 3:7).

NMR data:

^{1}H NMR (400 MHz, $CDCl_3$, 25 °C): δ= 7.53 (m, 2H, H_{arom}), 7.40-7.32 (m, 8H, H_{arom}), 5.52 (s, 1H, H-10), 5.13 (b.t., 1H, NH), 5.11 (s, 2H, -NHCOOC$\underline{H}_2$Ph), 4.83 (dd, 1H, $J_{3\text{-}2}$= 10.1 Hz, $J_{3\text{-}4}$= 3.6 Hz, H-3), 4.42 (dd, 1H, $J_{4\text{-}3}$= 3.6 Hz, $J_{4\text{-}5}$ < 1 Hz, H-4), 4.35 (d, 1H, $J_{1\text{-}2}$= 7.7 Hz, H-1), 4.34 (dd, 1H, $J_{6a\text{-}6b}$= 12.5 Hz, $J_{6a\text{-}5}$= 1.1 Hz, H-6a), 4.08 (dd, 1H, $J_{6b\text{-}6a}$= 12.2 Hz, $J_{6b\text{-}5}$= 1.5 Hz, H-6b), 4.03 (m, 2H, H-2 and H-7a), 3.63 (m, 1H, H-7b), 3.51 (m, 1H, H-5), 3.30 (m, 2H, H-9), 2.17 (s, 3H, -$COCH_3$), 1.89 (m, 1H, H-8a), 1.78 (m, 1H, H-8b) ppm.

^{13}C NMR (100.6 MHz, $CDCl_3$, 25 °C): δ= 170.9 (-$\underline{C}OCH_3$), 157.1 (-NH$\underline{C}OOCH_2$Ph), 129.0 (C_{arom}), 126.9 (C_{arom}), 103.3 (C-1), 101.2 (C-10), 72.4 (C-3), 73.4 (C-4), 69.1 (C-6), 68.4 (C-2), 66.9 (C-7, -NHCOO$\underline{C}H_2$Ph), 66.5 (C-5), 38.6 (C-9), 29.6 (C-8), 21.4 (-CO$\underline{C}H_3$) ppm.

MS (ESI+): theoretical mass: 501.53 m/z, experimental mass $[M+Na]^+$ 524.32 m/z.

2.2. Synthesis of fucoside donor 54

*Synthesis of methyl 2,3,4-tri-O-benzyl-α-L-fucopyranoside (**52**)*

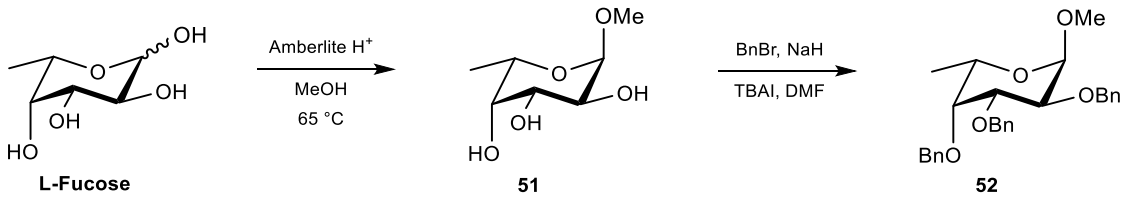

L-Fucose (5.00 g, 30.48 mmol) was dissolved in MeOH (50 ml, 0.6 M) and Amberlite IR120 (H^+ form) was added. The reaction mixture was warmed up to 65 ºC and after 17 h, the Amberlite was filtered off. The solvent was removed under vacuum and the product was re-crystalized with cold EtOH to obtain methyl α-L-fucopyranoside **51** (2.28 g, 12.80 mmol, 42 %).

The crystals (2.28 g, 12.80 mmol) were dissolved in dry DMF (70 ml, 0.18 M) and BnBr (9.1 ml, 76.83 mmol) was added. Sodium hydride (1.84 g, 76.67 mmol) was added portion-wise together with a spoon of TBAI to catalyze the reaction. The reaction was followed by TLC (Hex:EtOAc - 7:3) and after 24 h, the excess of NaH was quenched with MeOH and the crude was purified by column chromatography (Hex:EtOAc 9:1 → 8:2) to give compound **52** (5.17 g, 90 %) as a white solid.

TLC: R_f: 0.40 (Hex:EtOAc - 7:3).

NMR data:

^{1}H NMR (400 MHz, $CDCl_3$, 25 °C): δ= 7.47 – 7.25 (m, 15H, H_{arom}), 5.01 (d, 1H, J_{gem}= 11.7 Hz, -OC$\underline{H}_2$Ph), 4.90 (d, 1H, J_{gem}= 11.7 Hz, -OC$\underline{H}_2$Ph), 4.85 (d, 1H, J_{gem}= 12.2 Hz, -OC$\underline{H}_2$Ph), 4.76 (d, 1H, J_{gem}= 12.2 Hz, -OC$\underline{H}_2$Ph), 4.71 (d, 1H, J_{gem}= 12.2 Hz, -OC$\underline{H}_2$Ph), 4.68 (d, 1H, J_{gem}= 12.2 Hz, -OC$\underline{H}_2$Ph), 4.68 (d, 1H, $J_{1\text{-}2}$= 3.7 Hz, H-1), 4.06 (dd, 1H, $J_{2\text{-}1}$= 3.7 Hz, $J_{2\text{-}3}$= 9.9 Hz, H-2), 3.95 (dd, 1H, $J_{3\text{-}2}$= 9.9 Hz, $J_{3\text{-}4}$= 2.8 Hz, H-3), 3.86 (dq, 1H, $J_{5\text{-}4}$= 2.8 Hz, $J_{5\text{-}6}$= 6.5 Hz, H-5), 3.67 (dd, 1H, $J_{4\text{-}3}$= 2.8 Hz, $J_{4\text{-}5}$= 2.8 Hz, H-4), 1.14 (d, 1H, $J_{6\text{-}5}$= 6.5 Hz, H-6) ppm.

^{13}C NMR (100.6 MHz, $CDCl_3$, 25 °C): δ= 129.5 – 127.3 (C_{arom}), 99.5 (C-1), 79.7 (C-3), 77.9 (C-4), 76.6 (C-2), 74.6 (-O$\underline{C}H_2$Ph), 73.7 (-O$\underline{C}H_2$Ph), 73.6 (-O$\underline{C}H_2$Ph), 66.2 (C-5), 16.9 (C-6) ppm.

*Synthesis of 2,3,4-tri-O-benzyl-α,β-L-fucose (**53**)*

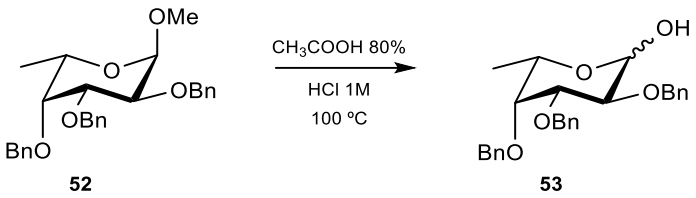

Compound **52** (1.98 g, 4.41 mmol) was dissolved in CH_3COOH 80% (50 ml) and HCl 1 M (15 ml) and the reaction mixture was refluxed at 100 °C. The progress was followed by TLC (Tol:EtOAc - 8:2). After 18 h, the reaction mixture was washed with DCM (3 x 20 ml), sat. $NaHCO_3$ until reaching a neutral pH and water (1 x 20 ml). The organic phase was dried over Na_2SO_4 and the solvent was removed under reduced pressure. The crude was purified by column chromatography (Hex:EtOAc 8:2 $\rightarrow$ 6:4) to give compound **53** (1.71 g, 89 %, α:β 8:2) as a white solid.

TLC: R_f: 0.68 (Tol:EtOAc - 8:2).

NMR data for α anomer:

^{1}H NMR (400 MHz, $CDCl_3$, 25 °C): δ= 7.49 – 7.26 (m, 15H, H_{arom}), 5.27 (d, 1H, $J_{1\text{-}2}$= 3.5 Hz, H-1), 4.98 (d, 1H, J_{gem}= 11.7 Hz, -OC$\underline{H}_2$Ph), 4.90 (d, 1H, J_{gem}= 11.7 Hz, -OC$\underline{H}_2$Ph), 4.83 (d, 1H, J_{gem}= 12.2 Hz, -OC$\underline{H}_2$Ph), 4.78 (d, 1H, J_{gem}= 12.2 Hz, -OC$\underline{H}_2$Ph), 4.71 (d, J_{gem}= 12.2 Hz, 1H, -OC$\underline{H}_2$Ph), 4.67 (d, 1H, J_{gem}= 12.2 Hz, -OC$\underline{H}_2$Ph), 4.04 (dd, 1H, $J_{2\text{-}1}$= 3.5 Hz, $J_{2\text{-}3}$= 9.8 Hz, H-2), 3.98 (dd, 1H, $J_{3\text{-}2}$= 9.8 Hz, $J_{3\text{-}4}$= 2.7 Hz, H-3), 3.67 (dd, 1H, $J_{4\text{-}3}$= 2.7 Hz, $J_{4\text{-}5}$= 2.8 Hz, H-4), 3.57 (m, 1H, H-5), 1.14 (d, 1H, $J_{6\text{-}5}$= 6.3 Hz, H-6) ppm.

^{13}C NMR (100.6 MHz, $CDCl_3$, 25 °C): δ= 129.6 – 127.2 (C_{arom}), 92.1 (C-1), 79.4 (C-3), 72.4 (C-4), 77.8 (C-2), 74.9 (-O$\underline{C}H_2$Ph), 73.7 (-O$\underline{C}H_2$Ph), 73.2 (-O$\underline{C}H_2$Ph), 67.0 (C-5), 17.0 (C-6) ppm.

MS (ESI+): theoretical mass: 434.52 m/z, experimental mass $[M+Na]^+$: 457.52 m/z.

*Synthesis of 2,3,4-tri-O-benzyl-α,β-L-fucopyranosyl trichloroacetimidate (**54**)*

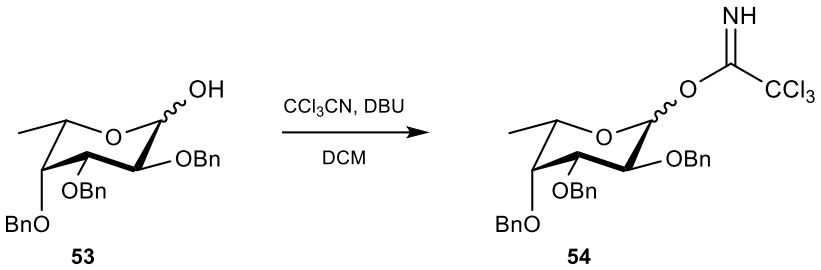

Compound **53** (0.51 g, 1.18 mmol) was dissolved in dry DCM (10 ml, 0.12 M). Trichloroacetonitrile (1.2 ml, 11.67 mmol) and catalytic amount of DBU were added under Ar atmosphere. The reaction mixture turned dark red, but the progress was difficult to monitor since the product **54** hydrolyzed on TLC. The excess of solvent was removed after 3 h and the crude was purified by short chromatographic column (Hex:EtOAc 9:1 → 7:3 + 0.5 % TEA) to afford trichloroacetimidate **54** (0.60 g, 1.03 mmol, 88 %, α:β 8:2) as a white foam.

TLC: R_f(α): 0.67 and R_f(β): 0.51 (Hex:EtOAc - 7:3)

NMR data for α anomer:

^{1}H NMR (400 MHz, $CDCl_3$, 25 °C): δ= 8.52 (s, 1H, -NH), 7.45 – 7.23 (m, 15H, H_{arom}), 6.54 (d, 1H, $J_{1\text{-}2}$= 3.5 Hz, H-1), 5.03 (d, 1H, J_{gem}= 11.6 Hz, -OC$\underline{H}_2$Ph), 4.88 (d, 1H, J_{gem}= 12.0 Hz, -OC$\underline{H}_2$Ph), 4.78 (m, 2H, -OC$\underline{H}_2$Ph), 4.70 (d, 1H, J_{gem}= 11.6 Hz, -OC$\underline{H}_2$Ph), 4.26 (dd, 1H, $J_{2\text{-}1}$= 3.5 Hz, $J_{2\text{-}3}$= 10.0 Hz, H-2), 4.12 (m, 1H, H-5), 4.04 (dd, 1H, $J_{3\text{-}2}$= 10.4 Hz, $J_{3\text{-}4}$= 2.8 Hz, H-3), 3.73 (dd, $J_{4\text{-}3}$= 2.8 Hz, $J_{4\text{-}5}$= 2.8 Hz, H-4), 1.18 (d, 3H, $J_{6\text{-}5}$= 6.5 Hz, H-6) ppm.

2.3. Synthesis of disaccharide antigen H derivative

*Synthesis of N-(benzyloxycarbonyl)aminopropyl 3-O-acetyl-4,6-O-benzylidene-2-O-(2',3',4'-tri-O-benzyl-α-L-fucopyranosyl)-β-D-galactopyranoside (**55**)*

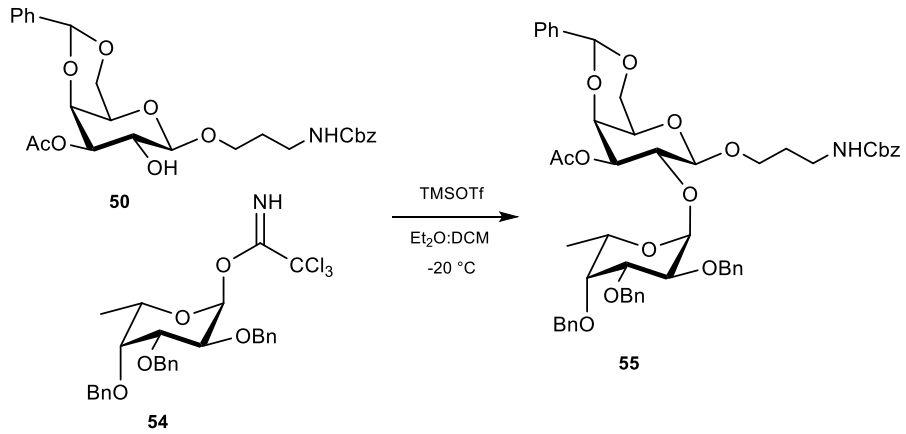

Acceptor **50** (0.24 g, 0.47 mmol) was co-evaporated with toluene and left in the pump overnight. After 15 h, it was dissolved in a mixture of dry Et_2O and dry DCM (9:1, 3.5 ml), brought to -20 ºC and TMSOTf (9 µl, 0.05 mmol) was added all under Ar atmosphere. A solution of the trichloroacetimidate **54** (0.73 g, 1.26 mmol) in Et_2O:DCM (9:1, 2 ml) was added dropwise into the reaction mixture. The reaction progress was monitored by HPTLC (Hex:EtOAc - 3:2) and after 1 h, the reaction mixture was neutralized with TEA and the crude was subjected to column chromatography (Hex:EtOAc 8:2 → 6:4) to separate the α anomer **55** (0.26 g, 60 %) from the β anomer (0.05 g, 12 %).

HPTLC: R_f(α): 0.22 and R_f(β): 0.37 (Hex:EtOAc - 3:2).

NMR data for α anomer:

^{1}H NMR (400 MHz, $CDCl_3$, 25 °C): δ= 7.50 (m, 2H, H_{arom}), 7.38 – 7.22 (m, 23H, H_{arom}), 5.49 (s, 1H, H-10), 5.32 (b.t., 1H, NH), 5.30 (d, 1H, $J_{1'-2'}$= 3.7 Hz, H-1'), 5.06 (s, 2H, -NHCOOC$\underline{H}_2$Ph), 5.04 (dd, 1H, J_{3-2}= 9.7 Hz, J_{3-4}= 3.6 Hz, H-3), 4.96 (d, 1H, J_{gem}= 11.7 Hz, -OC$\underline{H}_2$Ph), 4.79 – 4.73 (m, 2H, -OC$\underline{H}_2$Ph), 4.71 (d, 1H, J_{gem}= 11.9 Hz, -OC$\underline{H}_2$Ph), 4.63 (d, 1H, J_{gem}= 11.70 Hz, -OC$\underline{H}_2$Ph), 4.48 (d, 1H, J_{1-2}= 7.7 Hz, H-1), 4.36 (d, 1H, J_{4-3}= 3.6 Hz, J_{4-5} < 1 Hz, H-4), 4.33 (d, 1H, J_{6a-6b}= 12.5 Hz, J_{6a-5} < 1 Hz, H-6a), 4.24 (m, 1H, H-5') 4.12 (dd, 1H, J_{2-1}= 7.7 Hz, J_{2-3}= 9.7 Hz, H-2), 4.06 – 4.00 (m, 2H, H-6b and H-2'), 3.94 (m, 1H, H-7a), 3.88 (dd, 1H, $J_{3'-2'}$= 9.9 Hz, $J_{3'-4'}$= 2.7 Hz, H-3'), 3.67 (b.s, 1H, H-4'), 3.57 (m, 1H, H-7b), 3.47 (m, 1H, H-5), 3.28 (m, 2H, H-9), 1.86 (s, 3H, -$COCH_3$), 1.76 (m, 2H, H-8), 1.12 (d, 3H, $J_{6'-5'}$= 6.5 Hz, H-6') ppm.

^{13}C NMR (100.6 MHz, $CDCl_3$, 25 °C): δ= 171.2 (-$\underline{C}OCH_3$), 157.1 (-NH-$\underline{C}OOCH_2$Ph), 129.0 – 126.4 (C_{arom}), 102.2 (C-1), 101.1 (C-10), 98.1 (C-1'), 79.7 (C-3'), 77.9 (C-4'), 76.9 (C-2'), 75.0 (-O$\underline{C}H_2$Ph), 74.8 (C-3), 73.8 (-O$\underline{C}H_2$Ph), 73.7 (C-4), 73.2 (-O$\underline{C}H_2$Ph), 72.6 (C-2), 69.2 (C-6), 67.2 (C-5'), 66.6 (C-7 and -NHCOO$\underline{C}H_2$Ph), 66.3 (C-5), 39.3 (C-9), 31.3 (C-8), 21.9 (-CO$\underline{C}H_3$), 17.6 (C-6') ppm.

MS (ESI+): theoretical mass: 918.05 m/z, experimental mass $[M+Na]^+$: 941.24 m/z.

2.4. Synthesis of disaccharide acceptor 56

*Synthesis of N-(benzyloxycarbonyl)aminopropyl 4,6-O-benzylidene-2-O-(2',3',4'-tri-O-benzyl-α-L-fucopyranosyl)-β-D-galactopyranoside (**56**)*

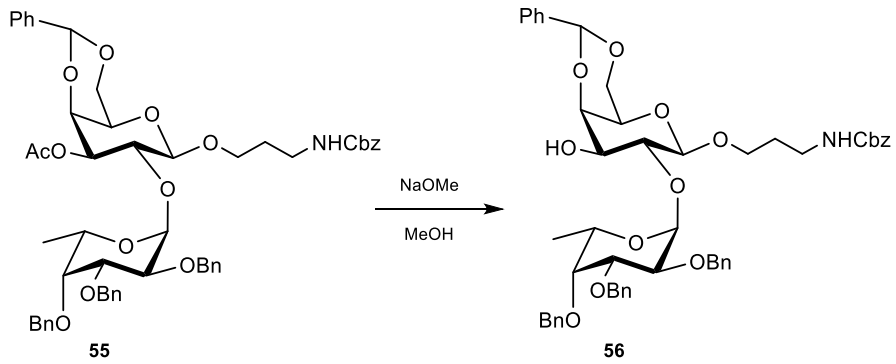

Compound **55** (0.21 g, 0.23 mmol) was dissolved in MeOH (3 ml, 0.08 M) and NaOMe (7 mg, 0.13 mmol) was added. The reaction mixture was stirred at r.t. until TLC (DCM:MeOH - 95:5) showed the consumption of the starting material. After 1 h, the reaction mixture was quenched using Amberlite IR120 (H^+ form), filtered and concentrated using the rotary evaporator to obtain compound **56** (0.20 g, 0.23 mmol, 99 %) as a white foam.

TLC: R_f: 0.37 (DCM:MeOH - 7:3).

NMR data:

^{1}H NMR (400 MHz, $CDCl_3$, 25 °C): δ= 7.56 (m, 2H, H_{arom}), 7.42 – 7.18 (m, 23H, H_{arom}), 5.58 (s, 1H, H-10), 5.38 (b.t., 1H, NH), 5.16 (d, 1H, $J_{1'-2'}$= 3.5 Hz, H-1'), 5.08 (s, 2H, -NHCOOC$\underline{H}_2$Ph), 4.98 (d, 1H, $J_{gem'}$= 11.7 Hz, -OC$\underline{H}_2$Ph), 4.78 (m, 4H, -OC$\underline{H}_2$Ph), 4.67 (d, 1H, $J_{gem'}$= 11.7 Hz, -OC$\underline{H}_2$Ph), 4.36 (d, 1H, J_{1-2}= 6.8 Hz, H-1), 4.31 (d, 1H, J_{6a-6b}= 12.4 Hz, J_{6a-5} < 1 Hz, H-6a), 4.23 (d, 1H, J_{4-3}= 2.4 Hz, H-4), 4.14 - 4.04 (m, 3H, H-2', H-5' and H-6b), 4.00 (dd, 1H, $J_{3'-2'}$= 10.1 Hz, $J_{3'-4'}$= 2.7 Hz, H-3'), 3.95 (m, 1H, H-7a), 3.83 (m, 2H, H-2 and H-3), 3.69 (b.s, 1H, H-4'), 3.65 (m, 1H, H-7b), 3.43 (b.s, 1H, H-5), 3.31 (m, 2H, H-9), 1.81 (m, 2H, H-8), 1.14 (d, 3H, $J_{6'-5'}$= 6.5 Hz, H-6') ppm.

^{13}C NMR (100.6 MHz, $CDCl_3$, 25 °C): δ= 156.9 (-NH$\underline{C}$OOCH$_2$Ph), 139.0 – 137.9 (C_{arom}), 128.9 – 126.7 (C_{arom}), 102.1 (C-1), 101.5 (C-10), 99.9 (C-1'), 79.7 (C-3'), 78.6 (C-2 or C-3), 77.7 (C-4'), 77.1 (C-2' or C-5'), 75.6 (C-4), 75.1 (-O$\underline{C}$H$_2$Ph), 74.2 (-O$\underline{C}$H$_2$Ph), 73.3 (C-2 or C-3), 73.1 (-O$\underline{C}$H$_2$Ph), 69.3 (C-6), 67.5 (C-2' or C-5'), 66.9 (C-5), 66.6 (-NHCOO$\underline{C}$H$_2$Ph), 66.5 (C-7), 38.1 (C-9), 29.5 (C-8), 17.2 (C-6') ppm.

2.5. Synthesis of galactoside donor 59

*Synthesis of 2,3,4,6-tetra-O-benzyl-β-D-galactopyranosyl trichloroacetimidate (**59**)*

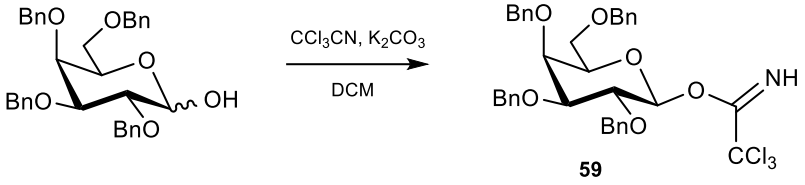

59

2,3,4,6-Tetra-O-benzyl-α,β-D-galctopyranose (0.50 g, 0.93 mmol) was dissolved in dry DCM (10 ml, 0.09 M). Trichloroacetonitrile (0.50 ml, 4.95 mmol) and K_2CO_3 (0.50 g, 3.62 mmol) were added under Ar atmosphere. The reaction mixture was vigorously stirred and after 5 h, the K_2CO_3 was filtered over celite. The crude was purified by short chromatographic column (Hex:EtOAc 9:1 + 1 % TEA) to isolate the desired β anomer **59** (0.58 g, 0.85 mmol, 90 %) as a white solid.

TLC: R_f(α): 0.73 and R_f(β): 0.60 (Hex:EtOAc 6:4).

NMR data for β anomer:

^{1}H NMR (400 MHz, $CDCl_3$, 25 °C): δ= 8.62 (s, 1H, -NH), 7.35 – 7.24 (m, 20H, H_{arom}), 5.74 (d, 1H, $J_{1\text{-}2}$= 8.0 Hz, H-1), 4.94 (d, 1H, J_{gem}= 11.8 Hz, -OC$\underline{H}_2$Ph), 4.91 (d, 1H, J_{gem}= 10.7 Hz, -OC$\underline{H}_2$Ph), 4.81 (d, J_{gem}= 10.7 Hz, -OC$\underline{H}_2$Ph), 4.72 (s, 2H, -OC$\underline{H}_2$Ph), 4.63 (d, 1H, J_{gem}= 11.8 Hz, -OC$\underline{H}_2$Ph), 4.47 (d, J_{gem}= 11.8 Hz, -OC$\underline{H}_2$Ph), 4.43 (d, J_{gem}= 11.8 Hz, -OC$\underline{H}_2$Ph), 4.09 (dd, 1H, $J_{2\text{-}1}$= 8.0 Hz, $J_{2\text{-}3}$= 9.8 Hz, H-2), 3.98 (dd, $J_{4\text{-}3}\sim J_{4\text{-}5}$ = 2.8 Hz, H-4), 3.75 (m, 1H, H-5), 3.65 (m, 3H, H-3, H-6a and H-6b) ppm.

2.6. Synthesis of trisaccharide antigen B derivative

*Synthesis of N-(benzyloxycarbonyl)aminopropyl 2-O-(2',3',4'-tri-O-benzyl-α-L-fucopyranosyl)-3-O-(2'',3'',4'',6''-tetra-O-benzyl-α-D-galactopyranosyl)-4,6-O-benzylidene-β-D-galactopyranoside (**60**)*

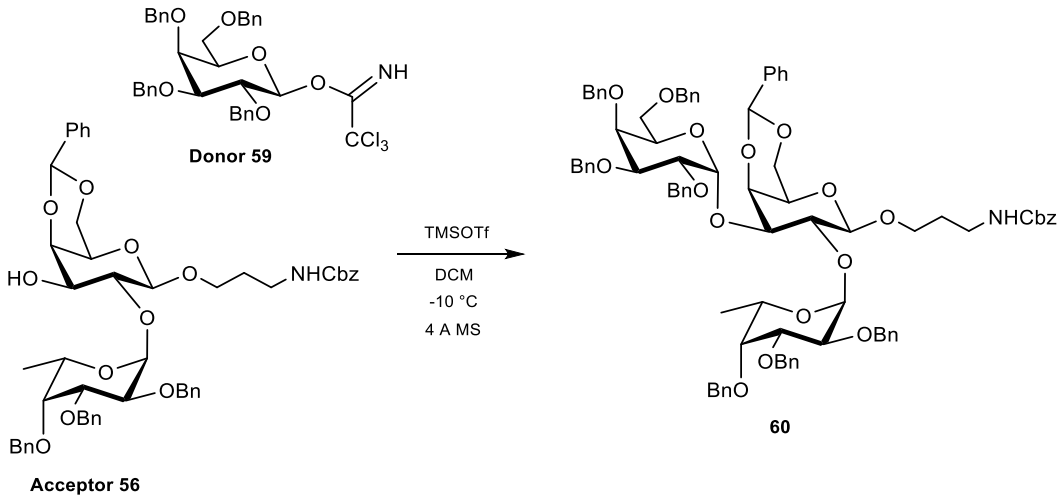

Compound **56** (68.6 mg, 0.078 mmol) was co-evaporated with toluene and after 12 h, it was dissolved in dry DCM (1 ml, 0.08 M) and 4 Å MS were added. After 30 mins, the reaction mixture was cooled down to -10 ºC and TMSOTf was added (3.2 µl, 0.008 mmol). A solution of donor **59** (0.13 g, 0.195 mmol) in DCM (1 ml) was added dropwise into the reaction mixture. The progress was monitored by HPTLC (Hex:EtOAc - 3:2) and after 2 h, the reaction mixture was neutralized with TEA and the crude was subjected to column chromatography (Hex:EtOAc 8:2 → 6:4) to afford compound **60** in α configuration (74.0 mg, 68 %).

TLC: R_f*(α)*: 0.38 (Hex:EtOAc - 1:1).

NMR data:

^{1}H NMR (400 MHz, $CDCl_3$, 25 °C): δ= 7.56 (m, 2H, H_{arom}), 7.48 – 7.10 (m, 43H, H_{arom}), 5.58 (s, 1H, H-10), 5.57 (d, 1H, $J_{1'',2''}$= 2.4 Hz, H-1''), 5.53 (s, 1H, H-10), 5.44 (d, 1H, $J_{1',2'}$= 3.4 Hz, H-1'), 5.16 (s, 2H, -NHCOOC$\underline{H}_2$Ph), 5.02 – 4.48 (m, 14H, , -OC$\underline{H}_2$Ph), 4.43 (d, 1H, $J_{4,3}$= 2.4 Hz, H-4), 4.36 (d, 1H, $J_{1,2}$= 7.6 Hz, H-1), 4.31 (d, 1H, $J_{6a,6b}$= 12.4 Hz, $J_{6a,5}$ < 1 Hz, H-6a), 4.29 (m, 1H, H-5'), 4.24 – 4.14 (m, 2H, H-2, H-5''), 4.12 – 3.94 (m, 7H, H-2', H-2'', H-3, H-3', H-4'', H-6b, H-7a), 3.71 (b.s, 1H, H-4'), 3.65 – 3.57 (m, 3H, H-3'', H-6a'', H-7b), 3.35 (m, 2H, H-9), 3.27 (m, 1H, H-6b''), 3.43 (b.s, 1H, H-5), 1.83 (m, 2H, H-8), 1.25 (d, 3H, $J_{6',5'}$= 6.4 Hz, H-6') ppm.

^{13}C NMR (100.6 MHz, $CDCl_3$, 25 °C): δ= 156.9 (-NH$\underline{C}$OOCH$_2$Ph), 140.1 – 137.2 (C_{arom}), 130.3 – 126.7 (C_{arom}), 102.5 (C-1), 101.4 (C-10), 98.0 (C-1''), 92.6 (C-1'), 80.1, 78.4, 78.15, 76.6, 75.6, 75.4 (C-2', C-2'', C-3, C-3', C-3'', C-4', C-4''), 75.0, 74.7, 74.0, 73.4, 73.2, 72.9 (-O$\underline{C}$H$_2$Ph), 73.0 (C-2 or C-5''), 72.0 (C-4), 70.3 (C-2 or C-5''), 70.2 (C-6''), 69.6 (C-6), 66.8 (C-5'), 66.7 (-NHCOO$\underline{C}$H$_2$Ph), 66.4 (C-7), 66.2 (C-5), 37.7 (C-9), 30.4 (C-8), 17.6 (C-6') ppm.

MS (ESI+): theoretical mass: 1398.65 m/z, experimental mass $[M+Na]^+$: 1421.65 m/z.

2.7. Synthesis of donor 62

Synthesis of imidazole-1-sulfonyl azide hydrogen sulfate

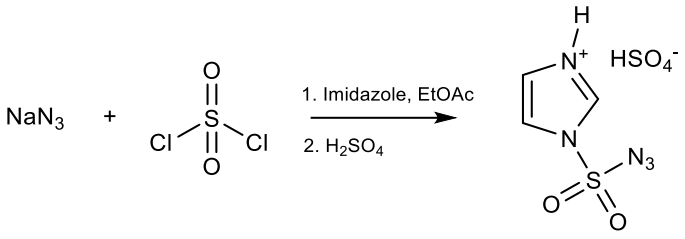

A suspension of NaN_3 (5 g, 77 mmol) in dry EtOAc (77 ml, 1 M) was cooled down to 0°C and sulfuryl chloride (6.2 ml, 77 mmol) was added dropwise. The reaction mixture was stirred at room temperature and after 16 h, the suspension was cooled down to 0°C and imidazole (10 g, 146 mmol) was added portionwise. After 4 h, the solution was basified with $NaHCO_3$ (150 ml), the organic phase was further washed with H_2O, dried over anhydrous Na_2SO_4 and filtered. An aqueous solution of H_2SO_4 98% (4.1ml, 77 mmol) was added slowly at 0°C and the mixture was stirred vigorously for 30 mins. The white precipitate was filtered using a Buchner funnel and washed with cold EtOAc. The solid was dried in the vacuum pump to obtain the target salt (9.2 g, 36 mmol, 44 %).

The spectroscopic data are in agreement with those reported in literature[303].

*Synthesis of acetyl 3,4,6-tri-O-acetyl-2-azido-2-deoxy-α,β-D-galactopyranoside (**61**)*

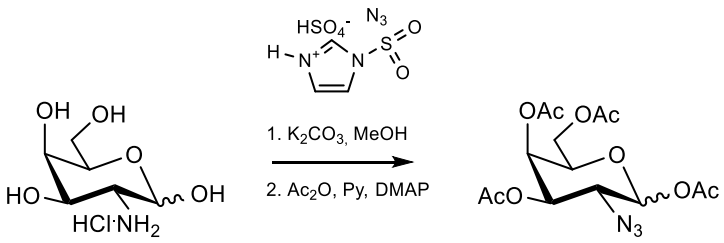

D-Galactosamine hydrochloride **61**

D-Galactosamine hydrochloride (4.50 g, 20.87 mmol) was dissolved in MeOH (100 ml, 0.2 M) and anhydrous K_2CO_3 (8.65 g, 62.59 mmol) was added portionwise at 0 °C. The reaction mixture was stirred for 15 mins and imidazole-1-sulfonyl azide hydrogen sulfate (7.01 g, 25.85 mmol) was added slowly, followed by the addition of $Cu_2SO_4 \cdot 5H_2O$ (52 mg, 0.21 mmol). The reaction progress was monitored by RPTLC (ACN:MeOH:H_2O - 5:2:0.1). After 10 h the starting material was consumed, and the excess of solvent was removed under vacuum. The crude product was dissolved in Py (30 ml) and DCM (70 ml), brought to 0°C before adding DMAP (50 mg, 0.41 mmol) and Ac_2O dropwise (15.8 ml, 167 mmol). The reaction progress was monitord by TLC (Hex:EtOAc 6:4) and after completion, it was neutralized with HCl 5% (3x 100ml) and washed with $NaHCO_3$ (1 x 100 ml) and brine (1 x 100 ml). The organic phase was dried over anhydrous Na_2SO_4, filtered and evaporated under vacuum. The crude was purified by column chromatography (Hex:EtOAc 8:2 → 6:4) to isolate compound **61** as a colorless foam (5.28 g, 68%, α:β 3:7).

RPTLC: *Rf:* 0.75 (ACN:MeOH:H_2O - 5:2:0.1).

NMR data for β anomer:

^{1}H NMR (400 MHz, $CDCl_3$, 25 °C): δ= 5.56 (d, 1H, $J_{1\text{-}2}$= 8.5 Hz, H-1), 5.39 (dd, $J_{4\text{-}3}$= 3.3 Hz, $J_{4\text{-}5}$ < 1 Hz, H-4), 4.91 (dd, 1H, $J_{3\text{-}2}$= 10.8 Hz, $J_{3\text{-}4}$= 3.3 Hz, H-3), 4.19-4.09 (m, 2H, H-6a and H-6b), 4.05 (m, 1H, H-5), 3.56 (dd, 1H, $J_{2\text{-}1}$= 8.5 Hz, $J_{2\text{-}3}$= 10.8 Hz, H-2), 2.22 (s, 3H, -$COCH_3$), 2.18 (s, 3H, -$COCH_3$), 2.08 (s, 3H, -$COCH_3$), 2.05 (s, 3H, -$COCH_3$) ppm.

^{13}C NMR (100.6 MHz, $CDCl_3$, 25 °C): δ= 170.6 – 168.8 (-$\underline{C}OCH_3$), 93.4 (C-1), 72.1 (C-5), 71.6 (C-3), 66.4 (C-4), 61.2 (C-6), 60.0 (C-2), 21.1 – 20.8 (-CO$\underline{C}H_3$) ppm.

*Synthesis of 3,4,6-tri-O-acetyl-2-azido-2-deoxy-α,β-D-galactopyranosyl trichloroacetimidate (**62**)*

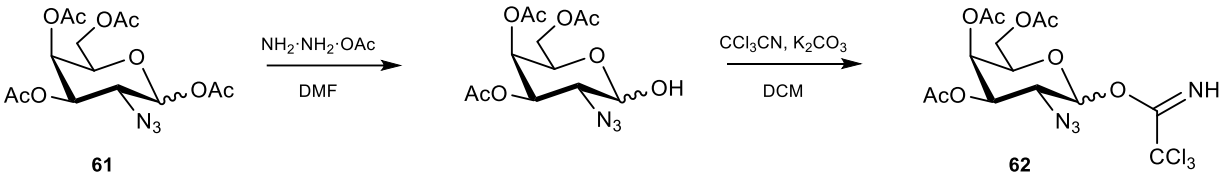

A solution of freshly prepared hydrazine acetate (0.30 ml, 3.42 mmol) was slowly added to a solution of compound **61** (0.97 g, 2.60 mmol) in dry DMF (9 ml, 0.3 M). The reaction was warmed up to 40 ºC and monitored by TLC (Hex:EtOAc - 2:8) until complete disappearance of the starting material and then diluted in EtOAc and washed with brine (2 x 15 ml) and water (2 x 15 ml). The organic phase was dried over anhydrous Na_2SO_4, filtered and evaporated. The crude was purified by column chromatography (Hex:EtOAc 5:5 → 5:6) to afford 3,4,6-tri-O-acetyl-2-azido-2-deoxy-α,β-D-galactopyranose (0.75 g, 86 %, α:β 1:1). TLC: R_f: 0.68 (Hex:EtOAc - 2:8).

The product (0.75 g, 2.26 mmol) was dissolved in dry DCM (12 ml, 0.19 M). CCl_3CN (1.2 ml, 11.98 mmol) and K_2CO_3 (1.27 g, 9.19 mmol) were added under Ar atmosphere. The reaction mixture was vigorously stirred and after 17 h, the K_2CO_3 was filtered over celite to afford compound **62** (0.90 g, 84 %, α:β 4:6).

NMR data for β anomer:

^{1}H NMR (400 MHz, $CDCl_3$, 25 °C): δ= 8.79 (s, 1H, -NH), 5.69 (d, 1H, $J_{1\text{-}2}$= 8.4 Hz, H-1), 5.37 (d, $J_{4\text{-}3}$= 3.31 Hz, H-4), 4.94 (dd, 1H, $J_{3\text{-}2}$= 10.5 Hz, $J_{3\text{-}4}$= 3.0 Hz, H-3), 4.16-4.00 (m, 3H, H-5, H-6a, H-6b), 3.99 (dd, 1H, $J_{2\text{-}1}$= 8.4 Hz, $J_{2\text{-}3}$= 10.5 Hz, H-2), 2.16 (s, 3H, -$COCH_3$), 2.05 (s, 3H, -$COCH_3$), 2.00 (s, 3H, -$COCH_3$) ppm.

^{13}C NMR (100.6 MHz, $CDCl_3$, 25 °C): δ= 170.4 – 168.6 (-$\underline{C}OCH_3$), 160.8 (-$\underline{C}NHCCl_3$), 96.7 (C-1), 71.7 (C-5), 71.3 (C-3), 66.1 (C-4), 61.0 (C-6), 60.6 (C-2), 20.6 – 20.5 (-CO$\underline{C}H_3$) ppm.

3. Experimental procedures Chapter III

3.1. Synthesis of 3'-aminopropyl 2-O-(α-D-mannopyranosyl)-α-D-mannopyranoside

*Synthesis of acetyl 3,4,6-tri-O-acetyl-2-O-(2',3',4',6'-tetra-O-acetyl-α-D-mannopyranosyl)-α,β-D-mannopyranoside (**65**)*

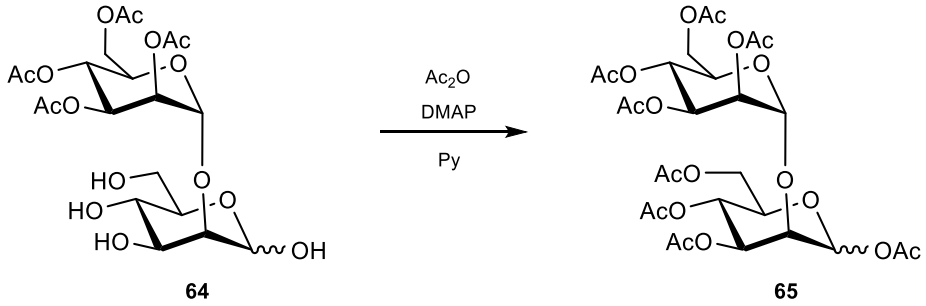

Compound **64** (0.14 g, 0.27 mmol) was dissolved in pyridine (4 ml, 0.07 M), acetic anhydride (0.4 ml, 4.23 mmol) and catalytic amount of DMAP were added. The reaction mixture was monitored by TLC (Hex:EtOAc - 4:6) and after 16 h the excess of solvent was removed in vacuo. The crude was purified by column chromatography (Hex:EtOAc 6:4 → 5:5) to obtain compound **65** as a white foam (0.18 g, quant., α:β 9:1).

TLC: R_f: 0.36 (Hex:EtOAc - 4:6).

NMR data for α anomer:

^{1}H NMR (400 MHz, $CDCl_3$, 25 °C): δ= 6.24 (d, 1H, $J_{1\text{-}2}$= 1.8 Hz, H-1), 5.46 to 5.38 (m, 2H, H-3' and H-4), 5.32 to 5.22 (m, 3H, H-2', H-3, H-4'), 4.95 (d, 1H, $J_{1\text{-}2}$= 1.4 Hz, H-1'), 4.23 (dd, 1H, $J_{6a\text{-}6b}$= 12.5 Hz, $J_{6a\text{-}5}$= 3.9 Hz, H-6a), 4.21 to 4.15 (m, 3H, H-6a', H-6b' and H-5'), 4.12 (dd, 1H, $J_{6b\text{-}6a}$= 12.5 Hz, $J_{6b\text{-}5}$= 2.1 Hz, H-6b), 4.04 (bt, 1H, $J_{2\text{-}1}$~$J_{2\text{-}3}$~1.8 Hz, H-2), 4.00 (ddd, 1H, $J_{5\text{-}4}$= 10.3 Hz, $J_{5\text{-}6a}$= 3.9 Hz, $J_{5\text{-}6b}$= 2.1 Hz, H-5), 2.15 (s, 6H, -$COCH_3$), 2.14 (s, 3H, -$COCH_3$), 2.10 (s, 3H, -$COCH_3$), 2.09 (s, 3H, -$COCH_3$), 2.04 (s, 6H, -$COCH_3$), 2.00 (s, 3H, -$COCH_3$) ppm.

^{13}C NMR (100.6 MHz, $CDCl_3$, 25 °C): δ= 170.2 – 169.53 (-$\underline{C}OCH_3$), 99.47 (C-1'), 91.7 (C-1), 76.07 (C-2), 70.87 (C-5), 69.97 (C-3, C-4', C-5'), 68.52 and 65.72 (C-3' and C-4), 66.39 (C-2'), 62.60 and 61.92 (C-6 and C-6'), 21.09 - 20.83 (-CO$\underline{C}H_3$) ppm.

*Synthesis of 3'-chloropropyl 3,4,6-tri-O-acetyl-2-O-(2',3',4',6'-tetra-O-acetyl-α-D-mannopyranosyl)-α-D-mannopyranoside (**66**)*

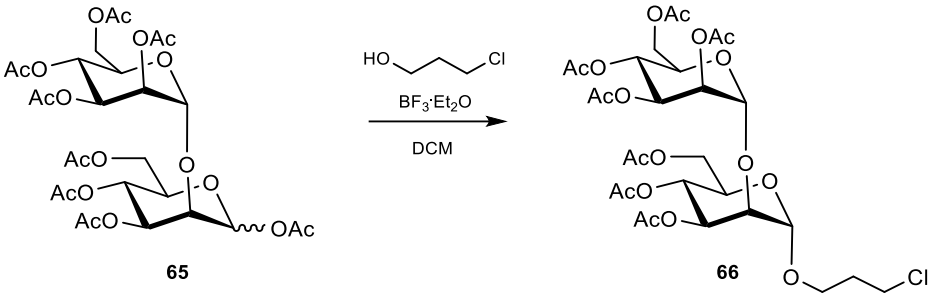

Compound **65** (52.8 mg, 0.08 mmol) was dissolved in dry toluene, co-evaporated three times and dried in the pump overnight in order to get rid of any traces of water. Compound **65** was dissolved in dry DCM (0.9 ml, 0.09 M) and 3-chloro-1-propanol (20 µl, 0.23 mmol) was added. The solution was ice-cooled to 0 °C and $BF_3 \cdot Et_2O$ (30 µl, 0.23 mmol) was added dropwise. The reaction mixture was stirred overnight at r.t and monitored by TLC (Hex:EtOAc - 4:6). After 48 h, when the spot corresponding to the starting material disappeared, the excess of acid was quenched with TEA and the solvent was removed. The crude was dissolved in pyridine (0.8 ml, 0.1 M) and Ac_2O was added (70 µl, 0.72 mmol), the reaction mixture was stirred overnight. The crude product was purified by column chromatography (Hex:EtOAc 5:5 → 4:6) to isolate glycoside **66** as a white foam (40.5 mg, 0.06 mmol, 73 %).

TLC: R_f: 0.43 (Hex:EtOAc - 4:6).

NMR data:

^{1}H NMR (400 MHz, $CDCl_3$, 25 °C): δ= 5.40 (dd, 1H, $J_{3\text{-}2}$= 2.3 Hz, $J_{3\text{-}4}$= 10.0 Hz, H-3'), 5.32 (dd, 1H, $J_{4\text{-}3}$= 10.0 Hz, $J_{4\text{-}5}$= 10.0 Hz, H-4 or H-4'), 5.27 (t, 1H, $J_{4\text{-}3}$= 10.0 Hz, $J_{4\text{-}5}$= ~1 Hz, H-4 or H-4'), 5.26 (dd, 1H, $J_{2'\text{-}1'}$= 1.5 Hz, $J_{2'\text{-}3'}$= 2.3 Hz, H-2'), 5.25 (dd, 1H, $J_{3\text{-}2}$= 2.3 Hz, $J_{3\text{-}4}$= 10.0 Hz, H-3), 4.95 (d, 1H, $J_{1\text{-}2}$= 1.5 Hz, H-1), 4.92 (d, 1H, $J_{1\text{-}2}$= 1.5 Hz, H-1'), 4.25 - 4.08 (m, 5H, H-6a', H-6b', H-6a, H-6b, H-5 or H-5'), 4.03 (dd, 1H, $J_{2\text{-}1}$= 1.5 Hz, $J_{2\text{-}3}$= 2.3 Hz H-2), 3.92 (m, 2H, H-5 or H-5' and H-7b), 3.65 (t, 2H, $J_{9\text{-}8}$= 6.1 Hz, H-9), 3.58 (dt, 1H, $J_{7a\text{-}7b}$= 9.8 Hz, $J_{7a\text{-}8}$= 5.3 Hz, H-7b), 2.06 (m, 2H, H-8), 2.14 (s, 3H, -$COCH_3$), 2.13 (s, 3H, -$COCH_3$), 2.08 (s, 6H, -$COCH_3$), 2.04 (s, 3H, -$COCH_3$), 2.03 (s, 3H, -$COCH_3$), 2.00 (s, 3H, -$COCH_3$) ppm.

^{13}C NMR (100.6 MHz, $CDCl_3$, 25 °C): δ= 170.7 – 169.5 (-$\underline{C}OCH_3$), 99.43 (C-1'), 98.60 (C-1), 77.23 (C-2), 70. 51 (C-3), 70.02 (C-2'), 69.43 and 68.94 (C-5 and C-5'), 68.57 (C-3'), 66.38 and 66.34 (C-4 and C-4'), 64.72 (C-7), 62.84 and 62.44 (C-6 and C-6'), 41.72 (C-9), 32.26 (C-8), 21.12 – 20.86 (-CO$\underline{C}H_3$) ppm.

MS (ESI+): theoretical mass: 713.08 m/z, experimental mass $[M+Na]^+$: 736.19 m/z.

*Synthesis of 3'-azidopropyl 3,4,6-tri-O-acetyl-2-O-(2',3',4',6'-tetra-O-acetyl-α-D-mannopyranosyl)-α-D-mannopyranoside (**67**)*

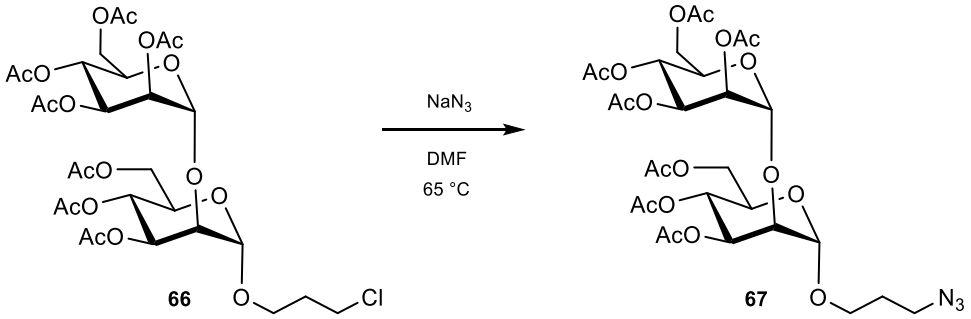

Sodium azide (10.2 mg, 0.16 mmol) was added to a suspension of compound **66** (31.0 mg, 0.04 mmol) in dry DMF (0.5 mL, 0.09 M). The reaction mixture was warmed up to 65 °C. The reaction could not be followed by TLC since the *Rf* of the starting material was analogous to the one of the product. After 14 h, the excess of solvent was removed under pressure and the crude was purified by column chromatography (Hex:EtOAc 5:5) to obtain compound **67** (31.3 mg, 0.04 mmol, quant.) as a colorless syrup.

NMR data:

^{1}H NMR (400 MHz, $CDCl_3$, 25 °C): δ= 5.39 (dd, 1H, $J_{3',-2'}$= 3.3 Hz, $J_{3',-4'}$= 9.9 Hz, H-3'), 5.32 (dd, 1H, J_{4-3}= 9.9 Hz, J_{4-5}= 9.5 Hz, H-4), 5.26 (m, 3H, H-4', H-3, H-2'), 4.93 (d, 1H, J_{1-2}= 1.7 Hz, H-1), 4.91 (d, 1H, $J_{1',-2',}$= 1.7 Hz, H-1'), 4.25 - 4.08 (m, 5H, H-6a', H-6b', H-6a, H-6b, H-5 or H-5'), 4.02 (dd, 1H, J_{2-1}= 1.7 Hz, J_{2-3}= 3.2 Hz, H-2), 3.89 (ddd, 1H, J_{5-4}= 9.5 Hz, J_{5-6a}= 4.3 Hz, J_{5-6b}= 2.4 Hz, H-5 or H-5'), 3.81 (m, 1H, H-7a), 3.51 (m, 1H, H-7b), 3.41 (dt, 2H, J_{9-7}= 6.4 Hz, J_{9a-8}= 2.7 Hz, H-9), 2.14 (s, 3H, -$COCH_3$), 2.13 (s, 3H, -$COCH_3$), 2.08 (s, 3H, -$COCH_3$), 2.07 (s, 3H, -$COCH_3$), 2.03 (s, 3H, -$COCH_3$), 2.02 (s, 3H, -$COCH_3$), 2.00 (s, 3H, -$COCH_3$), 1.88 (m, 2H, H-8) ppm.

^{13}C NMR (100.6 MHz, $CDCl_3$, 25 °C): δ= 171.2 – 169.4 (-$\underline{C}OCH_3$), 99.36 (C-1'), 98.51 (C-1), 77.11 (C-2), 70.41 and 69.92 (C-2' and C-3), 69.34 and 68.90 (C-5 and C-5'), 68.54 (C-3'), 66.58 and 66.33 (C-4 and C-4'), 65.00 (C-7), 62.76 and 62.40 (C-6 and C-6'), 48.30 (C-9), 28.90 (C-8), 21.04 – 20.72 (-CO$\underline{C}H_3$) ppm.

Synthesis of 3'-azidopropyl 2-O-(α-D-mannopyranosyl)-α-D-mannopyranoside

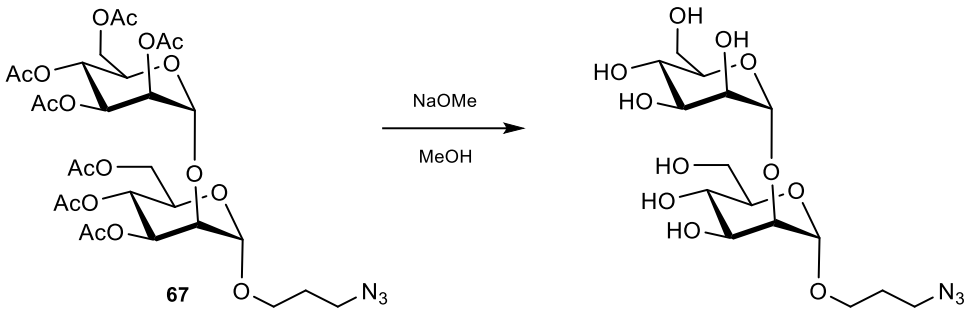

Compound **67** (79.3 mg, 0.11 mmol) was dissolved in MeOH (1 ml, 0.1 M) and NaOMe (6 mg, 0.11 mmol) was added. The reaction mixture was stirred at r.t. until TLC (DCM:MeOH 7:3) showed the consumption of the starting material. After 3 h, the reaction mixture was quenched using Amberlite IR120 (H^+ form), filtered and concentrated in vacuo to obtain the target compound (46.1 mg, 0.11 mmol, 98 %) as a colorless syrup.

TLC: R_f: 0.26 (DCM:MeOH 7:3).

NMR data:

^{1}H NMR (400 MHz, CD_3OD, 25 °C): δ= 5.12 (d, 1H, $J_{1\text{-}2}$= 1.37 Hz, H-1), 5.01 (d, 1H, $J_{1'\text{-}2'}$= 1.3 Hz, H-1'), 4.02 (dd, $J_{2'\text{-}1'}$= 1.3 Hz, $J_{2'\text{-}3'}$= 2.9 Hz, 1H, H-2'), 3.92-3.82 (m, 5H, H-2, H-3, H-6a and H-6a' and H-7a), 3.80-3.68 (m, 4H, H-3', H-6b and H-6b, H-5 or H-5'), 3.62 – 3.52 (m, 4H, H-4 and H-4', H-5 or H-5', H-7b), 3.45 (td, $J_{9\text{-}7}$= 6.4 Hz, $J_{9a\text{-}8}$= 2.7 Hz, 2H, H-9), 1.90 (m, 2H, H-8) ppm.

^{13}C NMR (100.6 MHz, CD_3OD, 25 °C): δ= 104.3 (C-1'), 99.8 (C-1), 80.7 (C-2), 75.03 and 74.75 (C-5 and C-5'), 72.41 and 72.17 (C-3 and C-3'), 71.85 (C-2'), 68.96 and 68.84 (C-4 and C-4'), 65.45 (C-7), 63.14 and 63.0 (C-6 and C-6'), 49.61 (C-9), 29.96 (C-8) ppm.

MS (ESI+): theoretical mass: 425.39 m/z, experimental mass $[M+Na]^+$: 448.08 m/z.

*Synthesis of 3'-aminopropyl 2-O-(α-D-mannopyranosyl)-α-D-mannopyranoside (**68**)*

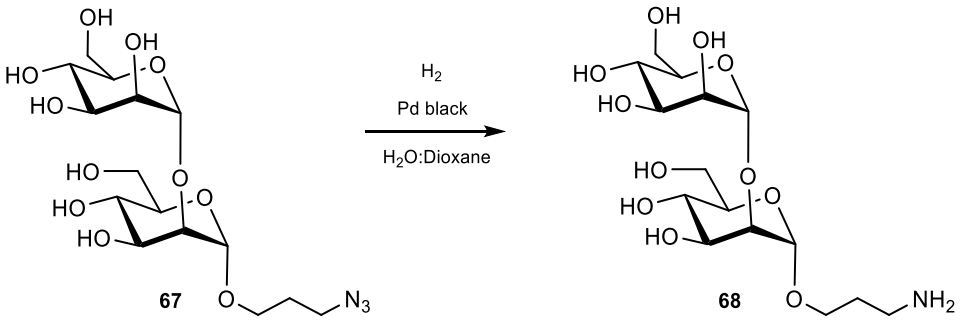

3'-Azidopropyl 2-O-(α-D-mannopyranosyl)-α-D-mannopyranoside (46.3 mg, 0.11 mmol) was dissolved in H_2O:dioxane 3:1 (4 ml, 0.03 M) and a catalytic amount of Pd black was added. The reaction atmosphere was purged with H_2/vacuum cycles and then, stirred under H_2 atmosphere. After 24 h, the Pd black was filtered through a Whatman syringe filter and concentrated in vacuo to obtain compound **68** as a colorless foam (42 mg, 0.11 mmol, 99 %).

NMR data:

^{1}H NMR (400 MHz, D_2O, 25 °C): δ= 5.11 (d, 1H, H-1), 5.03 (d, 1H, H-1'), 4.08 (m, 1H, H-2'), 3.99 – 3.56 (m, 13H, H-2, H-3, H-3', H-4, H-4', H-5, H-5', H-6a, H-6a', H-6b, H-6b', H-7a and H-7b), 2.97 (m, 2H, H-9), 1.91 (m, 2H, H-8) ppm.

^{13}C NMR (100.6 MHz, D_2O, 25 °C): δ= 104.14 (C-1), 99.86 (C-1'), 80.48 (C-2), 75.00, 74.59, 72.09, 71.69 and 68.78 (C-2', C-3, C-3', C-4, C-4', C-5 and C-5'), 67.08 (C-7), 62.89 and 62.72 (C-6 and C-6'), 39.31 (C-9), 30.35 (C-8) ppm.

MS (ESI+): theoretical mass: 399.39 m/z, experimental mass $[M+H]^+$: 440.21 m/z.

3.2. Synthesis of 3'-aminopropyl 3-O-(α-D-mannopyranosyl)-6-O-(α-D-mannopyranosyl)-α-D-mannopyranoside

*Synthesis of acetyl 2,4-di-O-acetyl-3-O-(2',3',4',6'-tetra-O-acetyl-α-D-mannopyranosyl)-6-O-(2'',3'',4'',6''-tetra-O-acetyl-α-D-mannopyranosyl)-α-D-mannopyranoside (**69**)*

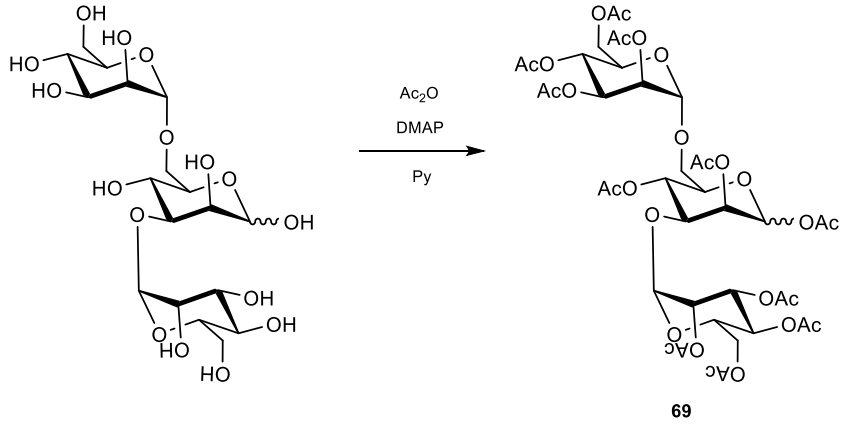

69

3-O-(α-D-mannopyranosyl)-6-O-(α-D-mannopyranosyl)-α,β-D-mannopyranose (94.5 mg, 0.19 mmol) was dissolved in pyridine (1.5 ml, 0.13 M), acetic anhydride (0.3 ml, 3.17 mmol) and catalytic amount of DMAP were added. The reaction mixture was monitored by TLC (Hex:EtOAc - 1:2) and after 16 h the excess of solvent was evaporated under reduced pressure. The crude was purified by column chromatography (Hex:EtOAc 5:5 → 4:6) to afford compound **69** as a white foam (192 mg, quant., α:β 8:2).

TLC: R_f: 0.35 (Hex:EtOAc - 1:2).

NMR data for α anomer:

^{1}H NMR (400 MHz, $CDCl_3$, 25 °C): δ= 6.04 (d, 1H, $J_{1\text{-}2}$= 1.6 Hz, H-1), 5.36 – 5.13 (m, 7H, H-2, H-2', H-2'', H-3' or H-3'', H-4, H-4', H-4''), 5.03 (m, 2H, H-1' or H-1'' and H-3' or H-3''), 4.77 (d, 1H, $J_{1\text{-}2}$= 1.5 Hz, H-1' or H-1''), 4.31 – 4.19 (m, 2H, H-6a' and H-6a''), 4.17 (dd, $J_{3\text{-}2}$= 3.3 Hz, $J_{3\text{-}4}$= 9.7 Hz 1H, H-3), 4.11 – 3.99 (m, 4H, H-5', H-5'', H-6b' and H-6b''), 3.88 (ddd, $J_{5\text{-}4}$= 9.5 Hz, $J_{5\text{-}6a}$= 5.6 Hz, $J_{5\text{-}6b}$= 2.9 Hz, 1H, H-5), 3.72 (dd, $J_{6a\text{-}6b}$= 11.2 Hz, $J_{6a\text{-}5}$= 5.6 Hz, 1H, H-6a), 3.55 (dd, $J_{6b\text{-}6a}$= 11.2 Hz, $J_{6b\text{-}5}$= 2.9 Hz, 1H, H-6b), 2.23 (s, 3H, -$COCH_3$), 2.15 (s, 3H, -$COCH_3$), 2.14 (s, 3H, -$COCH_3$), 2.13 (s, 6H, -$COCH_3$), 2.09 (s, 3H, -$COCH_3$), 2.08 (s, 3H, -$COCH_3$), 2.05 (s, 6H, -$COCH_3$), 1.99 (s, 3H, -$COCH_3$), 1.97 (s, 3H, -$COCH_3$) ppm.

^{13}C NMR (101 MHz, $CDCl_3$, 23 °C): δ= 171.0 – 169.7 (-$\underline{C}OCH_3$), 99.4 and 97.7 (C-1' and C-1''), 90.8 (C-1), 75.0 (C-3), 71.8 (C-5), 70.5 – 68.0 (C-2, C-2', C-2'', C-3', C-3'', C-4, C-4', C-4'', C-5' and C-5''), 67.4 (C-6), 62.6 and 62.5 (C-6' and C-6''), 21.1 – 20.7 (-CO$\underline{C}H_3$) ppm.

*Synthesis of 3'-chloropropyl 2,4-tri-O-acetyl-3-O-(2',3',4',6'-tetra-O-acetyl-α-D-mannopyranosyl)-6-O-(2'',3'',4'',6''-tetra-O-acetyl-α-D-mannopyranosyl)-α-D-mannopyranoside (**70**)*

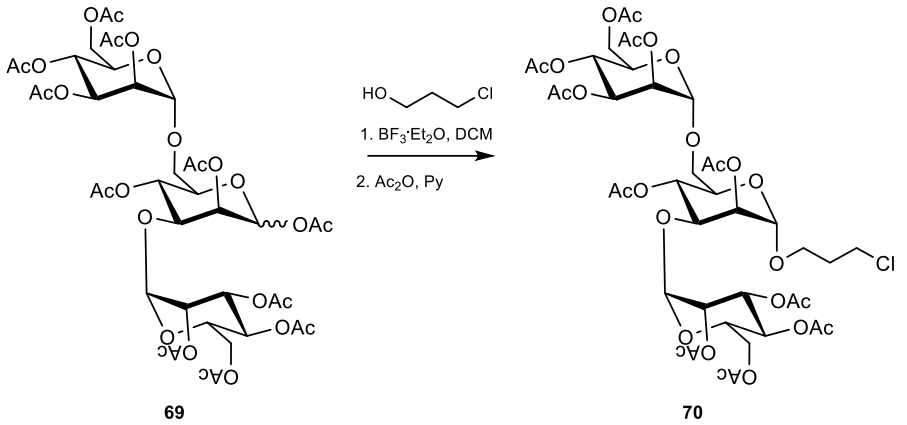

69 **70**

Compound **69** (50.4 mg, 0.05 mmol) was co-evaporated with toluene and dried in the pump overnight in order to get rid of any traces of water. Compound **69** was dissolved in dry DCM (0.5 ml, 0.1 M) and 3-chloro-1-propanol (13 µl, 0.15 mmol) was added. The solution was ice-cooled to 0 °C and $BF_3 \cdot Et_2O$ (13 µl, 0.10 mmol) was added dropwise. The reaction mixture was stirred overnight at r.t and monitored by TLC (Hex:EtOAc - 2:8). After 48 h, there was still some starting material and more $BF_3 \cdot Et_2O$ (7 µl, 0.05 mmol) was added at 0 °C. After 24 h, when the spot corresponding to the starting material disappeared, the excess of acid was quenched with TEA and the solvent was evaporated. The crude was dissolved in pyridine (0.5 ml, 0.1 M) and Ac_2O was added (43 µl, 0.45 mmol), the reaction mixture was stirred overnight. The excess of solvents was removed under vaccum and the crude product was purified by column chromatography (Hex:EtOAc 5:5 → 3:7) to obtain product **70** as a white foam (18.9 mg, 0.02 mmol, 37 %).

TLC: R_f: 0.54 (Hex:EtOAc 2:8).

NMR data:

^{1}H NMR (400 MHz, $CDCl_3$, 25 °C): δ= 5.35 – 5.15 (m, 7H, H-2, H-2', H-2'', H-3' or H-3'', H-4, H-4', H-4''), 5.00 (m, 2H, H-1' or H-1'' and H-3' or H-3''), 4.81 (d, 1H, $J_{1\text{-}2}$= 1.6 Hz, H-1), 4.80 (d, 1H, $J_{1\text{-}2}$= 1.5 Hz, H-1' or H-1''), 4.30 – 4.19 (m, 2H, H-6a' and H-6a''), 4.19 – 4.02 (m, 5H, H-3, H-5', H-5'', H-6b', H-6b''), 3.93 – 3.81 (m, 2H, H-5, H-7a), 3.77 (dd, 1H, $J_{6a\text{-}6b}$= 11.2 Hz, $J_{6a\text{-}5}$= 6.6 Hz, H-6a), 3.67 – 3.58 (m, 3H, H-9 and H-7b), 3.50 (dd, 1H, $J_{6b\text{-}6a}$= 11.2 Hz, $J_{6b\text{-}5}$= 2.1 Hz, H-6b), 2.07 (m, 2H, H-8), 2.20 (s, 3H, -$COCH_3$), 2.14 (s, 3H, -$COCH_3$), 2.13 (s, 6H, -$COCH_3$), 2.10 (s, 6H, -$COCH_3$), 2.05 (s, 3H, -$COCH_3$), 2.03 (s, 3H, -$COCH_3$), 1.99 (s, 3H, -$COCH_3$), 1.97 (s, 3H, -$COCH_3$) ppm.

^{13}C NMR (100.6 MHz, $CDCl_3$, 25 °C): δ= 171.2 – 169.7 (-$\underline{C}OCH_3$), 99.4 and 97.7 (C-1' and C-1''), 97.4 (C-1), 75.0 (C-3), 71.8 (C-5), 70.5 – 68.0 (C-2, C-2', C-2'', C-3', C-3'', C-4, C-4', C-4'', C-5' and C-5''), 67.4 (C-6), 65.0 (C-7), 62.6 and 62.5 (C-6' and C-6''), 42.2 (C-9), 32.8 (C-8), 21.1 – 20.7 (-CO$\underline{C}H_3$) ppm.

MS (ESI+): theoretical mass: 1001.32 m/z, experimental mass $[M+Na]^+$: 1024.50 m/z.

*Synthesis of 3'-azidopropyl 2,4-tri-O-acetyl-3-O-(2',3',4',6'-tetra-O-acetyl-α-D-mannopyranosyl)-6-O-(2'',3'',4'',6''-tetra-O-acetyl-α-D-mannopyranosyl)-α-D-mannopyranoside (**71**)*

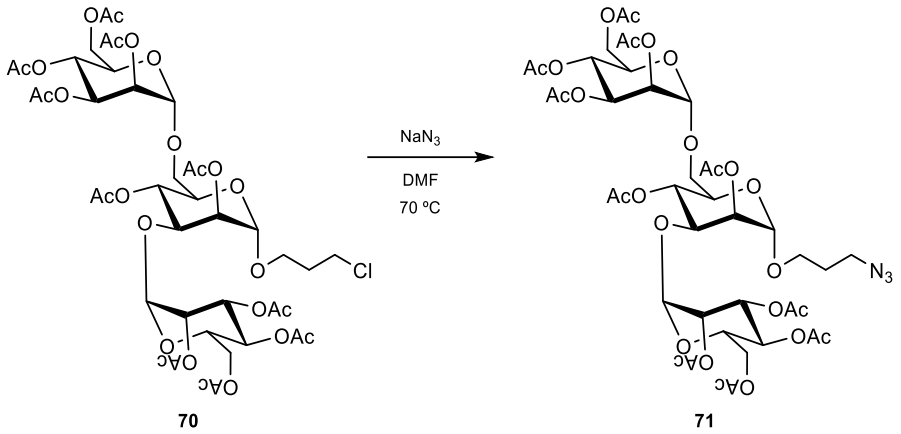

Sodium azide (11.1 mg, 0.17 mmol) was added to a stirring solution of compound **70** (39.0 mg, 0.04 mmol) in dry DMF (0.4 mL, 0.1 M). The reaction mixture was warmed up to 70 °C. The reaction could not be followed by TLC since the *Rf* of the starting material was similar to the one of the product. After 14 h, the excess of solvent was evaporated in vacuo and the crude was purified by column chromatography (Hex:EtOAc 4:6) to obtain compound **71** (38.1 mg, 97 %) as a transparent oil.

NMR data:

^{1}H NMR (400 MHz, $CDCl_3$, 25 °C): δ= 5.32 – 5.14 (m, 7H, H-2, H-2', H-2'', H-3' or H-3'', H-4, H-4', H-4''), 5.04 – 4.99 (m, 2H, H-1' or H-1'' and H-3' or H-3''), 4.82 (d, 1H, $J_{1\text{-}2}$= 1.6 Hz, H-1), 4.79 (d, 1H, $J_{1\text{-}2}$= 1.4 Hz, H-1' or H-1''), 4.31 – 4.20 (m, 2H, H-6a' and H-6a''), 4.18 – 4.04 (m, 5H, H-3, H-5', H-5'', H-6b', H-6b''), 3.87 – 3.74 (m, 3H, H-5, H-6a, H-7a), 3.54 (m, 1H, H-7b), 3.49 (dd, $J_{6b\text{-}6a}$= 10.5 Hz, $J_{6b\text{-}5}$= 1.9 Hz, 1H, H-6b), 3.42 (m, 2H, H-9), 2.21 (s, 3H, -$COCH_3$), 2.15 (s, 3H, -$COCH_3$), 2.14 (s, 6H, -$COCH_3$), 2.10 (s, 6H, -$COCH_3$), 2.05 (s, 3H, -$COCH_3$), 2.04 (s, 3H, -$COCH_3$), 1.98 (s, 3H, -$COCH_3$), 1.97 (s, 3H, -$COCH_3$), 1.90 (m, 2H, H-8) ppm.

^{13}C NMR (100.6 MHz, $CDCl_3$, 25 °C): δ= 171.1 – 169.7 (-$\underline{C}OCH_3$), 99.1 and 97.5 (C-1' and C-1''), 97.2 (C-1), 75.0 (C-3), 71.0 – 65.9 (C-2, C-2', C-2'', C-3', C-3'', C-4, C-4', C-4'', C-5, C-5' and C-5''), 66.8 (C-6), 65.2 (C-7), 62.6 and 62.5 (C-6' and C-6''), 48.5 (C-9), 28.8 (C-8), 21.7 – 20.2 (-CO$\underline{C}H_3$) ppm.

MS (ESI+): theoretical mass: 1007.90 m/z, experimental mass $[M+Na]^+$: 1030.99 m/z.

*Synthesis of 3'-azidopropyl 3-O-(α-D-mannopyranosyl)-6-O-(-α-D-mannopyranosyl)-α-D-mannopyranoside (**72**)*

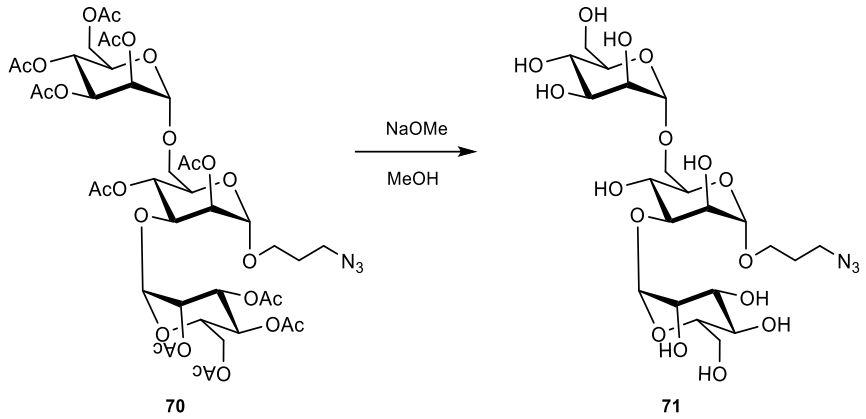

70 **71**

Compound **71** (42.9 mg, 0.04 mmol) was dissolved in MeOH (1 ml, 0.1 M) and NaOMe (5.2 mg, 0.08 mmol) was added. The reaction mixture was stirred at r.t. until TLC (DCM:MeOH - 7:3) showed the consumption of the starting material. After 3 h, the reaction mixture was quenched using Amberlite IR120 (H^+ form), filtered and concentrated in vacuo to give compound **72** (25.2 mg, quant.) as a colorless syrup.

NMR data:

^{1}H NMR (400 MHz, CD_3OD, 25 °C): δ= 5.09 (d, $J_{1\text{-}2}$= 1.4 Hz, 1H, H-1), 4.85 (d, 1H, $J_{1\text{-}2}$= 1.6 Hz, H-1), 4.73 (d, 1H, $J_{1\text{-}2}$= 1.5 Hz, H-1), 4.06 (m, 1H, H-2), 3.99 (m, 1H, H-2), 3.95 (dd, 1H, $J_{6a\text{-}6b}$= 10.8 Hz, $J_{6a\text{-}5}$= 5.3 Hz, H-6a) 3.89 (m, 1H, H-2), 3.85 – 3.59 (m, 15H, H-3, H-3', H-3'', H-4, H-4', H-4'', H-5, H-5', H-5'', H-6, H-6', H-6'', H-7a), 3.53 (1H, H-7b), 3.45 (td, 2H, $J_{9\text{-}8}$= 6.6 Hz, $J_{9\text{-}7}$= 2.1 Hz, H-9), 1.88 (m, 2H, H-8) ppm.

^{13}C NMR (100.6 MHz, CD_3OD, 25 °C): δ= 103.8, 101.6 and 101.3 (C-1, C-1' and C-1''), 80.3 (C-3), 74.8 – 67.5 (C-2, C-2', C-2'', C-3', C-3'', C-4, C-4', C-4'', C-5, C-5', C-5''), 67.1, 62.9 (C-6, C-6' and C-6''), 65.4 (C-7), 48.0 (C-9), 29.8 (C-8) ppm.

*Synthesis of 3'-aminopropyl 3-O-(α-D-mannopyranosyl)-6-O-(-α-D-mannopyranosyl)-α-D-mannopyranoside (**73**)*

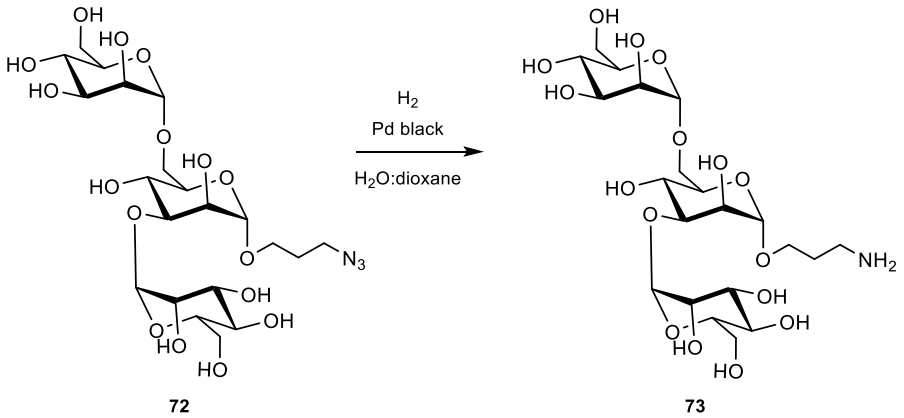

72 **73**

Compound **72** (25.2 mg, 0.04 mmol) was dissolved in H_2O:dioxane 5:1 (2 ml, 0.02 M) and a catalytic amount of Pd black was added. The reaction atmosphere was purged with H_2/vacuum cycles and then, stirred under H_2 atmosphere. After 24 h, the catalyst was filtered through a Whatman syringe filter and the excess of solvent was concentrated in vacuo to obtain compound **73** (23.0 mg, quant.) as a transparent foam.

NMR data:

^{1}H NMR (400 MHz, D_2O, 25 °C): δ= 5.12 (d, 1H, $J_{1\text{-}2}$= 1.4 Hz, H-1), 4.91 (d, 1H, $J_{1\text{-}2}$= 1.5 Hz, H-1), 4.83 (d, 1H, $J_{1\text{-}2}$= 1.5 Hz, H-1), 4.12 (m, 1H, H-2), 4.08 (m, 1H, H-2), 4.01 (m, 2H, H-2, H-6a), 3.95 – 3.56 (m, 16H, H-3, H-3', H-3'', H-4, H-4', H-4'', H-5, H-5', H-5'', H-6, H-6', H-6'', H-7), 2.97 (m, 2H, H-9), 1.91 (m, 2H, H-8) ppm.

^{13}C NMR (100.6 MHz, D_2O, 25 °C): δ= 104.5, 102.0 and 101.5 (C-1, C-1' and C-1''), 80.8 – 67.5 (C-2, C-2', C-2'', C-3, C-3', C-3'', C-4, C-4', C-4'', C-5, C-5', C-5''), 67.5, 63.2 (C-6, C-6' and C-6''), 67.5 (C-7), 39.8 (C-9), 30.6 (C-8) ppm.

MS (ESI+): theoretical mass: 561.23 m/z, experimental mass $[M+Na]^+$: 584.17 m/z.

REFERENCES

1. Feynman, R. P. There's plenty of room at the bottom. An invitation to open up a new field of physics. *Eng. Sci.* **XXIII**, 22 (1960).
2. Roco, M. C., Mirkin, C. A. & Hersam, M. C. Nanotechnology research directions for societal needs in 2020: Summary of international study. *J. Nanoparticle Res.* **13**, 897–919 (2011).
3. No Title. https://ec.europa.eu/environment/chemicals/nanotech/faq/definition_en.htm.
4. No Title. https://euon.echa.europa.eu/general-information.
5. Rizvi, S. A. A. & Saleh, A. M. Applications of nanoparticle systems in drug delivery technology. *Saudi Pharm. J.* **26**, 64–70 (2018).
6. Min, Y., Caster, J. M., Eblan, M. J. & Wang, A. Z. Clinical Translation of Nanomedicine. *Chem. Rev.* **115**, 11147–11190 (2015).
7. Teleanu, D. M., Chircov, C., Grumezescu, A. M., Volceanov, A. & Teleanu, R. I. Impact of nanoparticles on brain health: An up to date overview. *J. Clin. Med.* **7**, (2018).
8. Anselmo, A. C. & Mitragotri, S. Nanoparticles in the clinic. *Bioeng. Transl. Med.* **1**, 10–29 (2016).
9. Anselmo, A. C. & Mitragotri, S. Nanoparticles in the clinic: An update. *Bioeng. Transl. Med.* **4**, 1–16 (2019).
10. Anselmo, A. C. & Mitragotri, S. Nanoparticles in the clinic: An update post COVID-19 vaccines. *Bioeng. Transl. Med.* **6**, 1–20 (2021).
11. Gregoriadis, G. Liposomes and mRNA: Two technologies together create a COVID-19 vaccine. *Med. Drug Discov.* **12**, 100104 (2021).
12. Buglak, A. A. & Kononov, A. I. Comparative study of gold and silver interactions with amino acids and nucleobases. *RSC Adv.* **10**, 34149–34160 (2020).
13. Havaldar, D. V. *et al.* Differently synthesized gold nanoparticles respond differently to functionalization with L-amino acids. *Particuology* **52**, 97–104 (2020).
14. Reimers, J. R., Ford, M. J., Halder, A., Ulstrup, J. & Hush, N. S. Gold surfaces and nanoparticles are protected by Au(0)-thiyl species and are destroyed when Au(I)-thiolates form. *Proc. Natl. Acad. Sci. U. S. A.* **113**, E1424–E1433 (2016).
15. Kadhim, R. J., Karsh, E. H., Taqi, Z. J. & Jabir, M. S. Biocompatibility of gold nanoparticles: In-vitro and In-vivo study. *Mater. Today Proc.* **42**, 3041–3045 (2021).
16. Kang, M. S., Lee, S. Y., Kim, K. S. & Han, D. W. State of the art biocompatible gold nanoparticles for cancer theragnosis. *Pharmaceutics* **12**, 1–22 (2020).
17. Li, Z. *et al.* Small gold nanorods laden macrophages for enhanced tumor coverage in photothermal therapy. *Biomaterials* **74**, 144–154 (2016).
18. Popp, M. K. *et al.* Photothermal therapy using gold nanorods and near-infrared light in a murine melanoma model increases survival and decreases tumor volume. *J. Nanomater.* **2014**, (2014).
19. Sugiura, T. *et al.* Photothermal therapy of tumors in lymph nodes using gold nanorods and near-infrared laser light with controlled surface cooling. *Nano Res.* **8**, 3842–3852 (2015).
20. Cuiling Du, Anhe Wang, Jinbo Fei, Jie Zhao, J. L. Polypyrrole Stabilized Gold nanorods with Enhanced Photothermal Effect towards Two-Photon Photothermal Therapy. *J. Mater. Chem.B.* **3**, 4539–4545 (2015).
21. Qu, X., Yao, C., Wang, J., Li, Z. & Zhang, Z. Anti-CD30-targeted gold nanoparticles for photothermal therapy of L-428 Hodgkin's cell. *Int. J. Nanomedicine* **7**, 6095–6103 (2012).
22. Huang, X., Qian, W., El-Sayed, I. H. & El-Sayed, M. A. The potential use of the enhanced nonlinear properties of gold nanospheres in photothermal cancer therapy. *Lasers Surg. Med.* **39**, 747–753 (2007).
23. Carpin, L. B. *et al.* Immunoconjugated gold nanoshell-mediated photothermal ablation of trastuzumab-resistant breast cancer cells. *Breast Cancer Res. Treat.* **125**, 27–34 (2011).
24. Trinidad, A. J., Hong, S. J., Peng, Q., Madsen, S. J. & Hirschberg, H. Combined concurrent photodynamic and gold nanoshell loaded macrophage-mediated photothermal therapies: An in vitro study on squamous cell head and neck carcinoma. *Lasers Surg. Med.* **46**, 310–318 (2014).
25. Gao, L. *et al.* Hypocrellin-loaded gold nanocages with high two-photon efficiency for photothermal/photodynamic cancer therapy in vitro. *ACS Nano* **6**, 8030–8040 (2012).

26. Zhenxi Zhang, Sijia Wang, Hao Xu, Bo Wang, and C. Y. Role of 5-aminolevulinic acid-conjugated gold nanoparticles for photodynamic therapy of cancer. *J. Biomed. Opt.* **20**, 051043 (2015).
27. Kuo, W. S. *et al.* Gold nanomaterials conjugated with indocyanine green for dual-modality photodynamic and photothermal therapy. *Biomaterials* **33**, 3270–3278 (2012).
28. Wang, S. *et al.* Single continuous wave laser induced photodynamic/plasmonic photothermal therapy using photosensitizer-functionalized gold nanostars. *Adv. Mater.* **25**, 3055–3061 (2013).
29. Haume, K. *et al.* Gold nanoparticles for cancer radiotherapy: a review. *Cancer Nanotechnol.* **7**, (2016).
30. Zhang, X. D. *et al.* Size-dependent radiosensitization of PEG-coated gold nanoparticles for cancer radiation therapy. *Biomaterials* **33**, 6408–6419 (2012).
31. Chen, Y., Yang, J., Fu, S. & Wu, J. Gold nanoparticles as radiosensitizers in cancer radiotherapy. *Int. J. Nanomedicine* **15**, 9407–9430 (2020).
32. Tamarkin, L., Myer, L., Haynes, R. & Paciotti, G. CYT-6091 (Aurimune): a colloidal gold-based tumor-targeted nanomedicine. *Nanomedicine Nanotechnology, Biol. Med.* **2**, 273–274 (2006).
33. Giulio F. Paciotti, Jielu Zhao, Shugeng Cao, Peggy J. Brodie, L. T. & Marja Huhta, Lonnie D. Myer, Jay Friedman, and D. G. I. K. Synthesis and Evaluation of Paclitaxel-Loaded Gold Nanoparticles for Tumor-Targeted Drug Delivery. *Bioconjug. Chem.* **27**, 2647–2657 (2016).
34. Ruan, S. *et al.* Tumor microenvironment sensitive doxorubicin delivery and release to glioma using angiopep-2 decorated gold nanoparticles. *Biomaterials* **37**, 425–435 (2015).
35. Chen, Y. H. *et al.* Methotrexate conjugated to gold nanoparticles inhibits tumor growth in a syngeneic lung tumor model. *Mol. Pharm.* **4**, 713–722 (2007).
36. Fuller, M., Whiley, H. & Köper, I. Antibiotic delivery using gold nanoparticles. *SN Appl. Sci.* **2**, 1–7 (2020).
37. Saha, B. *et al.* In vitro structural and functional evaluation of gold nanoparticles conjugated antibiotics. *Nanoscale Res. Lett.* **2**, 614–622 (2007).
38. Shaker, M. A. & Shaaban, M. I. Formulation of carbapenems loaded gold nanoparticles to combat multi-antibiotic bacterial resistance: In vitro antibacterial study. *Int. J. Pharm.* **525**, 71–84 (2017).
39. Ding, Y. *et al.* Gold nanoparticles for nucleic acid delivery. *Mol. Ther.* **22**, 1075–1083 (2014).
40. Seferos, D. S., Prigodich, A. E., Giljohann, D. A., Patel, P. C. & Mirkin, C. A. Polyvalent DNA nanoparticle conjugates stabilize nucleic acids. *Nano Lett.* **9**, 308–311 (2009).
41. Giljohann, D. A., Seferos, D. S., Prigodich, A. E., Patel, P. C. & Mirkin, C. A. Gene regulation with polyvalent siRNA-nanoparticle conjugates. *J. Am. Chem. Soc.* **131**, 2072–2073 (2009).
42. Hao, L., Patel, P. C., Alhasan, A. H., Giljohann, D. A. & Mirkin, C. A. Nucleic acid-gold nanoparticle conjugates as mimics of microRNA. *Small* **7**, 3158–3162 (2011).
43. Ke Zhang, Liangliang Hao, Sarah J Hurst, C. A. M. Antibody-linked spherical nucleic acids for cellular targeting. *J. Am. Chem. Soc.* **134**, 16488–16491 (2012).
44. Zheng, D. *et al.* Topical delivery of siRNA-based spherical nucleic acid nanoparticle conjugates for gene regulation. *Proc. Natl. Acad. Sci. U. S. A.* **109**, 11975–11980 (2012).
45. Sandhu, K. K., McIntosh, C. M., Simard, J. M., Smith, S. W. & Rotello, V. M. Gold nanoparticle-mediated transfection of mammalian cells. *Bioconjug. Chem.* **13**, 3–6 (2002).
46. Ghosh, P. S., Kim, C. K., Han, G., Forbes, N. S. & Rotello, V. M. Efficient gene delivery vectors by tuning the surface charge density of amino acid-functionalized gold nanoparticles. *ACS Nano* **2**, 2213–2218 (2008).
47. Kim, S. T. *et al.* Dendronized gold nanoparticles for siRNA delivery. *Small* **8**, 3253–3256 (2012).
48. Elbakry, A. *et al.* Layer-by-layer assembled gold nanoparticles for sirna delivery. *Nano Lett.* **9**, 2059–2064 (2009).
49. Guo, S. *et al.* Enhanced gene delivery and siRNA silencing by gold nanoparticles coated with charge-reversal polyelectrolyte. *ACS Nano* **4**, 5505–5511 (2010).
50. Mateu Ferrando, R., Lay, L. & Polito, L. Gold nanoparticle-based platforms for vaccine development. *Drug Discov. Today Technol.* **38**, 57–67 (2020).

51. Dong, Y. C. *et al.* Effect of Gold Nanoparticle Size on Their Properties as Contrast Agents for Computed Tomography. *Sci. Rep.* **9**, 1–13 (2019).
52. Hainfeld, J. F., Slatkin, D. N., Focella, T. M. & Smilowitz, H. M. Gold nanoparticles: A new X-ray contrast agent. *Br. J. Radiol.* **79**, 248–253 (2006).
53. Hainfeld, J. F. *et al.* Micro-CT enables microlocalisation and quantification of Her2-targeted gold nanoparticles within tumour regions. *Br. J. Radiol.* **84**, 526–533 (2011).
54. Silvestri, A. *et al.* Design of functionalized gold nanoparticle probes for computed tomography imaging. *Contrast Media Mol. Imaging* **11**, 405–414 (2016).
55. Wang, H. *et al.* Folic acid-modified dendrimer-entrapped gold nanoparticles as nanoprobes for targeted CT imaging of human lung adencarcinoma. *Biomaterials* **34**, 470–480 (2013).
56. Zhou, C., Long, M., Qin, Y., Sun, X. & Zheng, J. Luminescent gold nanoparticles with efficient renal clearance. *Angew. Chemie - Int. Ed.* **50**, 3168–3172 (2011).
57. Luo, D. *et al.* Targeted Gold Nanocluster-Enhanced Radiotherapy of Prostate Cancer. *Small* **15**, 1–8 (2019).
58. Zhou, C. *et al.* Near-infrared emitting radioactive gold nanoparticles with molecular pharmacokinetics. *Angew. Chemie - Int. Ed.* **51**, 10118–10122 (2012).
59. Frigell, J., García, I., Gómez-Vallejo, V., Llop, J. & Penadés, S. 68Ga-labeled gold glyconanoparticles for exploring blood-brain barrier permeability: Preparation, biodistribution studies, and improved brain uptake via neuropeptide conjugation. *J. Am. Chem. Soc.* **136**, 449–457 (2014).
60. Zhu, M., Aikens, C. M., Hollander, F. J., Schatz, G. C. & Jin, R. Correlating the crystal structure of A thiol-protected Au25 cluster and optical properties. *J. Am. Chem. Soc.* **130**, 5883–5885 (2008).
61. Yang, J. *et al.* Gold/alpha-lactalbumin nanoprobes for the imaging and treatment of breast cancer. *Nat. Biomed. Eng.* **4**, 686–703 (2020).
62. Pyo, K. *et al.* Highly Luminescent Folate-Functionalized Au22 Nanoclusters for Bioimaging. *Adv. Healthc. Mater.* **6**, 1–8 (2017).
63. Szekeres, G. P. & Kneipp, J. SERS probing of proteins in gold nanoparticle agglomerates. *Front. Chem.* **7**, 1–10 (2019).
64. Wu, Y., Ali, M. R. K., Chen, K., Fang, N. & El-Sayed, M. A. Gold nanoparticles in biological optical imaging. *Nano Today* **24**, 120–140 (2019).
65. Kneipp, K. *et al.* Surface-enhanced raman spectroscopy in single living cells using gold nanoparticles. *Appl. Spectrosc.* **56**, 150–154 (2002).
66. Fasolato, C. *et al.* Folate-based single cell screening using surface enhanced Raman microimaging. *Nanoscale* **8**, 17304–17313 (2016).
67. Zavaleta, C. L. *et al.* Multiplexed imaging of surface enhanced Raman scattering nanotags in living mice using noninvasive Raman spectroscopy. *Proc. Natl. Acad. Sci. U. S. A.* **106**, 13511–13516 (2009).
68. Jimenez de Aberasturi, D. *et al.* Surface Enhanced Raman Scattering Encoded Gold Nanostars for Multiplexed Cell Discrimination. *Chem. Mater.* **28**, 6779–6790 (2016).
69. Reguera, J., Langer, J., Jiménez De Aberasturi, D. & Liz-Marzán, L. M. Anisotropic metal nanoparticles for surface enhanced Raman scattering. *Chem. Soc. Rev.* **46**, 3866–3885 (2017).
70. Li, M. *et al.* Design of SERS nanoprobes for Raman imaging: materials, critical factors and architectures. *Acta Pharm. Sin. B* **8**, 381–389 (2018).
71. Turkevich, J., Stevenson, P. C. & Hillier, J. A study of the nucleation and growth processes in the synthesis of colloidal gold. *Discuss. Faraday Soc.* **11**, 55–75 (1951).
72. Gao, Y. & Torrente-Murciano, L. Mechanistic insights of the reduction of gold salts in the Turkevich protocol. *Nanoscale* **12**, 2740–2751 (2020).
73. Ji, X., Song, X., Jun Li, Y. B., Yang, W. & Peng, X. Size Control of Gold Nanocrystals in Citrate Reduction: The Third Role of CitrateNo Title. *J. Am. Chem. Soc.* **129**, 13939–13948 (2007).
74. Kumar, S., Gandhi, K. S. & Kumar, R. Modeling of formation of gold nanoparticles by citrate method. *Ind. Eng. Chem. Res.* **46**, 3128–3136 (2007).
75. Wuithschick, M. *et al.* Turkevich in New Robes: Key Questions Answered for the Most Common Gold Nanoparticle Synthesis. *ACS Nano* **9**, 7052–7071 (2015).

76. Frens, G. Controlled nucleation for the regulation of the particle size in monodisperse gold suspensions. *Nat. Phys. Sci.* **241**, 20–22 (1973).
77. Kimling, J. *et al.* Turkevich method for gold nanoparticle synthesis revisited. *J. Phys. Chem. B* **110**, 15700–15707 (2006).
78. Tran, M., DePenning, R., Turner, M. & Padalkar, S. Effect of citrate ratio and temperature on gold nanoparticle size and morphology. *Mater. Res. Express* **3**, 1–10 (2016).
79. Yazdani, S. *et al.* Model for Gold Nanoparticle Synthesis: Effect of pH and Reaction Time. *ACS Omega* **6**, 16847–16853 (2021).
80. Ojea-Jiménez, I., Bastús, N. G. & Puntes, V. Influence of the sequence of the reagents addition in the citrate-mediated synthesis of gold nanoparticles. *J. Phys. Chem. C* **115**, 15752–15757 (2011).
81. Li, C., Li, D., Wan, G., Xu, J. & Hou, W. Facile synthesis of concentrated gold nanoparticles with low size-distribution in water: Temperature and pH controls. *Nanoscale Res. Lett.* **6**, 1–10 (2011).
82. Rahman, M. R., Saleh, F. S., Okajima, T. & Ohsaka, T. PH dependence of the size and crystallographic orientation of the gold nanoparticles prepared by seed-mediated growth. *Langmuir* **27**, 5126–5135 (2011).
83. Xia, H., Bai, S., Hartmann, J. & Wang, D. Synthesis of monodisperse quasi-spherical gold nanoparticles in water via silver(I)-assisted citrate reduction. *Langmuir* **26**, 3585–3589 (2010).
84. Liu, M. & Guyot-Sionnest, P. Mechanism of silver(I)-assisted growth of gold nanorods and bipyramids. *J. Phys. Chem. B* **109**, 22192–22200 (2005).
85. Jakhmola, A. *et al.* Experimental and theoretical study of biodirected green synthesis of gold nanoflowers. *Mater. Today Chem.* **14**, 100203 (2019).
86. Sau, T. K. & Murphy, C. J. Room Temperature, High-Yield Synthesis of Multiple Shapes of Gold Nanoparticles in Aqueous Solution. *J. Am. Chem. Soc* **126**, 8648–8649 (2004).
87. Brust, M., Walker, M., Bethell, D., Schiffrin, D. J. & Whyman, R. Synthesis of thiol-derivatised gold nanoparticles in a two-phase Liquid-Liquid system. *J. Chem. Soc., Chem. Commun.* 801–802 (1994).
88. Martin, M. N., Basham, J. I., Chando, P. & Eah, S. K. Charged gold nanoparticles in non-polar solvents: 10-min synthesis and 2D self-assembly. *Langmuir* **26**, 7410–7417 (2010).
89. Qian, H. & Jin, R. Ambient synthesis of Au144(SR)60 nanoclusters in methanol. *Chem. Mater.* **23**, 2209–2217 (2011).
90. E, X. T. F., Zhang, Y., Zou, J. J., Zhang, X. & Wang, L. Shape evolution in Brust-Schiffrin synthesis of Au nanoparticles. *Mater. Lett.* **118**, 196–199 (2014).
91. Goia, D. V. & Matijević, E. Tailoring the particle size of monodispersed colloidal gold. *Colloids Surfaces A Physicochem. Eng. Asp.* **146**, 139–152 (1999).
92. Perrault, S. D. & Chan, W. C. W. Synthesis and Surface Modification of Highly Monodispersed, Spherical Gold Nanoparticles of 50−200 nm. *J. Am. Chem. Soc* **131**, 17042–17043 (2009).
93. Tripathi, A., Kumari, S. & Kumar, A. Toxicity evaluation of pH dependent stable Achyranthes aspera herbal gold nanoparticles. *Appl. Nanosci.* **6**, 61–69 (2016).
94. Kunjiappan, S., Bhattacharjee, C. & Chowdhury, R. Hepatoprotective and antioxidant effects of Azolla microphylla based gold Accepted : acetaminophen nanoparticles against induced toxicity in a fresh water common carp fish (Cyprinus carpio L .). **2**, 88–110 (2015).
95. Gupta, R. & Padmanabhan, P. Biogenic synthesis and characterization of gold nanoparticles by a novel marine bacteria Marinobacter algicola: Progression from nanospheres to various geometrical shapes. *J. Microbiol. Biotechnol. Food Sci.* **8**, 732–737 (2018).
96. Sadhasivam, S., Shanmugam, P., Veerapandian, M., Subbiah, R. & Yun, K. Biogenic synthesis of multidimensional gold nanoparticles assisted by Streptomyces hygroscopicus and its electrochemical and antibacterial properties. *BioMetals* **25**, 351–360 (2012).
97. Ramakrishna, M., Rajesh Babu, D., Gengan, R. M., Chandra, S. & Nageswara Rao, G. Green synthesis of gold nanoparticles using marine algae and evaluation of their catalytic activity. *J. Nanostructure Chem.* **6**, 1–13 (2016).
98. Mukhoro, O. C. *et al.* Very Green Photosynthesis of Gold Nanoparticles by a Living Aquatic Plant: Photoreduction of AuIII by the Seaweed Ulva armoricana. *Chem. - A Eur. J.* **24**, 1657–1666 (2018).

99. Sreedharan, S. M., Gupta, S., Saxena, A. K. & Singh, R. Macrophomina phaseolina: microbased biorefinery for gold nanoparticle production. *Ann. Microbiol.* **69**, 435–445 (2019).
100. Bhaskaran, S., Sharma, N., Tiwari, P., Singh, S. R. & Sahi, S. V. Fabrication of innocuous gold nanoparticles using plant cells in culture. *Sci. Rep.* **9**, 1–9 (2019).
101. Khlebtsov, N. & Dykmana, L. Biodistribution and toxicity of engineered gold nanoparticles: A review of in vitro and in vivo studies. *Chem. Soc. Rev.* **40**, 1647–1671 (2011).
102. Adewale, O. B., Davids, H., Cairncross, L. & Roux, S. Toxicological Behavior of Gold Nanoparticles on Various Models: Influence of Physicochemical Properties and Other Factors. *Int. J. Toxicol.* **38**, 357–384 (2019).
103. Sani, A., Cao, C. & Cui, D. Toxicity of gold nanoparticles (AuNPs): A review. *Biochem. Biophys. Reports* **26**, 100991 (2021).
104. Connor, E. E., Mwamuka, J., Gole, A., Murphy, C. J. & Wyatt, M. D. Gold nanoparticles are taken up by human cells but do not cause acute cytotoxicity. *Small* **1**, 325–327 (2005).
105. Fan, J. ., Wung, W. ., Li, W. . & Yeh, J. M. Biocompatibility Study of Gold Nanoparticles to Human Cells. in *13th International Conference on Biomedical Engineering* 23 (2009).
106. Hwang, J. H. *et al.* Susceptibility to gold nanoparticle-induced hepatotoxicity is enhanced in a mouse model of nonalcoholic steatohepatitis. *Toxicology* **294**, 27–35 (2012).
107. Kim, K. T., Zaikova, T., Hutchison, J. E. & Tanguay, R. L. Gold nanoparticles disrupt zebrafish eye development and pigmentation. *Toxicol. Sci.* **133**, 275–288 (2013).
108. Pan, Y. *et al.* Gold nanoparticles of diameter 1.4 nm trigger necrosis by oxidative stress and mitochondrial damage. *Small* **5**, 2067–2076 (2009).
109. Jia, Y. P., Ma, B. Y., Wei, X. W. & Qian, Z. Y. The in vitro and in vivo toxicity of gold nanoparticles. *Chinese Chem. Lett.* **28**, 691–702 (2017).
110. Bhamidipati, B. & Fabris, L. Multiparametric Assessment of Gold Nanoparticle Cytotoxicity in Cancerous and Healthy Cells: The Role of Size, Shape, and Surface Chemistry. *Bioconjug. Chem.* **28**, 449–460 (2017).
111. Wang, Y. *et al.* A Comparison Study of Gold Nanohexapods, Nanorods, and Nanocages for Photothermal Cancer Treatment. *ACS Nano* **7**, 2068–2077 (2013).
112. Goodman, C. M., McCusker, C. D., Yilmaz, T. & Rotello, V. M. Toxicity of gold nanoparticles functionalized with cationic and anionic side chains. *Bioconjug. Chem.* **15**, 897–900 (2004).
113. Carnovale, C., Bryant, G., Shukla, R. & Bansal, V. Identifying Trends in Gold Nanoparticle Toxicity and Uptake: Size, Shape, Capping Ligand, and Biological Corona. *ACS Omega* **4**, 242–256 (2019).
114. Sadauskas, E. *et al.* Protracted elimination of gold nanoparticles from mouse liver. *Nanomedicine Nanotechnology, Biol. Med.* **5**, 162–169 (2009).
115. Di, J. *et al.* Size, shape, charge and "stealthy" surface: Carrier properties affect the drug circulation time in vivo. *Asian J. Pharm. Sci.* **16**, 444–458 (2021).
116. Longmire, M., Choyke, P. L. & Kobayashi, H. Clearance Properties of Nano-sized Particles and Molecules as Imaging Agents: Considerations and Caveats. *Nanomedicine* **3**, 703–717 (2008).
117. De Jong, W. H. *et al.* Particle size-dependent organ distribution of gold nanoparticles after intravenous administration. *Biomaterials* **29**, 1912–1919 (2008).
118. Sonavane, G., Tomoda, K. & Makino, K. Biodistribution of colloidal gold nanoparticles after intravenous administration: Effect of particle size. *Colloids Surfaces B Biointerfaces* **66**, 274–280 (2008).
119. Ohta, S. *et al.* Investigating the optimum size of nanoparticles for their delivery into the brain assisted by focused ultrasound-induced blood–brain barrier opening. *Sci. Rep.* **10**, 1–13 (2020).
120. Arnida, Janát-Amsbury, M. M., Ray, A., Peterson, C. M. & Ghandehari, H. Geometry and surface characteristics of gold nanoparticles influence their biodistribution and uptake by macrophages. *Eur. J. Pharm. Biopharm.* **77**, 417–423 (2011).
121. Zhang, J. *et al.* Quantitative biokinetics and systemic translocation of various gold nanostructures are highly dependent on their size and shape. *J. Nanosci. Nanotechnol.* **14**, 4124–4138 (2014).
122. Surface Charge Controls the Suborgan Biodistributions of Gold Nanoparticles. *Elci, Sukru G Jiang, Ying Yan, Bo Kim, Sung T Saha, Krishnendu Moyano, Daniel F Tonga, Gulen Y Jackson, Liam C Rotello, Vincent M Vachet, Richard W* **10**, (2016).

123. Clemente, E. *et al.* Probing the glycans accessibility in the nanoparticle biomolecular corona. *J. Colloid Interface Sci.* **613**, 563–574 (2022).
124. Monopoli, M. P., Åberg, C., Salvati, A. & Dawson, K. A. Biomolecular coronas provide the biological identity of nanosized materials. *Nat. Nanotechnol.* **7**, 779–786 (2012).
125. Piella, J., Bastús, N. G. & Puntes, V. Size-Dependent Protein–Nanoparticle Interactions in Citrate-Stabilized Gold Nanoparticles: The Emergence of the Protein Corona. *Bioconjug. Chem.* **28**, 88–97 (2017).
126. Walkey, C. D. *et al.* Protein Corona Fingerprinting Predicts the Cellular Interaction of Gold and Silver Nanoparticles. *ACS Nano* **8**, 2439–2455 (2014).
127. Casals, E., Pfaller, T., Duschl, A., Oostingh, G. J. & Puntes, V. Time evolution of the nanoparticle protein corona. *ACS Nano* **4**, 3623–3632 (2010).
128. Gagner, J. E., Lopez, M. D., Dordick, J. S. & Siegel, R. W. Effect of gold nanoparticle morphology on adsorbed protein structure and function. *Biomaterials* **32**, 7241–7252 (2011).
129. Cai, H. *et al.* Protein corona influences liver accumulation and hepatotoxicity of gold nanorods. *NanoImpact* **3**–**4**, 40–46 (2016).
130. Kah, J. C. Y. *et al.* Protein coronas on gold nanorods passivated with amphiphilic ligands affect cytotoxicity and cellular response to penicillin/streptomycin. *ACS Nano* **8**, 4608–4620 (2014).
131. D'Hollander, A. *et al.* Limiting the protein corona: A successful strategy for in vivo active targeting of anti-HER2 nanobody-functionalized nanostars. *Biomaterials* **123**, 15–23 (2017).
132. Chen, D., Ganesh, S., Wang, W. & Amiji, M. Plasma protein adsorption and biological identity of systemically administered nanoparticles. *Nanomedicine* **12**, 2113–2135 (2017).
133. Garcia-Alvarez, R., Hadjidemetriou, M., Sanchez-Iglesias, A., Liz-Marzán, L. M. & Kostarelos, K. In vivo formation of protein corona on gold nanoparticles. The effect of their size and shape. *Nanoscale* **10**, 1256–1264 (2017).
134. Nicoara, R., Ilies, M., Uifalean, A., Iuga, C. A. & Loghin, F. Quantification of the PEGylated gold nanoparticles protein corona. Influence on nanoparticle size and surface chemistry. *Appl. Sci.* **9**, (2019).
135. Caracciolo, G., Farokhzad, O. C. & Mahmoudi, M. Biological Identity of Nanoparticles In Vivo: Clinical Implications of the Protein Corona. *Trends Biotechnol.* **35**, 257–264 (2016).
136. Xiao, W. & Gao, H. The impact of protein corona on the behavior and targeting capability of nanoparticle-based delivery system. *Int. J. Pharm.* **552**, 328–339 (2018).
137. Sasidharan, A., Riviere, J. E. & Monteiro-Riviere, N. A. Gold and silver nanoparticle interactions with human proteins: impact and implications in biocorona formation. *J. Mater. Chem. B* **3**, 2075–2082 (2015).
138. Papini, E., Tavano, R. & Mancin, F. Opsonins and Dysopsonins of Nanoparticles: Facts, Concepts, and Methodological Guidelines. *Front. Immunol.* **11**, 1–19 (2020).
139. Dominguez-Medina, S. *et al.* Adsorption and Unfolding of a Single Protein Triggers Nanoparticle Aggregation. *ACS Nano* **10**, 2103–2112 (2016).
140. Bolaños, K., Kogan, M. J. & Araya, E. Capping gold nanoparticles with albumin to improve their biomedical properties. *Int. J. Nanomedicine* **14**, 6387–6406 (2019).
141. Tavanti, F. & Menziani, M. C. Computational insight on the interaction of common blood proteins with gold nanoparticles. *Int. J. Mol. Sci.* **22**, (2021).
142. Lee, H. Molecular modeling of protein corona formation and its interactions with nanoparticles and cell membranes for nanomedicine applications. *Pharmaceutics* **13**, (2021).
143. Chapman, R. G. *et al.* Surveying for surfaces that resist the adsorption of proteins. *J. Am. Chem. Soc.* **122**, 8303–8304 (2000).
144. Stiufiuc, R. *et al.* One-step synthesis of PEGylated gold nanoparticles with tunable surface charge. *J. Nanomater.* **2013**, (2013).
145. Quach, Q. H., Kong, R. L. X. & Kah, J. C. Y. Complement Activation by PEGylated Gold Nanoparticles. *Bioconjug. Chem.* **29**, 976–981 (2018).
146. Zhang, Y., Liu, A. T., Cornejo, Y. R., van Haute, D. & Berlin, J. M. A Systematic comparison of in vitro cell uptake and in vivo biodistribution for three classes of gold nanoparticles with saturated PEG coatings. *PLoS One* **15**, 1–16 (2020).
147. Polo, E. *et al.* Photothermal effects on protein adsorption dynamics of PEGylated gold nanorods. *Appl. Mater. Today* **15**, 599–604 (2019).

148. Walkey, C. D., Olsen, J. B., Guo, H., Emili, A. & Chan, W. C. W. Nanoparticle size and surface chemistry determine serum protein adsorption and macrophage uptake. *J. Am. Chem. Soc.* **134**, 2139–2147 (2012).
149. Uz, M., Bulmus, V. & Altinkaya, S. A. Effect of PEG Grafting Density and Hydrodynamic Volume on Gold Nanoparticle−Cell Interactions: An Investigation on Cell Cycle, Apoptosis, and DNA Damage. *Langmuir* **32**, 5997–6009 (2016).
150. Cruje, C. & Chithrani, D. B. Polyethylene Glycol Functionalized Nanoparticles for Improved Cancer Treatment. *Rev. Nanosci. Nanotechnol.* **3**, 20–30 (2014).
151. Sanchez-Cano, C. & Carril, M. Recent developments in the design of non-biofouling coatings for nanoparticles and surfaces. *Int. J. Mol. Sci.* **21**, 1–24 (2020).
152. Dai, Q., Walkey, C. & Chan, W. C. W. Polyethylene glycol backfilling mitigates the negative impact of the protein corona on nanoparticle cell targeting. *Angew. Chemie - Int. Ed.* **53**, 5093–5096 (2014).
153. Thanh, T., Thi, H., Pilkington, E. H., Nguyen, D. H. & Lee, J. S. The Importance of Poly (ethylene glycol) Alternatives for Overcoming PEG Immunogenicity in Drug. *Polymers (Basel).* **12**, 298 (2020).
154. Quach, Q. H. & Kah, J. C. Y. Non-specific adsorption of complement proteins affects complement activation pathways of gold nanomaterials. *Nanotoxicology* **11**, 382–394 (2017).
155. Mohamed, T., Matou-Nasri, S., Farooq, A., Whitehead, D. & Azzawi, M. Polyvinylpyrrolidone-coated gold nanoparticles inhibit endothelial cell viability, proliferation, and ERK1/2 phosphorylation and reduce the magnitude of endothelial-independent dilator responses in isolated aortic vessels. *Int. J. Nanomedicine* **12**, 8813–8830 (2017).
156. Georgiou, P. G. *et al.* 'tuning aggregative: Versus non-Aggregative lectin binding with glycosylated nanoparticles by the nature of the polymer ligand'. *J. Mater. Chem. B* **8**, 136–145 (2019).
157. Durand-Gasselin, C., Koerin, R., Rieger, J., Lequeux, N. & Sanson, N. Colloidal stability of zwitterionic polymer-grafted gold nanoparticles in water. *J. Colloid Interface Sci.* **434**, 188–194 (2014).
158. Pooja, D. *et al.* Natural polysaccharide functionalized gold nanoparticles as biocompatible drug delivery carrier. *Int. J. Biol. Macromol.* **80**, 48–56 (2015).
159. Jia, Y. *et al.* One step preparation of peptide-coated gold nanoparticles with tunable size. *Materials (Basel).* **12**, 1–12 (2019).
160. Varki, A. & Gagneux, P. *Essentials of Glycobiology. 3rd edition.* (2017).
161. Gabius, H. J., André, S., Jiménez-Barbero, J., Romero, A. & Solís, D. From lectin structure to functional glycomics: Principles of the sugar code. *Trends Biochem. Sci.* **36**, 298–313 (2011).
162. Reily, C., Stewart, T. J., Renfrow, M. B. & Novak, J. Glycosylation in health and disease. *Nat. Rev. Nephrol.* **15**, 346–366 (2019).
163. Hernando, P. J., Dedola, S., Marín, M. J. & Field, R. A. Recent Developments in the Use of Glyconanoparticles and Related Quantum Dots for the Detection of Lectins, Viruses, Bacteria and Cancer Cells. *Front. Chem.* **9**, 1–8 (2021).
164. García, I. *et al.* Glycans as Biofunctional Ligands for Gold Nanorods: Stability and Targeting in Protein-Rich Media. *J. Am. Chem. Soc.* **137**, 3686–3692 (2015).
165. De la Fuente, J. M. *et al.* Gold Glyconanoparticles as Water-Soluble Polyvalent Models to Study Carbohydrate Interactions. The first report of gold glyco NPs. *Angew. Chem. Int. Ed. Engl.* **40**, 2257–2261 (2001).
166. Adokoh, C. K., Obuah, C., Kinfe, H. H., Zinyemba, O. & Darkwa, J. Novel bio-friendly and non-toxic thiocarbohydrate stabilizers of gold nanoparticles. *New J. Chem.* **39**, 5249–5258 (2015).
167. Varela-Aramburu, S., Wirth, R., Lai, C. H., Orts-Gil, G. & Seeberger, P. H. Straightforward and robust synthesis of monodisperse surface-functionalized gold nanoclusters. *Beilstein J. Nanotechnol.* **7**, 1278–1283 (2016).
168. Sangabathuni, S. *et al.* Mapping the Glyco-Gold Nanoparticles of Different Shapes Toxicity, Biodistribution and Sequestration in Adult Zebrafish. *Sci. Rep.* **7**, 1–7 (2017).

169. Fyrner, T., Ederth, T., Aili, D., Liedberg, B. & Konradsson, P. Synthesis of oligo(lactose)-based thiols and their self-assembly onto gold surfaces. *Colloids Surfaces B Biointerfaces* **105**, 187–193 (2013).
170. Combemale, S., Assam-Evoung, J. N., Houaidji, S., Bibi, R. & Barragan-Montero, V. Gold nanoparticles decorated with mannose-6-phosphate analogues. *Molecules* **19**, 1120–1149 (2014).
171. Shiue, A. *et al.* Synthesis and cytotoxic analysis of thiolated xylose derivatives decorated on gold nanoparticles. *Biotechnol. Reports* **28**, e00549 (2020).
172. Chaudhary, P. M. *et al.* Assessing the effect of different shapes of glyco-gold nanoparticles on bacterial adhesion and infections. *Chem. Commun.* **51**, 15669–15672 (2015).
173. Compostella, F., Pitirollo, O., Silvestri, A. & Polito, L. Glyco-gold nanoparticles: Synthesis and applications. *Beilstein J. Org. Chem.* **13**, 1008–1021 (2017).
174. Hu, X. Le *et al.* Colorimetric and Plasmonic Detection of Lectins Using Core–Shell Gold Glyconanoparticles Prepared by Copper-Free Click Chemistry. *ACS Appl. matter interfaces* **7**, 1874–1878 (2015).
175. Telli, F. C. *et al.* Novel glyconanoconjugates: synthesis, characterization and bioapplications. *RSC Adv.* **6**, 105806–105813 (2016).
176. Chen, N. *et al.* N-Oxyamide-linked glycoglycerolipid coated AuNPs for receptor-targeting imaging and drug delivery. *Chem. commun.* **52**, 2284–2287 (2016).
177. Marradi, M., Chiodo, F., García, I. & Penadés, S. Glyconanoparticles as multifunctional and multimodal carbohydrate systems. *Chem. Soc. Rev.* **42**, 4728–4745 (2013).
178. Roskamp, M. *et al.* Multivalent interaction and selectivities in selectin binding of functionalized gold colloids decorated with carbohydrate mimetics. *Org. Biomol. Chem.* **9**, 7448–7456 (2011).
179. Fallarini, S. *et al.* Factors affecting T cell responses induced by fully synthetic glyco-gold-nanoparticles. *Nanoscale* **5**, 390–400 (2013).
180. Reynolds, M., Marradi, M., Imberty, A., Penadés, S. & Pérez, S. Influence of ligand presentation density on the molecular recognition of mannose-functionalised glyconanoparticles by bacterial lectin BC2L-A. *Glycoconj. J.* **30**, 747–757 (2013).
181. Toraskar, S., Gade, M., Sangabathuni, S., Thulasiram, H. V. & Kikkeri, R. Exploring the Influence of Shapes and Heterogeneity of Glyco-Gold Nanoparticles on Bacterial Binding for Preventing Infections. *ChemMedChem* **12**, 1116–1124 (2017).
182. Sangabathuni, S. *et al.* Glyco-gold nanoparticle shapes enhance carbohydrate–protein interactions in mammalian cells. *Nanoscale* **8**, 12729–12735 (2016).
183. Chien, Y. Y. *et al.* Globotriose-functionalized gold nanoparticles as multivalent probes for Shiga-like toxin. *ChemBioChem* **9**, 1100–1109 (2008).
184. Grant, O. C., Smith, H. M. K., Firsova, D., Fadda, E. & Woods, R. J. Presentation, presentation, presentation! Molecular-level insight into linker effects on glycan array screening data. *Glycobiology* **24**, 17–25 (2014).
185. Di Silvio, D., Silvestri, A., Lay, L., Polito, L. & Moya, S. E. Impact of ConcanavalinA affinity in the intracellular fate of Protein Corona on Glucosamine Au nanoparticles. *Sci. Rep.* **8**, 1–11 (2018).
186. Zheng, L. *et al.* Detection and differentiation of influenza viruses with glycan-functionalized gold nanoparticles. *Biosens. Bioelectron.* **91**, 46–52 (2017).
187. Baker, A. N. *et al.* The SARS-COV-2 Spike Protein Binds Sialic Acids and Enables Rapid Detection in a Lateral Flow Point of Care Diagnostic Device. *ACS Cent. Sci.* **6**, 2046–2052 (2020).
188. Chiodo, F. *et al.* High Sensitive Detection of Carbohydrate Binding Proteins in an ELISA-Solid Phase Assay Based on Multivalent Glyconanoparticles. *PLoS One* **8**, 1–11 (2013).
189. Arosio, D. *et al.* Effective Targeting of DC-SIGN by α-Fucosylamide Functionalized Gold Nanoparticles. *Bioconjug. Chem.* **25**, 2244–2251 (2014).
190. Budhadev, D. *et al.* Glycan-Gold Nanoparticles as Multifunctional Probes for Multivalent Lectin-Carbohydrate Binding: Implications for Blocking Virus Infection and Nanoparticle Assembly. *J. Am. Chem. Soc.* **142**, 18022–18034 (2020).

191. Ajish, J. K. *et al.* Self-Assembled Glycobis(acrylamide)-Stabilized Gold Nanoparticles for Fluorescent Turn-on Sensing of Lectin and Escherichia coli. *ACS Appl nano matter* **3**, 1307–1317 (2020).
192. Zhang, C. *et al.* A glycoconjugate-based gold nanoparticle approach for the targeted treatment of: Pseudomonas aeruginosa biofilms. *Nanoscale* **12**, 23234–23240 (2020).
193. Cagnoni, A. J., Pérez Sáez, J. M., Rabinovich, G. A. & Mariño, K. V. Turning-off signaling by siglecs, selectins, and galectins: Chemical inhibition of glycan-dependent interactions in cancer. *Front. Oncol.* **6**, 1–21 (2016).
194. Schofield, C. L. *et al.* Detection of mSiglec-E, in solution and expressed on the surface of Chinese hamster ovary cells, using sialic acid functionalised gold nanoparticles. *Analyst* **141**, 5799–5809 (2016).
195. García Calavia, P. *et al.* Targeted photodynamic therapy of breast cancer cells using lactose-phthalocyanine functionalized gold nanoparticles. *J. Colloid Interface Sci.* **512**, 249–259 (2018).
196. Adokoh, C. K., Keter, F. K., Kinfe, H. H., Tshikhudo, R. & Darkwa, J. Development and characterization of functionalized glyco thiolate capped gold nanoparticles for biological applications. *RSC Med. Chem.* **11**, 283–292 (2020).
197. Torres-Pérez, S. A., Torres-Pérez, C. E., Pedraza-Escalona, M., Pérez-Tapia, S. M. & Ramón-Gallegos, E. Glycosylated Nanoparticles for Cancer-Targeted Drug Delivery. *Front. Oncol.* **10**, 1–10 (2020).
198. Hockl, P. F. *et al.* Glyco-nano-oncology: Novel therapeutic opportunities by combining small and sweet. *Pharmacol. Res.* **109**, 45–54 (2016).
199. Aykaç, A. *et al.* B-Cyclodextrin-Bearing Gold Glyconanoparticles for the Development of Site Specific Drug Delivery Systems. *Langmuir* **30**, 234–242 (2014).
200. Yilmaz, G. *et al.* pH responsive glycopolymer nanoparticles for targeted delivery of anti-cancer drugs. *Mol. Syst. Des. Eng.* **3**, 150–158 (2018).
201. Adokoh, C. K. *et al.* Synthesis and evaluation of glycopolymeric decorated gold nanoparticles functionalized with gold-triphenyl phosphine as anti-cancer agents. *Biomacromolecules* **15**, 3802–3810 (2014).
202. Hu, C., Niestroj, M., Yuan, D., Chang, S. & Chen, J. Treating cancer stem cells and cancer metastasis using glucose-coated gold nanoparticles. *Int. J. Nanomedicine* **10**, 2065–2077 (2015).
203. Song, K. *et al.* Smart gold nanoparticles enhance killing effect on cancer cells. *Int. J. Oncol.* **42**, 597–608 (2013).
204. Adokoh, C. K. *et al.* Glyco disulfide capped gold nanoparticle synthesis: cytotoxicity studies and effects on lung cancer A549 cells. *Future Med. Chem.* **14**, 307–324 (2022).
205. Chiodo, F., Marradi, M., Calvo, J., Yuste, E. & Penadés, S. Glycosystems in nanotechnology: Gold glyconanoparticles as carrier for anti-HIV prodrugs. *Beilstein J. Org. Chem.* **10**, 1339–1346 (2014).
206. Mu, H., Liu, Q., Niu, H., Sun, Y. & Duan, J. Gold nanoparticles make chitosan–streptomycin conjugates effective towards Gram-negative bacterial biofilm. *RCS Adv.* **6**, 8714–8721 (2016).
207. Yuan, Y. *et al.* Recyclable Escherichia coli-Specific-Killing AuNP–Polymer (ESKAP) Nanocomposites. *ACS Appl. matter interfaces* **8**, 11309–11317 (2016).
208. Dykman, L. A. & Khlebtsov, N. G. Immunological properties of gold nanoparticles. *Chem. Sci.* **8**, 1719–1735 (2017).
209. Dykman, L. A. Gold nanoparticles for preparation of antibodies and vaccines against infectious diseases. *Expert Rev. Vaccines* **19**, 465–477 (2020).
210. Safari, D. *et al.* Gold nanoparticles as carriers for a synthetic Streptococcus pneumoniae type 14 conjugate vaccine. *Nanomedicine* **7**, 651–662 (2012).
211. Vetro, M. *et al.* Preparation and immunogenicity of gold glyco-nanoparticles as antipneumococcal vaccine model. *Nanomedicine* **12**, 13–23 (2017).
212. Muruato, L. A. *et al.* Use of reverse vaccinology in the design and construction of nanoglycoconjugate vaccines against burkholderia pseudomallei. *Clin. Vaccine Immunol.* **24**, 1–13 (2017).
213. Calderón-Gonzalez, R. *et al.* Pregnancy vaccination with gold glyco-nanoparticles carrying Listeria monocytogenes peptides protects against listeriosis and brain- and cutaneous-associated morbidities. *Nanomaterials* **6**, 1–11 (2016).

214. Martínez-Ávila, O. *et al.* Gold manno-glyconanoparticles: Multivalent systems to block HIV-1 gp120 binding to the lectin DC-SIGN. *Chem. - A Eur. J.* **15**, 9874–9888 (2009).
215. Chiodo, F., Enríquez-Navas, P. M., Angulo, J., Marradi, M. & Penadés, S. Assembling different antennas of the gp120 high mannose-type glycans on gold nanoparticles provides superior binding to the anti-HIV antibody 2G12 than the individual antennas. *Carbohydr. Res.* **405**, 102–109 (2015).
216. Climent, N. *et al.* Loading dendritic cells with gold nanoparticles (GNPs) bearing HIV-peptides and mannosides enhance HIV-specific T cell responses. *Nanomedicine Nanotechnology, Biol. Med.* **14**, 339–351 (2018).
217. Gianvincenzo, P. Di *et al.* Negatively charged glyconanoparticles modulate and stabilize the secondary structures of a gp120 V3 loop peptide: Toward fully synthetic HIV vaccine candidates. *Bioconjug. Chem.* **26**, 755–765 (2015).
218. Brinãs, R. P. *et al.* Design and synthesis of multifunctional gold nanoparticles bearing tumor-associated glycopeptide antigens as potential cancer vaccines. *Bioconjug. Chem.* **23**, 1513–1523 (2012).
219. Parry, A. L. *et al.* 'Multicopy multivalent' glycopolymer-stabilized gold nanoparticles as potential synthetic cancer vaccines. *J. Am. Chem. Soc.* **135**, 9362–9365 (2013).
220. Tavernaro, I. *et al.* Synthesis of tumor-associated MUC1-glycopeptides and their multivalent presentation by functionalized gold colloids. *Org. Biomol. Chem.* **13**, 81–97 (2015).
221. Mocan, T. *et al.* In vitro administration of gold nanoparticles functionalized with MUC-1 protein fragment generates anticancer vaccine response via macrophage activation and polarization mechanism. *J. Cancer* **6**, 583–592 (2015).
222. Terán-navarro, H., Calderon-gonzalez, R., Salcines-cuevas, D. & García, I. Pre-clinical development of Listeria -based nanovaccines as immunotherapies for solid tumours : insights from melanoma. *Oncoimmunology* **8**, 1–12 (2019).
223. Feng, G., Kong, B., Xing, J. & Chen, J. Enhancing multimodality functional and molecular imaging using glucose-coated gold nanoparticles. *Clin. Radiol.* **69**, 1105–1111 (2014).
224. Jølck, R. I. *et al.* Injectable colloidal gold for use in intrafractional 2D image-guided radiation therapy. *Adv. Healthc. Mater.* **4**, 856–863 (2015).
225. Marradi, M. *et al.* Paramagnetic Gd-based gold glyconanoparticles as probes for MRI: Tuning relaxivities with sugars. *Chem. Commun.* 3922–3924 (2009) doi:10.1039/b900957d.
226. Candiota, A. P. *et al.* A new ex vivo method to evaluate the performance of candidate MRI contrast agents: A proof-of-concept study. *J. Nanobiotechnology* **12**, 1–14 (2014).
227. Silvestri, A. *et al.* Influence of surface coating on the intracellular behaviour of gold nanoparticles: A fluorescence correlation spectroscopy study. *Nanoscale* **9**, 14730–14739 (2017).
228. Martinez-Moro, M., Di Silvio, D. & Moya, S. E. Fluorescence correlation spectroscopy as a tool for the study of the intracellular dynamics and biological fate of protein corona. *Biophys. Chem.* **253**, 106218 (2019).
229. Dominguez-Medina, S. *et al.* Measuring the Hydrodynamic Size of Nanoparticles Using Fluctuation Correlation Spectroscopy. *Annu. Rev. Phys. Chem.* **67**, 489–514 (2016).
230. Bojar, D. *et al.* A Useful Guide to Lectin Binding: Machine-Learning Directed Annotation of 57 Unique Lectin Specificities. *ACS Chem. Biol.* (2021) doi:10.1021/acschembio.1c00689.
231. Loke, I., Kolarich, D., Packer, N. H. & Thaysen-Andersen, M. Emerging roles of protein mannosylation in inflammation and infection. *Mol. Aspects Med.* **51**, 31–55 (2016).
232. Avvakumova, S. *et al.* Gold nanoparticles decorated by clustered multivalent cone-glycocalixarenes actively improve the targeting efficiency toward cancer cells. *Chem. Commun.* **50**, 11029–11032 (2014).
233. Borah, R., Deka, N. & Sarma, J. C. Iodine as an Acetyl Transfer Catalyst. *J. Chem. Res. - Part S* 110–111 (1997) doi:10.1039/a605061a.
234. Galili, U. Anti-Gal: An abundant human natural antibody of multiple pathogeneses and clinical benefits. *Immunology* **140**, 1–11 (2013).
235. Zhu, C. dong *et al.* Synthesis of novel galactose functionalized gold nanoparticles and its radiosensitizing mechanism. *J. Nanobiotechnology* **13**, 1–11 (2015).

236. Grellet, S. *et al.* Cancer-selective, single agent chemoradiosensitising gold nanoparticles. *PLoS One* **12**, 1–21 (2017).
237. Lemieux, R. U., Hendriks, K. B., Stick, R. V. & James, K. Halide Ion Catalyzed Glycosidation Reactions. Syntheses of α-Linked Disaccharides. *J. Am. Chem. Soc.* **97**, 4056–4062 (1975).
238. Becker, D. J. & Lowe, J. B. Fucose: Biosynthesis and biological function in mammals. *Glycobiology* **13**, (2003).
239. Daly, R., McCabe, T. & Scanlan, E. M. Development of fully and partially protected fucosyl donors for oligosaccharide synthesis. *J. Org. Chem.* **78**, 1080–1090 (2013).
240. Tolón Murguía, B. I. *et al.* An efficient synthetic route to O-(2-O-benzyl-3,4-di-O-acetyl-α/β-L-fucopyranosyl)-trichloroacetimidate. *Carbohydr. Res.* **499**, 4–9 (2021).
241. Schmidt, R. R. & Toepfer, A. Glycosylation with highly reactive glycosyl donors: efficiency of the inverse procedure. *Tetrahedron Lett.* **32**, 3353–3356 (1991).
242. Pedersen, C. M., Nordstrøm, L. U. & Bols, M. 'Super armed' glycosyl donors: Conformational arming of thioglycosides by silylation. *J. Am. Chem. Soc.* **129**, 9222–9235 (2007).
243. Uchiyama, T. & Hindsgaul, O. Per-O-Trimethylsilyl-α-L-Fucopyranosyl Iodide: A Novel Glycosylating Agent for Terminal α-L-Fucosylation. *Synlett* **6**, 499–501 (1996).
244. Maus, L., Dick, O., Bading, H., Spatz, J. P. & Fiammengo, R. Conjugation of peptides to the passivation shell of gold nanoparticles for targeting of cell-surface receptors. *ACS Nano* **4**, 6617–6628 (2010).
245. Pitirollo, O. *et al.* Gold nanoparticles morphology does not affect the multivalent presentation and antibody recognition of Group A Streptococcus synthetic oligorhamnans. *Bioorg. Chem.* **99**, 103815 (2020).
246. Arvizo, R. R. *et al.* Modulating pharmacokinetics, tumor uptake and biodistribution by engineered nanoparticles. *PLoS One* **6**, 3–8 (2011).
247. Oh, N. & Park, J. H. Surface chemistry of gold nanoparticles mediates their exocytosis in macrophages. *ACS Nano* **8**, 6232–6241 (2014).
248. Sun, H., Jiang, C., Wu, L., Bai, X. & Zhai, S. Cytotoxicity-Related Bioeffects Induced by Nanoparticles: The Role of Surface Chemistry. *Frontiers in Bioengineering and Biotechnology* vol. 7 (2019).
249. Coutinho, M. F., Prata, M. J. & Alves, S. Mannose-6-phosphate pathway: A review on its role in lysosomal function and dysfunction. *Mol. Genet. Metab.* **105**, 542–550 (2012).
250. Gary-Bobo, M., Nirde, P., Jeanjean, A., Morere, A. & Garcia, M. Mannose 6-Phosphate Receptor Targeting and its Applications in Human Diseases. *Curr. Med. Chem.* **14**, 2945–2953 (2007).
251. Dalle Vedove, E., Costabile, G. & Merkel, O. M. Mannose and Mannose-6-Phosphate Receptor–Targeted Drug Delivery Systems and Their Application in Cancer Therapy. *Adv. Healthc. Mater.* **7**, 1–37 (2018).
252. Vaillant, O. *et al.* Mannose-6-phosphate receptor: A target for theranostics of prostate cancer. *Angew. Chemie - Int. Ed.* **54**, 5952–5956 (2015).
253. Watanabe, Y., Komoda, Y., Ebisuya, K. & Ozaki, S. An efficient phosphorylation method using a new phosphitylating agent, 2-diethylamino-1,3,2-benzodioxaphosphepane. *Tetrahedron Lett.* **31**, 255–256 (1990).
254. Ramella, D. *et al.* A strategy for multivalent presentation of carba analogues from N. meningitidis a capsular polysaccharide. *European J. Org. Chem.* **2014**, 5915–5924 (2014).
255. Kiankarimi, M., Lowe, R., McCarthy, J. R. & Whitten, J. P. Diphenyl 2-pyridylphosphine and di-tert-butyl azodicarboxylate:convenient reagents for the Mitsunobu reaction. *Tetrahedron Lett.* **40**, 4497–4500 (1999).
256. Abdelkhaliq, A. *et al.* Impact of nanoparticle surface functionalization on the protein corona and cellular adhesion, uptake and transport 03 Chemical Sciences 0306 Physical Chemistry (incl. Structural). *J. Nanobiotechnology* **16**, 1–13 (2018).
257. Kwon, P. S. *et al.* Sulfated polysaccharides effectively inhibit SARS-CoV-2 in vitro. *Cell Discov.* **6**, 4–7 (2020).
258. Mycroft-West, C. J. *et al.* Heparin Inhibits Cellular Invasion by SARS-CoV-2: Structural Dependence of the Interaction of the Spike S1 Receptor-Binding Domain with Heparin. *Thromb. Haemost.* **120**, 1700–1715 (2020).

259. Goyal, V. *et al.* Commercial Pd/C-Catalyzed N-Methylation of Nitroarenes and Amines Using Methanol as Both C1 and H2 Source. *J. Org. Chem.* **84**, 15389–15398 (2019).
260. van de Wall, S., Santegoets, K. C. M., van Houtum, E. J. H., Büll, C. & Adema, G. J. Sialoglycans and Siglecs Can Shape the Tumor Immune Microenvironment. *Trends Immunol.* **41**, 274–285 (2020).
261. Jayant, S. *et al.* Targeted sialic acid-doxorubicin prodrugs for intracellular delivery and cancer treatment. *Pharm. Res.* **24**, 2120–2130 (2007).
262. Xu, X. L. *et al.* Sialic Acid-Functionalized pH-Triggered Micelles for Enhanced Tumor Tissue Accumulation and Active Cellular Internalization of Orthotopic Hepatocarcinoma. *ACS Appl. matter interfaces* **10**, 31903–31914 (2018).
263. Kim, Y. H. *et al.* Development of sialic acid-coated nanoparticles for targeting cancer and efficient evasion of the immune system. *Theranostics* **7**, 962–973 (2017).
264. Bondioli, L. *et al.* Sialic acid as a potential approach for the protection and targeting of nanocarriers. *Expert Opin. Drug Deliv.* **8**, 921–937 (2011).
265. Bondioli, L. *et al.* PLGA nanoparticles surface decorated with the sialic acid, N-acetylneuraminic acid. *Biomaterials* **31**, 3395–3403 (2010).
266. Spence, S. *et al.* Targeting Siglecs with a sialic acid-decorated nanoparticle abrogates inflammation. *Sci. Transl. Med.* **7**, 1–13 (2015).
267. Watkins, W. M. & Morgan, W. T. Specific inhibition studies relating to the Lewis blood-group system. *Nature* **16**, 4594 (1957).
268. Ravn, V. & Dabelsteen, E. Tissue distribution of histo-blood group antigens. *Apmis* **108**, 1–28 (2000).
269. Muschel, L. H. & Osawa, E. Human Blood Group Substance B and Escherichia coli 086. *Proc. Soc. Exp. Biol. Med.* **101**, 614–617 (1959).
270. Mahdavi, J. *et al.* A novel O-linked glycan modulates Campylobacter jejuni major outer membrane proteinmediated adhesion to human histo-blood group antigens and chicken colonization. *Open Biol.* **4**, (2014).
271. Tan, M. & Jiang, X. Norovirus and its histo-blood group antigen receptors: An answer to a historical puzzle. *Trends Microbiol.* **13**, 285–293 (2005).
272. Karki, G., Mishra, V. N. & Mandal, P. K. An expeditious synthesis of blood-group antigens, ABO histo-blood group type II antigens and xenoantigen oligosaccharides with amino type spacer-arms. *Glycoconj. J.* **33**, 63–78 (2016).
273. Nosaka, M. *et al.* Aberrant expression of histo-blood group a type 3 antigens in vascular endothelial cells in inflammatory sites. *J. Histochem. Cytochem.* **56**, 223–231 (2008).
274. Gao, S. *et al.* Histo-blood group ABO antigen in oral potentially malignant lesions and squamous cell carcinoma - Genotypic and phenotypic characterization. *Apmis* **112**, 11–20 (2004).
275. Abegaz, S. B. Human ABO Blood Groups and Their Associations with Different Diseases. *Biomed Res. Int.* **2021**, (2021).
276. Dean, L. Chapter 5 The ABO blood group. in *Blood Groups and Red Cell Antigens* (2005).
277. Zhang, H., Mooney, C. J. & Reilly, M. P. ABO blood groups and cardiovascular diseases. *Int. J. Vasc. Med.* **2012**, (2012).
278. Liu, Q. P. *et al.* Bacterial glycosidases for the production of universal red blood cells. *Nat. Biotechnol.* **25**, 454–464 (2007).
279. Hashemi-Najafabadi, S. *et al.* A method to optimize PEG-coating of red blood cells. *Bioconjug. Chem.* **17**, 1288–1293 (2006).
280. Mitra, R., Mishra, N. & Rath, G. P. Blood groups systems. *Indian J. Anaesth.* **58**, 524–528 (2014).
281. Zhang, S., Fu, Q., Zhang, Z. & Liu, Z. Surface loading of nanoparticles on engineered or natural erythrocytes for prolonged circulation time: strategies and applications. *Acta Pharmacol. Sin.* **42**, 1040–1054 (2021).
282. Harisa, G. E. din I., Ibrahim, M. F. & Alanazi, F. K. Characterization of human erythrocytes as potential carrier for pravas-tatin: An in vitro study. *Int. J. Med. Sci.* **8**, 222–230 (2011).
283. Bourgeaux, V., Lanao, J. M., Bax, B. E. & Godfrin, Y. Drug-loaded erythrocytes: On the road toward marketing approval. *Drug Des. Devel. Ther.* **10**, 665–676 (2016).

284. He, H., Ye, J., Wang, Y. & Yang, V. C. Cell-penetrating peptides meditated encapsulation of protein therapeutics into intact red blood cells and its application. *J Control Release* **176**, 123–132 (2014).
285. Pishesha, N. *et al.* Engineered erythrocytes covalently linked to antigenic peptides can protect against autoimmune disease. *Proc. Natl. Acad. Sci. U. S. A.* **114**, 3157–3162 (2017).
286. Glassman, P. M. *et al.* Vascular drug delivery using carrier red blood cells: Focus on RBC surface loading and pharmacokinetics. *Pharmaceutics* **12**, 1–21 (2020).
287. Villa, C. H. *et al.* Delivery of drugs bound to erythrocytes: new avenues for an old intravascular carrier. *Ther. Deliv.* **6**, 795–826 (2015).
288. Hu, C. M. J. *et al.* Erythrocyte membrane-camouflaged polymeric nanoparticles as a biomimetic delivery platform. *Proc. Natl. Acad. Sci. U. S. A.* **108**, 10980–10985 (2011).
289. Fu, Y. *et al.* Erythrocyte-Membrane-Camouflaged Nanoplatform for Intravenous Glucose-Responsive Insulin Delivery. *Adv. Funct. Mater.* **28**, 1–14 (2018).
290. Piao, J. G. *et al.* Erythrocyte membrane is an alternative coating to polyethylene glycol for prolonging the circulation lifetime of gold nanocages for photothermal therapy. *ACS Nano* **8**, 10414–10425 (2014).
291. Gao, W. *et al.* Surface functionalization of gold nanoparticles with red blood cell membranes. *Adv. Mater.* **25**, 3549–3553 (2013).
292. Rao, L. *et al.* Red Blood Cell Membrane as a Biomimetic Nanocoating for Prolonged Circulation Time and Reduced Accelerated Blood Clearance. *Small* **11**, 6225–6236 (2015).
293. Xia, Q., Zhang, Y., Li, Z., Hou, X. & Feng, N. Red blood cell membrane-camouflaged nanoparticles: a novel drug delivery system for antitumor application. *Acta Pharm. Sin. B* **9**, 675–689 (2019).
294. Doshi, N., Zahr, A. S., Bhaskar, S., Lahann, J. & Mitragotri, S. Red blood cell-mimicking synthetic biomaterial particles. *Proc. Natl. Acad. Sci. U. S. A.* **106**, 21495–21499 (2009).
295. Slaney, A. M. *et al.* Conjugation of A and B Blood Group Structures to Silica Microparticles for the Detection of Antigen-Specific B Cells. *Bioconjug. Chem.* **27**, 705–715 (2016).
296. Français, A., Urban, D. & Beau, J. M. Tandem catalysis for a one-pot regioselective protection of carbohydrates: The example of glucose. *Angew. Chemie - Int. Ed.* **46**, 8662–8665 (2007).
297. Wang, C. C., Lee, J. C. & Luo, S. Y. Regioselective one-pot protection of carbohydrates. *Nature* **446**, 896–899 (2007).
298. Gouasmat, A., Lemétais, A., Julien, S., Yann, B. & Beau, J. M. Catalytic Iron(III) Chloride Mediated Site-Selective Protection of Mono- and Disaccharides and One Trisaccharide. *European J. Org. Chem.* **2017**, 3355–3361 (2017).
299. Joseph, A. A. *et al.* TMSOTf-catalyzed silylation: Streamlined regioselective one-pot protection and acetylation of carbohydrates. *European J. Org. Chem.* 744–753 (2012) doi:10.1002/ejoc.201101267.
300. Zhou, Y., Li, J., Zhan, Y., Pei, Z. & Dong, H. Halide promoted organotin-mediated carbohydrate benzylation: Mechanism and application. *Tetrahedron* **69**, 2693–2700 (2013).
301. Ishihara, K., Kurihara, H. & Yamamoto, H. An Extremely Simple, Convenient, and Selective Method for Acetylating Primary Alcohols in the Presence of Secondary Alcohols. *J. Org. Chem.* **58**, 3791–3793 (1993).
302. Wegmann, B. & Schmidt, R. R. Synthesis of the H-disaccharide (2-O-α-l-fucopyranosyl-d-galactose) via the trichloroacetimidate method. *Carbohydr. Res.* **184**, 254–261 (1988).
303. Potter, G. T., Jayson, G. C., Miller, G. J. & Gardiner, J. M. An Updated Synthesis of the Diazo-Transfer Reagent Imidazole-1-sulfonyl Azide Hydrogen Sulfate. *J. Org. Chem.* **81**, 3443–3446 (2016).
304. Meloncelli, P. J. & Lowary, T. L. Synthesis of ABO histo-blood group type i and II antigens. *Carbohydr. Res.* **345**, 2305–2322 (2010).
305. Meloncelli, P. J., West, L. J. & Lowary, T. L. Synthesis and NMR studies on the ABO histo-blood group antigens: Synthesis of type III and IV structures and NMR characterization of type I-VI antigens. *Carbohydr. Res.* **346**, 1406–1426 (2011).
306. Kunetskiy, R. A., Pazynina, G. V., Ivanov, I. A. & Bovin, N. V. Synthesis of blood group A and B (type 2) tetrasaccharides. A strategy with fucosylation at the last stage. *Carbohydr. Res.* **498**, 108192 (2020).

307. Ryzhov, I. M. *et al.* Block synthesis of A (type 2) and B (type 2) tetrasaccharides related to the human ABO blood group system. *Carbohydr. Res.* **430**, 59–71 (2016).
308. Ryzhov, I. M. & Bovin, N. V. Synthesis of glycans functioning as antigens of the ABO blood group system. *Mendeleev Commun.* **29**, 597–612 (2019).
309. Neglia, L. *et al.* Mannose-binding lectin has a direct deleterious effect on ischemic brain microvascular endothelial cells. *J. Cereb. Blood Flow Metab.* **40**, 1608–1620 (2020).
310. Orsini, F. *et al.* Targeting mannose-binding lectin confers long-lasting protection with a surprisingly wide therapeutic window in cerebral ischemia. *Circulation* **126**, 1484–1494 (2012).
311. Longhi, L. *et al.* Mannose-binding lectin is expressed after clinical and experimental traumatic brain injury and its deletion is protective. *Crit. Care Med.* **42**, 1910–1918 (2014).
312. Osthoff, M. *et al.* Mannose-binding lectin deficiency is associated with smaller infarction size and favorable outcome in ischemic stroke patients. *PLoS One* **6**, (2011).
313. Wang, S. *et al.* Localized surface plasmon resonance-based abscisic acid biosensor using aptamer-functionalized gold nanoparticles. *PLoS One* **12**, 1–13 (2017).
314. Chen, H., Shao, L., Li, Q. & Wang, J. Gold nanorods and their plasmonic properties. *Chem. Soc. Rev.* **42**, 2679–2724 (2013).
315. Huang, X., Neretina, S. & El-Sayed, M. A. Gold nanorods: From synthesis and properties to biological and biomedical applications. *Adv. Mater.* **21**, 4880–4910 (2009).
316. Wang, L. *et al.* Side-by-side and end-to-end gold nanorod assemblies for environmental toxin sensing. *Angew. Chemie - Int. Ed.* **49**, 5472–5475 (2010).
317. Chang, H.-H. & Murphy, C. J. Mini Gold Nanorods with Tunable Plasmonic Peaks beyond 1000 nm. *Chem. Mater* **30**, 1427–1435 (2018).
318. Haine, A. T. & Niidome, T. Gold nanorods as nanodevices for bioimaging, photothermal therapeutics, and drug delivery. *Chem. Pharm. Bull.* **65**, 625–628 (2017).
319. Castellana, E. T., Gamez, R. C., Gómez, M. E. & Russell, D. H. Longitudinal surface plasmon resonance based gold nanorod biosensors for mass spectrometry. *Langmuir* **26**, 6066–6070 (2010).
320. Nusz, G. J., Curry, A. C., Marinakos, S. M., Wax, A. & Chilkoti, A. Rational Selection of Gold Nanorod Biosensors. *ACS Nano* **3**, 795–806 (2009).
321. Cao, J., Galbraith, E. K., Sun, T. & Grattan, K. T. V. Effective surface modification of gold nanorods for localized surface plasmon resonance-based biosensors. *Sensors Actuators, B Chem.* **169**, 360–367 (2012).
322. Cao, J., Sun, T. & Grattan, K. T. V. Gold nanorod-based localized surface plasmon resonance biosensors: A review. *Sensors Actuators, B Chem.* **195**, 332–351 (2014).
323. Pancaro, A. *et al.* The polymeric glyco-linker controls the signal outputs for plasmonic gold nanorod biosensors due to biocorona formation. *Nanoscale* **13**, 10837–10848 (2021).

This project has received funding from European Union's Horizon 2020 research and innovation program under the Marie Curie Sklodowska-Curie grant agreement No. 814236.